

Electron Spins in Dots and Rings:
Coherence, Read Out, and Transport

Inauguraldissertation
zur
Erlangung der Würde eines Doktors der Philosophie

vorgelegt der
Philosophisch-Naturwissenschaftlichen Fakultät
der Universität Basel

von
Hans-Andreas Engel
aus Eggwil

Basel, 2003

Genehmigt von der Philosophisch-Naturwissenschaftlichen Fakultät
auf Antrag von

Prof. Dr. Daniel Loss
Prof. Dr. Christoph Bruder
Prof. Dr. Leonid Levitov

Basel, den 16. Dezember 2003

Prof. Dr. Marcel Tanner
Dekan

Acknowledgements

First of all, I would like to thank Prof. Daniel Loss for accepting me as a diploma and PhD student. His deep understanding of physics, his patient explanations, and his precise questions provided a wonderful, stimulating support. In addition, I would like to thank Prof. Christoph Bruder and Prof. Leonid Levitov for co-refereeing this thesis.

The atmosphere in the Basel group has been friendly and inspiring. In particular, I would like to acknowledge my office mates, Dr. Felix Rembges, Dr. Guido Burkard, Dr. Eugene Sukhorukov, Dr. Alexander Khaetskii, Prof. Pascal Simon, and Dr. Hans-Benjamin Braun, with whom I shared good times talking about physics, computers, politics, and many other topics. It is a pleasure to thank all the other group members as well.

I would also like to acknowledge the contributions of my collaborators, Prof. David D. Awschalom, Bill Coish, Jeroen M. Elzerman, Prof. Andreas Engel, Ryan Epstein, Vitaly Golovach, Oliver Gywat, Ronald Hanson, Yui-chiro Kato, Prof. Leo P. Kouwenhoven, Dr. Christoph Leuenberger, Prof. Daniel J. Müller, Dr. Ansgar Philippsen, Dr. Simon Scheuring, Dr. Henning Stahlberg, and Prof. Lieven M.K. Vandersypen.

A number of other people contributed comments, advice, or questions from which I have learned during the last four years. Thanks to all of them, including particularly Dr. Ramón Aguado, Dr. Silvano De Franceschi, Prof. Klaus Ensslin, Dr. Diego Frustaglia, Dr. Ralf Häussler, Prof. Bert Hecht, Dr. Carol Leininger, Dr. Simon Rast, Dr. Stefan Oberholzer, Markus Popp, Prof. C. Schönenberger, Dr. Wilfred G. van der Wiel, and Dr. Maarten R. Wegewijs.

I acknowledge financial support from the Swiss NSF, NCCR Nanoscience Basel, DARPA, ARO, and from the Dissertationenfonds of the University of Basel.

Many thanks go to my parents Andreas and Barbara Engel and to my sister Eveline Engel for their love and support and for always having trust in me. To Caroline Logo I owe heartfelt thanks for her unwavering love and for always being a source of inspiration and happiness.

Summary

The spin of the electron leads to many effects in solid state physics. These effects provide the base for spintronics and promise many applications. One prominent proposal is to use individual electron spins as carriers of quantum information, as qubits, to build a quantum computer. Conversely, these effects can be used to assess the quantum mechanical properties of the spin using the well developed technologies of solid state physics. In this thesis, we consider semiconducting and metallic nanostructures and identify setups where new spin effects can be found. The main part of the thesis is focussed on quantum dots. These dots are small structures in which one can confine a single electron via its charge. Then, the spin of this electron can be addressed in a controlled way. One can apply an oscillating magnetic field which results in electron spin resonance (ESR) and drives the spin dynamics of the dot. We propose to assess the spin state of the dot by coupling to leads and driving an electrical current through the dot. This setup probes the quantum mechanical features of the single spin. In particular, the coherent Rabi oscillations and the decoherence time of the spin can be observed via the current through the dot. Furthermore, we describe how the electron spin on a dot can be assessed without requiring contact to leads. The combination of ESR and laser excitation with polarized light enables us to define schemes where the spin coherence and Rabi oscillations can be measured optically. In the absence of ESR, we consider the fluctuations (noise) of the dot current. Noise provides information on quantum effects which do not appear in the d.c. current itself. We study the asymmetric noise of dots in the quantum limit of high noise frequencies ω , where non-Markovian effects have to be taken into account. A further question is how to measure the state of a spin on a quantum dot, i.e., to detect if it is “up” or “down.” We propose several schemes for such a read out, including measuring the current through the dot coupled to spin-polarized leads and implementations based on a double

dot which electrostatically influences the current through a nearby quantum point contact. We also analyze the read-out statistics of an arbitrary two level system (qubit), taking into account possible imperfections of the measurement apparatus. Defining a measurement efficiency allows us to characterize a reliable n -shot read out. In the last part of this thesis, we consider electron spins in rings. In electron currents through mesoscopic rings one observes that each electron moves as a superposition simultaneously through the upper and lower arm of the ring and then interferes with itself. Additional interference effects can occur when the spins of the electrons evolve adiabatically and acquires a Berry phase, due to an inhomogeneous magnetic field or spin-orbit interaction. We study diffusive rings and determine the required field strength for the Berry phase to emerge and show that this phase leads to a suppression of the Aharonov-Bohm oscillations at certain magic angles of the magnetic field. Finally, for all setups proposed in this thesis, we discuss the experimental requirements and show that they can be satisfied under realistic conditions.

Contents

Acknowledgements	3
Summary	5
1 Introduction	11
1.1 The electron spin	12
1.2 Quantum dots	14
1.3 Decoherence	15
1.4 Quantum computing	17
1.5 Current fluctuations—quantum noise	21
1.6 Berry phase	24
2 Single Spin Dynamics and Decoherence in a Quantum Dot via Charge Transport	29
2.1 Introduction	30
2.2 Quantum dot in ESR Field	32
2.2.1 Model Hamiltonian	32
2.2.2 Dot spectrum and energetics	33
2.2.3 Systematic treatment of sequential tunneling	36
2.2.4 Master equation	38
2.2.5 Decoherence and measurement process	41
2.2.6 Cotunneling contribution to the sequential tunneling regime	41
2.3 Stationary current	42
2.3.1 Spin satellite peak	43
2.3.2 Spin decoherence time T_2	44
2.3.3 Universal conductance ratio	47
2.4 Even-to-odd sequential tunneling	49

2.5	Spin Inverter	50
2.5.1	Spin filter	51
2.5.2	Implementation of the spin inverter	53
2.6	Pumping	54
2.7	Rotating ESR fields	54
2.8	Cotunneling	56
2.9	Spin read out with spin-polarized leads	60
2.9.1	Counting statistics and signal-to-noise ratio	61
2.9.2	Measurement time	62
2.10	Rabi Oscillations of a single spin in the time domain	63
2.10.1	Observing Rabi oscillations via current	63
2.10.2	Decoherence in the time domain	65
2.10.3	Zeno effect	65
2.11	Pulsed ESR and Rabi oscillations	66
2.12	STM Techniques and ESR	69
2.13	Conclusion	70
3	Measurement Efficiency and n-shot Read Out of Spin Qubits	73
3.1	Introduction	73
3.2	n -shot read out and measurement efficiency e	74
3.2.1	Visibility v	75
3.3	Single spin read out	75
3.3.1	Read out with different Zeeman splittings.	76
3.3.2	Spin-dependent tunneling	77
3.3.3	Read out with Pauli principle	78
3.4	Read-out model	79
3.4.1	Incoherent tunneling	81
3.5	Read out with time-dependent currents	82
3.5.1	Read-out using a single dot only	82
3.6	Conclusion	83
4	Asymmetric Quantum Shot Noise and non-Markovian effects in Quantum Dots	85
4.1	Introduction	85
4.2	Quantum dots	86
4.3	Current	88
4.4	Quantum shot noise	88
4.5	Asymmetric steps in shot noise	91

4.5.1	Quantum dot with single level	92
4.5.2	Quantum dot with two and more levels	93
4.6	Conclusion	95
5	Optical Detection of Single-Electron Spin Decoherence in a Quantum Dot	97
5.1	Introduction	97
5.2	Charged excitons in quantum dots	98
5.3	Dynamics and Pauli blockade	100
5.4	Master equation	101
5.5	Spin decoherence time T_2 via cw excitation	102
5.6	Pulsed excitations and spin Rabi oscillations	106
5.7	Conclusion	107
6	Conductance fluctuations in diffusive rings: Berry phase effects and criteria for adiabaticity	109
6.1	Introduction and overview	110
6.2	Conductance fluctuations	113
6.2.1	Exact solution	113
6.2.2	Adiabatic approximation	116
6.2.3	Finite temperatures	118
6.3	Berry phase and Adiabaticity	120
6.3.1	Magic Angles—Qualitative criterion for Adiabaticity	120
6.3.2	Quantitative criterion for Adiabaticity	124
6.4	Exact calculations with spin-orbit interaction in diffusive limit	127
6.4.1	Magnetoconductance	129
6.4.2	Conductance fluctuations	129
6.5	Peak splittings in power spectra	131
6.5.1	Frequency shifts in δg and $\delta g^{(2)}$	131
6.5.2	Frequency shifts in $\delta g_{\text{hom}}^{(2)}$ for homogeneous fields	133
6.5.3	Numerical evaluations	134
6.6	Berry phase controlled Spin Filter	140
6.7	Conclusion	142
A	Energy Shifts due to Tunneling H_T	145
B	Stationary Current for cw ESR	149

C	Exact Current and Noise for a Quantum Dot	151
C.1	Current	152
C.1.1	Averaged current $\langle I_l \rangle$	153
C.2	Asymmetric shot noise	153
C.2.1	Symmetrized noise	155
C.2.2	Quantum noise in sequential tunneling regime	156
C.2.3	Quantum noise in coherent regime	156
D	Sequential Tunneling Quantum Noise	157
E	Double dot and QPC: Master Equation and Current	159
F	Two-level system in an electromagnetic field	163
F.1	Light-matter interaction with a classical field	163
F.2	Canonical quantization of the electromagnetic field	165
F.3	Interaction of a two-level system with the electromagnetic field	166
G	Differential equations for Cooperon and Diffuson	169
H	Finite Temperature Integrals for UCFs	173
I	UCFs $\delta g_{\text{hom}}^{(2)}$ for Homogeneous Fields	175
J	Energy Scales	179
	References	181
	Curriculum Vitae	199

Chapter 1

Introduction

The electron has spin, in addition to its charge and its mass. This electron spin leads to many effects in solid state systems and possibly to new applications. While control of the charge of the electron has been mastered in conventional electronics, the control and use of its spin are still emerging. Nevertheless, the enormous potential for using spin in electronic devices has been recognized [1] and has led to ongoing research in spintronics. First, conventional devices can be significantly improved by electron spin effects, e.g., magnetic read-out heads for computer hard drives [widely in use, based on the giant magnetoresistance (GMR) effect], non-volatile memories (e.g., MRAM which should be commercially available within two years), and future devices such as a spin transistor or memories based on single spins. Second, coherent properties of electron spins could be used for radically new designs in the field of quantum information [2]. In particular, the spins of electrons on arrays of quantum dots could be used for creating a quantum computer as proposed by D. Loss and D. DiVincenzo [3]. Such a quantum computer would provide large computational resources if it could eventually be built. It would also allow for a convincing test of properties of quantum mechanics such as phase coherence, non-locality, and entanglement. However, before that long term goal can be reached, a better understanding and control of spins in quantum dots is required.

The idea to use spins for electronics is strongly supported by experiments [4, 5, 6, 7, 8] showing unusually long spin dephasing times [4] in semiconductors (approaching microseconds in bulk and probably much longer in quantum dots), the injection of spin-polarized currents from a magnetic- to a non-magnetic semiconductor [5, 6], as well as by the phase-coherent spin

transport over distances of up to $100 \mu\text{m}$ [4]. Additionally, since the motion of the electron can be controlled through its charge, an electron spin can be transported along conducting wires [9]. This allows using spin-entangled electrons forming Einstein-Podolsky-Rosen (EPR) pairs, which can be created (e.g., in coupled quantum dots or near a superconductor-normal interface [10, 11]), transported, and detected [9, 12]. Such EPR pairs represent a fundamental prerequisite for quantum communication [13, 14].

1.1 The electron spin

Since this thesis deals with electron spins in solid state systems, we first review some basic properties of spin dynamics and introduce some standard notations. The electron has an “intrinsic” magnetic moment which takes the values $\pm \frac{1}{2}g\mu_B\hbar$. This corresponds to a spin $\frac{1}{2}$ having the two states “up”, $|\uparrow\rangle$, and “down”, $|\downarrow\rangle$, aligned parallel and antiparallel, resp., to a magnetic field, say, in the z direction. The general state $|\psi\rangle$ of the spin is an arbitrary superposition of up and down,

$$|\psi\rangle = \alpha|\uparrow\rangle + \beta|\downarrow\rangle. \quad (1.1)$$

Now we consider the operators which act on the spin system. They can be conveniently represented in terms of the identity operator and the Pauli matrices $\boldsymbol{\sigma} = (\sigma_x, \sigma_y, \sigma_z)$, with $\sigma_x = \begin{pmatrix} 0 & 1 \\ 1 & 0 \end{pmatrix}$, $\sigma_y = \begin{pmatrix} 0 & -i \\ i & 0 \end{pmatrix}$, and $\sigma_z = \begin{pmatrix} 1 & 0 \\ 0 & -1 \end{pmatrix}$ and which obey $\sigma_i\sigma_j = \delta_{ij} + i\sum_k \varepsilon_{ijk}\sigma_k$. We can use these operators to depict the spin state as a vector of unit length pointing in a particular direction, $\langle\boldsymbol{\sigma}\rangle = \langle\psi|\boldsymbol{\sigma}|\psi\rangle$, corresponding to a point on the so-called Bloch sphere [15] (see Fig. 1.2). Indeed, $\langle\uparrow|\boldsymbol{\sigma}|\uparrow\rangle$ points in the positive z direction. (This definition of the Bloch sphere is equivalent to geometrically representing the state of completely polarized light on the Poincaré sphere.) This picture implies the parametrization of an arbitrary spin state in terms of an azimuthal angle φ and a polar angle θ ,

$$|\psi\rangle = \cos\frac{\theta}{2}|\uparrow\rangle + e^{i\varphi}\sin\frac{\theta}{2}|\downarrow\rangle. \quad (1.2)$$

So far we have assumed that the spin is in a pure state $|\psi\rangle$. More generally, the spin state is described by a statistical ensemble which can be represented

in terms of the density matrix, $\rho = \rho_{\uparrow}|\uparrow\rangle\langle\uparrow| + \rho_{\downarrow}|\downarrow\rangle\langle\downarrow| + \rho_{\downarrow\uparrow}|\downarrow\rangle\langle\uparrow| + \rho_{\uparrow\downarrow}^*|\uparrow\rangle\langle\downarrow|$. The Bloch-vector then becomes $\mathbf{r} = \langle\boldsymbol{\sigma}\rangle = \text{Tr}\boldsymbol{\sigma}\rho$, with length less than one for a mixed state.¹

We now consider the dynamics of the spin. Placed in an magnetic field $\mathbf{B}(t)$, the spin is subjected to the Zeeman interaction,

$$H(t) = -\frac{1}{2}g\mu_B\mathbf{B}(t)\cdot\boldsymbol{\sigma}, \quad (1.3)$$

where g is the electron g factor and $\mu_B = e\hbar/2mc$ is the Bohr magneton.² We now evaluate the time derivative of the Bloch vector, $\dot{\mathbf{r}}$, using the Heisenberg equation (with $\hbar = 1$) and find

$$\dot{\mathbf{r}} = -\frac{i}{2}g\mu_B\langle[\mathbf{B}(t)\cdot\boldsymbol{\sigma}, \boldsymbol{\sigma}]\rangle = -g\mu_B\mathbf{B}(t)\times\mathbf{r}, \quad (1.4)$$

where we have evaluated the k^{th} component of the commutator as $[\sum_j B_j\sigma_j, \sigma_k] = 2i\sum_j B_j\varepsilon_{jkl}\sigma_l = -2i(\mathbf{B}\times\boldsymbol{\sigma})_k$. Equation (1.4) is the coherent part of the Bloch equation [15, 16] (we discuss the incoherent contributions in Sec. 1.3 below). It shows that the spin, pictured as a Bloch vector, precesses around the magnetic field $\mathbf{B}(t)$. This is like the precession of a classical magnetic moment in a magnetic field.

For a static magnetic field in the z direction, the spin precesses clockwise around the z axis with Larmor frequency $\omega_0 = g\mu_B B_z$. To create magnetic resonance [17], one applies an additional rotating field in the xy plane which approximately follows the spin precession, $B_x(t) = B_{\perp}\cos(\omega_1 t)$ and $B_y(t) = -B_{\perp}\sin(\omega_1 t)$. When transformed to the system which rotates at frequency ω_1 , with $U = \exp\{-i\omega_1 t\sigma_z/2\}$, one obtains the Hamiltonian in the rotating frame, $\tilde{H} = UHU^{\dagger} + i\hbar\dot{U}U^{\dagger} = -\frac{1}{2}g\mu_B\mathbf{B}^r\cdot\boldsymbol{\sigma}$, with a time-independent field $B_x^r = B_{\perp}$, $B_y^r = 0$, and $g\mu_B B_z^r = \omega_0 - \omega_1$. Thus, the rotating field component in the lab frame becomes, in the rotating frame, a static field in the x direction. In the z direction, the field is reduced by the frequency of rotation, ω_1 , i.e., the remaining field B_z^r is given by the detuning

¹One can easily recover the density matrix from \mathbf{r} with $\rho_{\uparrow} = (1-r_z)/2$, $\rho_{\downarrow} = (1+r_z)/2$, and $\rho_{\downarrow\uparrow} = (r_x + ir_y)/2$.

²Here, $e < 0$ is the electron charge, i.e., we define $\mu_B < 0$. In bulk GaAs, $g = -0.44$, thus $g\mu_B > 0$ and the spin ground state $|\uparrow\rangle$ is aligned parallel to the magnetic field. An arbitrary spin will precess clockwise around the field axis. The sign of g is reversed in vacuum, $g = 2.0023$. Then, the spin ground state is antiparallel to the magnetic field and the spin precession is anticlockwise.

$\omega_0 - \omega_1$. At the resonance, $\omega_0 = \omega_1$, only the field B_x^r remains. An initial spin $|\uparrow\rangle$ will rotate around B_x^r to the state $|\downarrow\rangle$ and then back to $|\uparrow\rangle$ and so forth. These rotations are called the Rabi oscillations of the spin.

1.2 Quantum dots

Semiconductor quantum dots are structures where charge carriers are confined in all three spatial dimensions. The dot size, typically between 10 nm and 1 μm [18], is on the order of the Fermi wavelength in the host material. The confinement of the quantum dots is usually achieved by electrical gating of a two-dimensional electron gas (2DEG), possibly combined with etching techniques. Small dots have charging energies in the meV range, resulting in quantization of charge on the dot (Coulomb blockade). This allows precise control of the number of electrons and of the spin ground state on the dot. Such a control of the number of electrons in the conduction band of a quantum dot (starting from zero) has been achieved with GaAs heterostructures, e.g., for vertical dots [19] and lateral dots [20]. Quantum dots have various tunable parameters. These include geometry, energy spectrum, coupling between dots, etc., which open up many possibilities by providing a versatile system for manipulation of electronic states, in particular the spin state. Further, the electronic dot-orbitals are highly sensitive to external magnetic and electric fields [18, 19], since the magnetic length corresponding to fields of $B \approx 1 \text{ T}$ is comparable to typical dot sizes. In coupled quantum dots Coulomb blockade effects [21], tunneling between neighboring dots [18, 21], and magnetization [22] have been observed as well as the formation of a delocalized single-particle state [23] and coherent charge oscillations [24].

Since the spin state of quantum dots can be controlled, it is possible to produce a spin $\frac{1}{2}$ ground state of the quantum dot. This can be achieved, e.g., if a single excess electron is left on the dot or if the dot has anti-ferromagnetic filling and contains an odd number of electrons. This system promises many applications, such as quantum computation [3] or single spin memory [25], and it also allows to probe single spin properties, such as dynamics and coherence.

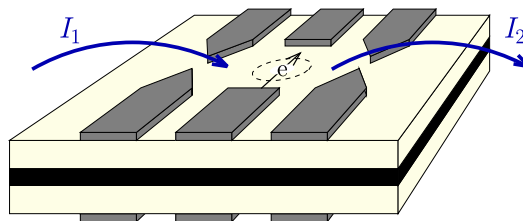


Figure 1.1: Schematic picture of a quantum dot. The electrodes (gray) confine electrons to the dot region (circle). The dot can be coupled to leads, allowing a current $I_{1,2}$ to flow through the dot. The spin state of the dot can be manipulated with external magnetic fields, shown by the wavy line.

1.3 Decoherence

The issue of decoherence is a fundamental problem in quantum physics, leading to the transition from quantum to classical behavior. It is an important issue in mesoscopic physics, since it puts an upper bound on the length and time scales on which electrons in small structures still show coherent effects. Due to this importance, there are many efforts to better understand and characterize decoherence. However, most of what has been probed, say, with weak localization or Aharonov-Bohm effects, is the *orbital* coherence of electrons. Orbital coherence stands for the preservation of the phase coherence if an electron is in a superposition of spatially separated states such as in the upper and lower arm of an Aharonov-Bohm ring. The corresponding coherence times, up to a few nanoseconds, found in such experiments are generally not related to the *spin* coherence time. Therefore, studies of the latter are a separate issue. If there are strong spin-orbit interaction effects, the spin and orbital decoherence are related. However, for some systems these effects can be small and thus there is a much longer spin than charge decoherence time, see below.

Now let us consider spin dynamics in the presence of decoherence. This can be described with the coherent time evolution, Eq. (1.4) and with additional (incoherent) damping terms. This leads to the standard Bloch equations [15, 16], where decoherence is characterized by two time scales: the (longitudinal) relaxation time T_1 and the decoherence (transverse relaxation) time T_2 , see Fig. 1.2. The spin relaxation time T_1 describes the lifetime of an

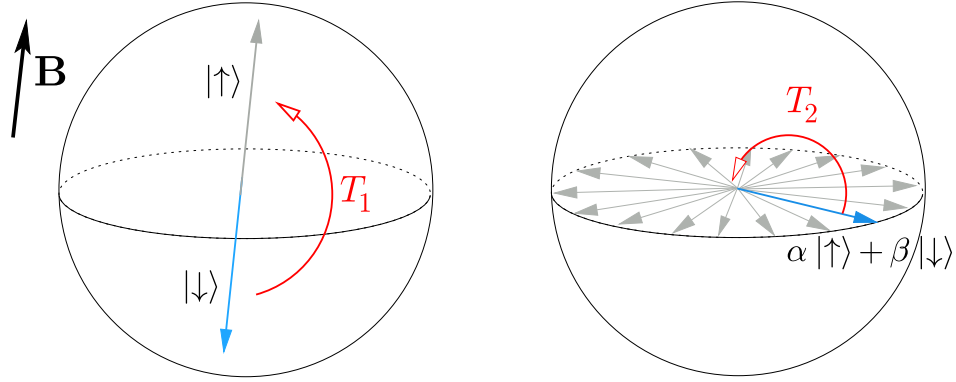


Figure 1.2: Spin in an external magnetic field, shown here on the Bloch sphere. Relaxation from the excited spin state to the ground state occurs on the time scale T_1 . The phase information of a superposition is lost after the decoherence time T_2 .

excited spin state aligned along the external field, and is classical in the sense of not involving the concept of quantum superpositions in its definition. On the other hand, the spin decoherence time T_2 gives the time over which a superposition of opposite spin states of a single electron remains coherent, i.e., the time it takes for a superposition $\alpha|\uparrow\rangle + \beta|\downarrow\rangle$ to decay into a mixture $|\alpha|^2|\uparrow\rangle\langle\uparrow| + |\beta|^2|\downarrow\rangle\langle\downarrow|$. Thus, coherent manipulations of electron spins, e.g., gate operations for quantum computation, must be performed faster than T_2 , cf. Sec. 1.4. We note that $T_2 \leq 2T_1$ and typically even $T_2 \ll T_1$ [16]. Thus, from the sole knowledge of T_1 no lower bound for T_2 follows. Therefore, it is of fundamental interest to investigate ways of measuring the decoherence time T_2 for a single spin. In particular, we are interested in spins on quantum dots (cf. Sec. 1.2) since this is a very versatile system and has promising applications as explained above. Finally, the loss of phase coherence of many but independent spins is described by the dephasing time T_2^* [4]. There, due to inhomogeneities in the Zeeman terms, the spins precess with a different period and eventually the precessions of different spins become out of phase. This results in a further suppression of phase coherence for an ensemble of (uncorrelated) spins but not necessarily for an individual spin, thus $T_2^* \leq T_2$.

For spins on quantum dots, a possible source of decoherence is due to spin-orbit interaction. There are calculations which show that phonon-assisted spin-flip rates ($1/T_1$) [26, 27] in quantum dots are unusually low. Coupling

to other electrons, which are for example present in gates, can lead to stronger relaxation in some regimes [28]. Also, the decoherence rates ($1/T_2$) are very low, since it turns out that $T_2 = 2T_1$ for decoherence due to spin-orbit interaction [29]. Another source of decoherence is the hyperfine coupling between electron spin and nuclear spins in a quantum dot [30, 31, 32]. The hyperfine interaction is always present in GaAs semiconductors, since all naturally occurring Ga and As isotopes have a nuclear spin $I = 3/2$. It is known that such decoherence can be controlled by an Overhauser field [30].

That spin coherence times can be orders of magnitude longer than charge coherence times has been shown in magneto-optical measurements, based on time-resolved Faraday rotation experiments on doped GaAs in the bulk [4]. At vanishing magnetic field and $T = 5$ K, a T_2^* time exceeding 100 ns was measured. For an ensemble of chemically synthesized semiconductor quantum dots, one has only found relatively small T_2^* times (a few ns at vanishing magnetic field), probably due to a large g factor inhomogeneity [33]. For single quantum dots, the T_1 time of a spin on the dot has been measured recently via transport and was shown to be longer than 50 microseconds [34, 35].

However, there are no experiments yet for the decoherence time T_2 of single electron spins in quantum dots. Due to this lack of experimental evidence, the existing results on somewhat different systems can not be viewed as conclusive for T_2 on dots. This makes experiments which determine the decoherence time highly desirable. In this thesis, we propose several schemes for how this time can be measured: in chapters 2 and 5 we describe how the T_2 time and the dynamics of single electron spins on quantum dots can be accessed via current or via photoluminescence.

1.4 Quantum computing

In quantum information, one makes use of the peculiarities of quantum mechanics to address tasks which are not feasible with conventional computing and communication devices [2, 13, 14]. Central in this field is the quantum computer. In contrast to the classical computer (based on bits with states 0 or 1), the quantum computer is based on quantum bits (qubits), which can be in an arbitrary superposition of 0 and 1: $\alpha|0\rangle + \beta|1\rangle$. These qubits in combination with controlled unitary time evolution allow a quantum computer to outperform classical computation through new and more powerful

quantum algorithms. Still, a classical computer can be used to simulate any quantum algorithm, using an (at most) exponentially increased amount of time relative to running the algorithm on a quantum computer. This implies that a quantum computer can speed up any task not more than exponentially.³ Is this upper limit of exponential speed up ever reached? There are two popular examples of quantum algorithms. First, for database searches, the Grover [36] algorithm only requires the square root of the time which is consumed by a classical algorithm. Second, for factorization of large numbers N , the speed up with the Shor [37] algorithm is even larger than any polynomial in the number of digits $n = \log N$. However, the speed up remains less than exponential, since the classical factorization algorithms [number field sieve (NFS) and multiple polynomial quadratic sieve (MPQS)] only need a sub-exponential amount of time, cf. table 1.1. Still, factorization remains a computationally hard problem which is required to ensure security of the RSA public key cryptosystems [38]. This security would be compromised by a quantum computer running the Shor algorithm. We now provide an example, where the speed gain of a quantum computer is even larger. Namely, one can also use Shor's algorithm to calculate discrete logarithms on arbitrary groups in polynomial time [2]. It can thus also be applied to the group which one defines on elliptic curves. However, the best currently known (classical) algorithm for finding discrete logarithms on this group⁴ requires an exponential amount of time [38, 39]. (This fact is used to build cryptosystems based on elliptic curves, using Diffie-Hellman key exchange.) Thus, for discrete logarithms on elliptic curves, the speed gain of the quantum computer is indeed exponential.

In addition to these computational advantages, there is a long list of other quantum tasks [13] such as cryptography [14], error correction schemes, quantum teleportation, etc. which indicates even more the desirability of physical implementations of quantum schemes. Still, a quantum computer does not yet exist,⁵ since a radically new approach to the design of the necessary

³Otherwise, there exists a task for which the best known classical algorithm could be sped up more than exponentially with a quantum algorithm. That quantum algorithm could then be simulated on a classical computer which would slow it down exponentially. Thus, in total, this simulation would still be faster than the original classical algorithm. This contradicts to the assumption that the classical algorithm was the best one known.

⁴This holds for "good" elliptic curves where the number of points contained in the curve satisfies some security conditions.

⁵In a liquid state NMR experiment, a new record of *seven* qubits was realized and the

	classical	quantum
search	n	\sqrt{n}
factorization	$\exp\{cn^{1/3} \log^{2/3} n\}$	$n^2 \log n \log \log n$
DL on elliptic curves	$\exp\{n/2\}$	n^3

Table 1.1: Time consumption of different problems as a function of input size n , using the best known classical and quantum algorithms. For database search, n is the number of database entries. For factorization of a number N and for finding a discrete logarithm (DL) on an elliptic curve with group order N , we set $n = \log_2 N$. Note that the speed gain of the problems listed here is \sqrt{n} , sub-exponential, and exponential, respectively.

hardware is required. Experimental progress as well as theoretical investigations are needed to provide guidance and support in the search for realizable implementations. There is a large number of proposed experimental implementations of qubits and quantum gates. A few examples are trapped ions [41], cavity QED [42], nuclear spins [43, 44, 45], superconducting devices [46, 47, 48, 49], and the already mentioned proposal based on the spin of the electron in quantum-confined nanostructures [3].

What physical systems can be used as a quantum computer? Any physical implementation must satisfy *all* five criteria of DiVincenzo's checklist for a quantum computer [50, 51].

i) *A scalable system with well characterized qubits.*

For implementing calculations on a quantum computer with the advantage of its speed up, one needs a large number of qubits, i.e., on the order of 10^5 . Thus, the underlying physical system must be scalable to such a number and allow gate operations [see iv) below] to be carried out in parallel (parallelism is required in known error correction schemes [2]). For characterizing a qubit, one can map any two-level system onto the qubit. Further, one can use a system with more degrees of freedom and map only a subspace of its Hilbert space onto the qubit. There, however it is important that the remaining part of the Hilbert space is not visited at the end of any gate operation, since this would correspond to *leakage* to an undefined state.

number 15 was factorized with the Shor algorithm [40]. However, this setup cannot be scaled to a higher number of qubits and thus does not satisfy criterion i) given below.

- ii) *The ability to initialize the state of the qubits.*

The quantum registers must be initialized to a known value at the beginning of a computation.

- iii) *Long decoherence times, much longer than the gate operation time.*

The concrete goal is to have an error rate not larger than one part in 10^4 . From that point on, an error-correction scheme [2] can remove the remaining errors and the quantum computer can be up-scaled. It is important to note that for most quantum computer proposals, this is the most difficult criterion to satisfy. Since any interaction can lead to decoherence, the qubits must be very isolated from their environment to obtain long coherence times. At the same time, a strong coupling to some controlled external degrees of freedom is required to produce fast quantum gate operations (see below).

- iv) *A universal set of gates.*

The physical system must provide mechanisms to control a particular unitary evolution of the involved qubits. These unitary evolutions are called quantum gates. It turns out that all quantum algorithms can be implemented by concatenating single-qubit gates and a universal two-qubit gate (e.g., XOR or square root of SWAP).

- v) *A qubit-specific measurement capability.*

At the end of the computation, its result must be read out by measuring specific qubits. Further, some error correcting schemes also require that qubits are read out during the computation.

We can now check if the proposal of using electron spins on quantum dots [3] can be used as quantum computer. It seems plausible that this proposal satisfies every item on this checklist. We summarize the most important facts for each item and refer to Ref. [52] for more details.

- i) The electron's spin $\frac{1}{2}$ provides a natural qubit, setting $|0\rangle \equiv |\uparrow\rangle$ and $|1\rangle \equiv |\downarrow\rangle$, cf. Eq. (1.1). Further, quantum dots provide a scalable system, say, lithographically defined quantum dots can be scaled with state-of-the-art techniques for defining nanostructures in semiconductors.

- ii) To initialize spin qubits, one can apply a large magnetic field $g\mu_B B \gg kT$ that allows them to relax to the thermal ground state. Alternatively, one can inject polarized electrons into the dot by using spin-polarizing materials [5, 6] or by spin-filtering with the help of another dot [25], see also Sec. 2.5.1.

iii) We can estimate the gate operation time, which for the spin qubits can be as low as $\tau_s \approx 30$ ps [52]. However, for the decoherence time of the spin qubit it would be desirable if it would be determined experimentally, as we have indicated in Sec. 1.3. So we propose simple schemes for accessing decoherence via current or via optical measurements.

iv) Single qubit gates can be produced by controlling the local magnetic fields or the local g factor (or g tensor), which can be achieved with a semiconductor heterostructure and electrical gating [52, 53, 54]. To build two qubit gates, one can use the exchange interaction of the spins on two neighboring dots, which can be controlled by tuning the tunnel coupling between the dots [3, 30, 55].

v) There are several proposals for measuring the spin in quantum dots. A very promising concept is to transfer the information from the spin to the charge state [3], e.g., by making use of the Pauli principle [25, 56, 57], via the spin-orbit interaction [28], or by making use of the Zeeman splitting [58]. We discuss the measurement efficiency for general qubit read out in Sec. 3.2 and concrete read-out schemes for spin qubits in Sec. 2.9 and chapter 3.

1.5 Current fluctuations—quantum noise

The electrical current and its fluctuations provide useful information about conducting systems. Let us consider the current operator I from a (quantum) statistical point of view. The quantity of primary interest is the expectation value, $\langle I(t) \rangle = \text{Tr } I(t)\rho = \text{Tr } I\rho(t)$. Here, the state of the system (including current leads) is described by the density matrix $\rho(t)$, corresponding to a pure state or to a statistical ensemble. We assume that the system has had sufficient time to relax to a stationary state, $\rho(t) = \bar{\rho}$. In this case, the expectation value becomes time-independent, $\langle I(t) \rangle = \langle I \rangle$. What are further interesting properties of the current beyond the expectation value? In the course of time, the current will fluctuate around its expectation value, i.e., at a given time t , the difference is $\delta I(t) = I(t) - \langle I \rangle$. We consider how the fluctuations evolve in time, i.e., if there is a fluctuation at time t' is it still present at time t . This is described by the (auto-)correlation function $\langle \delta I(t)\delta I(t') \rangle = \langle \delta I(t-t')\delta I \rangle = \langle I(t)I \rangle - \langle I \rangle^2$. This definition makes sense for a classical stochastic process, where for a given realization, the value of $\delta I(t)$ is known at every time t . For a quantum system, physical observables are described by Hermitian operators (ensuring real expectation values), e.g.,

$\delta I(t)$. However, since $\delta I(t)$ and δI do not necessarily commute, $\delta I(t)\delta I$ is non-Hermitian and is thus not an observable. Still, we find a physically relevant quantity by Fourier transforming the correlation function. This is the current noise,

$$S(\omega) = \int_{-\infty}^{\infty} dt e^{i\omega t} \langle \delta I(t)\delta I \rangle, \quad (1.5)$$

which is a real quantity and can be regarded as (an expectation value of) an observable. Alternatively, one can avoid the non-Hermitian operator by symmetrizing it, $\delta I(t)\delta I \rightarrow \frac{1}{2}[\delta I(t)\delta I + \delta I\delta I(t)]$. With this replacement in Eq. (1.5), one obtains the symmetrized noise, $S^{\text{sym}} = \frac{1}{2}[S(\omega) + S(-\omega)]$ [59]. However, now one has removed the quantum property of non-commuting operator; in chapter 4 we show that conversely the unsymmetrized noise contains more information about quantum effects. Another common definition of noise uses an additional factor of two, $S'(\omega) = 2S^{\text{sym}}(\omega)$. This is the noise power density which is measured after filtering the fluctuations at frequency $f = \omega/2\pi$ with some bandwidth Δf . Since the filter is assumed to pass both positive and negative frequencies, $\pm f$, this increases the noise power by a factor 2.⁶

A simple system for studying noise is a tunnel junction which can be described with two tunnel-coupled leads (reservoirs). Since the tunneling is weak, each of the leads remains at thermal equilibrium, even if a bias is applied across the junction. There are two limiting cases for noise which we now consider in the classical regime, $\omega < kT$. First, if the temperature T is larger than the bias, the directed tunneling events due to the bias give only negligible fluctuations while the thermal fluctuations across the junction will dominate. This is the Johnson-Nyquist noise $S(\omega) = 2kTG$ [60] with conductance G , and contains no additional information to what is already known from current measurements. Second, for a bias larger than temperature, the discrete charge of the electrons becomes important; each time an electron with charge e tunnels across the junction, this leads to a large fluctuation of the current, $\delta I(t) = e/\Delta t$ when averaged over an arbitrarily short time interval Δt . These fluctuations lead to so-called shot noise, $S(\omega) = e\langle I \rangle$, the name inspired by the “discrete” pellets coming out of a shotgun [61]. It is remarkable that by measuring current and shot noise of a tunnel junction, one can determine the charge of the electron. The crossover of these

⁶This prefactor, inconsistent in the literature, is eliminated when one regards the Fano factor which is defined as $F = S/e\langle I \rangle$ in the former case and $F = S'/2e\langle I \rangle$ in the latter.

two regimes is given by the nonequilibrium fluctuation-dissipation theorem (FDT), relating noise with the current through the junction for arbitrary bias.⁷

More generally, shot noise of mesoscopic systems provides a rich field of research [65, 66]. Since it allows to measure the charge of particles tunnelling across a junction, one can use it to access the charge of quasi particles, e.g., Cooper pairs tunneling between a superconductor and a normal metal. For systems with some correlations between different electrons, shot noise usually becomes suppressed, e.g., by a factor of $\frac{1}{3}$ in diffusive conductors [67]. The correlation effects become even richer if there is a part of the system which has some memory effects which is the case for quantum dots in the Coulomb blockade regime. There the correlations do not always lead to a suppression of noise. If an internal state of the dot switches the current from one to another value, this can even lead to super-Poissonian noise, i.e., $S > e\langle I \rangle$ [68, 63, 69].

Let us now go beyond shot noise. The counting statistics provides a generalization of the current fluctuations [70, 71]. There, one “counts” the charge which have been transferred since time $t = 0$ by a probability distribution $P_q(t)$. (In chapter 2, we use this description for quantum dots [72] to determine the statistics of the spin read out.) If the counting statistics is not calculated directly one can, e.g., use a nonequilibrium Green’s function method [73, 74]. The counting statistics is a generalization of shot noise, since the zero frequency noise $S(0)$ is recovered from the charge distribution, namely $\langle \delta q(t)^2 \rangle = t S(0)$ for sufficiently long t . Further, the higher moments of the current can be calculated. In particular, for the 3rd moment it was found in the tunneling regime that a similar effect as for shot noise appears, $\langle \delta I^3 \rangle = e^2 \langle I \rangle$ [75]. Remarkably, in contrast to shot noise, this relation holds even for arbitrary bias. This prediction was confirmed in a recent experiment [76], where also the contributions due to fluctuations in the measurement apparatus itself were taken into account [77].

Another interesting situation is the noise in the quantum limit of high frequencies ω . For tunneling junctions, this case is already described by the FDT (see footnote 7). There, one only considers the fluctuations between

⁷The FDT was derived for symmetrized noise S^{sym} [62]. For non-symmetrized noise, we evaluate current and noise in the spectral (Lehmann) representation and in lowest order in tunneling across the junction. For an applied bias $\Delta\mu/e$, we find the FDT $S(\omega) = \frac{e}{2} \sum_{\pm} \left[\coth \left(\frac{\Delta\mu \pm \omega}{2kT} \right) \pm 1 \right] \langle I(\Delta\mu \pm \omega) \rangle$. The antisymmetric noise contribution is given by the term ± 1 in the brackets. It can be rewritten using the linear response ac conductance G_{ω} [63], $S(\omega) - S^{\text{sym}}(\omega) = \omega \text{Re} G_{\omega}(\Delta\mu)$, recovering a known result [64].

two thermal reservoirs. However, the quantum effects become more apparent when the high-frequency fluctuations between a discrete system and a reservoir are considered, e.g., a quantum dot is coupled to leads. We show in chapter 4 that these quantum fluctuations leads to striking non-Markovian effects in (unsymmetrized) noise.

1.6 Berry phase

Just short of two decades old, Berry's phase [78] is a remarkably recent finding in quantum mechanics, considering that it follows directly from the fundamental laws of quantum mechanics. Even though it has been observed in single-particle experiments, the manifestation of the Berry phase in condensed matter systems is still under investigation and there are even some recent reports that the Berry phase might have been observed in such systems [79, 80, 81].

Let us now look for the origin of the Berry phase and consider a quantum system which depends on some external parameter $\mathbf{R}(t)$, e.g., a magnetic field. We make the important assumption [78] that the state of the system evolves adiabatically, i.e., it always remains in the n th eigenstate $|n, \mathbf{R}(t)\rangle$ of the Hamiltonian H . This assumption is satisfied if H varies slowly on time scales of the inverse energy level spacing. Then, the state is $|\psi_n(t)\rangle = c_n(t)|n, \mathbf{R}(t)\rangle$ with a phase factor $c_n(t)$. We insert it into the Schrödinger equation and get $c_n(t)E_n(t) = i\hbar \dot{c}_n(t) + i\hbar c_n(t)\langle n, \mathbf{R}(t)|\partial_t|n, \mathbf{R}(t)\rangle$, which we integrate to obtain $c_n(t) = \exp\left\{(-i/\hbar)\int_0^t E_n(t') dt' + i\gamma_g\right\}$. Thus, the time evolution of the system contains the usual dynamical phase but also an additional phase,

$$\gamma_g = -\text{Im} \int_{\mathbf{R}(0)}^{\mathbf{R}(t)} \langle n, \mathbf{R} | \nabla_{\mathbf{R}} |n, \mathbf{R}\rangle d\mathbf{R}. \quad (1.6)$$

This phase was ignored for a long time, since it can be eliminated by a basis change. Namely, in the basis $|\tilde{n}, \mathbf{R}(t)\rangle = e^{i\phi(\mathbf{R})}|n, \mathbf{R}(t)\rangle$, the additional phase of $c_n(t)$ becomes $\tilde{\gamma}_g = \gamma_g - [\phi(\mathbf{R}(t)) - \phi(\mathbf{R}(0))]$ and vanishes for the proper choice of $\phi(\mathbf{R}(t))$. However, for a closed contour, $\mathbf{R}(0) = \mathbf{R}(T)$, this argument obviously breaks down! Now, the phase γ_g is independent of $\phi(\mathbf{R})$ and can no longer be eliminated. This observation has led Berry to the remarkable conclusion that the phase γ_g can be observed. Note that the

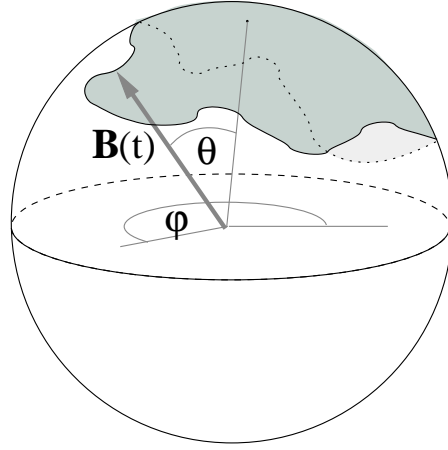


Figure 1.3: The Berry phase γ_g of a spin $\frac{1}{2}$ is half of the solid angle (gray) which is enclosed by the magnetic field \mathbf{B} ; the sign of γ_g is given by the parallel or antiparallel alignment of the spin.

phase only depends on the contour $\mathbf{R}(t)$ [cf. Eq. (1.6)] but does not depend how it is followed (adiabatically) in time.

To get a geometrical description of the Berry phase, we consider a spin $\frac{1}{2}$ in a time-dependent magnetic field $\mathbf{B}(t)$, which results, e.g., from an electron moving through an inhomogeneous magnetic field. The adiabatic assumption requires that the electron moves sufficiently slowly such that the spin of the electron retains its alignment (i.e., “up” or “down”) along the local field direction. This assumption is satisfied if the spin precesses many times around the local field. For a closed contour $\mathbf{B}(t)$, we can evaluate Eq. (1.6) using Stokes’ theorem and inserting the spin eigenstate of the local Zeeman field, Eq. (1.2), where the angles θ , φ are given by the direction of $\mathbf{B}(t)$. We find⁸ that the acquired Berry-Phase is half the solid angle spanned by $\mathbf{B}(t)$ [78], see Fig. 1.3, thus γ_g is indeed a geometrical object.

How can the Berry phase be observed experimentally? Even before Berry’s work, effects due to geometrical phases were known, see Ref. [82]. For mesoscopic systems, D. Loss, P.M. Goldbart and A.V. Balatsky have

⁸The line integral, $ds = \mathbf{e}_r dr + \mathbf{e}_\theta r d\theta + \mathbf{e}_\varphi r \sin \theta d\varphi$, becomes a surface integral over a part of the unit sphere, $d\mathbf{A}$, and we use $\text{curl } \mathbf{V} = \mathbf{e}_r \frac{1}{r \sin \theta} \left\{ \frac{\partial}{\partial \theta} (\sin \theta V_\varphi) - \frac{\partial V_\theta}{\partial \varphi} \right\} + \dots$ to find $\gamma_g = \int_0^t dt' \dot{\varphi} (\cos \theta - 1) = \frac{1}{2} \oint ds \cdot \frac{\cos \theta - 1}{r \sin \theta} \mathbf{e}_\varphi = -\frac{1}{2} \int \frac{d\mathbf{A} \cdot \mathbf{e}_r}{r^2} = -\frac{1}{2} \int d\Omega$.

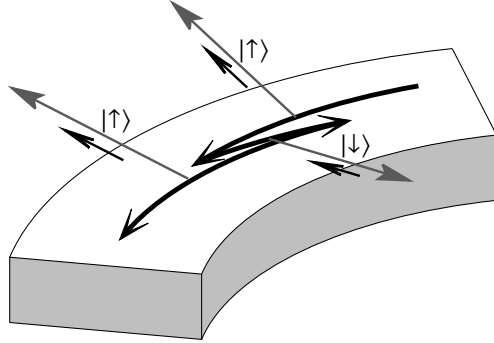


Figure 1.4: Electron in diffusive conductor with spin-orbit coupling. When the electron scatters while the motion is one dimensional and no external magnetic field is present, the spin remains aligned along the local effective field, parallel or antiparallel. If the external field is turned on, the effective field will change its direction abruptly at each scattering event and the picture of an electron moving adiabatically is no longer valid.

shown that the Berry phase can be observed [83]. They have proposed to consider the electrical current through a phase coherent ring (i.e., not larger than a few μm). The ring is placed in an inhomogeneous magnetic field, which changes direction but not magnitude, e.g., the field found above a bar magnet perpendicular to the ring plane. Each electron that enters from one side of the ring flows through both arms of the ring, analogous to the double slit experiment. During the passage through the inhomogeneous field, the electron spin acquires a Berry phase. This process is reminiscent of a charge moving through a vector potential and thereby collecting an Aharonov-Bohm phase. Finally, the contributions from both arms, which have acquired different phases, interfere at the other side of the ring, resulting in an increased or decreased current. This interference pattern in the current then contains effects of the Berry phase.

Besides having a spin following the direction of an inhomogeneous external field, there is another scenario which produces a Berry phase: spin-orbit coupling [84]. If an electron moves through an electric field perpendicular to the ring plane, an effective magnetic field, which is produced in the rest frame of the electron, couples to the electron spin. As this effective field is in the radial direction of the ring and perpendicular to the direction of motion, the field rotates while the electron moves around the ring and can

therefore produce a Berry phase. By additionally switching on an external (homogeneous) magnetic field, an arbitrary tilt angle of the total effective field can be realized and this Berry phase can be tuned. For ballistic motion, the Berry phase manifests itself in precisely the same way [84] as in the case with an inhomogeneous external magnetic field [83, 85, 86]. However, for diffusive motion the situation becomes more complicated, as the change of the direction of motion of the electron due to an elastic scattering event abruptly changes the effective field direction, see Fig. 1.4. Now the picture of a spin, moving adiabatically through a slowly varying field, is no longer valid and needs to be modified. This leads to a new physical situation which has to be considered separately from the situation with inhomogeneous fields.

Berry phase effects appear to their full extent only in the adiabatic limit described above. For semiconducting rings this assumption can be satisfied with experimentally achievable field strengths. However, in metals the Fermi velocity of electrons is much larger and a much larger field strength would be required. For diffusive rings (in the weak localization regime), this restriction can be overcome since the electrons remain much longer in an area with a given direction of the magnetic field [87]. The diffusive motion due to elastic scattering at an impurity potential does not destroy the phase coherence of the electrons and thus the interference effects are still present.

Chapter 2

Single Spin Dynamics and Decoherence in a Quantum Dot via Charge Transport

In this chapter, we investigate the spin dynamics of a quantum dot with a spin- $\frac{1}{2}$ ground state in the Coulomb blockade regime and in the presence of a magnetic rf field leading to electron spin resonance (ESR). We show that by coupling the dot to leads, spin properties on the dot can be accessed via the charge current in the stationary and nonstationary limits. We present a microscopic derivation of the current and the master equation of the dot using superoperators, including contributions to decoherence and energy shifts due to the tunnel coupling. We give a detailed analysis of sequential and cotunneling currents, for linearly and circularly oscillating ESR fields, applied in cw and pulsed modes. We show that the sequential tunneling current exhibits a spin satellite peak whose linewidth gives a lower bound on the decoherence time T_2 of the spin- $\frac{1}{2}$ state on the dot. Similarly, the spin decoherence can be accessed also in the cotunneling regime via ESR-induced spin flips. We show that the conductance ratio of the spin satellite peak and the conventional peak due to sequential tunneling saturates at the universal conductance ratio of 0.71 for strong ESR fields. We describe a double-dot setup which generates spin-dependent tunneling and acts as a current pump (at zero bias) and as a spin inverter which inverts the spin polarization of the current, even in a homogeneous magnetic field. We show that Rabi oscillations of the dot spin induce coherent oscillations in the time-dependent current. These oscillations are observable in the time-averaged current as function of ESR

pulse duration, and they allow the spin coherence to be accessed directly in the time domain. We analyze the measurement and read-out process of the dot spin via currents in spin-polarized leads and identify measurement time and efficiency by calculating the counting statistics, noise, and the Fano factor. We point out that single spin dynamics can also be accessed with STM techniques.

2.1 Introduction

The coherent control and manipulation of the electron spin has become the focus of an increasing number of experiments [4, 33, 89, 7, 5, 8, 34, 90]. From measurements it has become evident that the phase coherence of electron spins in semiconductors can be robust over unusually long times, exceeding hundreds of nanoseconds [4]. Thus, spins of electrons are suitable candidates for applications in the field of spintronics, in particular for quantum information processing [3, 30, 52, 44, 45, 91, 92, 93, 94, 95]. This has made it desirable to understand in more detail the coherent behavior of single electron spins which are confined to nanostructures such as quantum dots, molecules, or atoms, and to point to ways of how to access the coherence time T_2 (cf. Sec. 1.3) of a single spin experimentally. It is the goal of this chapter to address this issue and to propose and analyze transport scenarios involving a quantum dot attached to leads and with a spin-1/2 ground state.

In recent experiments, T_2^* was measured in bulk GaAs by using ultrafast time-resolved optical methods, yielding values for T_2^* exceeding 100 ns [4]. However, the measurement of the decoherence time T_2 for a single spin has—to our knowledge—not been reported yet. A first step into this direction are spin echo measurements on an ensemble of spins, where dephasing due to inhomogeneities of the magnetic field is eliminated. Indeed, such measurements being performed more than 30 years ago on P donors in Si, reported T_2 times up to $500\mu\text{s}$ [96]. However, it appears desirable to have a more direct method for single-spin measurements. To achieve this via direct coupling to the magnetic moment of the spin is rather challenging due to the extremely small magnetic moment, although it is believed to be within reach using cantilever techniques [97]. Here we concentrate on a further approach based on transport measurements. The key idea is to exploit the Pauli principle which connects spin and charge of the electron so intimately that all spin properties can be accessed via charge and charge currents, especially in the Coulomb

blockade regime [18] of a quantum dot attached to leads. Indeed, concrete scenarios based on such a spin-to-charge conversion have been proposed in the past [3, 25, 56, 52, 98], and it is our goal here to further elaborate on these concepts and to report on a variety of new results we have obtained.

There are two classes of spin decoherence contributions we have to distinguish in the following. First, rare tunneling events of electrons onto and off the dot change the spin state on the dot and in this way contribute to the decoherence of the dot spin. We account for this decoherence microscopically in terms of a tunneling Hamiltonian. Second, there are intrinsic decoherence contributions from processes which persist even if the dot is completely isolated from the leads. This decoherence is taken into account phenomenologically in the master equation developed in this thesis, with an intrinsic decoherence rate T_2^{-1} . The goal then is to show that this T_2 time can be extracted via current measurements, regardless of the microscopic processes leading to T_2 . Such a phenomenological approach to intrinsic decoherence makes the purpose of our considerations clearer and is applicable to different types of decoherence mechanisms, e.g., based on hyperfine and spin-orbit couplings. The microscopic study of such intrinsic decoherence, being an important subject in its own right, is not addressed in the present thesis.

The outline of this chapter is as follows. In Sec. 2.2, we define the system of interest, a quantum dot with spin-1/2 ground state in the Coulomb blockade regime tunnel coupled to leads and in the presence of an electron spin resonance (ESR) field. We derive the (generalized) master equation for the low-energy dot states in the sequential and cotunneling regime by evaluating the tunnel coupling to the leads microscopically in order to obtain tunneling rates, decoherence rates, and energy (Stark) shifts. For this we need to include diagonal and off-diagonal matrix elements of the reduced density operator. The stationary current through the dot and its dependence on the ESR field is discussed in Sec. 2.3. We find a spin satellite peak in the sequential tunneling current, whose linewidth as function of the ESR frequency gives a lower bound for the T_2 time. Thus, via the stationary current, the T_2 time can be measured in a regime that is experimentally accessible, as will be demonstrated by concrete numerical examples. We show that the ratio of this satellite peak and the main peak saturates at a universal conductance ratio for strong ESR fields. In Sec. 2.4, we extend our results to the even-to-odd transition, i.e., for the case where there is (on average) one electron less on the dot. In Sec. 2.5, we explain a mechanism for a spin-inverter device which inverts the spin polarization of the current passing through two

dots coupled in series in the presence of a homogeneous magnetic field. In Sec. 2.6, we discuss how spin-dependent tunneling can be used to pump a current through a system in the absence of a bias, where the ESR field provides the required energy. In Sec. 2.7, we consider rotating ESR fields which allows us to obtain the exact time evolution of the dot states and their decay rates. In Sec. 2.8, the cotunneling current through the quantum dot away from the sequential tunneling peak is discussed. We show that the T_2 time can also be accessed in this regime. Invoking spin-polarized leads, a read-out procedure for the dot spin is proposed and analyzed in Sec. 2.9, where counting statistics, noise, and the Fano factor are calculated, which allow us then to estimate the measurement time. In Sec. 2.10, we discuss coherent Rabi oscillations of the dot spin and their occurrence in the time-dependent current. In Sec. 2.11, we show that Rabi oscillations can also be observed in the time-averaged current if pulsed ESR fields are applied. In Sec. 2.12, we point out that our results also apply to scanning tunneling microscopy (STM) devices, and we finally conclude in Sec. 2.13.

2.2 Quantum dot in ESR Field

2.2.1 Model Hamiltonian

We consider a quantum dot in the Coulomb blockade regime [18], which has a spin- $\frac{1}{2}$ ground state. The dot is assumed to be tunnel coupled to two Fermi-liquid leads $l = 1, 2$, at chemical potentials μ_l . We start from the full Hamiltonian

$$H = H_{\text{lead}} + H_{\text{dot}} + H_{\text{ESR}}(t) + H_T, \quad (2.1)$$

which describes leads, dot, ESR field, and the tunnel coupling between leads and dot, respectively. For the leads we take $H_{\text{lead}} = \sum_{lk\sigma} \epsilon_{lk} c_{lk\sigma}^\dagger c_{lk\sigma}$, where $c_{lk\sigma}^\dagger$ creates an electron in lead l with orbital state k , spin σ , and energy ϵ_{lk} . We describe the coupling with the standard tunnel Hamiltonian

$$H_T = \sum_{lpk\sigma} t_{lp}^\sigma c_{lk\sigma}^\dagger d_{p\sigma} + \text{h.c.}, \quad (2.2)$$

with tunneling amplitude t_{lp}^σ and where $d_{p\sigma}^\dagger$ creates an electron on the dot in orbital state p . In Eq. (2.1), H_{dot} is time independent and includes charging and interaction energies of the electrons on the dot and coupling to a static

magnetic field B_z in z direction. The dot spin is coupled to a magnetic ESR field, $B_x(t) = B_x^0 \cos(\omega t)$, linearly oscillating in the x direction with frequency ω , thus $H_{\text{ESR}} = -\frac{1}{2}g\mu_B B_x(t) \sigma_x$. Such an oscillating field produces Rabi spin flips when its frequency is tuned to resonance, $\omega = \Delta_z$, as shown below. Then, the total Zeeman coupling of the dot spin is

$$-\frac{1}{2}g\mu_B \mathbf{B}(t) \cdot \boldsymbol{\sigma} = -\frac{1}{2}\Delta_z \sigma_z - \frac{1}{2}\Delta_x \cos(\omega t) \sigma_x, \quad (2.3)$$

with electron g factor g , Bohr magneton μ_B , and Pauli matrices σ_i . We have defined $\Delta_x = g\mu_B B_x^0$ and the Zeeman splitting $\Delta_z = g\mu_B B_z$. Ideally, we assume that the Zeeman splitting of the leads Δ_z^{leads} is different from Δ_z , and $\Delta_z^{\text{leads}} \ll \varepsilon_F$, where ε_F is the Fermi energy, such that the effects of the fields B_z and $B_x(t)$ on the leads are negligible (see below). Such a situation can be achieved by using materials of different g factors [5] and/or with local magnetic fields (B_x or B_z).

We are neglecting photon-assisted tunneling (PAT) processes [18, 99], in which oscillating electric potentials of the leads provide additional energy to electrons tunneling onto the dot. We note that PAT contributions to the current can be distinguished from ESR effects since the former contributions do not show resonant behavior as a function of B_z and/or ω , and they lead to several satellite peaks instead of one as for ESR effects (see below). Further, if one avoids electrical rf components parallel to the current, i.e., along the axis lead-dot-lead, no potential oscillations are produced, and thus PAT effects are excluded. Finally, electric rf fields can be avoided altogether, using a setup as in Ref. [49]. There, the oscillating current induced in a superconducting wire (via an rf source) generates only a magnetic rf component in the near-field region [100], with an the electric component that is negligibly small for $\omega \ll \omega_p$, where ω_p is the plasma frequency. Finally, for transport and ESR experiments in quantum Hall samples with and without quantum dots we refer to Refs. [101] and [102].

2.2.2 Dot spectrum and energetics

The electronic states of the quantum dot can be assumed as follows. For an odd number N of electrons on a dot with antiferromagnetic filling, the dot has a spin- $\frac{1}{2}$ ground state. The topmost (excess) electron can be either in the spin ground state $|\uparrow\rangle$ (σ_z eigenstate) or in the excited state $|\downarrow\rangle$ (see Fig. 2.1). This assumption is automatically satisfied if $N = 1$. Otherwise,

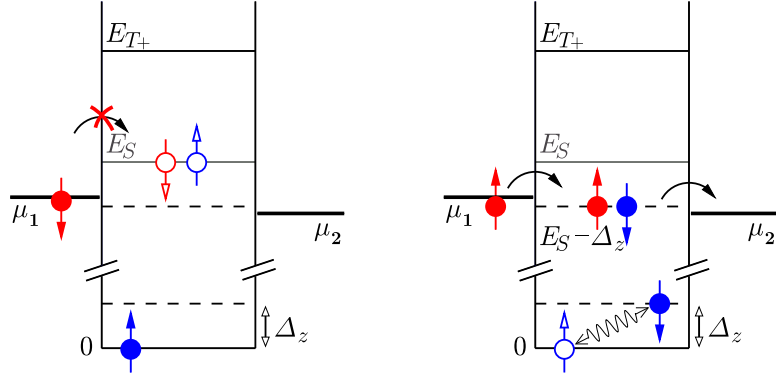


Figure 2.1: Quantum dot coupled to (unpolarized) leads $l = 1, 2$ with chemical potentials μ_l . The sequential tunneling regime $E_S > \mu_1 > E_S - \Delta_z > \mu_2$ (for $E_\uparrow = 0$) shown here corresponds to the satellite peak in the sequential tunneling current; cf. Sec. 2.3.1 and 2.3.2 and Figs. 2.2 and 2.3. Here, E_S (E_{T_+}) are the singlet (triplet) levels and the Zeeman splitting is $\Delta_z = g\mu_B B_z > kT$. (a) If the dot is initially in the spin ground state $|\uparrow\rangle$, sequential tunneling is blocked by energy conservation. (b) If the dot spin is excited by an ESR field (Rabi flip), spin up electrons can tunnel from lead 1 onto the dot, forming a singlet. Then, spin-up or -down electrons can tunnel into lead 2.

to obtain antiferromagnetic filling, Hund's rule must not apply. This can be achieved by breaking the orbital degeneracy on the dot, e.g., by using asymmetrically shaped dots or an appropriate magnetic field B_z [103]. For an additional electron on the dot, we assume for $N + 1$ the ground state to be the singlet $|S\rangle = (|\uparrow\downarrow\rangle - |\downarrow\uparrow\rangle)/\sqrt{2}$; i.e., the triplet state $|T_+\rangle = |\uparrow\uparrow\rangle$ has higher energy, which again can be achieved by tuning B_z [103]. The energy E_m of the dot, including charging energy, is defined by $H_{\text{dot}}|m\rangle = E_m|m\rangle$.

We shall give a brief overview of the energetics involved in tunneling through quantum dots in the Coulomb blockade regime [18] and in the presence of the Zeeman splitting and an ESR field. For simplicity, we assume that there is no electron-electron interaction on the dot apart from the classical charging effect. (Our work is not restricted to such an assumption, since we only require a spin- $\frac{1}{2}$ ground state and a large enough singlet-triplet spacing on the dot.) The total ground-state energy of a dot with antiferromagnetic

filling is

$$U(N) = \sum_{k=1}^N \varepsilon_k^\sigma + E_C^N, \quad (2.4)$$

for N electrons on the dot. Here, the single-particle energy of the k th electron, $\varepsilon_k^\sigma = \varepsilon_k + (-1)^k \Delta_z/2$, contains orbital and Zeeman energy contributions. The charging energy is $E_C^N = (Ne - Q_G)^2/2C$, with gate charge Q_G , and dot capacitance C . It is convenient to define the chemical potential of the dot, $\mu_{\text{dot}}(N+1) = U(N+1) - U(N)$, which is the energy required for an electron of lead l to tunnel onto the dot, which contains N electrons initially, i.e., tunneling onto the dot occurs for $\mu_l > \mu_{\text{dot}}$ [104]. In the Coulomb blockade regime, $kT \ll e^2/C$ (k : Boltzmann constant), no sequential tunneling current flows through the dot if the chemical potentials of dot and leads are such that $\mu_{\text{dot}}(N) < \mu_1, \mu_2 < \mu_{\text{dot}}(N+1)$. However, in the sequential tunneling regime $\mu_1 > \mu_{\text{dot}}(N+1) > \mu_2$, single electrons tunnel from lead 1 onto the dot and then on into lead 2, producing a sequential tunneling current.

In the presence of an ESR field, these concepts must be extended. Excitations of the dot states must be taken into account, since now the energy of the dot changes in time due to $B_x(t)$. A full analytical description of the current flow is derived in the following sections based on a time-dependent master equation. Here, we just intend to give a qualitative picture to provide some intuition for the underlying physical mechanism (it will not be needed later on). We define a time-dependent chemical potential of the dot, given as the energy required to add an electron at time t . We consider the two chemical potentials μ_{dot}^σ for initial spin- $\frac{1}{2}$ dot state $|\sigma\rangle$, i.e., $\Delta_{S\uparrow} = \mu_{\text{dot}}^\uparrow(N+1) = E_S - E_\uparrow$ and $\Delta_{S\downarrow} = \mu_{\text{dot}}^\downarrow(N+1) = E_S - E_\downarrow$, which simplify to $\Delta_{S\uparrow} = E_S$, and $\Delta_{S\downarrow} = E_S - \Delta_z$, respectively, for $E_\uparrow = 0$. Note that the μ_{dot}^σ is *lowered* if the dot is excited into state $|\downarrow\rangle$, since the Zeeman energy Δ_z has already been provided by a Rabi spin flip due to the ESR field. Therefore, we can identify the regime $\Delta_{S\uparrow} > \mu_1 > \Delta_{S\downarrow} > \mu_2$, where a sequential tunneling current will flow through the dot only after exciting the dot spin by a spin flip (see Fig. 2.1). In other words, the dot can be opened and closed via the ESR field, which thus allows one to modulate the current. This (dynamical) dependence of the current on the dot spin can be exploited to measure the T_2 time and the Rabi oscillations of the dot spin [56], as we will explain in detail in the following.

2.2.3 Systematic treatment of sequential tunneling

The electronic states on a quantum dot interact with their environment (heat bath), in particular with the Fermi leads, which provide and take up electrons. The state of the combined system, dot and environment, is given by the full density matrix $\rho(t)$. The states of interest are the electronic states on the dot, described by the reduced density matrix of the dot, $\rho_D = \text{Tr}_B \rho$. Here, Tr_B is the trace taken over the leads (environment), averaging over the (unobserved) degrees of freedom of the environment. The diagonal elements $\rho_n = \langle n | \rho_D | n \rangle$ of the density matrix of the dot describe the occupation probabilities of the dot levels, with $H_{\text{dot}} |n\rangle = E_n |n\rangle$. The off-diagonal elements $\rho_{nm} = \langle n | \rho_D | m \rangle = \rho_{mn}^*$ describe the coherence and the phase of superpositions of dot states.

The tunnel coupling H_T between leads and dot is switched on at $t = 0$. Prior to this, the dot and leads are assumed to be uncorrelated such that the full initial density matrix factorizes as $\rho(0) = \rho_D^0 \rho_B^0$, where ρ_B^0 is the density matrix of the leads in thermal equilibrium at $\mu_{1,2}$, and at temperature T . Next we derive the master equation for the reduced density matrix ρ_D by making use of the superoperator formalism [105]. In the following, we set $\hbar = 1$. Starting from the von Neumann equation $\dot{\rho} = -i[H, \rho]$ for the full density matrix and using standard manipulations [105], one finds the time evolution of the reduced density matrix

$$\dot{\rho}_D(t) = -i[H_{\text{dot}} + H_{\text{ESR}}(t), \rho_D(t)] - \int_0^t dt' M(t, t') \rho_D(t'), \quad (2.5)$$

$$M(t, t') = \text{Tr}_B L_V \left(\mathcal{T} e^{-i \int_{t'}^t dt'' Q L(t'')} \right) L_V \rho_B^0, \quad (2.6)$$

with time ordering \mathcal{T} and the Liouville operators (superoperators) defined by $L(t)X = [H(t), X]$, $L_V X = [H_T, X]$, and equivalently for L_{dot} , L_{lead} , and $L_{\text{ESR}}(t)$. The projectors are defined as $Q = 1 - P$ and $PX = \rho_B^0 \text{Tr}_B X$. The kernel M [Eq. (2.6)] is a superoperator describing processes involving tunneling of electrons to and from the leads. We consider here only sequential tunneling processes and refer for a discussion of cotunneling contributions to Secs. 2.2.6 and 2.8. Thus, we work in Born approximation by retaining only the terms in lowest order of L_V ; i.e., we replace L by $L_0 = L - L_V$ in Eq. (2.6). For further evaluation of M , it is self-consistent (see below) to neglect the effect of the ESR field, $L_{\text{ESR}}(t)$; i.e., we replace L_0 by $L_{\text{dot}} + L_{\text{lead}}$ in M . This removes explicitly the time dependence of M , making it time translation

invariant, $M(t, t') = M(t - t')$. We find that $M(\tau)$ decays on a time scale $\tau_c \sim 1/kT$; i.e., the correlations induced in the leads by H_T decay rapidly. Since this decay is typically much faster than the Rabi flips produced by the ESR field, $\tau_c \ll 1/\Delta_x$, we may indeed neglect the contribution of $L_{\text{ESR}}(t)$ to M . With these approximations, Eq. (2.5) becomes in the interaction picture

$$\dot{\rho}_{\text{D}}^{\text{I}}(t) = -iL_{\text{ESR}}^{\text{I}}(t)\rho_{\text{D}}^{\text{I}}(t) - \int_0^t d\tau M^{\text{I}}(\tau)\rho_{\text{D}}^{\text{I}}(t - \tau). \quad (2.7)$$

The rapid decay of $M(\tau)$ also justifies the Markovian assumption that the system has no memory about its past, i.e., that $\dot{\rho}_{\text{D}}(t)$ depends only on $\rho_{\text{D}}(t)$ and not on $\rho_{\text{D}}(t - \tau)$. This approximation is performed in the interaction picture, to keep track of the dynamical phase of the off-diagonal elements of ρ_{D} . Systematically we proceed as follows. Since the integrand in Eq. (2.7) only contributes for small τ , we may expand the integrand in τ , $M(\tau)\rho_{\text{D}}^{\text{I}}(t - \tau) = M(\tau)[\rho_{\text{D}}^{\text{I}}(t) - \tau\dot{\rho}_{\text{D}}^{\text{I}}(t) + O(\tau^2)]$. We then replace $\dot{\rho}_{\text{D}}^{\text{I}}(t)$ in the integrand by using Eq. (2.7) iteratively. However, since $M(\tau) \sim O(L_V^2)$, we can neglect the part of $\dot{\rho}_{\text{D}}^{\text{I}}(t)$ which is $O(L_V^2)$, since it corresponds to a higher-order term in our Born approximation. The remaining part of $\dot{\rho}_{\text{D}}^{\text{I}}(t)$ results from L_{ESR} , which can also be disregarded since, in the integrand, the ESR field only acts on the time scale $\tau_c \ll 1/\Delta_x$. We then extend the upper integration limit in Eq. (2.7) to ∞ , with negligible contributions due to the decay of $M(\tau)$. Therefore, the second term in Eq. (2.7) becomes $-\left\{\int_0^\infty d\tau M^{\text{I}}(\tau)\right\}\rho_{\text{D}}^{\text{I}}(t)$. Next, we evaluate the matrix elements $M_{bc|nm} = \langle b|(M|n\rangle\langle m|)|c\rangle$ explicitly in the interaction picture, which yields [106]

$$\begin{aligned} -\int_0^\infty d\tau M_{bc|nm}^{\text{I}}(\tau) &= \delta_{bc}\delta_{nm}\left(W_{cn} - \delta_{bn}\sum_k W_{kn}\right) \\ &\quad - (1 - \delta_{nm})\delta_{bn}\delta_{mc}\left[i\delta\epsilon_{nm} + \frac{1}{2}\sum_k (W_{kn} + W_{km})\right], \end{aligned} \quad (2.8)$$

with the rates W (see below) and energy shifts $\delta\epsilon_{nm}$ (Stark shifts). These shifts are small; e.g., the one between $|\downarrow\rangle$ and $|\uparrow\rangle$ is given by

$$\delta\epsilon_{\downarrow\uparrow} = \frac{1}{2\pi}\sum_l \mathcal{P}\int_0^\infty d\epsilon f_l(\epsilon)\left(\frac{\gamma_l^\uparrow}{\epsilon - \Delta_{S\downarrow}} - \frac{\gamma_l^\downarrow}{\epsilon - \Delta_{S\uparrow}}\right), \quad (2.9)$$

and similarly for $\delta\epsilon_{S\downarrow}$ and $\delta\epsilon_{S\uparrow}$. For $|\mu_l - \Delta_{S\sigma}| > kT$, the energy shift becomes

$$\delta\epsilon_{\downarrow\uparrow} = \sum_l \left(\frac{\gamma_l^\downarrow}{2\pi} \ln \left| \frac{\Delta_{S\uparrow}}{\mu_l - \Delta_{S\uparrow}} \right| - \frac{\gamma_l^\uparrow}{2\pi} \ln \left| \frac{\Delta_{S\downarrow}}{\mu_l - \Delta_{S\downarrow}} \right| \right), \quad (2.10)$$

which, for $\gamma_l^\uparrow = \gamma_l^\downarrow$, reduces to $\delta\epsilon_{\downarrow\uparrow} \approx \sum_l (\gamma_l/2\pi) \ln [|\mu_l - \Delta_{S\downarrow}|/|\mu_l - \Delta_{S\uparrow}|]$ and, thus, to a small correction $|\delta\epsilon_{\downarrow\uparrow}| \lesssim \gamma \ln(\Delta_z/kT)$, for $\Delta\mu < \Delta_z$.

The sequential tunneling rates in Eq. (2.8) are

$$W_{S\downarrow} = \sum_l W_{S\downarrow}^l, \quad W_{S\downarrow}^l = \gamma_l^\uparrow f_l(\Delta_{S\downarrow}), \quad (2.11)$$

$$W_{\downarrow S} = \sum_l W_{\downarrow S}^l, \quad W_{\downarrow S}^l = \gamma_l^\uparrow [1 - f_l(\Delta_{S\downarrow})], \quad (2.12)$$

with the Fermi function $f_l(\Delta_{S\downarrow}) = [1 + e^{(\Delta_{S\downarrow} - \mu_l)/kT}]^{-1}$ of lead l . The rates $W_{S\uparrow}$, $W_{\uparrow S}$, $W_{S\uparrow}^l$, and $W_{\uparrow S}^l$ are defined analogously as functions of γ_l^\downarrow and $f_l(\Delta_{S\uparrow})$, and $W_{mn} = 0$. The transition rates

$$\gamma_l^\uparrow = 2\pi\nu_\uparrow |t_l^\uparrow|^2, \quad \gamma_l^\downarrow = 2\pi\nu_\downarrow |t_l^\downarrow|^2 \quad (2.13)$$

consist of (possibly) spin-dependent densities of states $\nu_{\uparrow,\downarrow}$ at the Fermi energy and tunneling amplitude $t_l^{\uparrow,\downarrow}$. (Spin-dependent densities of states are considered in Sec. 2.9 for spin read out.) For later convenience, we define for $\sigma = \uparrow, \downarrow$

$$\gamma^\sigma = (\gamma_1^\sigma + \gamma_2^\sigma)/2, \quad \gamma = (\gamma^\uparrow + \gamma^\downarrow)/2. \quad (2.14)$$

2.2.4 Master equation

So far we have considered only coupling to an environment consisting of Fermi leads. However, the electronic dot states are affected also by intrinsic degrees of freedom such as hyperfine coupling, spin-orbit interaction, or spin-phonon coupling, which lead to intrinsic spin relaxation and decoherence. Treating such couplings microscopically is beyond the present scope (see, e.g., Ref. [26]). Thus, we treat these couplings phenomenologically by introducing corresponding rates in the master equation. First, the spin *relaxation* rates $W_{\uparrow\downarrow}$ and $W_{\downarrow\uparrow}$ describe processes in which the dot spin is

flipped. We can assume $W_{\uparrow\downarrow} \gg W_{\downarrow\uparrow}$, for $\Delta_z > kT$ (consistent with detailed balance, $W_{\uparrow\downarrow}/W_{\downarrow\uparrow} = e^{\Delta_z/kT}$). These relaxation processes correspond to the phenomenological rate $1/T_1 = W_{\uparrow\downarrow} + W_{\downarrow\uparrow}$; see also Sec. 2.2.5. Second, the rate $1/T_2$ describes the intrinsic *decoherence* of the spin on the dot, which is present even in the absence of coupling to the leads. This type of decoherence destroys the information about the relative phase in a superposition of $|\uparrow\rangle$ and $|\downarrow\rangle$, without changing the populations of the opposite spin states. Formally, this leads to a decay of the off-diagonal matrix element $\rho_{\downarrow\uparrow}$. Including the decoherence contribution of H_T [Eqs. (2.8) and (2.11)], the total spin decoherence rate is

$$V_{\downarrow\uparrow} = \frac{W_{S\uparrow} + W_{S\downarrow}}{2} + \frac{1}{T_2}; \quad (2.15)$$

i.e., electrons tunneling onto the dot further destroy spin coherence on the dot (see Sec. 2.2.5 for an interpretation).

With the above results, we obtain from Eq. (2.5) the master equation of the dot,

$$\dot{\rho}_{\uparrow} = -(W_{\downarrow\uparrow} + W_{S\uparrow})\rho_{\uparrow} + W_{\uparrow\downarrow}\rho_{\downarrow} + W_{\uparrow S}\rho_S - \Delta_x \cos(\omega t) \text{Im}[\rho_{\downarrow\uparrow}], \quad (2.16)$$

$$\dot{\rho}_{\downarrow} = W_{\downarrow\uparrow}\rho_{\uparrow} - (W_{\uparrow\downarrow} + W_{S\downarrow})\rho_{\downarrow} + W_{\downarrow S}\rho_S + \Delta_x \cos(\omega t) \text{Im}[\rho_{\downarrow\uparrow}], \quad (2.17)$$

$$\dot{\rho}_S = W_{S\uparrow}\rho_{\uparrow} + W_{S\downarrow}\rho_{\downarrow} - (W_{\uparrow S} + W_{\downarrow S})\rho_S, \quad (2.18)$$

$$\dot{\rho}_{\downarrow\uparrow} = -i\Delta_z\rho_{\downarrow\uparrow} + i\frac{\Delta_x}{2}\cos(\omega t)(\rho_{\uparrow} - \rho_{\downarrow}) - V_{\downarrow\uparrow}\rho_{\downarrow\uparrow}, \quad (2.19)$$

$$\dot{\rho}_{S\uparrow} = -i\Delta_{S\uparrow}\rho_{S\uparrow} - V_{S\uparrow}\rho_{S\uparrow}, \quad (2.20)$$

$$\dot{\rho}_{S\downarrow} = -i\Delta_{S\downarrow}\rho_{S\downarrow} - V_{S\downarrow}\rho_{S\downarrow}. \quad (2.21)$$

Here, the time evolution of the matrix elements $\rho_{nm} = \langle n|\rho_D|m\rangle$ of the density matrix of the dot is described for the states $|n\rangle = |\uparrow\rangle, |\downarrow\rangle, |S\rangle$; e.g., for the diagonal element we write $\rho_{\uparrow} = \langle\uparrow|\rho_D|\uparrow\rangle$, for the off-diagonal element, $\rho_{S\uparrow} = \langle S|\rho_D|\uparrow\rangle$, etc. The rate W_{mn} describes transitions from state $|n\rangle$ to $|m\rangle$. Equations (2.16)–(2.18) are rate equations with gain and loss terms, up to the contributions from the ESR field. Then, the population of, say, state $|\uparrow\rangle$ is changed by $d\rho_{\uparrow}$ after time dt by the following contributions [Eq. (2.16)]. The population ρ_{\uparrow} is increased when the dot is previously in state $|S\rangle$ (with probability ρ_S), and a spin \downarrow electron tunnels out of the dot with probability

$W_{\uparrow S} dt$. However, the population ρ_{\uparrow} is decreased when the system was already in state $|\uparrow\rangle$, and a spin \downarrow electron tunnels onto the dot with probability $W_{S\uparrow} dt$. The spin-flip rates $W_{\uparrow\downarrow}$ and $W_{\downarrow\uparrow}$ enter Eq. (2.16) analogously. In the absence of an ESR field, the off-diagonal elements [Eqs. (2.19)–(2.21)] of the density matrix decouple from the diagonal ones and decay with the decoherence rates $V_{nm} = V_{mn}$.

In the presence of an ESR field, the diagonal [Eqs. (2.16) and (2.17)] and the off-diagonal [Eq. (2.19)] matrix elements become coupled by the term proportional to Δ_x . This coupling of populations (ρ_{\uparrow} and ρ_{\downarrow}) and coherence ($\rho_{\uparrow\downarrow}$) shows the coherent nature of Rabi spin flips and makes it apparent that we are studying a resonant process, which requires that we take H_{ESR} fully into account.

The current $I_2 = e\langle dq/dt \rangle$ from the dot into lead 2 is defined by the number of charges dq that accumulate in lead 2 after time dt . With probability ρ_S , the dot is in state $|S\rangle$ and a charge e will tunnel into lead 2 with probability $(W_{\uparrow S}^2 + W_{\downarrow S}^2) dt$. However, if the dot is in state $|\uparrow\rangle$ or $|\downarrow\rangle$, a charge may tunnel from lead 2 onto the dot, reducing the number of charges in lead 2. Thus, in total we obtain for the current in lead 2

$$I_2 = e(W_{\uparrow S}^2 + W_{\downarrow S}^2)\rho_S - eW_{S\uparrow}^2\rho_{\uparrow} - eW_{S\downarrow}^2\rho_{\downarrow}. \quad (2.22)$$

The current in lead 1, I_1 , is obtained analogously and is given by Eq. (2.22) after changing sign and replacing the index 2 by 1. We show in Sec. 2.3 that $I_1 = I_2$ in the stationary limit, due to charge conservation.

Finally we note that Eqs. (2.20) and (2.21), which describe a superposition of an odd and an even number of electrons on the dot, decouple from Eqs. (2.16)–(2.19) and are thus not of relevance for our considerations. Further, since the coupling to the leads is switched on only at $t = 0$, initially the number of particles on the dot is well defined. Therefore $\rho_{S\uparrow}$ and $\rho_{S\downarrow}$ vanish at $t = 0$ and at all later times, as seen from Eqs. (2.20) and (2.21). In particular, no superposition of a state with an even and a state with an odd number of electrons on the dot is produced by the coupling to the leads, since this would require a coherent superposition of corresponding states in the leads; however, for times larger than τ_c (which is typically the case), we can safely neglect any coherence in the Fermi-liquid leads.

2.2.5 Decoherence and measurement process

We elucidate the connection between spin decoherence and measurement, first in the absence of leads and ESR field. We consider a coherent superposition $\alpha|\uparrow\rangle + \beta|\downarrow\rangle$ as the initial state of the dot. This pure state corresponds to the reduced density matrix $\rho_\uparrow(0) = |\alpha|^2$, $\rho_\downarrow(0) = |\beta|^2$, and $\rho_{\uparrow\downarrow}(0) = \alpha^*\beta$, and the master equation contains only the rates $W_{\uparrow\downarrow}$, $W_{\downarrow\uparrow}$, and $V_{\uparrow\downarrow} = 1/T_2$. The off-diagonal terms $\rho_{\uparrow\downarrow} = \rho_{\uparrow\downarrow}^*$, decay with the decoherence time T_2 , $\rho_{\uparrow\downarrow}(t) = e^{-t/T_2 - it\Delta_z} \rho_{\uparrow\downarrow}(0)$, while the diagonal terms (occupation probabilities) decay with the spin relaxation time $T_1 = (W_{\uparrow\downarrow} + W_{\downarrow\uparrow})^{-1}$ and $\rho_\downarrow(t) = \rho_\downarrow^{\text{eq}} + e^{-t/T_1} [\rho_\downarrow(0) - \rho_\downarrow^{\text{eq}}]$ toward their stationary value $\rho_\downarrow^{\text{eq}} = W_{\uparrow\downarrow}/(W_{\uparrow\downarrow} + W_{\downarrow\uparrow})$ and $\rho_\uparrow = 1 - \rho_\downarrow$. In total, for $T_2 < T_1$, we can picture the decay of ρ_D as

$$\begin{pmatrix} |\alpha|^2 & \alpha\beta^* \\ \alpha^*\beta & |\beta|^2 \end{pmatrix} \xrightarrow{T_2} \begin{pmatrix} |\alpha|^2 & 0 \\ 0 & |\beta|^2 \end{pmatrix} \xrightarrow{T_1} \begin{pmatrix} \rho_\uparrow^{\text{eq}} & 0 \\ 0 & \rho_\downarrow^{\text{eq}} \end{pmatrix}; \quad (2.23)$$

i.e., the off-diagonal terms vanish first on the time scale T_2 , and then the diagonal ones equilibrate on the time scale T_1 .

As shown in Sec. 2.2.3, when electrons tunnel onto the dot, the decoherence rate $V_{\uparrow\downarrow}$ [Eq. (2.15)] and thus the decay of the off-diagonal elements are increased further. We note now the formal equivalence to the quantum measurement process (in the σ_z basis), where the dot spin is projected onto $|\uparrow\rangle$ or $|\downarrow\rangle$, and thus the off-diagonal matrix elements vanish. This projection can be understood as a decoherence process. Conversely, we can consider the decoherence due to tunneling as a measurement performed by the tunneling electrons. We note that this process is a *weak* measurement in the following sense. The electrons in the leads attempt to tunnel on the dot, but only with small probability $\propto W_{S\sigma}$ are these attempts successful. Thus, the current I , which carries away the information of the dot state to the observer, is formed by these successful electrons, while the unsuccessful electrons are not detected. Another way to say this is that a given electron from the lead has only a small probability $\propto W_{S\sigma}$ to “measure” (i.e., decohere) the dot state.

2.2.6 Cotunneling contribution to the sequential tunneling regime

We work in the sequential tunneling regime, defined by $\mu_1 > \Delta_{S\downarrow} > \mu_2$. One can see that higher-order—cotunneling—contributions can be neglected

[18, 25] for $\gamma_l < \Delta_z$, kT , and $\Delta\mu < \Delta_z$, the regime of interest here. Most importantly, the cotunneling contributions to $V_{\downarrow\uparrow}$ are of the order γ_l^2/Δ_z (see Sec. 2.8); i.e., they are suppressed compared to the sequential tunneling contributions by a factor of γ_l/Δ_z ($\approx 5 \times 10^{-5}$ for the parameters of Fig. 2.3). Formally, the cotunneling contributions to the master equation can be absorbed into T_1 and T_2 . For a discussion of cotunneling currents away from the sequential tunneling resonance see Sec. 2.8.

2.3 Stationary current

We now consider the stationary current I in the presence of a continuous-wave (cw) ESR field. Therefore we calculate the stationary solution $\rho(t \rightarrow \infty)$ of the master equation [Eqs. (2.16)–(2.21)]. We will apply the rotating-wave approximation (RWA)[107], where only the leading frequency contributions of H_{ESR} are retained. Higher-order contributions would include the simultaneous absorption of two photons and the emission of another photon. In lowest order, only single photons can be absorbed or emitted, producing a spin flip on the dot. To perform this approximation, we write $\Delta_x \cos(\omega t) = \frac{1}{2}\Delta_x (e^{i\omega t} + e^{-i\omega t})$; i.e., we decompose the linearly oscillating magnetic field into a superposition of a clockwise and an anticlockwise rotating field. Integrating Eqs. (2.16), (2.17), and (2.19), one finds that for $\omega \approx \Delta_z$, the anticlockwise rotating field leads to rapidly oscillating terms in the integrands, which nearly average to zero. Therefore, we retain only the clockwise rotating field, which is given by the term proportional to $e^{i\omega t}$ (see also Sec. 2.7). Note that since only one field component contributes, the field amplitude is halved. This leads to the period T_Ω of one Rabi oscillation,

$$T_\Omega = \frac{4\pi}{\Delta_x}. \quad (2.24)$$

The RWA is valid for $\Delta_x, V_{\downarrow\uparrow}, |\Delta_z - \omega| \ll \omega$ (see, e.g., Ref. [108]) and is well justified for the parameters considered here. In the stationary case and using the RWA, the dependence of ρ_\uparrow and ρ_\downarrow [Eqs. (2.16) and (2.17)] on $\rho_{\downarrow\uparrow}$ is eliminated, leading to the effective spin-flip rate

$$W_\omega = \frac{\Delta_x^2}{8} \frac{V_{\downarrow\uparrow}}{(\omega - \Delta_z)^2 + V_{\downarrow\uparrow}^2}, \quad (2.25)$$

which is a Lorentzian as a function of ω with maximum $W_\omega^{\text{max}} = \Delta_x^2/8V_{\downarrow\uparrow}$ at resonance $\omega = \Delta_z$.

Now it is straightforward to find the stationary solution of the effective rate equations for ρ_\uparrow , ρ_\downarrow and ρ_S ,

$$\rho_\uparrow = \eta [W_{\uparrow S}W_{S\downarrow} + (W_{\uparrow\downarrow} + W_\omega)(W_{\uparrow S} + W_{\downarrow S})], \quad (2.26)$$

$$\rho_\downarrow = \eta [W_{\downarrow S}W_{S\uparrow} + (W_{\downarrow\uparrow} + W_\omega)(W_{\uparrow S} + W_{\downarrow S})], \quad (2.27)$$

$$\rho_S = \eta [W_{S\uparrow}W_{S\downarrow} + W_{S\uparrow}(W_{\uparrow\downarrow} + W_\omega) + W_{S\downarrow}(W_{\downarrow\uparrow} + W_\omega)], \quad (2.28)$$

where the normalization factor η is such that $\sum_n \rho_n = 1$. We see from Eqs. (2.26)–(2.28) that the effective spin-flip rates are $W_{\uparrow\downarrow} + W_\omega$ and $W_{\downarrow\uparrow} + W_\omega$; i.e., the ESR field flips up and down spin with equal rate W_ω .

We can now calculate the spin- \uparrow polarized current in lead 2, $I_2^\uparrow = e W_{\downarrow S}^2 \rho_S - e W_{S\downarrow}^2 \rho_\downarrow$ [cf. Eq. (2.22)]. The result is displayed in Eq. (B.1) in the Appendix. The spin- \downarrow polarized current I_2^\downarrow is obtained from Eq. (B.1) by interchanging \uparrow with \downarrow in the numerator (the denominator remains unaffected by such an interchange). The currents in lead 1, $I_1^{\uparrow,\downarrow}$, are obtained from the formulas for $I_2^{\uparrow,\downarrow}$ by changing sign and interchanging indices 1 with 2. Note that generally $I_1^\uparrow \neq I_2^\uparrow$, since the ESR field generates spin flips on the dot, and thus the spin on the dot is not a conserved quantity. However, the stationary charge current $I_l = \sum_\sigma I_l^\sigma$ is the same in both leads, $I = I_1 = I_2$, due to charge conservation.

2.3.1 Spin satellite peak

In this subsection we discuss the stationary current I through the dot, in particular, its behavior as function of $\mu = (\mu_1 + \mu_2)/2$ or, equivalently, as a function of the gate voltage V_g . We will see that an additional sequential tunneling peak (satellite peak) will appear due to the ESR field. Before explicit evaluation of the current, we briefly describe this situation in qualitative terms. We assume a large Zeeman splitting $\Delta_z > \Delta\mu$, kT , with applied bias $\Delta\mu = \mu_1 - \mu_2 > 0$. If the potentials are such that $\mu_1 > \Delta_{S\uparrow} > \mu_2$ —i.e., the chemical potential of the dot (relative to the ground state $|\uparrow\rangle$) is between the chemical potentials of the leads—the state of the dot changes between $|\uparrow\rangle$ and $|S\rangle$ due to sequential tunneling events, leading to the standard sequential tunneling peak in $I(\mu)$ at $\mu \approx \Delta_{S\uparrow}$.

However, we also have to consider the regime $\Delta_{S\uparrow} > \mu_1 > \Delta_{S\downarrow} > \mu_2$, as shown in Fig. 2.1. Without an ESR field, the dot relaxes into its ground state $|\uparrow\rangle$ (since $W_{\downarrow\uparrow} \ll W_{\uparrow\downarrow}$), and the sequential tunneling current through the dot is blocked since the chemical potential $\Delta_{S\uparrow}$ of the dot is higher than

those of the leads. However, if an ESR field generates Rabi spin flips (on the dot only), the current flows through the dot involving the state $|\downarrow\rangle$, since $\Delta_{S\downarrow}$ is lower than μ_1 . Therefore, a sequential tunneling current appears also for gate voltages V_g corresponding to $\Delta_{S\downarrow}$; i.e., $I(\mu)$ exhibits a spin satellite peak due to the ESR field at $\mu \approx \Delta_{S\downarrow}$. This new peak is shifted away from the main peak by Δ_z (Fig. 2.2). The presence of such a satellite peak and its sensitivity to changes in B_z allows identification of spin effects [109]. Further, we note that via the position of the peak in $I(\omega)$, $I(B_z)$, or $I(\mu)$, the Zeeman splitting and also the g factor of a single dot can be measured. Such a measurement could provide a useful technique to study g -factor-modulated materials, where the g factor can be controlled by shifting the equilibrium position of the electrons in the dot from one layer to another by electrical gating [52]. Note that measurement of the peak position would also allow to access the Stark shifts [Eq. (2.9)].

We consider now the analytic expression for the current I , as given in Eq. (B.1), for the regime of the spin satellite peak. In this regime, $\Delta_{S\uparrow} - \mu_1 = \Delta_{S\downarrow} + \Delta_z - \mu_2 - \Delta\mu > \Delta_z - \Delta\mu \approx \Delta_z > kT$, and thus $f_l(\Delta_{S\uparrow}) = 0$, $W_{S\uparrow}^l = 0$, and $W_{\uparrow S}^l = \gamma_l^\downarrow$. For simplicity, we consider $\gamma_l = \gamma_l^\uparrow = \gamma_l^\downarrow$ here (cf. Sec. 2.6 for pumping due to $\gamma_l^\uparrow \neq \gamma_l^\downarrow$). The expression for the stationary current [Eq. (B.1)] considerably simplifies to

$$\begin{aligned}
 I(\omega, \mu) = & 2e(W_{\uparrow\downarrow} + W_\omega)\gamma_1\gamma_2[f_1(\Delta_{S\downarrow}) - f_2(\Delta_{S\downarrow})] \left\{ (2\gamma - W_{\uparrow\downarrow} - W_\omega) \right. \\
 & \left. \times [\gamma_1 f_1(\Delta_{S\downarrow}) + \gamma_2 f_2(\Delta_{S\downarrow})] + 4\gamma(W_{\uparrow\downarrow} + W_{\downarrow\uparrow} + 2W_\omega) \right\}^{-1}.
 \end{aligned}
 \tag{2.29}$$

For a plot of I vs ω and μ and some explanations of its characteristics, see Fig. 2.2.

2.3.2 Spin decoherence time T_2

Around the spin satellite peak, it is possible to measure W_ω via the current and thereby access the spin decoherence time of the spin- $\frac{1}{2}$ state on the dot. For this, we identify a regime where the Rabi spin flips on the dot become the bottleneck for electron transport through the quantum dot such that the current becomes proportional to the spin-flip rate W_ω . For $kT < \Delta\mu$ and

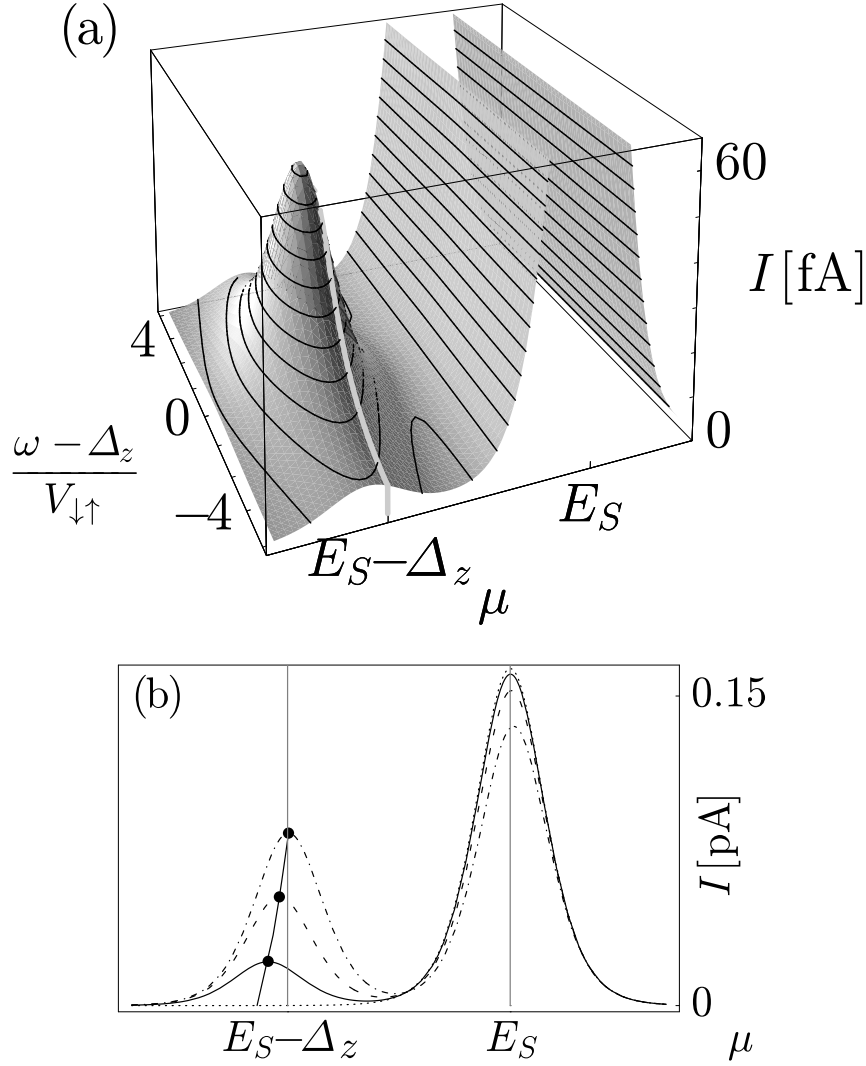


Figure 2.2: The stationary current I [Eq. (B.1)] vs $\mu = (\mu_1 + \mu_2)/2$ and ESR frequency ω . We take $T = 70\text{mK}$, $\Delta\mu/e = 6\mu\text{V}$, $B_z = 0.5\text{T}$, $g = 2$, $T_1 = 1\mu\text{s}$, $T_2 = 100\text{ns}$, $\gamma_1 = 5 \times 10^6\text{s}^{-1}$, and $\gamma_2 = 5\gamma_1$, i.e., $\Delta_z = 10kT$ and $\Delta\mu = kT$. The width of the sequential tunneling peaks in $I(\mu)$ is determined by the temperature; see Eq. (2.31). (a) The current $I(\mu, \omega)$ shows a spin satellite peak near $\mu = E_S - \Delta_z$ (for $E_{\uparrow} = 0$) due to the ESR field. Note that the spin satellite peak is slightly shifted from this position [see Eq. (2.35)], which is indicated by the line at $E_S - \Delta_z$ (light gray line) in (a). Here, $B_x^0 = 1.5\text{G}$, i.e., $W_{\omega}^{\text{max}} = \gamma_1$ at resonance and $\mu = \Delta_{S1}$. (b) The current $I(\mu)$ for $W_{\omega} = 0$ (dotted line), $\gamma_1/5$ (solid line), γ_1 (dashed line), and $9\gamma_1$ (dash-dotted line). The position of the spin satellite peak as function of W_{ω} is shown as black dots and the connecting solid line.

$W_\omega^{\max} < \max\{W_{\uparrow\downarrow}, \gamma_1\}$ we obtain for the stationary current [Eq. (2.29)]

$$I(\omega) = \frac{2e \gamma_1 \gamma_2 (W_{\uparrow\downarrow} + W_\omega)}{\gamma_1(\gamma_1 + \gamma_2) + W_{\uparrow\downarrow}(\gamma_1 + 2\gamma_2)}; \quad (2.30)$$

see Fig. 2.3. We have used $W_{\downarrow\uparrow} < W_{\uparrow\downarrow}$ here. In the linear response regime $kT > \Delta\mu$ and for $W_\omega^{\max} < \max\{W_{\uparrow\downarrow}, \gamma f_1(\Delta_{S\downarrow} + \Delta\mu/2)\}$, the current is

$$I(\omega) = \frac{e \gamma_1 \gamma_2 (W_{\uparrow\downarrow} + W_\omega) \Delta\mu}{2(\gamma_1 + \gamma_2) kT h(T)} \cosh^{-2}\left(\frac{\Delta_{S\downarrow} - \mu}{2kT}\right). \quad (2.31)$$

The current $I(\mu)$ shows the standard sequential tunneling peak shape, determined by the usual cosh dependence on temperature, which is slightly modified by

$$h(T) = 2W_{\uparrow\downarrow} + (2\gamma - W_{\uparrow\downarrow}) f_1(\Delta_{S\downarrow} + \Delta\mu/2). \quad (2.32)$$

Most importantly, the current $I(\omega)$ of the satellite peak [Eqs. (2.30) and (2.31)] is proportional to the spin-flip rate W_ω . Thus, $I(\omega)$ or, equivalently, $I(B_z)$ has a Lorentzian shape with resonance peak at $\omega = \Delta_z$ of width $2V_{\uparrow\downarrow}$. Since $V_{\uparrow\downarrow} \geq 1/T_2$, this width provides a lower bound on the *intrinsic* spin decoherence time T_2 of a single dot spin. For weak tunneling $\gamma_1 < 2/T_2$, this bound saturates; i.e., the width $2V_{\uparrow\downarrow}$ becomes $2/T_2$. Note that the current also shows resonant behavior for $\Delta\mu = 0$ and $\gamma_i^\uparrow \neq \gamma_i^\downarrow$ [Eq. (B.2)]; i.e., a lower bound for T_2 can also be measured via a current due to pumping.

We point out the similarity of our proposal to ESR spectroscopy [16], where absorption or emission linewidths of the ESR field provide information on decoherence. In contrast to these techniques, we are considering here linewidths in resonances of the current, which allows us to access even single spins, since very low currents can be measured accurately.

For Eqs. (2.30) and (2.31) we have assumed that W_ω is small compared to the tunneling or the spin relaxation rates. Therefore, we have neglected the contributions of W_ω in the denominator of these expressions. To take these contributions into account, we note that $W_\omega/(\alpha + W_\omega)$ as a function of ω is still a Lorentzian, but with an increased width $w = 2V_{\uparrow\downarrow}\sqrt{1 + W_\omega^{\max}/\alpha}$. Therefore, the current $I(\omega)$ has the linewidth

$$w = 2V_{\uparrow\downarrow}\sqrt{1 + \frac{W_\omega^{\max} (3\gamma_1 + 4\gamma_2)}{\gamma_1(\gamma_1 + \gamma_2) + W_{\uparrow\downarrow}(\gamma_1 + 2\gamma_2)}}, \quad (2.33)$$

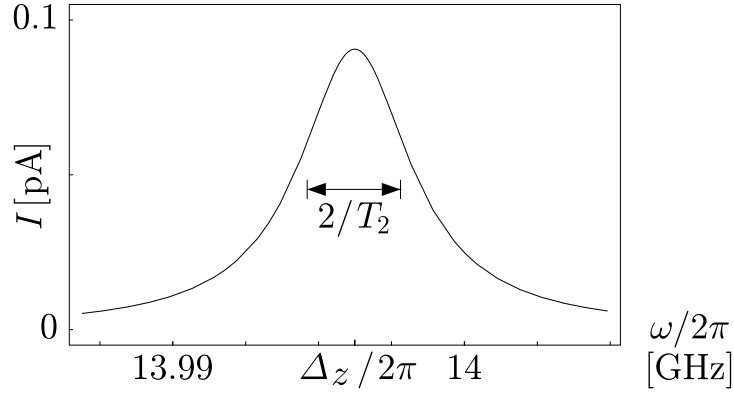


Figure 2.3: The stationary current $I(\omega)$ [Eq. (2.30)] for $kT < \Delta\mu$, $B_z = 0.5\text{T}$, $B_x^0 = 0.45\text{ G}$, $T_1 = 1\ \mu\text{s}$, $T_2 = 100\text{ ns}$, $\gamma_1 = 5 \times 10^6\text{ s}^{-1}$, and $\gamma_2 = 5\gamma_1$, i.e., satisfying $W_\omega^{\text{max}} < \gamma_1 < 1/T_2$. Here, the linewidth gives a lower bound for the intrinsic spin decoherence time T_2 (shown schematically by the arrow), while it becomes equal to $2/T_2$ for $B_x^0 = 0.08\text{ G}$ and $W_\omega^{\text{max}} \ll \gamma_1 = 5 \times 10^5\text{ s}^{-1} \ll 2/T_2$, where $I(\omega = \Delta_z) \approx 1.3\text{ fA}$.

for $kT < \Delta\mu$ [Eq. (2.30)], and

$$w = 2V_{\uparrow\downarrow} \sqrt{1 + W_\omega^{\text{max}} [4 - f_1(\Delta_{S\downarrow} + \Delta\mu/2)]/h(T)} , \quad (2.34)$$

for $kT > \Delta\mu$ [Eq. (2.31)]. Since the linewidth is increased by this correction, the inverse linewidth is still a lower bound for T_2 .

2.3.3 Universal conductance ratio

For increasing W_ω , the satellite peak in the current $I(\mu)$ increases while the main peak decreases, as shown in Fig. 2.2(b). Further, as function of kT , the peak is slightly shifted. Explicitly, for $\gamma_i^\uparrow = \gamma_i^\downarrow$ and $\Delta_z > \Delta\mu$, kT , we find from Eq. (2.29) the position of the satellite peak

$$\mu_{\text{ESR}} = \Delta_{S\downarrow} - \frac{kT}{2} \ln \left\{ \frac{W_{\uparrow\downarrow}/2 + W_{\downarrow\uparrow} + 3W_\omega/2 + \gamma}{W_{\uparrow\downarrow} + W_{\downarrow\uparrow} + 2W_\omega} \right\} . \quad (2.35)$$

The position of the main peak is

$$\mu_0 = \Delta_{S\uparrow} + \frac{kT}{2} \ln \left\{ \frac{W_{\uparrow\downarrow} + 2W_{\downarrow\uparrow} + 3W_\omega + 2\gamma}{W_{\uparrow\downarrow} + W_{\downarrow\uparrow} + 2W_\omega + 2\gamma} \right\} . \quad (2.36)$$

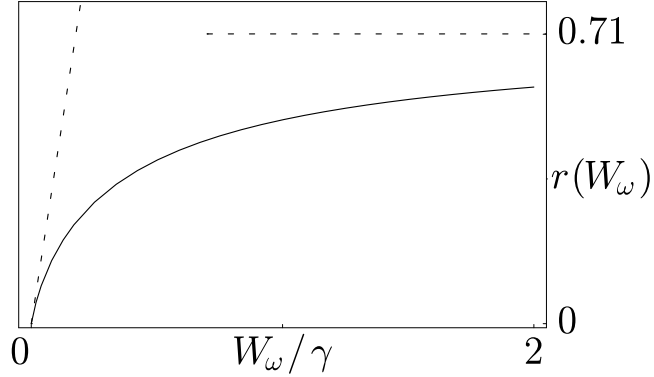


Figure 2.4: The current ratio r of the main and the satellite peak as a function of the effective spin-flip rate W_ω [Eq. (2.37)]. The dashed line shows the saturation of r for $W_\omega \gg \gamma$ at the universal conductance ratio $r_0 \approx 0.71$ [Eq. (2.38)].

An experimentally accessible quantity is the ratio of the two current peaks or, equivalently (for linear response $\Delta\mu < kT$), the ratio of the conductances $r(W_\omega) = I(\mu_{\text{ESR}})/I(\mu_0) = G(\mu_{\text{ESR}})/G(\mu_0)$. For this, we evaluate the stationary current at the gate voltages defined by Eqs. (2.35) and (2.36), and find, for $\Delta\mu < kT$ and $W_{\uparrow\downarrow} < W_\omega$,

$$r(W_\omega) = \frac{2W_\omega \left(1 + \sqrt{1 + \frac{W_\omega}{2W_\omega + 2\gamma}}\right)^2}{4\sqrt{W_\omega}\sqrt{3W_\omega + 2\gamma} + (7W_\omega + 2\gamma)}; \quad (2.37)$$

see Fig. 2.4. On the one hand, for small spin-flip rates, $W_\omega < \gamma$, the ratio r is $4W_\omega/\gamma$; i.e., at ESR resonance, $r(B_x^0) = (g\mu_B B_x^0)^2/(2V_{\uparrow\downarrow}\gamma)$. If the tunneling rates and field strengths are known, this provides a further method for measuring a lower bound of the single-spin decoherence time. On the other hand, this peak ratio [Eq. (2.37)] can be used to measure the ratio W_ω/γ , useful for estimating the additional peak broadening due to other limiting processes, as discussed in Sec. 2.3.2; cf. Eqs. (2.33) and (2.34).

It is noteworthy that the ratio r saturates for $W_\omega \gg \gamma$ at the *universal conductance ratio*

$$r_0 = \frac{5 + 2\sqrt{6}}{7 + 4\sqrt{3}} \approx 0.71. \quad (2.38)$$

For a larger bias, but still $\Delta\mu < \Delta_z$, and for $W_\omega \gg \gamma$, the ratio becomes

$$r_0 \left(\frac{\Delta\mu}{kT} \right) = \frac{\left(\sqrt{3} + \sqrt{2} e^{\frac{\Delta\mu}{2kT}} \right)^2 \gamma_1 + \left(\sqrt{2} + \sqrt{3} e^{\frac{\Delta\mu}{2kT}} \right)^2 \gamma_2}{\left(2 + \sqrt{3} e^{\frac{\Delta\mu}{2kT}} \right)^2 \gamma_1 + \left(\sqrt{3} + 2 e^{\frac{\Delta\mu}{2kT}} \right)^2 \gamma_2}. \quad (2.39)$$

For $\gamma_1 = \gamma_2$, the numerical value of r_0 remains 0.71 for all values $\Delta\mu$. Generally, r_0 is between $2/3$ (for $\gamma_1 \gg \gamma_2$) and $3/4$ (for $\gamma_1 \ll \gamma_2$), where r_0 takes these extremal values for $\Delta\mu > kT$.

Note that the current at the satellite peak is never larger than at the main peak. This asymmetry is best explained in the limit $\Delta\mu > kT$, when the ratio becomes $r_0(\infty) = (2\gamma_1 + 3\gamma_2)/(3\gamma_1 + 4\gamma_2)$. Since $W_\omega > \gamma$, the Rabi spin flips equilibrate the populations ρ_\uparrow and ρ_\downarrow . Thus, the stationary populations of the states are $\rho_S = \eta W_{\text{in}}$, and $\rho_\uparrow = \rho_\downarrow = \eta W_{\text{out}}$, where $\eta = 1/(W_{\text{in}} + 2W_{\text{out}})$ is a normalization factor, η_{ESR} at the satellite peak, and η_0 at the main peak. The rates $W_{\text{in(out)}}$ include all processes of electrons tunneling into (out of) the dot. Note that at the satellite peak $\mu = \mu_{\text{ESR}}$, a spin-up electron tunneling from lead 1 is the only process where an electron tunnels onto the dot, i.e., $W_{\text{in}}(\mu_{\text{ESR}}) = \gamma_1$, whereas at the main peak, $\mu = \mu_0$, the only tunnel process out of the dot is an electron with spin down into the right lead, i.e., $W_{\text{out}}(\mu_0) = \gamma_2$. At the satellite peak, both spin-up and -down electrons can tunnel from the dot to lead 2; thus, the current is given by $I(\mu_{\text{ESR}}) = 2\gamma_2\rho_S = 2\gamma_1\gamma_2\eta_{\text{ESR}}$, with $\eta_{\text{ESR}} = 1/(3\gamma_1 + 4\gamma_2)$. At the main peak, electrons can tunnel from lead 1 onto the dot, and the current is $I(\mu_0) = \gamma_1(\rho_\uparrow + \rho_\downarrow) = 2\gamma_1\gamma_2\eta_0$, with $\eta_0 = 1/(2\gamma_1 + 3\gamma_2)$. Thus, the conductance ratio is given as $r_0 = \eta_{\text{ESR}}/\eta_0$, and we immediately obtain $r_0(\infty)$ in accordance with Eq. (2.39). Therefore, the reason for $r_0 < 1$ is that at the satellite peak three out of four tunnel processes contribute to W_{out} , and thus $\eta_{\text{ESR}} < \eta_0$, while only one contributes at the main peak.

2.4 Even-to-odd sequential tunneling

Up to now we have considered sequential tunneling currents with odd-to-even transitions of the number of electrons on the dot. Now we consider a different filling on the dot, with even-to-odd transitions. The state with N even is $|\bar{S}\rangle$ (involving different orbital states as for $|S\rangle$), and the states with $N + 1$ are $|\uparrow\rangle$ and $|\downarrow\rangle$. This system can be described with the same formalism as

before, but with the tunneling rates $W_{\bar{S}\downarrow} = \sum_l W_{\bar{S}\downarrow}^l$, $W_{\downarrow\bar{S}} = \sum_l W_{\downarrow\bar{S}}^l$,

$$W_{\bar{S}\downarrow}^l = \gamma_l^\downarrow [1 - f_l(\Delta_{\downarrow\bar{S}})], \quad W_{\downarrow\bar{S}}^l = \gamma_l^\downarrow f_l(\Delta_{\downarrow\bar{S}}), \quad (2.40)$$

and with $W_{\bar{S}\uparrow}$, $W_{\uparrow\bar{S}}$, $W_{\bar{S}\uparrow}^l$, and $W_{\uparrow\bar{S}}^l$ defined analogously. The master equation of this system is given by Eqs. (2.16)–(2.21) upon replacing the subscripts S by \bar{S} . Since $W_{\downarrow\bar{S}}$ describes an electron tunneling onto the dot, whereas $W_{\downarrow S}$ describes an electron tunneling out of the dot, the stationary current through the dot is given by Eq. (2.22) after changing its sign and replacing the subscripts, resulting in

$$I_2 = -e(W_{\uparrow\bar{S}}^2 + W_{\downarrow\bar{S}}^2)\rho_{\bar{S}} + eW_{\bar{S}\uparrow}^2\rho_{\uparrow} + eW_{\bar{S}\downarrow}^2\rho_{\downarrow}. \quad (2.41)$$

By comparing Eqs. (2.11) and (2.12) with Eq. (2.40) and Eq. (2.22) with Eq. (2.41), we find that the formulas for the current are modified by the replacements $f_l(\Delta_{S\downarrow}) \rightarrow [1 - f_l(\Delta_{\downarrow\bar{S}})]$, $\gamma_l^\uparrow \rightarrow \gamma_l^\downarrow$, $I_l^\uparrow \rightarrow -I_l^\downarrow$, and analogously for opposite spins. For completeness, we give in the Appendix the formula for the stationary current I_2^\downarrow [Eq. (B.3)], which is obtained by applying the above replacements to Eq. (B.1).

In Sec. 2.3.2 we have identified the regime of the spin satellite peak, which can be used to measure the decoherence time T_2 . For the setup considered here, an analogous regime is $\mu_1 > \Delta_{\downarrow\bar{S}} > \mu_2 > \Delta_{\uparrow\bar{S}}$; see Fig. 2.5(a). The current at the spin satellite peak is then given by Eqs. (2.30) and (2.31) in the corresponding regimes, after interchanging γ_1 with γ_2 , replacing $f_1 \rightarrow (1 - f_1)$ and $\Delta_{S\downarrow} \rightarrow \Delta_{\downarrow\bar{S}}$.

For antiferromagnetic filling of the dot, one can use particle-hole symmetry to show that the two cases, odd-to-even and even-to-odd transitions, are equivalent. Indeed, the tunneling from, say, a spin \uparrow electron from the dot into the lead, $|\uparrow\rangle \rightarrow |\bar{S}\rangle$, can be regarded as a spin \uparrow hole which tunnels from the lead onto the dot, which was initially occupied by a spin \downarrow hole and now forms a hole singlet, i.e., $|\downarrow_h\rangle \rightarrow |S_h\rangle$. With this picture in mind, above modifications become obvious.

2.5 Spin Inverter

In this section we describe a setup with which spin-dependent tunneling $\gamma_l^\downarrow \neq \gamma_l^\uparrow$ can be achieved. Alternatively, spin-polarized leads (see Sec. 2.9 for details) or spin-dependent tunneling barriers could be used. This setup,

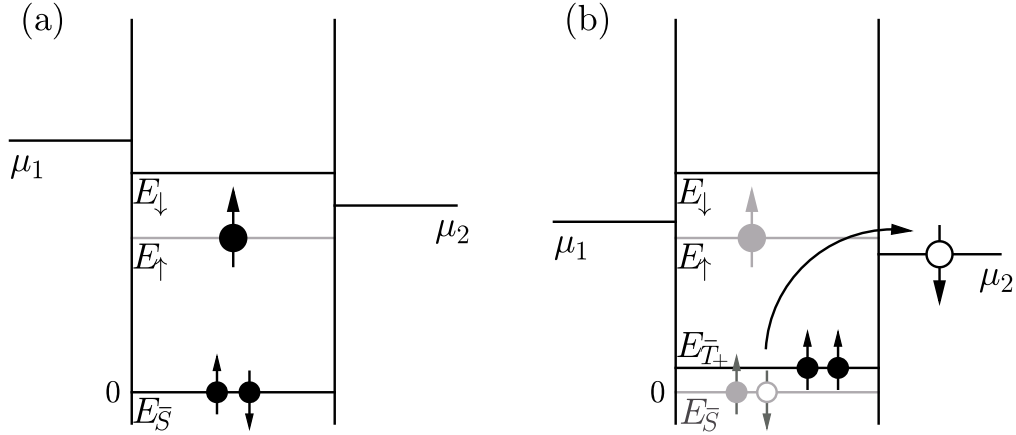


Figure 2.5: (a) Setup for measuring T_2 , with $\mu_1 > E_{\downarrow} > \mu_2$ (for $E_{\bar{S}} = 0$). A lower-lying state occupied by a singlet (corresponding to state $|\bar{S}\rangle$) illustrates the antiferromagnetic filling of the dot. (b) Dot which should act as spin filter, allowing only spin \uparrow to pass. However, in the setup (b), the singlet-triplet spacing $E_{T_+} - E_{\bar{S}}$ is too small compared to $\Delta\mu = \mu_1 - \mu_2$. Here, if the initial dot state is $|\uparrow\rangle$ (shown in gray), an electron with spin \downarrow from a lower-lying state can tunnel onto the right dot, leaving a triplet on the dot (black), thus the spin filter does not operate properly. This problem disappears if the number of electrons on the dot can be reduced down to zero.

shown in Fig. 2.6, consist of two dots, “dot 1” and “dot 2,” which are coupled in series with interdot tunneling amplitude t_{DD} . Dot 2 acts as a spin filter [25] and is coupled to the lead 2 with tunneling amplitude t_{DL} . We write the Zeeman splitting Δ_z^d , the energy E_n^d of state $|n\rangle$, and the chemical potential $\Delta_{S\sigma}^d$ with an index for dot $d = 1, 2$. We assume that dot 2 remains unaffected by the ESR field, which can be achieved, e.g., by applying B_x and/or B_z locally or with different g factors for dot 1 and dot 2. This assumption is taken into account by choosing $\Delta_z^1 \not\approx \Delta_z^2$.

2.5.1 Spin filter

We briefly review the concept of using a quantum dot as spin filter [25], as it is important for the description of the spin inverter. If the dot is initially in state $|\uparrow\rangle$, only a spin \downarrow electron can tunnel onto the dot, forming a singlet. Most importantly, the Zeeman splitting in the dot should be such

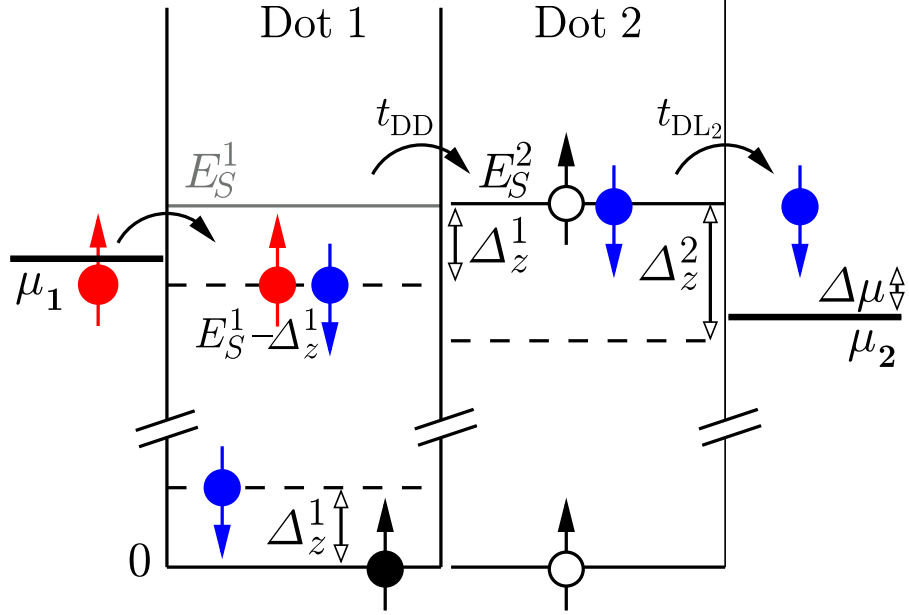


Figure 2.6:

Spin-inverter setup, where the ESR field generates spin flips on dot 1 and the (additional) dot 2 acts as a spin filter, allowing only spin- \downarrow electrons to tunnel into lead 2. We consider the regime $|t_{DD}| < |t_{DL}|$, $E_S^1 \approx E_S^2$, $\Delta_z^1 \neq \Delta_z^2$, and $E_S^i > \mu_i > E_S^i - \Delta_z^i$, for $i = 1, 2$. The allowed transition sequence is schematically given by $\uparrow \uparrow \uparrow \uparrow \xrightarrow{\text{ESR}} \uparrow \downarrow \uparrow \uparrow \rightarrow \uparrow \downarrow \uparrow \uparrow \rightarrow \uparrow \uparrow \downarrow \uparrow \leftrightarrow \uparrow \uparrow \downarrow \downarrow$ (see text), where “ \leftrightarrow ” means a coherent tunneling process.

that $\Delta_z > \Delta_{S\downarrow} - \mu_2$. This ensures proper operation of the spin filter: because of energy conservation, only the electron with spin \downarrow can tunnel from the dot to the lead, leaving the dot always in state $|\uparrow\rangle$ after an electron has passed. Therefore, the sequential tunneling current is spin \downarrow polarized. There is a small spin- \uparrow cotunneling current, however, which is suppressed by a factor [25] $\gamma \max\{kT, \Delta\mu\} / (E_{T_+} - E_S)^2$. Note that for efficient spin filtering, it is favorable to have the singlet state $|S\rangle$ as ground state with an even number of electrons on the dot, since the denominator of the suppression factor can become large, i.e., $E_{T_+} - E_S > \Delta_z$. Otherwise, if the triplet state $|T_+\rangle = |\uparrow\uparrow\rangle$ is the ground state, only spin- \uparrow sequential tunneling current can flow through the dot. However, the spin- \downarrow cotunneling current involves the

triplet state $|T_0\rangle = (|\uparrow\downarrow\rangle + |\downarrow\uparrow\rangle)/\sqrt{2}$, and the suppression factor is given by $\gamma \max\{kT, \Delta\mu\}/(\Delta_z)^2$; i.e., the cotunneling current is not suppressed efficiently [110].

2.5.2 Implementation of the spin inverter

For implementation of the spin inverter, the Zeeman splitting in dot 2 should be such that $\Delta_z^2 > \Delta_{S\downarrow}^1 - \mu_2$, ensuring that dot 2 acts as a spin filter. The coupling of dot 2 to the lead shall be strong such that electrons escape rapidly from dot 2 into lead 2. This leads to resonant tunneling with resonance width $\Gamma_2 = 2\pi\nu_\downarrow|t_{DL}|^2$. We require $\Gamma_2 < \Delta_{S\uparrow}^2 - \mu_2$, i.e., that the broadened level of dot 2 be above μ_2 . This excludes contributions from electrons tunneling from lead 2 onto dot 2, as shown in Ref. [10].

We calculate the rates $\hat{\gamma}^\uparrow$ and $\hat{\gamma}^\downarrow$ for tunneling from dot 1 via dot 2 into lead 2 in a T -matrix approach [111, 10]. We use the tunnel Hamiltonian $H_T = H_{DD} + H_{DL}$, where H_{DD} describes tunneling from dot 1 to dot 2 and H_{DL} from dot 2 to lead 2. The transition rates are $W_{fi} = 2\pi|\langle f|T(\varepsilon_i)|i\rangle|^2\delta(\varepsilon_f - \varepsilon_i)$, where lead 2 is initially at equilibrium and with the T matrix

$$T(\varepsilon_i) = \lim_{\eta \rightarrow +0} H_T \sum_{n=0}^{\infty} \left(\frac{1}{\varepsilon_i + i\eta - H_{\text{dot}} - H_{\text{lead}}} H_T \right)^n. \quad (2.42)$$

We take the leading order in H_{DD} and sum up the contributions from all orders in H_{DL} . We then integrate over the final states in lead 2 and obtain the Breit-Wigner transition rate of an electron with spin \downarrow to tunnel from dot 1 to lead 2 via the resonant level E_S^2 of dot 2,

$$\hat{\gamma}^\downarrow = \frac{|t_{DD}|^2 \Gamma_2}{(\Delta_{S\uparrow}^1 - \Delta_{S\uparrow}^2)^2 + (\Gamma_2/2)^2}. \quad (2.43)$$

In the spin filter regime considered here, dot 2 is always in state $|\uparrow\rangle$. Thus, tunneling of an electron with spin \uparrow would involve the triplet level E_{T_+} on dot 2, which is out of resonance, and thus $\hat{\gamma}^\uparrow$ is suppressed to zero (up to cotunneling contributions, see Sec. 2.2.6). The state of dot 1 and the current through the setup is again described by the master equation [Eqs. (2.16)–(2.21)] with the tunneling rates $W_{S\downarrow}^2 = W_{\downarrow S}^2 = W_{S\uparrow}^2 = 0$ and $W_{\uparrow S}^2 = \hat{\gamma}^\downarrow$. Thus, we can use all previous results for one dot in Sec. 2.3.1, but with $\gamma_2^\downarrow \rightarrow \hat{\gamma}^\downarrow$, $\gamma_2^\uparrow \rightarrow 0$, and $f_2(\Delta_{S\uparrow}) = 0$. Note that even for zero bias $\Delta\mu = 0$, a pumping

current flows from lead 1 via the dots 1 and 2 to lead 2; see Eq. (2.44) and Sec. 2.6. We point out that this setup (see Fig. 2.6) acts as a *spin inverter*; i.e., only spin- \uparrow electrons are taken as input (lead 1), while the output (lead 2) consists of spin- \downarrow electrons. In particular, the spin inverter does not require a change in the direction of the external magnetic field [56].

2.6 Pumping

The ESR field provides energy to the system by exciting the spin state on the dot. When the dot is initially in the excited state $|\downarrow\rangle$, a spin up electron can tunnel onto the dot, followed by the spin down tunneling out of the dot. In total, the Zeeman energy Δ_z is gained. This energy input can be exploited to induce a current through the dot, even at zero bias $\Delta\mu = 0$. However, to obtain a directed current, the spin symmetry between lead 1 and 2 must be broken. This can be achieved by spin-dependent tunneling, $\gamma_i^\downarrow \neq \gamma_i^\uparrow$, e.g., produced with a double-dot, see Sec. 2.5. At the spin satellite peak and for zero bias, i.e., $f_1 = f_2$, there is a finite current [Eq. (B.2)] due to “pumping” [112] by the ESR source,

$$I(\omega) = e(W_{\downarrow\uparrow} + W_\omega)(\gamma_1^\uparrow\gamma_2^\downarrow - \gamma_1^\downarrow\gamma_2^\uparrow)f_1(\Delta_{S\downarrow}) \left[2\gamma^\uparrow f_1(\Delta_{S\downarrow}) \times (2\gamma^\downarrow - W_{\uparrow\downarrow} - W_\omega) + 4\gamma(W_{\uparrow\downarrow} + W_{\downarrow\uparrow} + 2W_\omega) \right]^{-1}. \quad (2.44)$$

Here, $\text{sgn}(\gamma_1^\uparrow\gamma_2^\downarrow - \gamma_1^\downarrow\gamma_2^\uparrow)$ determines the direction of the current. Note that for spin-independent tunneling, $\gamma_i^\downarrow = \gamma_i^\uparrow$, and the pumping current vanishes.

2.7 Rotating ESR fields

It is interesting to study *rotating* magnetic fields in addition to linearly oscillating fields as studied above. With rotating fields, it is possible to calculate the time evolution of the density matrix of the dot exactly. In particular, the stationary solution of the master equation is obtained in a controlled approach and no rotating wave approximation is necessary. However, rotating fields are experimentally more difficult to produce than linearly oscillating fields.

We consider a clockwise rotating field with amplitude B_{\perp}^0 , described by

$$H_{\text{ESR}} = -\frac{1}{4} \Delta_{\perp} [\sigma_x \cos(\omega t) - \sigma_y \sin(\omega t)], \quad (2.45)$$

where $\Delta_{\perp} = 2g\mu_{\text{B}}B_{\perp}^0$. Thus, for $\Delta_x = \Delta_{\perp}$ we have chosen the amplitude of the rotating field to be only half the amplitude of the linearly oscillating field, since both lead to the same effective spin-flip rate W_{ω} . Using Eq. (2.5) we immediately obtain the master equation, which is given by Eqs. (2.16)–(2.21) after the following replacements. The last terms in Eqs. (2.16) and (2.17) become $\mp(\Delta_{\perp}/2) \text{Im}[e^{i\omega t} \rho_{\uparrow\downarrow}]$, respectively. Equation (2.19) is replaced by

$$\dot{\rho}_{\uparrow\downarrow} = -i\Delta_z \rho_{\uparrow\downarrow} + i\frac{\Delta_{\perp}}{4} e^{-i\omega t} (\rho_{\uparrow} - \rho_{\downarrow}) - V_{\uparrow\downarrow} \rho_{\uparrow\downarrow}. \quad (2.46)$$

We transform to the rotating frame $|\uparrow\rangle_r = e^{i\omega t/2} |\uparrow\rangle$ and $|\downarrow\rangle_r = e^{-i\omega t/2} |\downarrow\rangle$ such that $\rho_{\uparrow\downarrow} = e^{-i\omega t} \rho_{\uparrow\downarrow}^r$. This transformation removes the time dependence of the coefficients in the master equation, which we shall now write as $\dot{\rho}_{\text{D}}^r = \mathcal{M} \rho_{\text{D}}^r$. The equations for $\dot{\rho}_{S\uparrow}^r$ and $\dot{\rho}_{S\downarrow}^r$ decouple and we write the remaining part of the superoperator \mathcal{M} as matrix in the basis $\{\rho_{\uparrow}^r, \rho_{\downarrow}^r, \rho_S^r, \text{Re}[\rho_{\uparrow\downarrow}^r], \text{Im}[\rho_{\uparrow\downarrow}^r]\}$,

$$\mathcal{M} = \begin{pmatrix} -(W_{\uparrow\downarrow} + W_{S\uparrow}) & W_{\uparrow\downarrow} & W_{\uparrow S} & 0 & -\Delta_{\perp}/2 \\ W_{\uparrow\downarrow} & -(W_{\uparrow\downarrow} + W_{S\downarrow}) & W_{\downarrow S} & 0 & \Delta_{\perp}/2 \\ W_{S\uparrow} & W_{S\downarrow} & -(W_{\uparrow S} + W_{\downarrow S}) & 0 & 0 \\ 0 & 0 & 0 & -V_{\uparrow\downarrow} & (\Delta_z - \omega) \\ \Delta_{\perp}/4 & -\Delta_{\perp}/4 & 0 & -(\Delta_z - \omega) & -V_{\uparrow\downarrow} \end{pmatrix}. \quad (2.47)$$

The master equation can now be solved exactly by calculating the eigenvalues λ_i of \mathcal{M} . Since the total probability is conserved, $\sum_n \dot{\rho}_n = 0 = \sum_{nm} \mathcal{M}_{nm} \rho_m$, where n is summed over the diagonal elements, and m over diagonal and off-diagonal elements of ρ_{D} . By considering linearly independent initial conditions for ρ_{D} , we see that $\sum_n \mathcal{M}_{nm} = 0$, for every m . Thus, adding up the rows in \mathcal{M} for the diagonal elements of ρ_{D} gives zero, which is satisfied explicitly by adding the first three rows in Eq. (2.47). Therefore, \mathcal{M} does not have full row rank and there is an eigenvalue $\lambda_0 = 0$ with eigenspace describing the stationary solution. The eigenvalues of \mathcal{M} are

$$\left\{ 0, -V_{\uparrow\downarrow}, -3W, -\frac{1}{2} \left(\Sigma_W + V_{\uparrow\downarrow} \pm \sqrt{(\Sigma_W - V_{\uparrow\downarrow})^2 - \Delta_{\perp}^2} \right) \right\}, \quad (2.48)$$

with $\Sigma_W = W + W_{\uparrow\downarrow} + W_{\downarrow\uparrow}$ and where we have considered $W = W_{S\uparrow} = W_{S\downarrow} = W_{\uparrow S} = W_{\downarrow S}$ and resonance $\Delta_z = \omega$ for simplicity. If all λ_i are different, the time evolution of the density matrix is $\rho_D(t) = \sum_i c_i e^{\lambda_i t} \rho_i$ [113]. The decay of the contribution of the eigenvectors ρ_i is exponential and generally all decay rates λ_i are involved. Further, we see from the last two eigenvalues in Eq. (2.48) that the decay rates of ρ_D may be a nontrivial function of the rates involved in the master equation. This should be kept in mind when one uses time-dependent ensemble properties, i.e., $\rho_D(t)$, to measure intrinsic rates, e.g., T_1 and T_2 . We point out that the presence of very small decay rates does not necessarily prevent a decay of the initial conditions. If, say, the tunneling rates are smaller than the spin relaxation rate, $W \ll W_{\uparrow\downarrow}$, it would be interesting to study a density matrix which is described as a linear combination of the eigenvector with eigenvalue $-3W$ [Eq. (2.48)] and the stationary solution ρ_0 , i.e., $\rho_D(t) = \rho_0 + c e^{-3Wt} \rho_{3W}$, where the decay rate $3W$ is independent of $W_{\uparrow\downarrow}$. However, such an initial condition always contains contributions from state $|S\rangle$ such that, in particular, it is not possible to construct an initial spin- $\frac{1}{2}$ state which would decay only with the slow rate $3W$.

The (exact) stationary solution of the master equation can be readily obtained from Eq. (2.47). By eliminating $\rho_{\uparrow\uparrow}^r$ from the coupled equations, we obtain the effective spin-flip rate

$$W_\omega = \frac{\Delta_\perp^2}{8} \frac{V_{\uparrow\downarrow}}{(\omega - \Delta_z)^2 + V_{\uparrow\downarrow}^2}, \quad (2.49)$$

which is equivalent to Eq. (2.25). Thus, all the results for the stationary currents from Sec. 2.3 apply and are exact for the case of rotating magnetic fields.

2.8 Cotunneling

We now consider the cotunneling regime [114, 115, 63] $\Delta_{S\uparrow}, \Delta_{S\downarrow} > \mu_1, \mu_2 \gg E_\downarrow, E_\uparrow$, where the number of electrons on the dot is odd; thus the state on the dot is described by $|\uparrow\rangle$ and $|\downarrow\rangle$. The leading-order tunnel processes is now the tunneling of electrons from lead l onto the dot, forming a virtual state $|n\rangle$, followed by tunneling into lead l' . The spin state on the dot changes $\sigma \rightarrow \sigma'$. This process is called elastic cotunneling for $\sigma = \sigma'$ and inelastic cotunneling for $\sigma \neq \sigma'$. Note that in the absence of an ESR field, the dot relaxes into

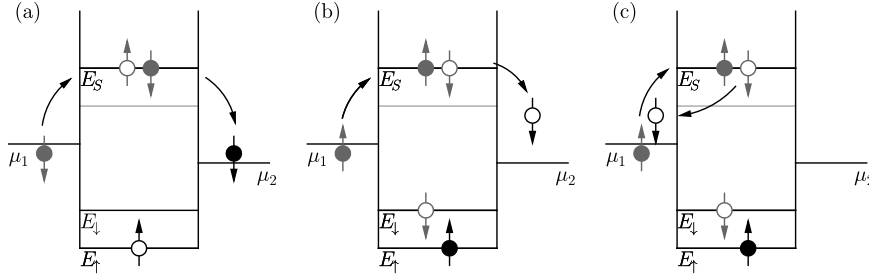


Figure 2.7: Cotunneling processes involving $|S\rangle$ for $\Delta_z > \Delta\mu$. (a) Elastic cotunneling. The cotunneling sequence $\downarrow\uparrow \rightarrow \uparrow\downarrow \rightarrow \uparrow\downarrow$, involving the virtual state $|S\rangle$ on the dot with virtual energy cost $\Delta_{S\uparrow} - \mu_1$. An equivalent process is possible when the initial and final dot state is $|\downarrow\rangle$, however, with a virtual energy cost reduced by Δ_z . These elastic cotunneling processes contribute to transport and to spin decoherence, while they do not contribute to spin relaxation (i.e., T_1). (b) Inelastic cotunneling from lead 1 into lead 2 via the sequence $\uparrow\downarrow \rightarrow \uparrow\downarrow \rightarrow \uparrow\downarrow$. Note that tunneling of an electron from lead 2 into lead 1 is also possible, since the energy gain Δ_z from the dot relaxation is larger than the bias $\Delta\mu$. (c) Inelastic cotunneling, where only one lead is involved. The process shown here leads to a particle-hole excitation in lead 1. While it does not directly contribute to transport, it contributes to spin relaxation and spin decoherence of the dot.

its spin ground state and no inelastic cotunneling processes, exciting the dot spin, occur for $\Delta\mu < \Delta_z$. However, if an ESR field is present, the dot spin can be excited by spin flips. Then, inelastic cotunneling processes, which relax the dot spin, can occur. These processes either contribute to transport or produce a particle-hole excitation in lead 1 or 2 [see Figs. 2.7(b) and 2.7(c)].

These cotunneling rates are calculated in a “golden rule” approach [25], which is known to be consistent with a microscopic derivation [63],

$$W_{\sigma'\sigma}^{\nu l} = 2\pi\nu^2 \int d\epsilon f_l(\epsilon) [1 - f_l(\epsilon - \Delta_{\sigma'\sigma})] \left| \sum_n \frac{t_{\nu\sigma'n} t_{l\sigma n}^*}{\Delta_{n\sigma} - \epsilon} \right|^2, \quad (2.50)$$

where the possible spin dependence of ν has been absorbed into t , $\Delta_{\sigma'\sigma} = E_{\sigma'} - E_{\sigma}$ is the change of Zeeman energy on the dot, and $\Delta_{n\sigma} = E_n - E_{\sigma}$ is the energy cost of the virtual intermediate state. Here, $t_{l\sigma n}$ are the tunneling amplitudes, where $t_{l\downarrow S} = t_l^{\uparrow}$ has already been introduced in Eq. (2.13). The cotunneling current through the dot can be calculated by summing up the

contributing tunneling rates, as we have done for Eq. (2.22),

$$I_{\text{CT}} = e \sum_{\sigma\sigma'} (W_{\sigma'\sigma}^{21} - W_{\sigma'\sigma}^{12}) \rho_{\sigma}. \quad (2.51)$$

We point out that by treating the cotunneling processes with golden rule rates, only classically allowed dot states are considered. Thus, the number of charges on the dot is fixed and no charge can temporarily accumulate as for sequential tunneling. In particular, we have neglected quantum charge fluctuations on the dot. Therefore, within our master equation approach for cotunneling, the charge currents in both leads are equal, $I_1(t) = I_2(t)$. This equality is valid for “coarse-grained” expectation values of the current (and other physical observables). In this approximation, one smoothens out the quantum fluctuations by averaging over the short-time behavior; i.e., one considers only the behavior on time scales larger than the lifetime $1/(\Delta_{S\sigma} - \mu)$ of the virtual states on the dot. However, when the charge imbalance due to the virtual states is taken into account in a microscopic treatment, one can find pronounced peaks in the noise $S(\omega)$ for $|\omega|$ corresponding to the virtual energy cost, as was shown in Ref. [116].

The inelastic cotunneling provides spin relaxation processes in addition to those contributing to T_1 , totaling in $W_{\uparrow\downarrow}^{\text{CT}} = W_{\uparrow\downarrow} + \sum_{l'} W_{\uparrow\downarrow}^{l'l}$. For processes with $l' = l$, particle-hole excitations are produced in lead l . We are interested in the regime $\Delta\mu < \Delta_z$, where (inelastic) cotunneling does not excite the dot spin, i.e., $W_{\uparrow\downarrow}^{\text{CT}} = W_{\uparrow\downarrow}$. In analogy to Eq. (2.15), we take a phenomenological total spin decoherence rate

$$V_{\uparrow\downarrow}^{\text{CT}} = \frac{1}{T_2} + \frac{1}{2} \sum_{l'\sigma\sigma'} W_{\sigma'\sigma}^{l'l}, \quad (2.52)$$

where all spin relaxation and tunneling processes are taken into account. The master equation for the dot in the cotunneling regime and in the presence of a linearly polarized ESR field becomes

$$\dot{\rho}_{\uparrow} = -W_{\uparrow\downarrow}^{\text{CT}} \rho_{\uparrow} + W_{\uparrow\downarrow}^{\text{CT}} \rho_{\downarrow} - \Delta_x \cos(\omega t) \text{Im}[\rho_{\uparrow\downarrow}], \quad (2.53)$$

$$\dot{\rho}_{\downarrow} = W_{\uparrow\downarrow}^{\text{CT}} \rho_{\uparrow} - W_{\uparrow\downarrow}^{\text{CT}} \rho_{\downarrow} + \Delta_x \cos(\omega t) \text{Im}[\rho_{\uparrow\downarrow}], \quad (2.54)$$

$$\dot{\rho}_{\uparrow\downarrow} = -i\Delta_z \rho_{\uparrow\downarrow} + i\frac{\Delta_x}{2} \cos(\omega t) (\rho_{\uparrow} - \rho_{\downarrow}) - V_{\uparrow\downarrow}^{\text{CT}} \rho_{\uparrow\downarrow}. \quad (2.55)$$

Note that away from the sequential tunneling regime, the master equation becomes much simpler while the formulas for the rates are more involved.

For the time-averaged current we evaluate the stationary solution of the master equation in the rotating wave approximation (see Sec. 2.3) for linearly or exactly (see Sec. 2.7) for circularly polarized ESR fields. This yields an effective spin-flip rate W_ω [Eqs. (2.25) and (2.49), respectively] and eliminates Eq. (2.55). We obtain

$$\rho_\downarrow = \frac{W_\omega + W_{\downarrow\uparrow}}{2W_\omega + W_{\downarrow\uparrow} + W_{\uparrow\downarrow} + \sum_{ll'} W_{\uparrow\downarrow}^{ll'}} \quad (2.56)$$

and $\rho_\uparrow = 1 - \rho_\downarrow$. We consider the case close to a sequential tunneling resonance (but still in the cotunneling regime), $\Delta_{S\sigma} - \mu_l < E_{T_+} - E_S$, such that the virtual energy cost of an intermediate triplet state is much higher than that for a singlet state. Since $(E_{T_+} - E_\sigma - \mu)/(E_S - E_\sigma - \mu) < 1$, with $\mu = (\mu_1 + \mu_2)/2$, we have to consider only cotunneling processes involving state $|S\rangle$ in Eq. (2.50). For $\Delta\mu$, $kT < \Delta_{S\sigma} - \mu < E_{T_+} - E_S$, the relevant elastic rates are

$$W_{\sigma\sigma}^{21} = \frac{\gamma_1\gamma_2}{2\pi} \frac{\Delta\mu}{(\Delta_{S\sigma} - \mu)^2}. \quad (2.57)$$

The inelastic rates are, for lead indices $l, l' = 1, 2$,

$$W_{\uparrow\downarrow}^{l'l} = \frac{\gamma_1\gamma_2}{2\pi} \frac{\Delta_z + (l' - l)\Delta\mu}{(\Delta_{S\downarrow} - \mu)(\Delta_{S\downarrow} + \Delta_z - \mu)} \quad (2.58)$$

$$\approx \frac{\Delta_z + (l' - l)\Delta\mu}{\Delta\mu} W_{\downarrow\downarrow}^{21}, \quad (2.59)$$

where Eq. (2.59) is valid for $\Delta_z < \Delta_{S\downarrow} - \mu$. Note that for $\Delta\mu < \Delta_z$ the inelastic rates can be much larger (by a factor of $\Delta_z/\Delta\mu$) than the elastic ones, while their contribution to the current, $W_{\uparrow\downarrow}^{21} - W_{\downarrow\uparrow}^{12} = 2W_{\downarrow\downarrow}^{21}$, is of the same order as for the elastic rates.

For W_ω^{\max} , $W_{\uparrow\downarrow} < W_{\uparrow\downarrow}^{21}$, we obtain the cotunneling current from Eqs. (2.51) and (2.56)–(2.58),

$$I_{\text{CT}} = \frac{e}{2\pi} \frac{\Delta\mu \gamma_1\gamma_2}{(\Delta_{S\uparrow} - \mu)^2} + eW_\omega \frac{\Delta\mu}{4\Delta_z} \left[3 - \frac{\Delta_{S\downarrow} - \mu}{\Delta_{S\uparrow} - \mu} + \frac{\Delta_z}{\Delta_{S\downarrow} - \mu} \right] \quad (2.60)$$

$$\approx \frac{e}{2\pi} \frac{\Delta\mu \gamma_1\gamma_2}{(\Delta_{S\uparrow} - \mu)^2} + eW_\omega \frac{\Delta\mu}{2\Delta_z}. \quad (2.61)$$

The first term in Eq. (2.60) results from elastic cotunneling with spin ground state $|\uparrow\rangle$ on the dot. The second term represents the increased current if the

spin is flipped into state $|\downarrow\rangle$ before cotunneling occurs, since then both elastic and inelastic cotunneling processes contribute to the current. The current I_{CT} is proportional to W_ω , up to a constant background and thus shows, as a function of ω , a resonant peak at $\omega = \Delta_z$ of width $2V_{\downarrow\uparrow}$. Thus, the intrinsic spin decoherence time T_2 is accessible in the cotunneling current as well as in the sequential tunneling (see Sec. 2.3.2). Generally, the cotunneling current is much smaller than the sequential tunneling current, and thus it might seem more difficult to detect T_2 in the cotunneling regime. However, since the current and the decoherence rate due to tunneling are proportional to γ^2 , the small currents can be compensated by choosing more transparent tunnel barriers, i.e., larger γ . Then, the current and the decoherence rate in the cotunneling regime can become comparable to the sequential tunneling values given in Sec. 2.3.2. For illustration we give the following estimates. For $B_z = 1$ T, $B_x^0 = 2$ G, $g = 2$, $\gamma_1 = \gamma_2 = 5 \times 10^9$ s $^{-1}$, $T_1 = 1$ μ s, $T_2 = 100$ ns, $\Delta_{S\downarrow} - \mu = \Delta_z$, and $\Delta\mu = \Delta_z/5$, the cotunneling current as a function of the ESR frequency ω is 0.18 pA away from resonance and exhibits a resonance peak of $I_{\text{CT}}^{\text{max}} = 0.28$ pA, with half-width $V_{\downarrow\uparrow}^{\text{CT}} = 3.5 \times 10^7$ s $^{-1}$.

2.9 Spin read out with spin-polarized leads

An electron spin on a quantum dot can be used as a single spin memory (or as a quantum bit for quantum computation [52]) if the spin state of the quantum dot can be measured. It was shown that a quantum dot connected to fully spin-polarized leads, $\Delta_z^{\text{leads}} > \varepsilon_F > \Delta_z$, can be used for reading the spin state of the quantum dot via the charge current [25]. Such a situation can be realized with magnetic semiconductors (with effective g factors exceeding 100) [5] or in the quantum Hall regime where spin-polarized edge states are coupled to a quantum dot [117]. If the spin polarization in both leads is \uparrow , no electron with spin \downarrow can be provided or taken by the leads (since $\nu_{\downarrow} = 0$), and the rates $W_{S\uparrow}$ and $W_{\uparrow S}$ vanish. Thus, if the dot is initially in state $|\uparrow\rangle$, no electron can tunnel onto the dot (the formation of the triplet is forbidden by energy conservation) and $I = 0$, up to negligible cotunneling contributions. However, if the dot is in state $|\downarrow\rangle$, a current can flow via the sequential tunneling transitions $\uparrow\downarrow \rightarrow \uparrow\uparrow \rightarrow \downarrow\uparrow$. Therefore, the initial spin state of the quantum dot can be detected by measuring the current through the dot. Note that for this read-out scheme, it is not necessary to have $\Delta_z > kT$ on the dot; the constraint of having spin-polarized leads is already sufficiently

strong.

In the stationary regime and for $\Delta_z > kT$, the current becomes blocked due to spin relaxation ($W_{\uparrow\downarrow}$). However, this blocking can be removed by the ESR field producing spin flips on the dot (with rate W_ω). For $W_\omega < W_{\uparrow\downarrow}$, this competition leads again to a stationary current with resonant structure,

$$I(\omega) = e (W_{\uparrow\downarrow} + W_\omega) \frac{\gamma_1 \gamma_2}{\gamma_2 W_{\uparrow\downarrow} + (\gamma_1 + \gamma_2) W_{\downarrow\uparrow}}, \quad (2.62)$$

from which $V_{\uparrow\downarrow}$ (and $1/T_2$) can be measured. Note that the relaxation rate $W_{\uparrow\downarrow}$ is rather small; thus only small ESR fields can be used, which leads to small currents.

2.9.1 Counting statistics and signal-to-noise ratio

We analyze now the time dynamics of the read out of a dot spin via spin-polarized currents. The goal is to obtain the full counting statistics and to characterize a measurement time t_{meas} for the spin read out. While we have considered only averaged currents so far, we now need to keep track of the number of electrons q which have accumulated in lead 2 since $t = 0$ [70, 71, 72]. The time evolution of $\rho_D(q, t)$, now charge dependent, is described by Eqs. (2.16)–(2.21), but with replacements $W_{\downarrow S}^2 \rho_S(q) \rightarrow W_{\downarrow S}^2 \rho_S(q - 1)$ in Eq. (2.17) and $W_{S\downarrow}^2 \rho_\downarrow(q) \rightarrow W_{S\downarrow}^2 \rho_\downarrow(q + 1)$ in Eq. (2.18). Next, we consider the distribution function $P_i(q, t) = \sum_n \rho_n(q, t)$ that q charges have accumulated in lead 2 after time t when the dot was in state $|i\rangle$ at $t = 0$. For a meaningful measurement of the dot spin, the spin-flip times $W_{\uparrow\downarrow}^{-1}$, $W_{\downarrow\uparrow}^{-1}$ and $1/\Delta_x$ must be smaller than t_{meas} and are neglected. Equations (2.16)–(2.21) then decouple except Eqs. (2.17) and (2.18), which we solve for $\rho_\uparrow = 1$ and for $\rho_\downarrow = 1$ at $t = 0$. The general solution follows by linear combination. First, if the dot is initially in state $|\uparrow\rangle$, no charges tunnel through the dot, and thus $P_\uparrow(q, t) = \delta_{q0}$. Second, for the initial state $|\downarrow\rangle$, we consider $kT < \Delta\mu$ and equal rates $W_{S\downarrow}^1 = W_{\downarrow S}^2 = W$. We relabel the density matrix $\rho_\downarrow(q) \rightarrow \rho_{m=2q}$ and $\rho_S(q) \rightarrow \rho_{m=2q+1}$, and Eqs. (2.17) and (2.18) become

$$\dot{\rho}_m = W(\rho_{m-1} - \rho_m), \quad (2.63)$$

with solution $\rho_m(t) = (Wt)^m e^{-Wt}/m!$ (Poissonian distribution). We obtain the counting statistics

$$P_\downarrow(q, t) = \frac{(Wt)^{2q} e^{-Wt}}{(2q)!} \left(1 + \frac{Wt}{2q+1} \right). \quad (2.64)$$

Experimentally, $P_{\downarrow}(q, t)$ can be determined by time series measurements or by using an array of independent dots (see Sec. 2.10.1). The inverse signal-to-noise ratio is defined as the Fano factor [65, 118], which we calculate as

$$F_{\downarrow}(t) = \frac{\langle \delta q(t)^2 \rangle}{\langle q(t) \rangle} = \frac{1}{2} + \frac{3 - 2e^{-2Wt}(4Wt + 1) - e^{-4Wt}}{4(2Wt - 1 + e^{-2Wt})}, \quad (2.65)$$

with F_{\downarrow} decreasing monotonically from $F_{\downarrow}(0) = 1$ to $F_{\downarrow}(t \rightarrow \infty) = \frac{1}{2}$. Note that for dot spin $|\uparrow\rangle$, only weak cotunneling occurs with Fano factor $F_{\uparrow} = 1$ [63].

If we are interested in the current and noise for long times $t > W^{-1}$, we can follow the steps used in Ref. [119]. We decouple the differential equations with respect to q by taking the inverse Fourier transform $\rho_{\text{D}}(k) = \sum_q e^{-ikq} \rho_{\text{D}}(q)$. Note that, for $k = 0$, we recover the density matrix $\rho_{\text{D}} = \rho_{\text{D}}(k = 0)$, where the accumulated charge is not taken into account. The probability $P_{\downarrow}(q, t)$ is then approximated by a Gaussian wave packet in q space with group velocity $I/e = W_{S\downarrow}^1 W_{\downarrow S}^2 / (W_{S\downarrow}^1 + W_{\downarrow S}^2)$ and width $\sqrt{2F(I/e)t}$, and

$$F = \frac{(W_{S\downarrow}^1)^2 + (W_{\downarrow S}^2)^2}{(W_{S\downarrow}^1 + W_{\downarrow S}^2)^2} \quad (2.66)$$

is the Fano factor [119]. However, within this approximation, valid for $Wt > 1$, we cannot access the short-time behavior where only a few electrons have tunneled through the dot, which is of importance for the read-out process considered here.

2.9.2 Measurement time

Using the counting statistics, we can now quantify the measurement efficiency. If, after time t_{meas} , some charges $q > 0$ have tunneled through the dot, the initial state of the dot was $|\downarrow\rangle$ with probability 1 [assuming that single charges can be detected via a single electron transistor (SET) (Ref. [118])]. However, if no charges were detected ($q = 0$), the initial state of the spin memory was $|\uparrow\rangle$ with probability

$$1 - P_{\downarrow}(0, t) = 1 - \frac{W_{S\downarrow}^1 e^{-W_{\downarrow S}^2 t} - W_{\downarrow S}^2 e^{-W_{S\downarrow}^1 t}}{W_{S\downarrow}^1 - W_{\downarrow S}^2}, \quad (2.67)$$

which reduces to $1 - e^{-Wt}(1 + Wt)$, for equal rates. Thus, roughly speaking, we find that $t_{\text{meas}} \gtrsim 2W^{-1}$, as expected, while the Fano factor is $0.5 < F_{\downarrow} \lesssim$

0.72. If, more generally, the threshold for detection is at m charges, $m \geq 1$, Eq. (2.67) is replaced by $1 - \sum_{q=0}^{m-1} P_1(q, t)$.

We insert now realistic numbers to obtain an estimate of the fastest possible measurement time which can be achieved with this setup. For a fast spin read out, the tunneling rates and the current through the dot should be large, limited by the fact that the conductance of the dot should not exceed the single-channel conductance e^2/h . In the linear response regime and for a small bias $\Delta\mu/e$, the current is $I = e\gamma^\uparrow \Delta\mu/8kT < (\Delta\mu/e)(e^2/h)$ for $\gamma_1^\uparrow = \gamma_2^\uparrow$. Thus, the tunneling rates are limited by $\gamma^\uparrow < 8kT/h = 1.66 \times 10^{11} (T/\text{K})\text{s}^{-1}$. For $W = \gamma^\uparrow = 1.25 \times 10^{10} \text{ s}^{-1}$ (corresponding to $kT < \Delta\mu$ and a current $I = 1 \text{ nA}$) and $m = 1$, the spin state can be determined with more than 95% probability for a measurement time of $t_{\text{meas}} = 400 \text{ ps}$ and with more than 99.99% probability for $t_{\text{meas}} = 1 \text{ ns}$ [120].

2.10 Rabi Oscillations of a single spin in the time domain

2.10.1 Observing Rabi oscillations via current

The ESR field generates coherent Rabi oscillations of the dot spin, leading to oscillations in $\rho_D(t)$. Since the time-dependent currents $I(t)$ in the leads are given by the populations $\rho_n(t)$ [Eq. (2.22)], current measurements give access to these Rabi oscillations. First, we consider a dot coupled to unpolarized leads in the regime of the spin satellite peak (see Fig. 2.1 and Sec. 2.3.1). For $kT < \Delta\mu$, the current in lead 2 is $I_2(t) = e(\gamma_2^\uparrow + \gamma_2^\downarrow) \rho_S(t)$; i.e., ρ_S is directly accessible via measurement of $I_2(t)$ [121]. Further, for $\gamma_1^\uparrow = \gamma_1^\downarrow$, the current in lead 1 is $I_1(t) = e\gamma_1(\rho_\downarrow - \rho_S)$, which gives access to $\rho_\downarrow(t)$, if the ratio γ_1/γ_2 is known. We calculate the oscillations of $I_{1,2}(t)$ explicitly by numerical integration of the master equation [Eqs. (2.16)–(2.19)]; see Fig. 2.8(b).

The measurement of ρ_D can be refined by using the spin read-out setup with spin-polarized leads (Sec. 2.9). For $kT < \Delta\mu$, the current is $I_1(t) = I_1^\uparrow(t) = e\gamma_1^\uparrow \rho_\downarrow(t)$ in lead 1 and $I_2(t) = I_2^\uparrow(t) = e\gamma_2^\uparrow \rho_S(t)$ in lead 2 [121]. Thus, the time dependence of ρ_\downarrow and ρ_S (and also of $\rho_\uparrow = 1 - \rho_\downarrow - \rho_S$) can be directly measured via the currents $I_{1,2}$; see Fig. 2.8(a).

Note that the electrons which tunnel onto the dot decohere the spin state on the dot (see Sec. 2.2.5). Thus, to observe Rabi oscillations in $I_{1,2}(t)$ experimentally, the Rabi frequency Δ_x must be larger than the coupling to

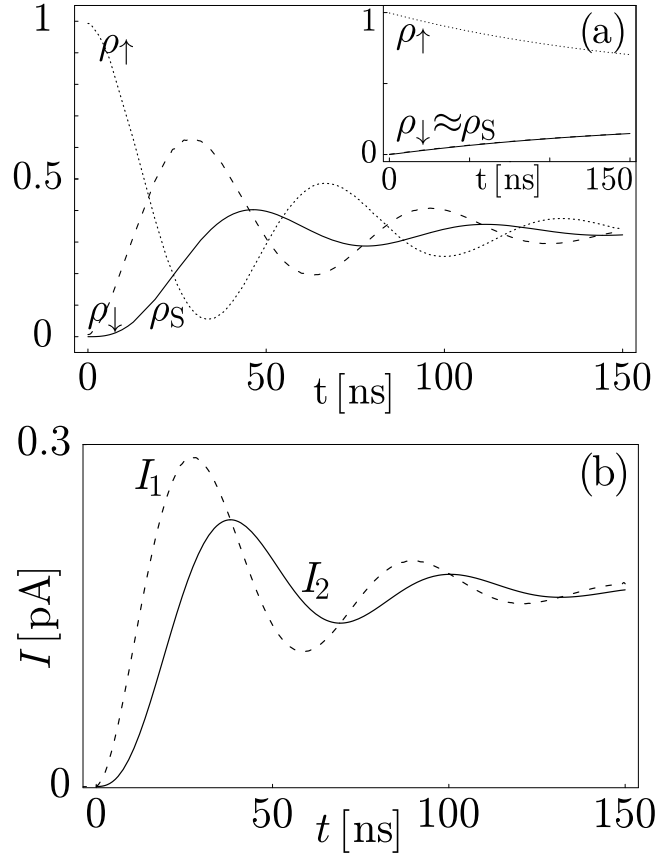


Figure 2.8: Rabi oscillations of the electron spin on the dot in the time domain. We consider the regime at the spin satellite peak, $\Delta_{S\uparrow} > \mu_1 > \Delta_{S\downarrow} > \mu_2$, (see Fig. 2.1), and take $T_1 = 1 \mu\text{s}$, $T_2 = 300 \text{ ns}$, $\Delta_x = 5W_{S\downarrow}$ (corresponding to $B_x^0 = 11 \text{ G}$ for $g = 2$), and $\rho_\uparrow = 1$ at $t = 0$. During the time span shown here, fewer than three electrons have tunneled through the dot on average. Here, the spin decoherence is dominated by the tunneling process, i.e., $W_{S\downarrow} \gg 1/T_2$. (a) Spin-polarized leads with the only nonvanishing tunnel rates $W_{S\downarrow} = W_{\downarrow S} = 4 \times 10^7 \text{ s}^{-1}$. The Rabi oscillations show up in ρ_\uparrow (dotted line), ρ_\downarrow (dashed line), and ρ_S (solid line), which is directly visible in the current, since $I_1^\uparrow(t) \propto \rho_\downarrow$ and $I_2^\uparrow(t) \propto \rho_S$, for $kT < \Delta\mu$. In the inset, we show the case of large tunneling, $W_{S\downarrow} = W_{\downarrow S} = 10^9 \text{ s}^{-1} \gg \Delta_x$. As a consequence of the Zeno effect (see Sec. 2.10.3), the Rabi oscillations are suppressed. Further, ρ_\downarrow and ρ_S are indistinguishable since $|\downarrow\rangle$ and $|S\rangle$ equilibrate rapidly due to the increased tunneling. (b) The time-dependent currents in unpolarized leads, $I_1(t) = e\gamma_1(\rho_\downarrow - \rho_S)$ and $I_2(t) = 2e\gamma_2\rho_S$, for $kT < \Delta\mu$, and $\gamma_i^\uparrow = \gamma_i^\downarrow = 4 \times 10^7 \text{ s}^{-1}$, for $l = 1, 2$.

the leads $W_{S\downarrow}$; otherwise, the strong decoherence (equivalent to a continuous measurement) suppresses the Rabi oscillations (Zeno effect; see Sec. 2.10.3). Then, however, only very few electrons tunnel per Rabi oscillation period through the dot. To overcome the limitations of such a weak current signal and to obtain $I_{1,2}(t)$ experimentally, an ensemble average is required.

There are two possibilities to obtain averages: namely, using many dots or performing a time series measurement. First, many independent dots can be measured simultaneously by arranging the dots in parallel to increase the total current. For example, an array (ensemble) of dots and leads could be produced with standard techniques for defining nanostructures or self-assembled, or chemically synthesized dots could be placed within an insulating barrier between two electrodes. Second, time series measurement over a single dot can be performed. For this, the procedure of preparing the dot to the desired initial state—applying an ESR field and measuring the current—has to be repeated many times (see Sec. 2.9.1 for counting statistics of the read-out process). Then, assuming ergodicity, the current average of all these individual measurements corresponds to the ensemble-averaged value.

2.10.2 Decoherence in the time domain

In Fig. 2.8, we plot the numerical solution of Eqs. (2.16)–(2.21), showing the coherent oscillations of ρ_D and I_l , for (a) spin-polarized and (b) unpolarized leads. The decay of these oscillations is dominated by the spin decoherence rate $V_{\downarrow\uparrow}$. Since this decay can be measured via the current, $V_{\downarrow\uparrow}$ (and $1/T_2$) can be accessed directly in the time domain (see also Sec. 2.11, Ref. [122] and Fig. 2.9).

2.10.3 Zeno effect

When the rate for electrons tunneling onto the dot, $W_{S\sigma}$, is increased, the coherent oscillations of $\rho_{\uparrow}, \rho_{\downarrow}$ become suppressed [see inset of Fig. 2.8(a)]. This suppression is caused by the increased spin decoherence rate $V_{\downarrow\uparrow}$ [Eq. (2.15)] and can be interpreted as a continuous strong measurement of the dot spin, performed by an increased number of charges tunneling onto the dot. This suppression of coherent oscillations is known as the Zeno effect [123]. Since it is visible in ρ_D , it can be observed via the currents $I_{1,2}(t)$.

2.11 Pulsed ESR and Rabi oscillations

We now show that it is possible to observe the coherent Rabi oscillations of a single electron spin even without the requirement of measuring time-resolved currents. This can be achieved by applying ESR pulses of length t_p and by measuring time-averaged currents (over arbitrarily long times). Then, the time-averaged current $\bar{I}(t_p)$ as function of t_p gives access to the time evolution of the spin state on the dot for both polarized and unpolarized leads [124]. In particular, since arbitrarily long times, and thus a large number of electrons, can be used to measure \bar{I} , the required experimental setups are significantly simpler compared to setups which aim at measuring time-dependent currents with high resolution.

We assume a rectangular envelope for the ESR pulse with length t_p and repetition time t_r (thus $t_p < t_r$). The time when no ESR field is present, $t_r - t_p$, should be long enough such that the dot can relax into its ground state $|\uparrow\rangle$; i.e., at the beginning of the next pulse, we have $\rho_\uparrow = 1$. We calculate $\bar{I}(t_p)$ by numerical integration of the master equation [Eqs. (2.16)–(2.19)] and by subsequently averaging the (time-dependent) current [Eq. (2.22)] over the time interval $[0, t_r]$. The results are shown in Fig. 2.9(b) for unpolarized leads at the spin satellite peak (see Sec. 2.3.1) and in Fig. 2.9(c) for spin-polarized leads in the regime for spin read out (see Sec. 2.9). In both cases, $\bar{I}(t_p)$ as a function of pulse length t_p shows the Rabi oscillations of the dot spin; i.e., the Rabi oscillations can be observed in the time domain even without time-resolved measurements.

In addition to the exact numerical evaluation of the master equation (see Fig. 2.9), we now give an approximate analytical expression for $\bar{I}(t_p)$. We first consider the case of unpolarized leads at the spin satellite peak (Sec. 2.3.1); for the case of spin-polarized leads, see below. For this, we need to evaluate the time average of Eq. (2.22). For $kT < \Delta\mu$, we get

$$\bar{I}(t_p) = e(\gamma_2^\uparrow + \gamma_2^\downarrow) \frac{1}{t_r} \int_0^{t_r} dt \rho_S(t). \quad (2.68)$$

First, we consider times t with $0 \leq t \leq t_p$, for which an ESR field is present, and ρ_D oscillates with Rabi frequency Δ_x [see Fig. 2.9(a) for $t \leq 200$ ns]. Qualitatively speaking, when $\rho_S(t)$ is integrated in Eq. (2.68) up to t_p , the oscillating contribution averages nearly to zero, and we obtain a background contribution \bar{I}_0 approximately proportional to $e(\gamma_2^\uparrow + \gamma_2^\downarrow)t_p/t_r$, i.e., linear in t_p , in agreement with Fig. 2.9(b). For experiments, this linearity of \bar{I}_0 provides

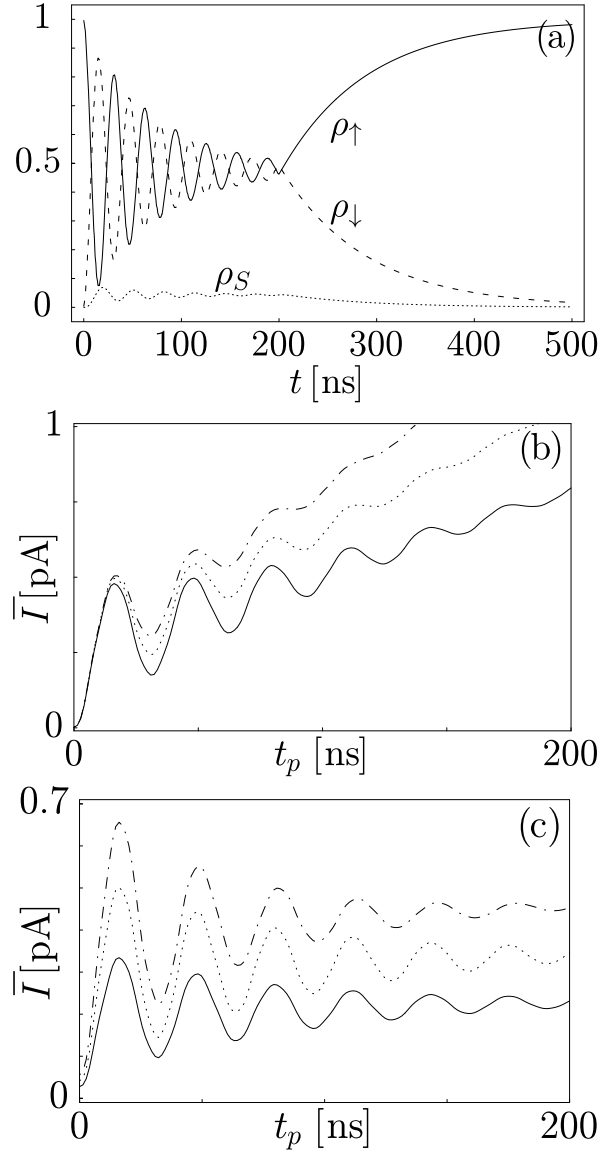


Figure 2.9: Single-spin Rabi oscillations in the current $\bar{I}(t_p)$ generated by ESR pulses of length t_p . Here, $\Delta\mu > kT$, Rabi frequency $\Delta_x = 4 \times 10^8 \text{ s}^{-1}$ (corresponding to $g = 2$ and $B_x^0 = 23\text{G}$), $\gamma_1 = 2 \times 10^7 \text{ s}^{-1}$, $\gamma_2 = 5\gamma_1$, $T_1 = 1\mu\text{s}$, and $T_2 = 150 \text{ ns}$. (a) Evolution of the density matrix for unpolarized leads where a pulse of length $t_p = 200 \text{ ns}$ is switched on at $t = 0$, obtained by numerical integration of the master equation [Eqs. (2.16)–(2.19)]. (b) Time-averaged current $\bar{I}(t_p)$ (solid line) for unpolarized leads and a pulse repetition time $t_r = 500 \text{ ns}$. We also show the current where γ_1 and γ_2 are increased by a factor of 1.5 (dotted line) and 2 (dash-dotted line). (c) Time-averaged current $\bar{I}(t_p)$ (solid line) for spin-polarized leads, $\gamma_1^{\uparrow} = 2 \times 10^7 \text{ s}^{-1}$, $\gamma_2^{\uparrow} = 5\gamma_1^{\uparrow}$, $\gamma_{1,2}^{\downarrow} = 0$. The pulse repetition time $t_r = 10 \mu\text{s}$ is chosen larger than T_1 .

Again, we show the current for tunneling rates $\gamma_{1,2}^{\uparrow}$ increased by a factor of 1.5 (dotted line) and 2 (dash-dotted line). Note that in this figure $t_p < T_1$; i.e., most electrons tunnel through the dot after the pulse is switched off, thus the linear background is negligibly small.

a first check that t_r is sufficiently long such that the dot has indeed relaxed into its ground state before the next pulse is applied. We also give an upper bound for \bar{I}_0 by using the inequality $\rho_S \leq \rho_S^{\max} = W_{S\downarrow}/(W_{S\downarrow} + W_{S\uparrow} + W_{\uparrow S})$. This is seen as follows. For $\rho_S(t) > \rho_S^{\max}$, we would have $\dot{\rho}_S(t) < 0$, and thus $\rho_S(t') > \rho_S^{\max}$, for all $0 \leq t' \leq t$, which would be in contradiction to the initial condition $\rho_S(0) = 0$; hence indeed $\rho_S(t) \leq \rho_S^{\max}$. From Eq. (2.68), we then obtain $\bar{I}_0 < e \min\{\gamma_1^\uparrow, \gamma_2^\uparrow + \gamma_2^\downarrow\} t_p/t_r$. Note that for pulse lengths t_p , over which the dot spin evolves coherently, $t_p \gamma_1^\uparrow \lesssim 1$. Thus, by comparing the upper bound with Eq. (2.69), we see that for $\gamma_1^\uparrow < \gamma_2$ the background current \bar{I}_0 never becomes dominant.

Second, we consider $t_p \leq t \leq t_r$; i.e., the ESR field is switched off, and the dot state relaxes into its ground state $|\uparrow\rangle$. Making the reasonable assumption that the tunnel processes dominate the spin relaxation, $\gamma > W_{\uparrow\downarrow}$, we neglect $W_{\uparrow\downarrow}$ here. We then calculate the contribution for $t \geq t_p$ to the integral in Eq. (2.68) analytically and obtain

$$\bar{I}(t_p) - \bar{I}_0(t_p) = \frac{e}{t_r} \frac{\gamma_2^\uparrow + \gamma_2^\downarrow}{\gamma_1^\uparrow + \gamma_2^\downarrow} [\rho_\downarrow(t_p) + \rho_S(t_p)] \propto 1 - \rho_\uparrow(t_p). \quad (2.69)$$

We now give a physical explanation for Eq. (2.69). We consider different tunneling events (after the pulse is switched off) and their contributions to the current, $\int_{t_p}^{t_r} dt \rho_S(t)$. Since we assume that at t_r the dot has relaxed into its ground state $|\uparrow\rangle$ and thus $\rho_S(t_r) = \rho_\downarrow(t_r) = 0$, it is sufficient to consider only one pulse and to extend the upper integration limit to infinity. For the population $\rho_\downarrow(t_p)$ of state $|\downarrow\rangle$, the only allowed transition is $|\downarrow\rangle \rightarrow |S\rangle$ (neglecting again the intrinsic spin relaxation rate $W_{\uparrow\downarrow}$). Thus, eventually this population ρ_\downarrow will be transferred to ρ_S and thus to the current. Note that sequences with $|S\rangle \rightarrow |\downarrow\rangle$ contribute to the current at a later time again, since the only possible decay into the ground state $|\uparrow\rangle$ involves $|S\rangle$. Therefore, concerning current contributions, we introduce the effective population $\rho_I = \rho_\downarrow + \rho_S$, which is the probability that at some later time an electron can still tunnel from the dot to lead 2. This ρ_I decays to state $|\uparrow\rangle$ with the rate $\gamma_S = \gamma_1^\downarrow + \gamma_2^\downarrow$, i.e., with the rate for the process $|S\rangle \rightarrow |\uparrow\rangle$. In total, integrating over $\rho_S(t)$ for $t > t_p$ yields $\int_0^\infty dt \rho_I(t_p) e^{-\gamma_S t} = [\rho_\downarrow(t_p) + \rho_S(t_p)]/\gamma_S$, and with Eq. (2.68) we immediately recover Eq. (2.69), as expected.

Next, we consider the case for spin-polarized leads. Here, no spin relaxation process due to tunneling occurs and the dot spin can only relax via intrinsic spin flips, given by the rate $W_{\uparrow\downarrow}$ (corresponding to the relaxation

time T_1 ; we neglect $W_{\downarrow\uparrow}$ for $W_{\downarrow\uparrow} \ll W_{\uparrow\downarrow}$). Thus, we now consider the relaxation rate $W_{\uparrow\downarrow}$ instead of γ_S . The relaxation occurs only from $|\downarrow\rangle$ to $|\uparrow\rangle$; i.e., the roles of $|S\rangle$ and $|\downarrow\rangle$ are interchanged compared to the case for unpolarized leads considered above. The above argument now applies analogously by considering the (spin-polarized) current in lead 1, $I_1^\uparrow(t) = e\gamma_1^\uparrow\rho_\downarrow(t)$. We obtain

$$\bar{I}^\uparrow(t_p) \approx \frac{e}{t_r} \frac{\gamma_1^\uparrow}{W_{\uparrow\downarrow}} [1 - \rho_\uparrow(t_p)], \quad (2.70)$$

with equality for $t_p \ll T_1$. We point out that for $\gamma_1^\uparrow \gg 1/T_1$, the (total) decoherence of the dot spin occurs much faster than its (intrinsic) relaxation. Then, pulse lengths t_p , for which Rabi oscillations can be observed, are limited, $1/t_p \gtrsim V_{\downarrow\uparrow} > \gamma_1^\uparrow \gg W_{\uparrow\downarrow}$. In this case, the current contribution for $t \leq t_p$ can be neglected since it is suppressed by a factor of $t_p W_{\uparrow\downarrow} \ll 1$ compared to the contribution for $t \geq t_p$ [Eq. (2.70)], see Fig. 2.9(c). Note that for spin-polarized leads, the relaxation time $W_{\uparrow\downarrow}^{-1}$ is usually much longer than for unpolarized leads, γ_S^{-1} ; thus the required pulse repetition time $t_r > W_{\uparrow\downarrow}^{-1}$ might become very long. However, if one chooses a pulse repetition time $t_r = c/\gamma$, for $c > 1$, and with the relevant relaxation rate γ , the current is proportional to $(1/t_r) \int_0^\infty dt e^{-\gamma t} = 1/c$, i.e., independent of γ . Thus, roughly speaking, the slow relaxation rate in the case of spin-polarized leads has no influence on the attainable maximum current since the decay from ρ_S and ρ_\downarrow is much slower and thus per pulse there are more electrons passing the dot.

To conclude, we would like to emphasize again that the Rabi oscillations of the dot spin can be observed directly in the time domain by using pulsed ESR and measuring time-averaged currents (see Fig. 2.9). Observing Rabi oscillations also allows one to determine T_2 in the time domain; see Sec. 2.10.2 [122].

2.12 STM Techniques and ESR

So far, we have considered a quantum dot coupled to leads. In this section, we would like to note that our description applies to more general structures showing Coulomb blockade behavior, such as Au nanoparticles [125] or C_{60} molecules [126], which has been observed with STM techniques. This justifies that instead of a quantum dot, we now consider a localized surface state or an atom, molecule, or nanoparticle adsorbed on a substrate. This particle can then be probed with the STM tip by measuring the tunnel current through

the particle. The current arises from electrons tunneling from the STM tip onto the particle and further tunneling, possibly through an insulating overlayer, into the bulk of the substrate.

In standard STM theory, the tunneling from the STM tip to the sample is treated perturbatively [127]. Evaluation of the golden rule matrix element, in the simplest model of a one-dimensional tunnel barrier, gives a tunneling amplitude, which is dominated by an exponential decay of the electronic wave function into the barrier; thus $t_l^\sigma \propto e^{-\kappa d}$ [cf. Eq. (2.13)], with $\kappa = \sqrt{2m\phi}$, tip-particle distance d , and barrier height ϕ (roughly given by the work function of the tip and sample). In particular, the perturbative description of STM is equivalent to our treatment of the tunneling Hamiltonian in first (sequential tunneling) order. Therefore, if the particle of interest shows Coulomb blockade behavior and has a spin- $\frac{1}{2}$ ground state, the master equation [Eqs. (2.16)–(2.21)] applies. Thus, using an ESR field, coherent Rabi oscillations and the T_2 time of the spin state of the particle can be accessed via the current. Further, if spin-polarized tips and/or substrates are available (spin-polarized STM), such a particle can act as single spin memory with read out via current. Note that the tunneling rates from the STM tip into the particle can be controlled by changing the distance d ; thus the total decoherence $V_{\downarrow\uparrow}$ [Eq. (2.15)], containing tunneling contributions, can be varied. This allows one, e.g., to vary the current linewidth $2V_{\downarrow\uparrow}$ (Sec. 2.3.2) and to suppress the Rabi spin flips for strong decoherence (Zeno effect, Sec. 2.10.3). One apparent restriction of atomic or molecular systems is that it is difficult to apply a gate voltage to the particle, shifting its energy levels. However, the same effect can be achieved if the Fermi energies in the STM tip and the substrate can be shifted, such as by varying electron densities.

2.13 Conclusion

We have shown how the single-spin dynamics of quantum dots can be accessed by current measurements. We have derived and analyzed coupled master equations of a quantum dot, which is tunnel coupled to leads, in the presence of an ESR field. The current through the dot in the sequential tunneling regime shows a new resonance peak (satellite peak) whose linewidth provides a lower bound on the single-spin decoherence time T_2 . We have shown that also the cotunneling current has a resonant current contribution, giving access to T_2 . The coherent Rabi oscillations of the dot spin can be

observed by charge measurements, since they lead to oscillations in the time-dependent current and in the time-averaged current as function of ESR pulse length. We have shown how the ESR field can pump current through a dot at zero bias if spin-dependent tunneling or a spin inverter is available. We have discussed the concept of measuring a single spin via charge in detail. We have identified the measurement time of the dot spin via spin-polarized leads. Finally, we have noted that the concepts presented here are not only valid for quantum dots but also for “real” atoms or molecules if they are contacted with an STM tip.

Chapter 3

Measurement Efficiency and n -shot Read Out of Spin Qubits

In this chapter, we consider a general apparatus for measuring a qubit and define a measurement efficiency e to characterize reliable measurements via n -shot read outs. We consider electron spin qubits in quantum dots and propose various read-out implementations based on a double dot and quantum point contact (QPC). We show that the associated efficiencies e vary between 50% and 100%, allowing single-shot read out in the latter case. We model the read out microscopically and derive its time dynamics in terms of a generalized master equation, calculate the QPC current and show that it allows spin read out under realistic conditions.

3.1 Introduction

The read out of a qubit state is of central importance for quantum information processing [2], see Sec. 1.4. In special cases, the qubit state can be determined in a single measurement, referred to as single shot read out. In general, however, the measurement needs to be performed not only once but n times, where n depends on the qubit, the efficiency e of the measurement device, and on the tolerated inaccuracy (infidelity) α . In the next section, we analyze such n -shot read outs for general qubit implementations and derive a lower bound on n in terms of e and α . In Sec. 3.3, we then turn to spin-based qubits and GaAs quantum dots [3, 128] and analyze their n -shot read out based on a spin-charge conversion and charge measurement via QPCs.

3.2 n -shot read out and measurement efficiency e

How many times n do the preparation and measurement need to be performed until the state of the qubit is known with some given infidelity α (n -shot read out)? We consider a well-defined qubit, i.e., we take only a two-dimensional qubit Hilbert space into account and exclude leakage to other degrees of freedom. We define a set of positive operator-valued measure (POVM) operators [123], $E_{A_0} = p_0|0\rangle\langle 0| + (1-p_1)|1\rangle\langle 1|$ and $E_{A_1} = (1-p_0)|0\rangle\langle 0| + p_1|1\rangle\langle 1|$, where p_0 and p_1 are probabilities. These operators describe measurements with outcomes A_0 and A_1 , *resp.* They are positive and $E_{A_0} + E_{A_1} = 1$. This model of the measurement process can be pictured as follows. First, the qubit is coupled to some other device (e.g., to a reference dot, see below). Then this coupled system is measured and thereby projected onto some internal state. That state is accessed via an external “pointer” observable \hat{A} [123] (e.g., a particular charge distribution, a time-averaged current, or noise). We assume that only two measurement outcomes are possible, either A_0 or A_1 , which are classically distinguishable [129]. For initial qubit state $|0\rangle$ the expectation value is $\langle \hat{A} \rangle_0 = p_0 A_0 + (1-p_0) A_1$, while for initial state $|1\rangle$ it is $\langle \hat{A} \rangle_1 = (1-p_1) A_0 + p_1 A_1$. Let us take an initial qubit state $|0\rangle$ and consider a single measurement. With probability p_0 , the measurement outcome is A_0 which one would interpret as “qubit was in state $|0\rangle$ ”. However, with probability $1-p_0$, the outcome is A_1 and one might incorrectly conclude that “qubit was in state $|1\rangle$ ”. Conversely, the initial state $|1\rangle$ leads with probability p_1 to A_1 and with $1-p_1$ to A_0 . We now determine n for a given α , for a qubit either in state $|0\rangle$ or $|1\rangle$ (no superposition allowed [130]). For an accurate read out we need, roughly speaking, that $\langle \hat{A} \rangle_0$ and $\langle \hat{A} \rangle_1$ are separated by more than the sum of the corresponding standard deviations. More precisely [131], we consider a parameter test of a binomial distribution of the measurement outcomes, one of which is A_0 with probability p . The null hypothesis is that the qubit is in state $|0\rangle$, thus $p = p_0$. The alternative is a qubit in state $|1\rangle$, thus $p = 1-p_1$. For sufficiently large n , namely $n p_{0,1}(1-p_{0,1}) > 9$, one can approximate the binomial with a normal distribution [132]. The state of the qubit can then be determined with significance level (“infidelity”) α for

$$n \geq z_{1-\alpha}^2 \left(\frac{1}{e} - 1 \right), \quad (3.1)$$

$$e = \left(\sqrt{p_0 p_1} - \sqrt{(1-p_0)(1-p_1)} \right)^2, \quad (3.2)$$

with the quantile (critical value) $z_{1-\alpha}$ of the standard normal distribution function, $\Phi(z_{1-\alpha}) = 1 - \alpha = \frac{1}{2}[1 + \text{erf}(z_{1-\alpha}/\sqrt{2})]$. We interpret e as *measurement efficiency*. Indeed, it is a single parameter $e \in [0, 1]$ which tells us if n -shot read out is possible. For $p_0 = p_1 = 1$, the efficiency is maximal, $e = 100\%$, and single-shot read out is possible ($n = 1$). Conversely, for $p_1 = 1 - p_0$ (e.g., $p_0 = p_1 = \frac{1}{2}$), the state of the qubit cannot be determined, not even for an arbitrarily large n , and the efficiency is $e = 0\%$. For the intermediate regime, $0\% < e < 100\%$, the state of the qubit is known after several measurements, with n satisfying Eq. (3.1).

3.2.1 Visibility v

When coherent oscillations between $|0\rangle$ and $|1\rangle$ are considered, the amplitude of the oscillating signal is $|\langle \hat{A} \rangle_1 - \langle \hat{A} \rangle_0|$, i.e., smaller than the value $|A_1 - A_0|$ by a factor of $v = |p_0 + p_1 - 1|$. Thus, we can take v as a measure of the visibility of the coherent oscillations. With v and the shift of the oscillations, $s = \frac{1}{2}(p_1 - p_0) = \frac{1}{2}(\langle \hat{A} \rangle_0 + \langle \hat{A} \rangle_1 - A_0 - A_1)/(A_1 - A_0)$, we can get e . We find the general relation $v^2 \leq e \leq v$, where the left inequality becomes exact for $p_0 = p_1$ and the right for $p_0 = 1$ or $p_1 = 1$. Further, for every $0 < \epsilon < 1$ we can take $p_0 = \frac{1}{2}$ and $p_1 = \frac{1}{2} + \frac{\epsilon}{2}$, thus $e < \epsilon v$. Hence, given these natural interpretations of e and v , we see that somewhat unexpectedly the efficiency can be much smaller than the visibility (of course, $e = 0 \Leftrightarrow v = 0$).

3.3 Single spin read out

We now discuss several concrete read-out setups and their measurement efficiency. We consider a promising qubit, which is an electron spin confined in a quantum dot [3, 128]. For the read out of such a spin qubit, the time scale is limited by the spin-flip time T_1 , which has a lower bound of $\approx 100 \mu\text{s}$ [133, 35] (while T_2 is not of relevance here). One setup proposed in Ref. [3] is read out via a neighboring paramagnetic dot, where the qubit spin nucleates formation of a ferromagnetic domain. This leads to $p_0 = p_1 = \frac{3}{4}$ and thus $e = 25\%$. Another idea is to transfer the qubit information from spin to charge [3, 128, 134, 25, 56, 57]. For this, we propose to couple the qubit dot to a second (“reference”) dot [135] and discuss several possibilities how that coupling can be made spin-dependent, see also Fig 3.1. The resulting charge distribution on the double dot will then depend on the qubit spin state

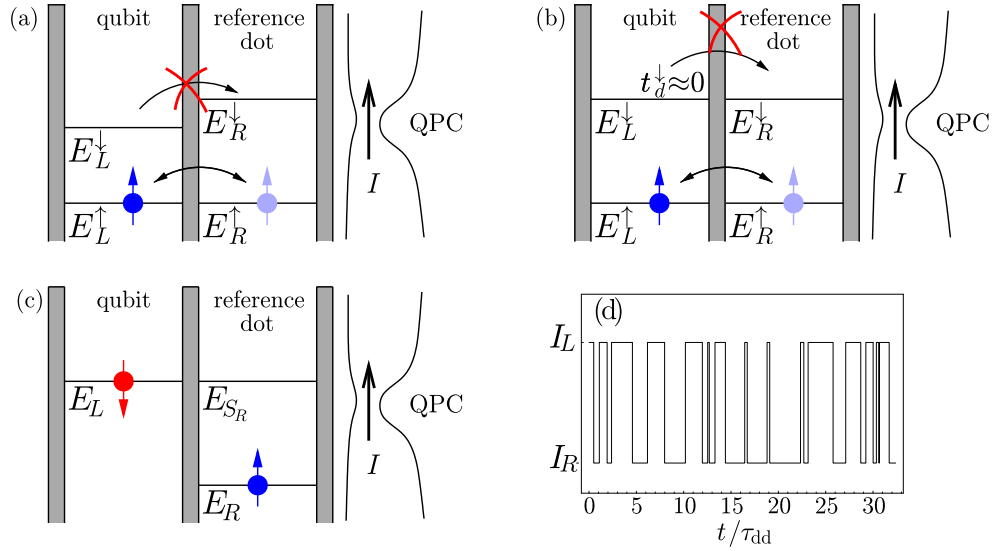


Figure 3.1: Electron spin read-out setup consisting of a double dot. The right “reference” dot is coupled capacitively to a QPC shown on the right. (a) Read out using different Zeeman splittings. For \uparrow , the electron tunnels between the two dots. For \downarrow , tunneling is suppressed by the detuning and the stationary state has a large contribution of the left dot since it has lower energy. This allows single-shot read out, i.e., $e = 100\%$. (b) Spin-dependent tunneling amplitudes, $t_d^\downarrow < t_d^\uparrow$, also enable efficient read out. (c) Read out with the singlet state. Tunneling of spin \uparrow to the reference dot is blocked due to the Pauli principle. (d) Schematic current vs. time during a single measurement. Here, τ_{dd} is the time scale for tunneling and we assume $\Gamma_{\text{tot}} > t_d$, i.e., that the tunneling events can be resolved in the current.

and can be detected by coupling the double dot to an electrometer, such as a quantum point contact (QPC) [136, 20], see Fig 3.1 (or, alternatively, a single-electron transistor [137]).

3.3.1 Read out with different Zeeman splittings.

First, we propose a setup where efficiencies up to 100% can be reached, see Fig. 3.1a. We take a double dot with different Zeeman splittings, $\Delta_z^{L,R} = E_{L,R}^\downarrow - E_{L,R}^\uparrow$, in each dot [138] and consider a single electron on the double dot. For initial qubit state $|\uparrow\rangle$, the electron can tunnel from state $|L_\uparrow\rangle \hat{=} \uparrow_1 \circ_2$

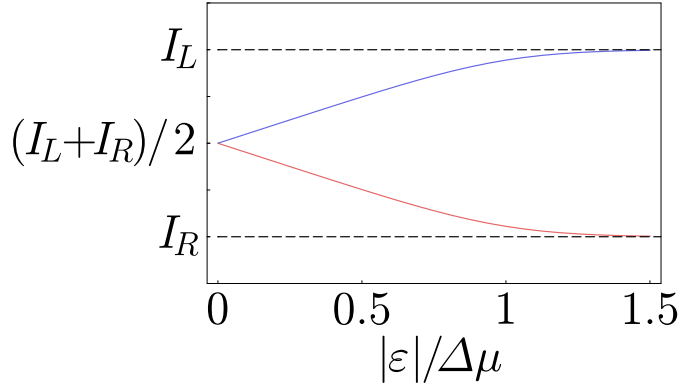


Figure 3.2: QPC current [Eq. (3.12)] as function of detuning ε where $\varepsilon > 0$ (lower curve) and $\varepsilon < 0$ (upper curve) and for small t_d . Note that for $|\varepsilon| > \Delta\mu$, the factor η [Eq. (3.10)] ensures saturation of the current at the values $I_{L,R}$.

to state $|R_\uparrow\rangle \hat{=} \bigcirc_1 \uparrow_2$ and vice versa, and analogously for qubit state $|\downarrow\rangle$. We consider time scales shorter than T_1 , thus the states with different spins are not coupled. Next, we define the detunings $\varepsilon_{\uparrow,\downarrow} = E_L^{\uparrow,\downarrow} - E_R^{\uparrow,\downarrow}$, which are different for the up and down states, $\varepsilon_\downarrow - \varepsilon_\uparrow = \Delta_z^L - \Delta_z^R \neq 0$. The stationary state of the double dot depends on $\varepsilon_{\uparrow,\downarrow}$ and so does the QPC current $\bar{I}_{\uparrow,\downarrow}$ [we show this below, see Eq. (3.12) and \bar{I}_{incoh}]. Therefore, initial states $|\uparrow\rangle$ and $|\downarrow\rangle$ can be identified through distinguishable stationary currents [129], $\bar{I}_\uparrow \neq \bar{I}_\downarrow$, thus $e = 100\%$ and single-shot read out is possible.

3.3.2 Spin-dependent tunneling

Spin-dependent tunneling provides another read-out scheme, see Fig. 3.1b, which we describe with spin-dependent tunneling amplitudes $t_d^{\uparrow,\downarrow}$. For $t_d^\downarrow \ll t_d^\uparrow$, only spin \uparrow tunnels onto the reference dot while tunneling of spin \downarrow is suppressed. We assume the same Zeeman splitting in both dots and resonance $\varepsilon = 0$. It turns out [Eq. (3.12)] that $\bar{I}_{\uparrow,\downarrow}$ depends on $t_d^{\uparrow,\downarrow}$ and thus the state of the qubit can be measured. However, the decay to the stationary state is quite slow in case the qubit is $|\downarrow\rangle$, due to the suppressed tunneling amplitude t_d^\downarrow . Since the difference in charge distribution between qubit $|\uparrow\rangle$ and $|\downarrow\rangle$ is larger at short timescales, it can thus be advantageous to measure

the time-dependent current (discussed toward the end).

3.3.3 Read out with Pauli principle

We now consider the case where the reference dot contains initially an electron in spin up ground state, see Fig. 3.1c. We assume gate voltages such that there are either two electrons on the right dot or one electron on each dot. Thus, we consider the 5 dimensional Hilbert space $|S_R\rangle \hat{=} \bigcirc_1 \bigcirc_2$, $|\uparrow\downarrow\rangle \hat{=} \bigcirc_1 \bigcirc_2$, $|\downarrow\uparrow\rangle \hat{=} \bigcirc_1 \bigcirc_2$, $|T_+\rangle \hat{=} \bigcirc_1 \bigcirc_2$, $|T_-\rangle \hat{=} \bigcirc_1 \bigcirc_2$. We define the “delocalized” singlet $|S_{LR}\rangle = (|\uparrow\downarrow\rangle - |\downarrow\uparrow\rangle)/\sqrt{2}$ and the triplet $|T_0\rangle = (|\uparrow\downarrow\rangle + |\downarrow\uparrow\rangle)/\sqrt{2}$. In the absence of tunneling, the corresponding energies are $E_{S_R} = 2\epsilon_R + U$ and $E_{S_{LR}} = E_{T_{0,\pm}} = \epsilon_L + \epsilon_R$ with charging energy U and single particle energies $\epsilon_{L,R}$. We can neglect states with two electrons on the qubit dot and the triplet states with two electrons on the reference dot, since they have a much larger energy (their admixture due to tunneling is small). We denote the state with an “extra” electron on the right dot as $|R\rangle \equiv |S_R\rangle$ with corresponding QPC current I_R . For state $|L\rangle \equiv |S_{LR}\rangle$ and for all triplet states, $|T_{0,\pm}\rangle$, the current is I_L . When tunneling is switched on and the qubit is initially in state $|\uparrow\rangle$, tunneling to the reference dot is blocked due to the Pauli exclusion principle [139]. Thus, the double dot will remain in the (stationary) state $|T_+\rangle\langle T_+|$ and the current in the quantum dot remains $\langle I \rangle = I_L$ (a so-called non-demolition measurement). On the other hand, for an initial qubit state $|\downarrow\rangle$, the initial state of the double dot is $|\downarrow\uparrow\rangle = (|T_0\rangle - |S_{LR}\rangle)/\sqrt{2}$. The contribution $|S_{LR}\rangle$ of this superposition is tunnel coupled to $|S_R\rangle$ and will decay to the stationary state $\bar{\rho}$ with corresponding QPC current \bar{I} (see below for an explicit evaluation). In contrast, the triplet contribution $|T_0\rangle$ is not tunnel-coupled to $|S_R\rangle$ due to spin conservation and does not decay. In total, the density matrix of the double dot decays into the stationary value $\frac{1}{2}(|T_0\rangle\langle T_0| + \bar{\rho})$. For $\varepsilon = 0$, the ensemble-averaged QPC current for qubit $|\downarrow\rangle$ is $\langle I \rangle = \frac{1}{2}(I_L + \bar{I}) \approx \frac{1}{4}(3I_L + I_R)$ and can thus be distinguished from I_L for qubit $|\uparrow\rangle$. However, in a single run of such a measurement, an initial qubit $|\downarrow\rangle$ decays either into $|T_0\rangle\langle T_0|$ or into $\bar{\rho}$, with 50% probability each. Since $|T_0\rangle\langle T_0|$ and $|T_+\rangle\langle T_+|$ lead to the same QPC current I_L , these two states are not distinguishable within this read-out scheme and single-shot read-out is not possible. The read out can now be described with the POVM model given above, with $|\uparrow\rangle \equiv |0\rangle$ and $|\downarrow\rangle \equiv |1\rangle$ and $A_\uparrow = I_L$; $A_\downarrow = \bar{I}$; $p_\uparrow = 1$; and $p_\downarrow = \frac{1}{2}$. Thus, the *measurement efficiency* is $e = 50\%$, i.e., to achieve a fidelity of $1 - \alpha = 99\%$, we need $n \geq 7$ read outs [132].

An analogous read out is possible if the ground state of the reference dot is a triplet, say $|RT_+\rangle \hat{=} \bigcirc_1 \bigcirc_2$ which is lower than the other triplets ($|RT_{0,-}\rangle$, $|RT_-\rangle$) due to Zeeman splitting. Again, we assume that the reference dot is initially $|\uparrow\rangle$. First, for a qubit state $|\uparrow\rangle$ and at resonance, $\varepsilon = 0$, tunneling into $|RT_+\rangle$ always occurs and $p_\uparrow = 1$. Second, the qubit state $|\downarrow\rangle$ has an increased energy by the Zeeman splitting Δ_z and is thus at resonance with $|RT_0\rangle$ (which has also an increased energy). If the double dot is not projected onto the singlet (in 50% of the cases), tunneling onto the reference dot will also occur, i.e., $p_\downarrow = \frac{1}{2}$. Thus, when one detects an additional charge on the reference dot, the initial state of the qubit is not known. We find again $e = 50\%$.

3.4 Read-out model

So far we have introduced various spin read out schemes and the corresponding measurement efficiencies. In order to evaluate the signal strength $A_0 - A_1$ for these schemes, we now calculate the stationary charge distribution $\bar{\rho}$ and QPC current \bar{I} for the case when the electron can tunnel coherently between the two dots (as a function of the detuning and the tunnel coupling). We describe the read-out setup with the Hamiltonian

$$H = H_{\text{dot}} + V_d + H_{\text{QPC}} + V. \quad (3.3)$$

Here, H_{QPC} contains the energies of the (uncoupled) Fermi leads of the QPC. Further, H_{dot} describes the double dot in the absence of tunneling, including orbital and electrostatic charging energies, $H_{\text{dot}}|n\rangle = E_n|n\rangle$. It thus contains $\varepsilon = E_L - E_R$, the detuning of the tunneling resonance. The inter-dot tunneling Hamiltonian is defined as

$$V_d = t_d(|R\rangle\langle L| + |L\rangle\langle R|). \quad (3.4)$$

(Note that for tunneling between $|S_{LR}\rangle$ and $|S_R\rangle$, t_d is $\sqrt{2}$ times the one-particle tunneling amplitude, since both states $|\uparrow\downarrow\rangle$ and $|\downarrow\uparrow\rangle$ are involved). V is a tunneling Hamiltonian describing transport through the QPC. The tunneling amplitudes, t_L^Q and t_R^Q , will be influenced by electrostatic effects, in particular by the charge distribution on the double dot. Thus, we model the measurement of the dot state via the QPC with [140, 141, 142]

$$V = \left(t_L^Q |L\rangle\langle L| + t_R^Q |R\rangle\langle R| \right) \sum (c_{\text{in}}^\dagger c_{\text{out}} + \text{h.c.}). \quad (3.5)$$

Here, c_{in}^\dagger and c_{out}^\dagger create electrons in the incoming and the outgoing leads of the QPC, where the sum is taken over all momentum and spin states. We derive the master equation for the reduced density matrix ρ of the double dot. We use standard techniques and make a Born-Markov approximation in V [107, 143]. We allow for an arbitrary inter-dot tunnel coupling, i.e., we keep V_{d} exactly, with energy splitting $E = \sqrt{4t_{\text{d}}^2 + \varepsilon^2}$ in the eigenbasis of $H_{\text{dot}} + V_{\text{d}}$. We obtain the master equation [144]

$$\dot{\rho}_L = -\dot{\rho}_R = 2t_{\text{d}} \text{Im} [\rho_{RL}], \quad (3.6)$$

$$\begin{aligned} \dot{\rho}_{RL} = & \left[it_{\text{d}} + t_{\text{d}} \frac{\Gamma_{\text{Q}} \varepsilon}{E^2} (g_{\Sigma} - 2g_0) \right] (\rho_R - \rho_L) \\ & - \frac{t_{\text{d}} \Gamma_{\text{Q}}}{\Delta\mu} - (\kappa \Gamma_{\text{Q}} + \Gamma_{\text{i}} - i\varepsilon) \rho_{RL}, \end{aligned} \quad (3.7)$$

for $\rho_n = \langle n|\rho|n\rangle$ and $\rho_{RL} = \langle R|\rho|L\rangle$. In comparison to previous work [140, 141, 142], we find an additional term, $-t_{\text{d}} \Gamma_{\text{Q}}/\Delta\mu$, which comes from treating V_{d} exactly. We find that the current through the QPC is $I_L = 2\pi\nu^2 e \Delta\mu |t_L^{\text{Q}}|^2$ for state $|L\rangle$ and analogously I_R for state $|R\rangle$, and we choose $I_L, I_R \geq 0$. Here, $\Delta\mu > 0$ is the applied bias across the QPC and ν is the DOS at the Fermi energy of the leads connecting to the QPC. We define $g_{\pm} = g(\Delta\mu \pm E)$, $g_{\Sigma} = g_+ + g_-$ and $g_0 = g(\Delta\mu)$ with $g(x) = x/\Delta\mu (e^{x/kT} - 1)$. The values $g_{\pm, \Sigma, 0}$ vanish for $\Delta\mu \pm E > kT$. In this case, the decay rate due to the current assumes the known value [140, 141, 142],

$$\Gamma_{\text{Q}} = \left(\sqrt{I_L} - \sqrt{I_R} \right)^2 / 2e. \quad (3.8)$$

Generally, the factor $\kappa = 1 + (4t_{\text{d}}^2 g_{\Sigma} + 2\varepsilon^2 g_0)/E^2$ accounts for additional relaxation/dephasing due to particle hole excitations, induced, e.g., by thermal fluctuations of the QPC current. For almost equal currents, $I_{L,R} = I (1 \pm \frac{1}{2}x)$, we have $\Gamma_{\text{Q}} = Ix^2/8e + O(x^4)$. Finally, by introducing the phenomenological rate Γ_{i} we have allowed for some intrinsic charge dephasing, which occurs on the time scale of nanoseconds [24]. For an initial state in the subspace $\{|L\rangle, |R\rangle\}$, we find the stationary solution of the double dot,

$$\begin{aligned} \bar{\rho} = & \frac{1}{2} \left(1 - \eta \frac{\varepsilon}{\Delta\mu} \right) |L\rangle\langle L| + \frac{1}{2} \left(1 + \eta \frac{\varepsilon}{\Delta\mu} \right) |R\rangle\langle R| \\ & - \eta \frac{t_{\text{d}}}{\Delta\mu} (|R\rangle\langle L| + |L\rangle\langle R|), \end{aligned} \quad (3.9)$$

where

$$\eta = \frac{\Gamma_Q}{\Gamma_Q(1 + g_\Sigma) + \Gamma_i}. \quad (3.10)$$

Positivity of $\bar{\rho}$ is satisfied since $\eta \leq \Delta\mu/E$. The time decay to $\bar{\rho}$ is described by three rates, given as the roots of $P(X) = X^3 + 2\Gamma_{\text{tot}}X^2 + (E^2 + \Gamma_{\text{tot}}^2)X + 4t_d^2[\Gamma_{\text{tot}} + \Gamma_Q(g_\Sigma - 2g_0)\varepsilon^2/E^2]$, with $\Gamma_{\text{tot}} = \kappa\Gamma_Q + \Gamma_i$. The stationary current through the QPC is given by

$$\bar{I} = \bar{\rho}_L I_L + \bar{\rho}_R I_R + 2e t_d \lambda (\Gamma_Q / \Delta\mu) \text{Re } \bar{\rho}_{\text{RL}} \quad (3.11)$$

and thus becomes

$$\bar{I} = \frac{I_L + I_R}{2} + \eta \frac{\varepsilon}{2\Delta\mu} (I_R - I_L) - \eta \lambda \frac{2e \Gamma_Q t_d^2}{\Delta\mu^2}, \quad (3.12)$$

where $\lambda = 1 - \Delta\mu(g_- - g_+)/E$. We note that η quantifies the effect of the detuning ε on the QPC current. To reach maximal sensitivity, $\eta = 1$, we need $I_R \lesssim I_L/10$ for $I \sim 1 \text{ nA}$ and $\Gamma_i \sim 10^9 \text{ s}^{-1}$. In linear response, the current becomes

$$\begin{aligned} \bar{I} = & \frac{I_L + I_R}{2} + (I_R - I_L) \frac{\varepsilon}{2E} \tanh\left(\frac{E}{2kT}\right) \left[1 - \frac{\Gamma_i \Delta\mu}{\Gamma_Q E} \tanh\left(\frac{E}{2kT}\right)\right] \\ & + e \frac{t_d^2 \Gamma_i \Delta\mu}{E^3 \cosh^2(E/kT)} \left[\sinh\left(\frac{E}{kT}\right) - \frac{E}{kT}\right] \left[1 - \frac{\Gamma_i \Delta\mu}{\Gamma_Q E} \tanh\left(\frac{E}{2kT}\right)\right] \\ & - 2e \frac{t_d^2 \Gamma_Q}{E^2} \left[1 - \frac{E}{kT \sinh(E/kT)}\right]. \end{aligned} \quad (3.13)$$

Note that the second term in Eq. (3.12) depends on ε , a property which can be used for read out, as we have discussed above. For example, for different Zeeman splittings and $\varepsilon_{\uparrow,\downarrow} = \pm\Delta\mu/2$, $\Gamma_i = 10^9 \text{ s}^{-1}$, $I_L = 1 \text{ nA}$, and $I_R = 0$, the current difference is $\bar{I}_\downarrow - \bar{I}_\uparrow = 0.4 \text{ nA}$, which reduces to 0.05 nA for $I_R = 0.5 \text{ nA}$. However, typical QPC currents currently reachable are $I_L = 10 \text{ nA}$ and $I_R = 9.9 \text{ nA}$, i.e., the relaxation of the double dot due to the QPC is suppressed, $\eta < 10^{-3}$, and other relaxation channels become important.

3.4.1 Incoherent tunneling

So far, we have discussed coherent tunneling. We can also take incoherent tunneling into account, e.g., phonon assisted tunneling, by introducing relaxation rates in Eqs. (3.6),(3.7). For example, for detailed balance rates

and neglecting coherent tunneling, we find the stationary current $\bar{I}_{\text{incoh}} = \frac{1}{2}(I_L + I_R) + \frac{1}{2}(I_R - I_L) \tanh(\varepsilon/2kT)$ (which becomes I_R for $\varepsilon > kT$). The QPC current again depends on ε and can be used for spin read out. The current can also be measured on shorter time scales as we discuss now.

3.5 Read out with time-dependent currents

Read out with time-dependent currents is possible if there is sufficient time to distinguish I_L from I_R between two tunneling events to or from the reference dot, i.e., we consider $\Gamma_{\text{tot}} > t_d$. In this incoherent regime, the tunneling from qubit to reference dot occurs with a rate W_{\uparrow} or W_{\downarrow} , depending on the qubit state, with, say, $W_{\downarrow} \ll W_{\uparrow}$. Such rates arise from spin-dependent tunneling, $t_d^{\uparrow,\downarrow}$, or from different Zeeman splittings and tuning to tunneling resonance for, say, qubit $|\uparrow\rangle$ while qubit $|\downarrow\rangle$ is off-resonant, see Figs. 3.1a and 3.1b. For read out, the electron is initially on the left dot and the QPC current is I_L . Then, if the electron tunnels onto the reference dot within time t and thus changes the QPC current to I_R , such a change would be interpreted as qubit in state $|\uparrow\rangle$, otherwise as qubit $|\downarrow\rangle$. For calculating the measurement efficiency e , we note that $p_{\uparrow} = p_0 = 1 - e^{-tW_{\uparrow}}$ and $p_{\downarrow} = p_1 = e^{-tW_{\downarrow}}$ (with this type of read out, W_{\downarrow} corresponds to a loss of the information, i.e., describes “mixing” [119]). We then maximize e by choosing a suitable t and find efficiencies $e \gtrsim 50\%$ for $W_{\uparrow}/W_{\downarrow} \gtrsim 8.75$ and $e \gtrsim 90\%$ for $W_{\uparrow}/W_{\downarrow} \gtrsim 80$.

A more involved read out is to measure the current through the QPC at different times. The current as function of time switches between the values I_L and I_R , i.e., shows telegraph noise, as sketched in Fig. 3.1d. Since the frequency of these switching events (roughly W_{\uparrow} or W_{\downarrow}) depends on the spin, the QPC noise reveals the state of the qubit. Finally, at times of the order of the spin relaxation time T_1 , the information about the qubit is lost. At each spin flip, the switching frequency changes ($W_{\uparrow} \leftrightarrow W_{\downarrow}$), which thus provides a way to measure T_1 .

3.5.1 Read-out using a single dot only

Finally, we consider the qubit dot coupled to a lead instead of a reference dot. Due to Zeeman splitting, the energy levels can be tuned such that only the qubit \downarrow (electron) can tunnel to the lead [56, 57] with rate γ_{out} (spin \uparrow electrons can tunnel only *onto* the dot). This produces a pulse in the QPC

current, whose duration must exceed t_m to be detected (given by the time-resolution of the current measurement), until a spin \uparrow electron tunnels onto the dot, with rate γ_{in} . After waiting a time t to detect such a signal, we have $p_{\uparrow} = 1$ and $e = p_{\downarrow} = e^{-t_m \gamma_{\text{in}}} (1 - e^{-t \gamma_{\text{out}}})$.

3.6 Conclusion

In conclusion, we have given the criterion when n -shot measurements are possible and have introduced the measurement efficiency e . For electron spin qubits, we have proposed several read-out schemes and have found efficiencies up to 100%, which allow single-shot read out. Other schemes, which are based on the Pauli principle (Sec. 3.3.3), have a lower efficiency, $e = 50\%$.

Chapter 4

Asymmetric Quantum Shot Noise and non-Markovian effects in Quantum Dots

We analyze the frequency-dependent noise correlation of a current through a quantum dot that is coupled to Fermi leads and is in the Coulomb blockade regime. We show that asymmetric shot noise as function of frequency shows steps and becomes super-Poissonian. This provides experimental access to quantum fluctuations. We present an exact calculation for a single dot level and a systematic calculation of the noise in lowest-order Born approximation (sequential tunneling regime) for the general case of many levels with charging interaction.

4.1 Introduction

Shot noise is a striking consequence of charge quantization and allows to characterize the transport of individual electrons [65]. The symmetry of the noise $S(\omega)$ is important: For a classical stationary system, noise (for autocorrelations) is always symmetric in the frequency ω . However, for a quantum system, noise can be asymmetric due to the non-commutativity of current operators at different times. It was recently found that such an asymmetric noise can be detected since the noise frequency ω corresponds to a quantum of energy $\hbar\omega$ which is transferred from the system to the measurement apparatus [64, 145, 146]. This means that antisymmetric quantum effects in noise

can be measured and isolated from the classical (symmetric) effects [147]. In this work, we show that striking asymmetric effects appear in the shot noise $S(\omega)$ of a quantum dot with steps as function of ω , giving a super-Poissonian Fano factor. Our analysis is based on a systematic microscopic theory which remains valid in the quantum limit, $\omega > kT$ (where a Markov approximation typically involved would not be valid). We verify our theory by exactly calculating the noise of a dot with a single level. We note that quantum dots are good candidates for an experimental test of our predictions since such systems have been studied extensively over the years, both experimentally and theoretically [148, 149, 150, 151, 116, 63].

We consider the operator I_l which describes the current in a lead l . We define the current noise,

$$S_{ll'}(\omega) = \int_{-\infty}^{\infty} dt e^{i\omega t} [\langle I_l(t)I_{l'} \rangle - \langle I_l \rangle \langle I_{l'} \rangle], \quad (4.1)$$

in terms of the (non-symmetrized) correlation function, $\langle I_l(t)I_{l'} \rangle = \text{Tr } I_l(t)I_{l'}\bar{\rho}$. Here, $\bar{\rho}$ is the stationary density matrix (of the full quantum system). Note that $I_l(t)I_{l'}$ is not a Hermitian operator and thus does not correspond to a classical observable. How should we interpret Eq. (4.1)? On the one hand, one can avoid the non-Hermitian operator by arguing heuristically that Eq. (4.1) is “unphysical” and by instead considering the correlation function in terms of the symmetrized operator $\frac{1}{2}[I_l(t)I_{l'} + I_{l'}I_l(t)]$ [59]. One then obtains the symmetrized noise, $S_{ll'}^{\text{sym}}(\omega) = \frac{1}{2}[S_{ll'}(\omega) + S_{l'l}(-\omega)]$. For $l = l'$, this noise does not depend on the sign of ω . This corresponds to a measurement apparatus [64, 145, 146] which does not discriminate between absorption and emission of energy by the system, and thus cannot detect all noise characteristics. On the other hand, we have $\langle I_l(-t)I_{l'} \rangle = \langle I_{l'}(t)I_l \rangle^*$ and thus $S_{ll'}(\omega) = S_{l'l}(\omega)^*$, since I_l is Hermitian and $\bar{\rho}$ stationary. Thus, $S_{ll}(\omega)$ is a real quantity which can be regarded as an observable. Indeed, there are setups, where $S_{ll}(\omega)$ can be accessed experimentally [64, 145, 146]. This justifies to consider asymmetric quantum noise [Eq. (4.1)] as we do in the following.

4.2 Quantum dots

To illustrate the presence of asymmetric shot noise contributions due to quantum effects, we consider now a concrete system of a quantum dot in the

Coulomb blockade regime [18], coupled to Fermi leads $l = 1, 2, \dots$ at chemical potentials μ_l . When only a single dot level is present, the noise can be calculated even exactly [149] (see below). This is however not possible for systems with many levels and charging interaction, for which we now develop a perturbative approach. We assume weak coupling such that current and noise are dominated by the sequential tunneling (ST) contributions, valid for $kT > \gamma$ with temperature T and level width γ . We model the combined system with the Hamiltonian $H = H_{\text{lead}} + H_{\text{dot}} + H_T$, which describes leads, dot, and the tunnel coupling between leads and dot, resp., and with $H_0 = H_{\text{lead}} + H_{\text{dot}}$. We let $H_{\text{lead}} = \sum_{lk\sigma} \epsilon_{lk} c_{lk\sigma}^\dagger c_{lk\sigma}$, where $c_{lk\sigma}^\dagger$ creates an electron in lead l with orbital state k , spin σ , and energy ϵ_{lk} . The electronic dot states $|n\rangle$ are described by $H_{\text{dot}}|n\rangle = E_n|n\rangle$, including charging and interaction energies. We use the standard tunneling Hamiltonian $H_T = \sum_{lpk\sigma} t_{lp}^\sigma c_{lk\sigma}^\dagger d_{p\sigma} + \text{H.c.}$, with tunneling amplitude t_{lp}^σ and where $d_{p\sigma}^\dagger$ creates an electron on the dot with orbital state p and spin σ . The state of the combined system is given by the full density matrix ρ , while the electronic states of the dot are described by the reduced density matrix, $\rho = \text{Tr}_R \rho$, where the trace is taken over the leads. We assume that at some initial time t_0 the full density matrix factorizes, $\rho(t_0) = \rho^0 \rho_R^0$, with the equilibrium density matrix of the leads, ρ_R^0 . From the von Neumann equation $\dot{\rho} = -i[H, \rho]$ one finds [105] the generalized master equation for the reduced density matrix, $\dot{\rho}_D(t) = -iL_D \rho(t) - \int_{t_0}^t dt' \hat{M}(t') \rho(t-t')$, where the kernel \hat{M} is the self-energy superoperator. Since we consider the weak coupling regime, we proceed with a systematic lowest-order expansion in H_T . We obtain $\hat{M}(\tau) = \text{Tr}_R L_T e^{-iL_0\tau} L_T \rho_R^0$, where we define the superoperators $L_D X = [H_{\text{dot}}, X]$, $L_0 X = [H_0, X]$, and $L_T X = [H_T, X]$. In the following, we work in the Laplace space, $f(t) \mapsto f(\omega) = \int_0^\infty dt e^{i\omega t} f(t)$ (we take $\text{Im } \omega > 0$ but our results remain well-defined for $\text{Im } \omega \rightarrow 0$). Then, the time evolution of ρ reads

$$-\rho(t_0) - i\omega \rho(\omega) = \mathcal{M}(\omega) \rho(\omega), \quad (4.2)$$

with $\mathcal{M}(\omega) = -iL_D - \hat{M}(\omega)$ and with the lower boundary of the Laplace transformation shifted to t_0 . We take $t_0 \rightarrow -\infty$ and assume that the system has relaxed at the much later time $t = 0$ into its stationary state $\bar{\rho} = \rho(0) = \lim_{\omega \rightarrow 0} (-i\omega) \rho(\omega)$. We multiply Eq. (4.2) by $-i\omega$, take $\omega \rightarrow 0$, and find the equation $\mathcal{M}(0) \bar{\rho} = 0$ from which we get $\bar{\rho}$.

4.3 Current

We calculate the current I_l flowing from the dot into lead l and vice versa. The current operators are $I_l(t) = (-1)^l e \dot{q}_l(t) = (-1)^l i e [H_T, q_l(t)]$ where $q_l = \sum_{k\sigma} c_{lk\sigma}^\dagger c_{lk\sigma}$ is the number of electrons in lead l . We choose the sign of I_l such that $\langle I_1 \rangle = \langle I_2 \rangle$ in the case of two leads. We now introduce the projectors $P = \rho_{\text{R}}^0 \text{Tr}_{\text{R}}$ and $Q = \mathbb{1} - P$ with the properties $PL_T P = 0 = PI_l P$ and $PL_0 = L_0 P$. We evaluate $\langle I_l \rangle$ by inserting $P + Q = \mathbb{1}$ and find $\langle I_l(t) \rangle = \text{Tr} I_l Q e^{-i(L_0 + L_T)(t-t_0)} \rho(t_0) = -i \text{Tr} I_l \int_{t_0}^t dt' Q e^{-iL_0(t-t')} L_T P \rho(t') + O(H_T^3)$. This motivates introducing the following superoperators, $W_l^f = W_l^> + W_l^<$ with $W_l^>(\tau) = -i \text{Tr}_{\text{R}} I_l e^{-iL_0 \tau} L_T \rho_{\text{R}}^0$ and $W_l^<(\tau) = -i \text{Tr}_{\text{R}} L_T e^{-iL_0 \tau} I_l \rho_{\text{R}}^0$, and $W_{l,l'}(\tau) = \text{Tr}_{\text{R}} I_l e^{-iL_0 \tau} I_{l'} \rho_{\text{R}}^0$. Note that these superoperators act only on the dot space, which considerably simplifies further evaluations. In the ST regime, the current is

$$\langle I_l \rangle = \text{Tr}_{\text{D}} W_l^f(\omega=0) \bar{\rho}. \quad (4.3)$$

This indicates that the superoperator W_l^f accounts for the current through the dot. This interpretation becomes very apparent if we keep track of the number of electrons in the leads, q_l , by including them into the reduced density matrix and using the canonical ensemble for the leads. We then find the identity $W_l^f = (-1)^l e [q_l, \mathcal{M}]$ for arbitrary frequency ω , which in Markovian approximation can be interpreted as follows. The superoperator for the master equation corresponds to $\mathcal{M}(\omega=0) \sim (\mathcal{U}(dt) - 1)/dt$, where \mathcal{U} stands for the time evolution of the system density matrix. Thus, $W_l^f(\omega=0) \sim (-1)^l e [q_l, \mathcal{U}(dt)]/dt \sim (-1)^l e \dot{q}_l(t)$, which is just our definition of the current.

4.4 Quantum shot noise

Next, we evaluate the noise [Eq. (4.1)] in lowest order in H_T but without any further approximation. It is sufficient to consider $t > 0$, since $\langle I_l(-t) I_{l'} \rangle = \langle I_{l'}(t) I_l \rangle^*$. Using again $P + Q = \mathbb{1}$ we get $\langle I_l(t) I_{l'} \rangle = \text{Tr} I_l Q e^{-iL t} P I_{l'} Q \bar{\rho} + \text{Tr} I_l Q e^{-iL t} Q I_{l'} P \bar{\rho}$, while we neglect the higher-order term $\text{Tr} I_l Q e^{-iL t} Q I_{l'} Q \bar{\rho}$ in H_T . The goal is to factor out one of the following expressions. First, we expand $Q e^{-iL Q t} Q = Q e^{-iL_0 t} Q + O(H_T)$ to leading order. Second, we evaluate the conditional time evolution $\rho_{\text{D}}^c(t) := \text{Tr}_{\text{R}} e^{-iL t} \rho_{\text{R}}^0$. We find that ρ_{D}^c is the formal solution of Eq. (4.2) with initial value $\mathbb{1}$, thus $\rho_{\text{D}}^c(\omega) = -[i\omega + \mathcal{M}(\omega)]^{-1}$ [152]. Finally, we use $\text{Tr}_{\text{R}} I_l Q e^{-iL t} \rho_{\text{R}}^0 = \int_0^t dt' W_l^>(t-t') \rho_{\text{D}}^c(t')$

and $\text{Tr}_R I_l Q e^{-iLt} Q I_{l'} \rho_R^0 = W_{l,l'}(t) + \int_0^t dt' \int_0^{t'} dt'' W_l^>(t-t') \rho_D^c(t'-t'') W_{l'}^<(t'')$. We obtain the noise correlation in ST regime,

$$\begin{aligned} S_{ll'}(\omega) = & 2\text{Tr}_D \left\{ W_l^f(\omega) \rho_D^c(\omega) [W_{l'}^>(0) + W_{l'}^<(\omega)] + \right. \\ & + W_{l'}^f(-\omega) \rho_D^c(-\omega) [\overline{W}_l^>(0) + \overline{W}_l^<(-\omega)] \\ & \left. + W_{l,l'}(\omega) + \overline{W}_{l',l}(-\omega) \right\} \bar{\rho}. \end{aligned} \quad (4.4)$$

Here, ω is real and the limit $\omega \rightarrow 0$ is well behaved [the $\delta(\omega)$ contribution is cancelled by $\langle I_l \rangle \langle I_{l'} \rangle$ in Eq. (4.1)]. For a superoperator \mathcal{S} , we have defined $\overline{\mathcal{S}}$ such that $(\mathcal{S}A)^\dagger = \overline{\mathcal{S}}A^\dagger$, thus $\mathcal{S}_{bc|nm} := \langle b | (\mathcal{S}|n\rangle\langle m|) |c\rangle = (\overline{\mathcal{S}}_{cb|mn})^*$, and $\overline{\mathcal{S}}(\omega)A = \int_0^\infty dt e^{i\omega t} [\mathcal{S}(t)A]^\dagger$.

For deriving Eqs. (4.3)-(4.4), we have made no Markov approximation where we would evaluate $\hat{M}(t)e^{itL_0}$ at $\omega = 0$ and equivalently for the other superoperators [153]. We note that for the current [Eq. (4.3)], \mathcal{M} and W_l^f are both evaluated at $\omega = 0$, thus the stationary current does not contain non-Markovian effects. We now show how the Markov approximation changes the noise. We obtain for the noise correlator,

$$\begin{aligned} S_{ll'}^{\text{Mkov}}(\omega) = & 2\text{Tr}_D \left[-W_l^f(i\omega + \mathcal{M})^{-1} W_{l'}^f \right. \\ & \left. - W_{l'}^f(-i\omega + \mathcal{M})^{-1} W_l^f + W_{l,l'} + \overline{W}_{l',l} \right] \bar{\rho}. \end{aligned} \quad (4.5)$$

Note that $(i\omega + \mathcal{M})^{-1}$ corresponds to $e^{\mathcal{M}t}$ in time space, which transforms a given initial system state $\rho(t_i)$ to the state at a later time, $\rho(t_i+t) = e^{\mathcal{M}t}\rho(t_i)$, and is thus called conditional time evolution. Now, the first term in Eq. (4.5) can be interpreted by reading from right to left as follows. After equilibration, the dot is in the stationary state $\bar{\rho}$, then an electron tunnels to/from lead l' and the dot is in state proportional to $W_{l'}^f \bar{\rho}$, the state now evolves for a time t and finally an electron tunnels to/from lead l . The second term in Eq. (4.5) arises from $t < 0$ and the third and the fourth term is due to the instantaneous correlation of a single electron with itself, i.e., corresponds to shot noise. We stress that the Markov approximation changes the noise, which for $l = l'$ becomes symmetrized, $S_{ll}^{\text{Mkov}}(\omega) = S_{ll}^{\text{Mkov}}(-\omega)$ [154]. In particular, the antisymmetric noise contribution showing pure quantum effects cannot be obtained in the Markov approximation. We can decompose the noise, $S_{ll} = S_{ll}^{\text{Mkov}} + S_{ll}^{\text{Q, sym}} + S_{ll}^{\text{Q, antisym}}$, where the antisymmetric part, $S_{ll}^{\text{Q, antisym}}$, is purely

due to quantum effects, while the symmetric part consists of a Markovian and a non-Markovian contribution.

We now return to the exact expression of the noise in Born approximation [Eq. (4.4)] and explicitly calculate the matrix elements of the various superoperators,

$$-\hat{M}(t)e^{itL_0}\rho = \sum_l (G_+^l\rho - g_+^l\rho) + \text{h.c.}, \quad (4.6)$$

$$W_l^<(t)e^{itL_0} = (-1)^l e(G_-^l - g_-^l), \quad (4.7)$$

$$W_l^>(t)e^{itL_0} = (-1)^l e(\tilde{G}_-^l + g_-^l), \quad (4.8)$$

$$W_{l,l'}(t)e^{itL_0} = \delta_{ll'} e^2 g_+^l, \quad (4.9)$$

with $G_\pm^l = G_\pm^{l,\text{out}}(t) \pm G_\pm^{l,\text{in}}(t)$ and $g_\pm^l = \sum_{bn} |b\rangle\langle n| \text{Tr}_D \{ G_\pm^l |n\rangle\langle b| \}$ [155]. We define $t_{nm}^{l\sigma} = \sqrt{2\pi\nu_{l\sigma}} \sum_p t_{lp}^\sigma \langle n|d_{p\sigma}|m\rangle$, with spin dependent density of states $\nu_{l\sigma}$ in lead l . The matrix elements of the remaining superoperators are

$$G_{bc|nm}^{l,\text{in}}(\omega) = \sum_\sigma \frac{t_{mc}^{l\sigma} t_{nb}^{l\sigma*}}{2} \left(f_l(\Delta_{bn} - \omega) + \frac{ip_{bn}^+}{\pi} \right), \quad (4.10)$$

$$G_{bc|nm}^{l,\text{out}}(\omega) = \sum_\sigma \frac{t_{cm}^{l\sigma*} t_{bn}^{l\sigma}}{2} \left(1 - f_l(\Delta_{nb} + \omega) + \frac{ip_{nb}^-}{\pi} \right), \quad (4.11)$$

with $\Delta_{bn} = E_b - E_n$, and $p_{bn}^\pm = \log\{2\pi kT/[(1 \mp 1)\epsilon_c/2 \pm \Delta_{bn} - \omega]\} + \text{Re}\psi[\frac{1}{2} + i(\Delta_{bn} \mp \omega - \mu_l)/2\pi kT]$. Here, ψ is the digamma function. The terms p_{bn}^\pm arise from the principal values $\mathcal{P} \int_0^\infty d\epsilon f_l(\epsilon)/(\epsilon - \Delta_{bn} + \omega)$ and $\mathcal{P} \int_0^{\epsilon_c} d\epsilon [1 - f_l(\epsilon)]/(\Delta_{nb} - \epsilon + \omega)$ with bandwidth cutoff ϵ_c . If we neglect ω with respect to the large energies Δ_{bn} and $\epsilon_c - \Delta_{nb}$, the first term of p^\pm (and thus ϵ_c) drops out in $S_{ll'}(\omega)$. We note that the contribution corresponding to Eq. (4.9) has been calculated for the symmetrized noise of a single electron transistor with a continuous spectrum, using a phenomenological Langevin approach [156]. With these results, Eqs. (4.4) and (4.6)-(4.11), it is straightforward to find $S_{ll'}(\omega)$ for an arbitrary dot spectrum; one only needs to evaluate simple algebraic expressions.

We now identify the regime where the asymmetric noise properties become most apparent. Asymmetries arise from the ω dependence of Eqs. (4.10)-(4.11), i.e., are most prominent for $|\omega| > kT$. In this regime, the Markov approximation breaks down [153] and noise probes non-Markovian

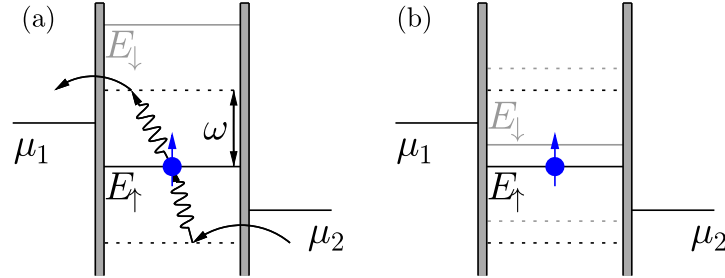


Figure 4.1: Quantum dot coupled to two leads and in the sequential tunneling regime. (a) Large Zeeman splitting, $\Delta_z > \Delta\mu + \omega$. When the dot is empty and $\omega \geq E_\uparrow - \mu_2$, an electron from lead 2 absorbs energy ω and tunnels for a short time onto the dot, contributing to the noise S_{22} . Similarly, for $\omega > \mu_1 - E_\uparrow$, the electron on the dot can tunnel into lead 1, contributing to S_{11} . (b) Smaller Zeeman splitting, here $\Delta_z = \Delta\mu/4$. The noise in this regime is shown in Fig. 4.2 (solid line).

effects. Further, since the ST regime is valid for $kT > |t|^2$, we have $\omega > |t|^2$. Thus, the conditional time evolution becomes $\rho_D^c(\omega) \approx i/\omega$, since $\mathcal{M}(\omega) \sim t^2$. For the noise [Eq. (4.4)] only the two last terms are relevant, since they are of order t^2 while the other terms are of order t^4/ω and can be neglected. Less formally, this is because multiple tunneling processes [described by $\rho_D^c(\omega)$] do not occur on the short time scales corresponding to large ω . Thus, only the individual (uncorrelated) tunneling events contribute, leading to shot noise.

4.5 Asymmetric steps in shot noise

Let us now consider a specific case, see Fig. 4.1, where a dot is coupled to two leads $l = 1, 2$ and a voltage bias $\Delta\mu = \mu_1 - \mu_2$ is applied. We assume single energy level spacing and Coulomb charging energy larger than temperature, bias, and noise frequency. We consider the dot states $|0\rangle$, with an even number of electrons and state $|\sigma\rangle$ where an electron with spin $\sigma = \uparrow, \downarrow$ is added to the dot [157]. For an applied magnetic field B , the Zeeman splitting is $\Delta_z = g\mu_B B = E_\downarrow - E_\uparrow > 0$. We consider the ST regime, $\mu_1 > E_\uparrow > \mu_2$, and define the tunneling rates $\gamma_l^\sigma = |t_{0\sigma}^{l\sigma}|^2$.

4.5.1 Quantum dot with single level

First, we assume a large Zeeman splitting such that only the spin ground state $|\uparrow\rangle$ is relevant, see Fig. 4.1(a), and we omit the index \uparrow . Since in this regime only one dot level is involved, there are no charging effects between different levels. Thus, $H_{\text{dot}} = E_{\uparrow} d^{\dagger} d$ and so the full Hamiltonian H is bilinear and can be solved exactly. The symmetrized noise was calculated for this system and discussed for $\omega = 0$ [149]. We now calculate the asymmetric noise for finite ω exactly. For this, we solve the Heisenberg equations for $d(t)$ and $c_{lk}(t)$ and evaluate the current operator, $I_l(t)/e(-1)^l = \sum_{kl'k''} [j_{k'} c_{l'k'}^{\dagger} c_{lk} + \text{H.c.}] + \sum_{l'k'l''k''} (\gamma_l/|t_l|^2) j_{k'} j_{k''}^* c_{l'k'}^{\dagger} c_{l''k''}$. Here, the lead operators c_{lk} are evaluated at time t_0 (i.e., when the leads are at equilibrium) and we have defined $j_{k'} = i t_l^* t_{l'} e^{i(\epsilon_{l'k'} - \epsilon_{lk})(t-t_0)} / (\epsilon_{l'k'} - E_{\uparrow} - i\gamma)$ and $\gamma = (\gamma_1 + \gamma_2)/2$. Now we insert this into Eq. (4.1) and readily obtain the asymmetric noise, containing all quantum effects. We consider the coherent non-perturbative regime of strong coupling to the leads in the quantum limit of large frequencies, $\omega > \gamma > kT$. The shot noise becomes

$$S_{ll}^a(\omega) = \sum_{l', \pm} \frac{\pm \gamma_1 \gamma_{l'}}{2\pi\gamma} \theta(\omega \pm \mu_{l'} \mp \mu_l) [h(\mu_{l'}) - h(\mu_l \mp \omega)], \quad (4.12)$$

where $h(\epsilon) = \arctan[(\epsilon - E_{\uparrow})/\gamma]$. Note that the noise shows steps at $\omega = \pm|E_{\uparrow} - \mu_l|$ with width γ [158]. Furthermore, for $\omega > |E_{\uparrow} - \mu_l|, \Delta\mu$, the noise is asymmetric and saturates at $S_{ll}^a(\omega) = e^2 \gamma_l$, while $S_{ll}^a(-\omega) = 0$.

Let us now return to the ST regime $kT > \gamma$. For large frequencies, $\omega > \gamma$, we find the (asymmetric) shot noise

$$S_{ll}^a(\omega) = \sum_{l', \pm} \frac{\gamma_l \gamma_{l'}}{2\gamma} [\delta_{1, \mp 1} \pm f_{l'}(E_{\uparrow})] [\delta_{1, \pm 1} \mp f_l(E_{\uparrow} \pm \omega)]. \quad (4.13)$$

We can now compare this result [Eq. (4.13)] with the noise in our systematic lowest order expansion. Indeed, in this regime, the result from Eq. (4.4) agrees with Eq. (4.13). Again, the noise shows a pronounced asymmetry. For simplicity, we take $\omega > \Delta\mu + kT$ (thus, also $\omega > \gamma_l$) such that $f_l(E_{\uparrow} + \omega) = 0$ and $f_l(E_{\uparrow} - \omega) = 1$, leaving $f_l(E_{\uparrow})$ unrestricted. In this case, the (asymmetric) shot noise is

$$S_{ll}^a(\omega) = e^2 \gamma_l \quad (4.14)$$

whereas $S_{ll}^a(-\omega) = S_{12}^a(\pm\omega) = 0$; this is the same result as we have found for strong coupling. The interpretation is that for $S_{ll}^a(-\omega)$ the detector absorbs

energy ω , which, however, cannot be provided by any tunneling process. On the other hand, for $S_{ll}^a(\omega)$ the detector provides energy ω . Thus, if the dot is empty, an electron with energy $E_{\uparrow} - \omega$ can tunnel from the Fermi sea l into the dot, and, if the dot is filled, an electron can tunnel from the dot into an unoccupied lead state of energy $E_{\uparrow} + \omega$, see Fig. 4.1(a). In both cases, the tunneling occurs with rate γ_l and thus the contribution to the autocorrelation is $e^2\gamma_l\delta(t)$. Note that for $|E_{\uparrow} - \mu_l| > kT$, the noise is $S_{11}^a(\omega) = e\langle I \rangle (\gamma_1 + \gamma_2)/\gamma_2$. Thus, the frequency dependent Fano factor, $F_{11}(\omega) = S_{11}(\omega)/e\langle I \rangle$, is 2 for large ω and $\gamma_1 = \gamma_2$, and can even become larger for $\gamma_1 > \gamma_2$, in contrast to the Markovian case where we find it to be 1. Thus, we find that the quantum shot noise is *super-Poissonian*. Moreover, away from the ST regime, say for $E_{\uparrow} + kT > \mu_l$, the dot remains always in state $|0\rangle$ and only a small (higher-order in H_T) cotunneling current $\langle I \rangle$ flows through the dot [63]. However, the noise can still be of lower order, it is $S_{ll}^a(\omega) = e^2\gamma_l f_l(E_{\uparrow} - \omega)$ for large $|\omega|$, resulting in a large Fano factor $F_{ll}(\omega)$.

Finally, in Markov approximation the noise [Eq. (4.5)] is $S_{ll}^{\text{Mkv},a}(\omega) = e^2\gamma_1\gamma_2/(\gamma_1 + \gamma_2) \{1 - 2\gamma_1\gamma_2/[\omega^2 + (\gamma_1 + \gamma_2)^2]\}$, for $|E_{\uparrow} - \mu_l| > kT$, in accordance with [150]. We point out that $S_{11}^{\text{Mkv},a}(\omega) = S_{22}^{\text{Mkv},a}(\omega)$ is not generally true; it holds only if either $kT < \Delta\mu$ or if $\omega = 0$. Now, for large $|\omega|$, the noise is Poissonian, $e^2\gamma_1\gamma_2/(\gamma_1 + \gamma_2) = e\langle I \rangle$, which can be interpreted as follows. The electrons with charge e tunnel onto the dot with rate γ_1 , leading to a shot noise contribution of $e^2\gamma_1\delta(t)$. This can only occur if the dot is empty, reducing noise with a probability factor $\gamma_2/(\gamma_1 + \gamma_2)$. However, the energy transfer to or from the detector is not taken into account in the Markovian approximation S_{ll}^{Mkv} .

4.5.2 Quantum dot with two and more levels

Second, we consider the regime where the state $|\downarrow\rangle$ becomes relevant and charging interaction enters (here no exact solution is available). Within the Markov approximation and neglecting temperature effects, this regime corresponds to $\mu_1 > E_{\uparrow,\downarrow} > \mu_2$ with $f_l(E_{\uparrow}) = f_l(E_{\downarrow}) = \delta_{l1}$, see Fig. 4.1(b). If tunneling out of the dot is spin-independent, $\gamma_2 = \gamma_2^{\uparrow} = \gamma_2^{\downarrow}$, this system is equivalent to the case discussed above, but with an increased rate for tunneling onto the dot, replacing $\gamma_1 \rightarrow \gamma_1^{\uparrow} + \gamma_1^{\downarrow}$. The noise ($S_{ll}^{\text{Mkv},b}$) is given by $S_{ll}^{\text{Mkv},a}$ after this replacement. We plot the noise in Markov approximation, see the dotted line in Fig. 4.2, whose single feature is a dip near $\omega = 0$, which

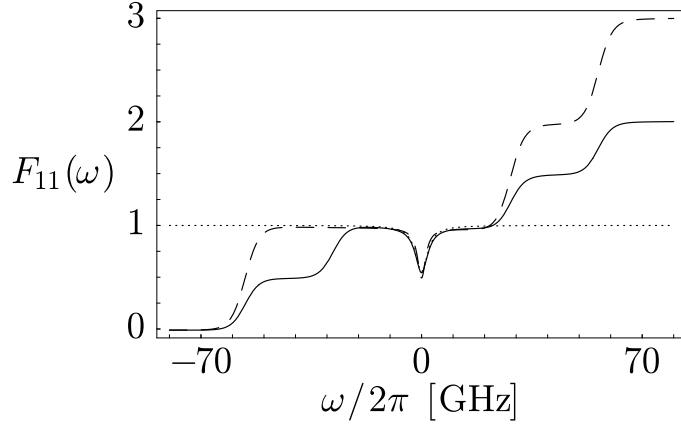


Figure 4.2: The Fano factor $F_{11}(\omega) = S_{11}(\omega)/e\langle I \rangle$ in the shot noise regime $\Delta\mu > kT$ as function of noise frequency ω . (Asymmetric noise at frequencies up to 90 GHz has been measured [159].) We consider $T = 100$ mK, $\Delta\mu/e = 460$ μ V, $E_{\uparrow} = (\mu_1 + \mu_2)/2$, $\gamma_1 = \gamma_2 = 5 \times 10^9$ s $^{-1}$, and $g = 2$. We use the full expression for the noise S_{11}^b [Eq. (4.4)] (solid line) and within Markov approximation, $S_{11}^{b,\text{Mkov}}$, (dotted line), for $B = 1$ T [see Fig. 4.1(b)], thus $\Delta_z = \Delta\mu/4$ and $\langle I \rangle = 530$ pA. Note that the steps disappear when the noise S_{11}^b is symmetrized (some features remain for $\gamma_1 \neq \gamma_2$). We also show S_{11}^c (dashed line), being strongly asymmetric, where $B = 3$ T, $\Delta_z = 3\Delta\mu/4$, and $\langle I \rangle = 400$ pA. The dip near $\omega = 0$ is due to the charging effect of the dot, while the steps arise from additional transitions for increasing ω , see text.

is due the charging effect of the dot and described by a Lorentzian. Without Markov approximation, we have the additional energy scale ω which leads to new features. Now, two regimes are relevant. We consider again a small Zeeman splitting such that $\mu_1 > E_{\uparrow,\downarrow} > \mu_2$ and $f_l(E_{\uparrow}) \approx f_l(E_{\downarrow})$. We plot the noise $S_{11}^b(\omega)$ in Fig. 4.2 (solid line). For increasing ω , more energy is available and more tunneling processes are allowed. Namely, if $\omega \geq -(\mu_1 - E_{\uparrow})$, an electron with spin \uparrow from lead 1 can emit energy ω and tunnel onto the dot, and if $\omega \geq \mu_1 - E_{\uparrow}$, an electron on the dot with spin \uparrow can absorb energy ω and tunnel into lead 1. Analogous processes occur for spin \downarrow . Thus, the noise S_{11}^b shows four steps at $\omega_i = \pm(\mu_1 - E_{\uparrow,\downarrow})$, corresponding to the dashed lines in Fig. 4.1(b). These steps are broadened due to finite γ_l and temperature, and for small γ_l the step is $\propto \tanh[(\omega - \omega_i)/2kT]$. The height of the steps changes for spin-dependent tunneling, $\gamma_l^{\uparrow} \neq \gamma_l^{\downarrow}$. For large $|\omega|$, such that

$f_l(E_\sigma + |\omega|) = 0$ and $f_l(E_\sigma - |\omega|) = 1$, the noise vanishes for $\omega < 0$ while for $\omega > 0$ it saturates at

$$S_{ll}^b(\omega) = 2e^2\gamma_l \frac{\gamma_1 + \gamma_2}{\gamma_1[1 + f_1(E_\uparrow)] + \gamma_2[1 + f_2(E_\uparrow)]}. \quad (4.15)$$

Next, we consider an intermediate Zeeman splitting, $E_\downarrow > \mu_1 + kT$. In this regime (c), the dot is either in state $|0\rangle$ or $|\uparrow\rangle$, while the state $|\downarrow\rangle$ is never occupied and so no additional tunneling process occurs for $\omega \geq -(E_\downarrow - \mu_1)$. Thus, the steps in the noise are at $\omega = \pm(\mu_1 - E_\uparrow)$ and at $\omega = E_\downarrow - \mu_1$, see Fig. 4.2 (dashed line). For large ω , the noise saturates at

$$S_{ll}^c(\omega) = e^2 \sum_{\nu=1,2} \gamma_\nu^\uparrow \frac{\gamma_l^\uparrow + \gamma_l^\downarrow[1 - f_\nu(E_\uparrow)]}{\gamma_1^\uparrow + \gamma_2^\uparrow}. \quad (4.16)$$

Here, we have allowed for spin-dependent tunneling. If we exclude the contributions involving state $|\downarrow\rangle$ by setting $\gamma_l^\downarrow = 0$, we recover Eq. (4.14). Generally, we see that the noise $S_{ll}(\omega)$ of a quantum dot consists of a series of steps and is monotonically increasing, apart from features near $\omega = 0$. We stress that the highly asymmetric $S_{ll}(\omega)$ can be observed with an appropriate measurement apparatus [64, 145, 146]. For sufficiently large $|\omega|$, the antisymmetric contribution becomes $\frac{1}{2}[S_{ll}(\omega) - S_{ll}(-\omega)] = \frac{1}{2}\text{sign}(\omega)S_{ll}(|\omega|)$ and is given by Eqs. (4.13)-(4.16).

4.6 Conclusion

In this chapter, we have derived the asymmetric shot noise of a quantum dot exactly for a single dot level and in the weak coupling regime for many dot levels. We have shown that the noise exhibits striking asymmetric and super-Poissonian effects in the quantum limit, see Fig. 4.2. In particular, the noise shows steps a function of frequency, with step positions depending on the bias and on the level spectrum. Since these parameters can be determined in independent transport measurements, this allows a prediction of shot noise features for a given experimental implementation. These features can then be accessed in a realistic experiment and the quantum fluctuations beyond the classical limit can be measured.

Chapter 5

Optical Detection of Single-Electron Spin Decoherence in a Quantum Dot

We propose a method based on optically detected magnetic resonance (ODMR) to measure the decoherence time T_2 of a single electron spin in a semiconductor quantum dot. The electron spin resonance (ESR) of a single excess electron on a quantum dot is probed by circularly polarized laser excitation. Due to Pauli blocking, optical excitation is only possible for one of the electron spin states. The photoluminescence is modulated due to the ESR which enables the measurement of electron spin decoherence. We study different possible schemes for such an ODMR setup.

5.1 Introduction

As we have explained in chapter 1, experimental measurement of the T_2 time of single spins in quantum dots are highly desirable. In chapter 2 we have proposed a setup how T_2 and the Rabi oscillations of the spin can be accessed via current measurements. An alternative method to access quantum dots are optical measurement. Recent optical experiments have even demonstrated the coherent control and the detection of *excitonic* states of single quantum dots [161]. Is it then possible to measure the T_2 time of a single *electron* spin in a quantum dot using optical methods? However, this has turned out to be an intricate problem. This is mainly due to the interaction of the electron and

the hole inside an exciton.¹ The electron and hole spin are decoupled only if the hole spin couples (via spin-orbit interaction) stronger to the environment than to the electron spin. Recent experiments, measuring Faraday rotation, have suggested that this does not apply to excitons in quantum dots [162]. Alternatively, if electron-hole pairs are excited inside the barrier material of a quantum dot heterostructure, the carriers diffuse after their creation to the dots and are captured inside them within typically tens of ps [163, 164]. By that time, electron and hole spins have decoupled. In such an experiment, the Hanle effect would allow the measurement of electron spin decoherence. However, this approach has not yet given conclusive results for T_2 [165].

What is a promising approach to measure the electron spin decoherence time T_2 by optical methods? For this, initially some coherence of the electron spin must be produced, preferably in the absence of holes. This can be done using ESR. The coherence decays and, after some time, the remaining coherence is measured optically. This implies using ODMR. Such ODMR schemes have been applied to single nitrogen-vacancy centers in diamond [166]. For quantum dots, ODMR has recently been applied to electrons and holes in CdSe dots [167] and to excitons in InAs/GaAs dots [168]. While these two experiments have not considered single spin coherence, the feasibility of the combination of ESR and optical methods in quantum dot experiments has been demonstrated.

In this chapter, we we make use of Pauli blocking of exciton creation [169] in an ODMR setup. We show that the linewidth of the photoluminescence as function of the ESR field frequency provides a lower bound on T_2 . Further, if pulsed laser and cw ESR excitation is applied, electron spin Rabi oscillations can be detected via the photoluminescence.

5.2 Charged excitons in quantum dots

We consider quantum dots which confine electrons as well as holes (type I dots). We assume a ground state where the dot is charged with one single electron. This can be achieved, e.g., by n-doping [170] or by electrical injection [171]. Such a single electron state can be optically excited, which leads

¹Alternatively, one can measure T_2 via currents through quantum dots in an ESR field, see Chapter 2. However, using an optical detection scheme there is no need for contacting dots with current leads (thus reducing decoherence) and one can benefit from the high sensitivity of photodetectors.

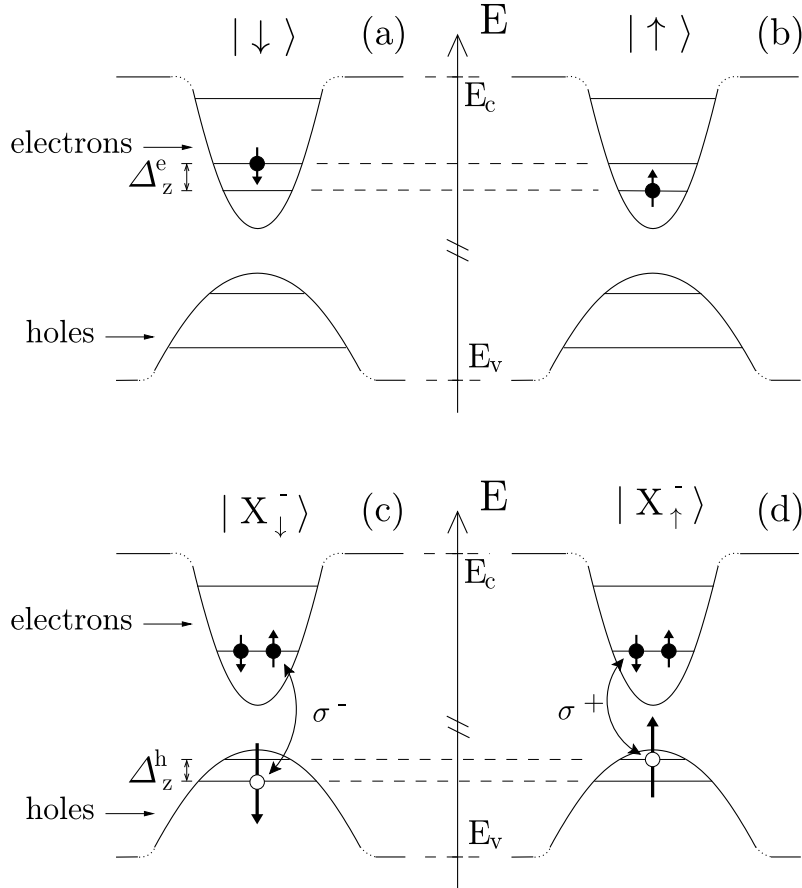


Figure 5.1: The states of a single quantum dot in a static magnetic field, (a) $|\downarrow\rangle$, (b) $|\uparrow\rangle$, (c) $|X_{\downarrow}^{-}\rangle$, and (d) $|X_{\uparrow}^{-}\rangle$. The Zeeman splittings are $\Delta_z^e = g_e^z \mu_B B_z$ for the electron and $\Delta_z^h = g_{hh}^z \mu_B B_z$ for the hole. Coherent transitions occur between (a) and (b) due to the ESR field and between (a) and (c) due to the σ^- -polarized laser field. The arrows in (c) and (d) indicate which electron-hole pair couples with the photon field of polarization σ^{\pm} .

to the formation of a negatively charged exciton, consisting of two electrons and one hole. Recent experiments on InAs dots [172, 173] and GaAs dots [174] have shown that in the charged exciton ground state, the two electrons form a spin singlet in the lowest (conduction-band) electron level and the hole occupies the lowest (valence-band) hole level. Note that single-electron level spacings can be relatively large, e.g., on the order of 50 meV for InAs dots [175]. Typically, the level spacing of confined hole states is smaller than the one of electrons [176]. We assume that the lowest heavy hole (hh, with total angular momentum projection $J_z = \pm 3/2$) and light hole (lh, $J_z = \pm 1/2$) dot levels are split by an energy δ_{hh-lh} . Additionally, mixing of hh and lh states should be negligible [177]. These conditions are satisfied for several types of quantum dots [172, 173, 174, 178, 179]. Then, circularly polarized optical excitation that is restricted to either hh or lh states excites spin-polarized electrons. In this chapter, we first assume a hh ground state for holes. We discuss then different hole configurations.

The states of a quantum dot, in a static magnetic field B_z in z direction, can be taken as follows, see also Fig. 5.1. A single electron in the lowest orbital state is either in the spin ground state, $|\uparrow\rangle$, or in the excited spin state, $|\downarrow\rangle$. Adding an electron-hole pair, the negatively charged exciton (in the orbital ground state) is either in the excited spin state, $|X_\downarrow^- \rangle$, or in the spin ground state, $|X_\uparrow^- \rangle$. For these excitonic states, the subscript \downarrow, \uparrow refers to the hh spin and we apply the usual time-inverted notation for hole spins. For simplicity, we assume $\text{sign}(g_e^z) = \text{sign}(g_{hh}^z)$ for the electron and the hh g factors in z direction. Note that the very same scheme can also be applied if the sign of g_{hh}^z is reversed. Then, one would use a σ^+ laser field and all results apply after interchanging $|X_\downarrow^- \rangle$ and $|X_\uparrow^- \rangle$.²

5.3 Dynamics and Pauli blockade

We describe the coherent dynamics of a quantum dot, charged with a single excess electron, in this ODMR setup with the Hamiltonian

$$H = H_{\text{dot}} + H_{\text{ESR}} + H_L + H_{\text{d-L}}, \quad (5.1)$$

coupling the three states $|\uparrow\rangle$, $|\downarrow\rangle$, and $|X_\downarrow^- \rangle$. Here, H_{dot} comprises the quantum dot potential, the Zeeman energies due to a constant magnetic field in

²Alternatively, one could still use a σ^- laser, as long as the rate $W_{X_\uparrow, X_\downarrow}$ remains sufficiently large, i.e., for large enough kT in comparison to the hole Zeeman splitting.

z direction, and the Coulomb interaction of electrons and holes. It defines the dot energy E_n by $H_{\text{dot}}|n\rangle = E_n|n\rangle$. Here, the electron Zeeman splitting is $g_e^z \mu_B B_z = E_\downarrow - E_\uparrow$, where μ_B is the Bohr magneton [180]. The ESR term $H_{\text{ESR}}(t)$ couples $|\uparrow\rangle$ and $|\downarrow\rangle$ via $\mathbf{B}_\perp(t)$, which rotates with frequency ω_{ESR} in the xy plane [181, 56, 57]. The ESR Rabi frequency is $\Omega_{\text{ESR}} = g_e^\perp \mu_B B_\perp$, with g factor g_e^\perp . Even if the ESR field is also resonant with the hole Zeeman splitting, it has a negligible effect on the charged exciton states since they recombine quickly. An oscillating field, $\mu_B \overleftrightarrow{\mathbf{g}} \mathbf{B}$, can also be produced with voltage-controlled modulation of the electron g -tensor $\overleftrightarrow{\mathbf{g}}$ [54]. A σ^- -polarized laser beam is applied in z direction (typically parallel to [001]), with free laser field Hamiltonian $H_L = \omega_L a_L^\dagger a_L$, where the laser frequency is ω_L , $a_L^{(\dagger)}$ are photon operators, and we set $\hbar = 1$. The coupling of $|\downarrow\rangle$ and $|X_\downarrow^-\rangle$ to the laser field is described by $H_{\text{d-L}}$ which introduces the complex optical Rabi frequency, Ω_L [182]. Since the dot is only coupled to a single circularly polarized laser mode via $H_{\text{d-L}}$, the terms that violate energy conservation vanish due to selection rules. If the laser bandwidth is smaller than δ_{hh-lh} , the absorption of a σ^- photon in the spin ground state, $|\uparrow\rangle$, is excluded due to Pauli blocking [183]. We neglect all multi-photon processes via other levels since they are only relevant to high-intensity laser fields. For this configuration, the σ^- photon absorption is switched “on” and “off” by the ESR-induced electron spin flips. Here, the laser bandwidth and the temperature can safely exceed the electron Zeeman splitting. We transform H into the rotating frame with respect to ω_{ESR} and ω_L . The laser detuning is $\delta_L = (E_{X_\downarrow^-} - E_\downarrow) - \omega_L$ and the ESR detuning $\delta_{\text{ESR}} = g_e^z \mu_B B_z - \omega_{\text{ESR}}$. The coupling of the described system to its environment is taken into account in the next section.

5.4 Master equation

We next consider the reduced density matrix for the dot, $\rho = \text{Tr}_R \rho_F$, where ρ_F is the full density matrix and Tr_R is the trace taken over the environment (or reservoir). In the von Neumann equation, $\dot{\rho}_F = -i[H, \rho_F]$, we treat the interaction with the ESR and laser fields exactly with the Hamiltonian in the rotating frame. We describe the coupling with the environment (radiation field, nuclear spins, phonons, spin-orbit interaction, etc.) with phenomenological rates. We write $W_{nm} \equiv W_{n \leftarrow m}$ for (incoherent) transitions from state $|m\rangle$ to $|n\rangle$ and V_{nm} for the decay of off-diagonal elements of ρ . Note that

usually $V_{nm} \geq \frac{1}{2} \sum_k (W_{kn} + W_{km})$. The electron spin relaxation time [184] is $T_1 = (W_{\uparrow\downarrow} + W_{\downarrow\uparrow})^{-1}$, with spin flip rates $W_{\uparrow\downarrow}, W_{\downarrow\uparrow}$. In the absence of the ESR and laser excitations, the off-diagonal matrix elements of the electron spin decay with the (intrinsic) single-spin decoherence rate $V_{\downarrow\uparrow} = 1/T_2$. The linewidth of the optical σ^- transition is denoted by $V_X = V_{X\downarrow,\downarrow}$. We use the notation $\rho_n = \langle n|\rho|n\rangle$ and $\rho_{nm} = \langle n|\rho|m\rangle$. The master equation is given in the rotated basis $|\uparrow\rangle, |\downarrow\rangle, |X_{\uparrow}^-\rangle, |X_{\downarrow}^-\rangle$ as $\dot{\rho}_D = \mathcal{M}\rho$, where \mathcal{M} is a superoperator. Explicitly,

$$\dot{\rho}_{\uparrow} = \Omega_{\text{ESR}} \text{Im} \rho_{\downarrow\uparrow} + W_{\text{em}} \rho_{X\uparrow} + W_{\uparrow\downarrow} \rho_{\downarrow} - W_{\downarrow\uparrow} \rho_{\uparrow}, \quad (5.2)$$

$$\begin{aligned} \dot{\rho}_{\downarrow} = & -\Omega_{\text{ESR}} \text{Im} \rho_{\downarrow\uparrow} + \frac{i}{2} (\Omega_L \rho_{X\downarrow,\downarrow}^* - \Omega_L^* \rho_{X\downarrow,\downarrow}) + W_{\text{em}} \rho_{X\downarrow} \\ & + W_{\downarrow\uparrow} \rho_{\uparrow} - W_{\uparrow\downarrow} \rho_{\downarrow}, \end{aligned} \quad (5.3)$$

$$\begin{aligned} \dot{\rho}_{X\downarrow} = & -\frac{i}{2} (\Omega_L \rho_{X\downarrow,\downarrow}^* - \Omega_L^* \rho_{X\downarrow,\downarrow}) + W_{X\downarrow,X\uparrow} \rho_{X\uparrow} - (W_{\text{em}} + W_{X\uparrow,X\downarrow}) \rho_{X\downarrow}, \end{aligned} \quad (5.4)$$

$$\dot{\rho}_{X\uparrow} = W_{X\uparrow,X\downarrow} \rho_{X\downarrow} - (W_{\text{em}} + W_{X\downarrow,X\uparrow}) \rho_{X\uparrow}, \quad (5.5)$$

$$\dot{\rho}_{\downarrow\uparrow} = \frac{i}{2} \Omega_{\text{ESR}} (\rho_{\downarrow} - \rho_{\uparrow}) - \frac{i}{2} \Omega_L^* \rho_{X\downarrow,\uparrow} - (i\delta_{\text{ESR}} + T_2^{-1}) \rho_{\downarrow\uparrow}, \quad (5.6)$$

$$\dot{\rho}_{X\downarrow,\uparrow} = \frac{i}{2} \Omega_{\text{ESR}} \rho_{X\downarrow,\downarrow} - \frac{i}{2} \Omega_L \rho_{\downarrow\uparrow} - [i(\delta_{\text{ESR}} + \delta_L) + V_{X\downarrow,\uparrow}] \rho_{X\downarrow,\uparrow}, \quad (5.7)$$

$$\dot{\rho}_{X\downarrow,\downarrow} = \frac{i}{2} \Omega_{\text{ESR}} \rho_{X\downarrow,\uparrow} - \frac{i}{2} \Omega_L (\rho_{\downarrow} - \rho_{X\downarrow}) - (i\delta_L + V_X) \rho_{X\downarrow,\downarrow}. \quad (5.8)$$

The remaining matrix elements of ρ are decoupled and are not important here.

5.5 Spin decoherence time T_2 via cw excitation

We first consider the photoluminescence for a cw ESR and laser field. For this, we calculate the stationary density matrix $\bar{\rho}_D$ with $\dot{\bar{\rho}}_D = 0$. We introduce the rate

$$W_L = \frac{|\Omega_L|^2}{2} \frac{V_X}{V_X^2 + \delta_L^2} \quad (5.9)$$

for the optical excitation, with maximum value W_L^{max} at $\delta_L = 0$. We first solve $\dot{\rho}_{X\downarrow,\uparrow} = 0$ and find that the coupling to the laser field produces an additional

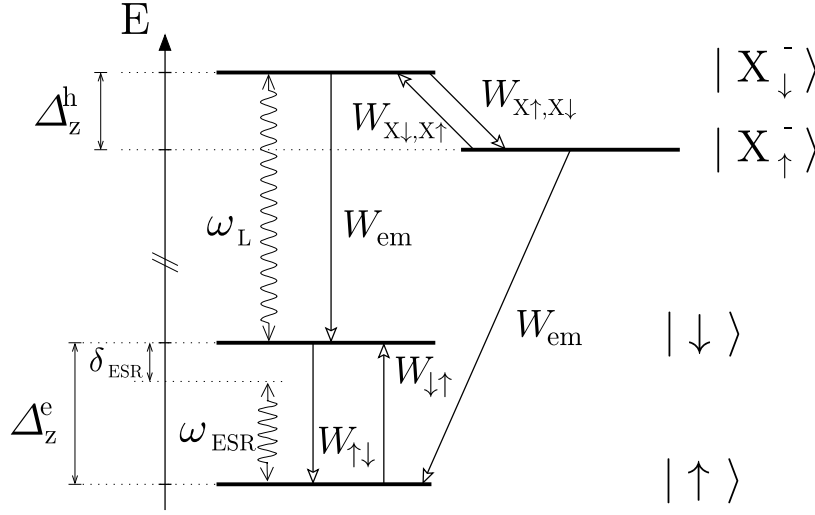


Figure 5.2: Scheme of the transitions between $|\uparrow\rangle$, $|\downarrow\rangle$, $|X_{\uparrow}^{-}\rangle$, and $|X_{\downarrow}^{-}\rangle$. Wavy arrows describe the transitions driven by the ESR field and the laser field with frequencies ω_{ESR} and ω_L , respectively. The corresponding Rabi frequencies are Ω_{ESR} and $|\Omega_L|$, respectively. A detuning $\delta_{\text{ESR}} = \Delta_z^e - \omega_{\text{ESR}}$ is shown for the ESR field, with Zeeman splitting Δ_z^e . Incoherent transitions are depicted with arrows and occur at rates W_{nm} . We consider $W_{\downarrow, X_{\downarrow}^{-}} = W_{\uparrow, X_{\uparrow}^{-}} =: W_{\text{em}}$.

decoherence channel to the electron spin. We obtain the renormalized spin decoherence rate V_{ESR} which satisfies

$$V_{\text{ESR}} \leq \frac{1}{T_2} + \frac{|\Omega_L|^2}{4V_{X_{\downarrow}, \uparrow}} \approx \frac{1}{T_2} + \frac{1}{2}W_L^{\text{max}}. \quad (5.10)$$

Further, the ESR detuning is also renormalized, $\tilde{\delta}_{\text{ESR}} \geq \delta_{\text{ESR}} [1 - |\Omega_L|^2 / (W_{\text{em}} + W_{X_{\uparrow}, X_{\downarrow}})^2]$. We assume that these renormalizations and δ_L are small compared to the linewidth of the optical transition, i.e., W_L^{max} , $|\tilde{\delta}_{\text{ESR}} - \delta_{\text{ESR}}| < V_X$. Then, if both transitions are near resonance, $\delta_L \lesssim V_X$ and $|\tilde{\delta}_{\text{ESR}}| \lesssim V_{\text{ESR}}$, no additional terms appear in the renormalized master equation. We solve $\dot{\rho}_{X_{\downarrow}, \downarrow} = 0$ and $\dot{\rho}_{\uparrow} = 0$ and introduce the rate

$$W_{\text{ESR}} = \frac{\Omega_{\text{ESR}}^2}{2} \frac{V_{\text{ESR}}}{V_{\text{ESR}}^2 + \tilde{\delta}_{\text{ESR}}^2}, \quad (5.11)$$

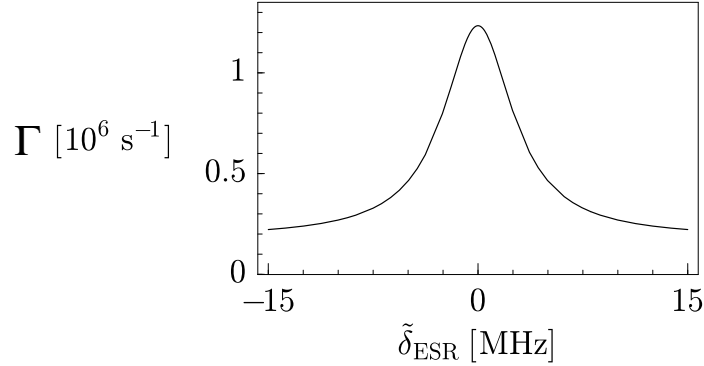


Figure 5.3: The total photoluminescence rate Γ is a Lorentzian as function of the ESR detuning $\tilde{\delta}_{\text{ESR}}$. Its linewidth w gives an upper bound for $2/T_2$. Here, we use $g_e = 0.5$, $B_{\perp} = 1$ G, $T_2 = 100$ ns, $W_{\uparrow\downarrow} = W_{\downarrow\uparrow} = (20 \mu\text{s})^{-1}$, $W_{\text{em}} = 10^9 \text{ s}^{-1}$, $W_{X\uparrow, X\downarrow} = W_{X\downarrow, X\uparrow} = W_{\text{em}}/2$, $\delta_L = 0$, $V_{X\downarrow, \uparrow} = V_X = (W_{\text{em}} + W_{X\uparrow, X\downarrow})/2$, and $\Omega_L = 2\Omega_{\text{ESR}}\sqrt{T_2 V_X}$. With these parameters, the requirement $W_L \lesssim T_2^{-1} \lesssim V_{\text{ESR}}$ is satisfied.

which together with W_L eliminates Ω_L , V_X , δ_L , Ω_{ESR} , V_{ESR} , and $\tilde{\delta}_{\text{ESR}}$ from the remaining equations for the diagonal elements of ρ . These now contain the effective spin flip rates $\tilde{W}_{\uparrow\downarrow} = W_{\uparrow\downarrow} + W_{\text{ESR}}$ and $\tilde{W}_{\downarrow\uparrow} = W_{\downarrow\uparrow} + W_{\text{ESR}}$. We find the stationary solution

$$\begin{aligned} \bar{\rho}_{\uparrow} &= \eta W_L W_{\text{em}} W_{X\uparrow, X\downarrow} + \eta \tilde{W}_{\uparrow\downarrow} W_{\text{em}} W_{X\uparrow, X\downarrow} + \eta \tilde{W}_{\uparrow\downarrow} (W_L + W_{\text{em}}) \\ &\quad \times (W_{\text{em}} + W_{X\downarrow, X\uparrow}), \end{aligned} \quad (5.12)$$

$$\bar{\rho}_{\downarrow} = \eta \tilde{W}_{\downarrow\uparrow} (W_L + W_{\text{em}}) (W_{\text{em}} + W_{X\downarrow, X\uparrow}) + \eta \tilde{W}_{\downarrow\uparrow} W_{\text{em}} W_{X\uparrow, X\downarrow}, \quad (5.13)$$

$$\bar{\rho}_{X\downarrow} = \eta W_L \tilde{W}_{\downarrow\uparrow} (W_{\text{em}} + W_{X\downarrow, X\uparrow}), \quad (5.14)$$

$$\bar{\rho}_{X\uparrow} = \eta W_L \tilde{W}_{\downarrow\uparrow} W_{X\uparrow, X\downarrow}, \quad (5.15)$$

where the normalization factor η is such that $\sum_n \rho_n = 1$. Note that $\bar{\rho}_{\uparrow} \geq \bar{\rho}_{\downarrow}$ is satisfied for $W_{\uparrow\downarrow} \geq W_{\downarrow\uparrow}$. Thus, electron spin polarization is achieved due to the hole spin relaxation channel, analogously to an optical pumping scheme. Now, photons with σ^- (σ^+) polarization are emitted from the dot at the rate $\Gamma^- = W_{\text{em}} \bar{\rho}_{X\downarrow}$ ($\Gamma^+ = W_{\text{em}} \bar{\rho}_{X\uparrow}$). These rates are proportional to $W_{\text{ESR}}/(\gamma + W_{\text{ESR}})$ for a given γ , up to a constant background which is negligible for $W_{\downarrow\uparrow} < W_{\text{ESR}}$. In particular, the total rate $\Gamma = \Gamma^- + \Gamma^+$ as function of $\tilde{\delta}_{\text{ESR}}$ is a Lorentzian with linewidth $w = 2V_{\text{ESR}}\sqrt{1 + W_{\text{ESR}}^{\text{max}}/\gamma}$, see Fig. 5.3. Analyzing the expression for γ , we find the relevant parameter

regime with the inequality

$$w \leq 2 V_{\text{ESR}} \left[1 + \frac{2 W_{\text{ESR}}^{\text{max}}}{W_{\text{L}}} \left(1 + \frac{W_{\text{em}}}{W_{\text{r}}} + \frac{W_{X\downarrow, X\uparrow}}{W_{\text{r}}} \right) + \frac{3 W_{\text{ESR}}^{\text{max}}}{W_{\text{r}}} + \frac{W_{\text{ESR}}^{\text{max}}}{W_{\text{em}}} \left(1 + \frac{3 W_{X\downarrow, X\uparrow}}{W_{\text{r}}} \right) \right]^{1/2}, \quad (5.16)$$

which saturates for vanishing $W_{\downarrow\uparrow}$ and $W_{\uparrow\downarrow}$. Here, the rate $W_{\text{r}} = W_{X\uparrow, X\downarrow} + W_{\uparrow\downarrow} (1 + W_{\text{em}}/W_{\text{L}})$ describes different relaxation channels, all leading to the ground state $|\uparrow\rangle$, and thus correspond to “switching off” the laser excitations. If W_{r} is large, e.g., due to efficient hole spin relaxation [185], $w \approx 2 V_{\text{ESR}}$. From the linewidth w one can extract a *lower bound for T_2* : $T_2 \geq 1/V_{\text{ESR}} \geq 2/w$. Further, this lower bound saturates when the expression in brackets in Eq. (5.16) becomes close to 1 and thus $T_2^{-1} \approx V_{\text{ESR}}$ [see Eq. (5.10)], i.e., the T_2 time is given by the linewidth. Comparing with the exact solution, we find that our analytical approximation gives the value of Γ within 0.2 % for the parameters of Fig. 5.3. Due to possible imperfections in this ODMR scheme, e.g., mixing of hh and lh states or a small contribution of the σ^+ polarization in the laser light, also the state $|\uparrow\rangle$ can be optically excited. We describe this with the effective rate $W_{\text{L},\uparrow}$ which leads to an additional linewidth broadening [similar to Eq. (5.16)]. This effect is small for $W_{\text{L},\uparrow} < W_{\text{ESR}}$. Detection of the laser stray light can be avoided by only measuring Γ^+ . Otherwise, the laser could be distinguished from Γ^- by using two-photon absorption. As an alternative, the optical excitation could be tuned to an excited hole state (hh or lh),³ possibly with a reversal of laser polarization. A *pulsed* laser, finally, would enable the distinction between luminescence and laser light by time gated detection.

³After excitation, the hole relaxes into its ground state within an intraband relaxation time less than a few hundred ps [164]. Recombination mostly takes place at a later time, typically after 1 ns. Thus, the emission is red-shifted and can be discriminated from the stray light of the laser. However, excitations into higher electron levels must still be excluded. This is possible for the first few excited hole levels, since the level spacing is smaller for holes than for electrons.

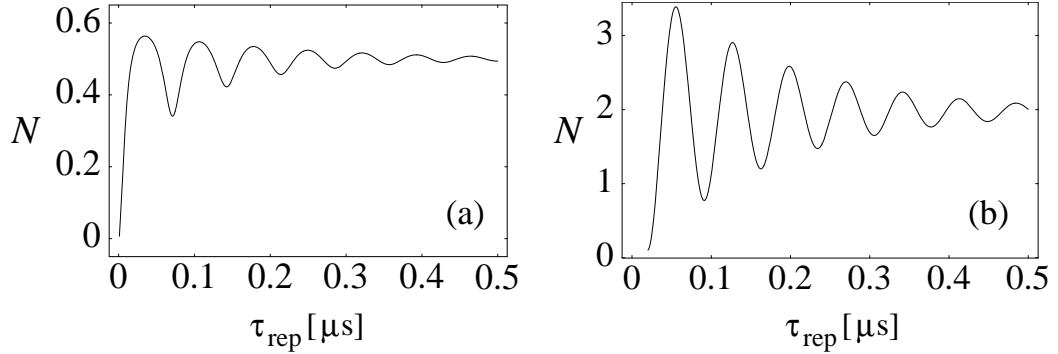


Figure 5.4: Average number N of photons emitted per period τ_{rep} as function of the laser pulse repetition time for (a) π pulses with $\Delta t = 5$ ps and $\Omega_L = \pi/\Delta t$, and (b) pulses with $\Delta t = 20$ ns and $\Omega_L = \pi/(500$ ps). We have set $\delta_{\text{ESR}} = 0$. The other parameters are as in Fig. 5.3. The decay of the oscillation is given by V_{ESR} and therefore depends on T_2 .

5.6 Pulsed excitations and spin Rabi oscillations

For a pulsed σ^- laser, one can also measure the photoluminescence, Γ , as function of the pulse repetition time τ_{rep} instead of $\tilde{\delta}_{\text{ESR}}$. We still use cw ESR (or, alternatively, a static transverse magnetic field, i.e., in the Voigt geometry). We stress that the same restrictions on the laser bandwidth as in the cw case apply. Due to hole spin flips, followed by emission of a photon, the dot is preferably in the state $|\uparrow\rangle$ rather than $|\downarrow\rangle$ at the end of a laser pulse. The magnetic field then acts on the electron spin until the next laser pulse arrives. Finally, the spin state $|\downarrow\rangle$ is read out optically and, therefore, the Rabi oscillations (or spin precessions) can be observed in the photoluminescence as function of τ_{rep} , see Fig. 5.4. For simplicity, we consider square pulses of length Δt . We write in the master equation $\mathcal{M}(t) = \mathcal{M}_L$ during a laser pulse and otherwise $\mathcal{M}(t) = \mathcal{M}_0$, setting $\Omega_L = 0$. We find the steady-state density matrix ρ_∞ of the dot just after the pulse with $U_p \rho_\infty = \rho_\infty$, where $U_p = \exp(\mathcal{M}_L \Delta t) \exp[\mathcal{M}_0(\tau_{\text{rep}} - \Delta t)]$ describes the time evolution during τ_{rep} .

The photoluminescence rate is now evaluated by $\Gamma = W_{\text{em}} \overline{(\rho_{X\downarrow} + \rho_{X\uparrow})}$, where the bar designates time averaging over many periods τ_{rep} . For $\Delta t \geq \pi/\Omega_L$, W_{em}^{-1} , the spin oscillations become more pronounced, see Fig. 5.4 (b).

This results from an enhanced relaxation to the state $|\uparrow\rangle$ during each pulse and thus from a much larger ρ_{\uparrow} than ρ_{\downarrow} just after the pulse. (Alternatively, a group of short pulses can be used to simulate the long pulse.)

The same cw and pulsed optical detection schemes can be combined with pulsed instead of cw ESR, allowing spin echo and similar techniques. Such pulses can, e.g., be produced via the AC Stark effect [90, 186].

5.7 Conclusion

We have proposed an ODMR setup with ESR and polarized optical excitation. We have shown that this setup allows the optical measurement of the single electron spin decoherence time T_2 in semiconductor quantum dots. The discussed cw and pulsed optical detection schemes can also be combined with pulsed instead of cw ESR, allowing spin echo and similar standard techniques. Such pulses can, e.g., be produced via the AC Stark effect [186]. Further, as an alternative to photoluminescence detection, photocurrent can be used to read out the charged exciton[171], and the same ODMR scheme can be applied.

Chapter 6

Conductance fluctuations in diffusive rings: Berry phase effects and criteria for adiabaticity

We study Berry phase effects on conductance properties of diffusive mesoscopic conductors, which are caused by an electron spin moving through an orientationally inhomogeneous magnetic field. Extending previous work by D. Loss *et al.* [87], we start with an exact, i.e. not assuming adiabaticity, calculation of the universal conductance fluctuations in a diffusive ring within the weak localization regime. As part of this calculation, we derive a differential equation for the diffuson in the presence of Zeeman coupling to an inhomogeneous magnetic field. We calculate the field strength required for adiabaticity and show that this strength is reduced by the diffusive motion. We demonstrate that not only the phases but also the amplitudes of the $h/2e$ Aharonov-Bohm oscillations are strongly affected by the Berry phase. In particular, we show that these amplitudes are completely suppressed at certain *magic tilt angles* of the external fields, and thereby provide a useful criterion for experimental searches. We also discuss Berry phase-like effects resulting from spin-orbit interaction in diffusive conductors and derive exact formulas for both magnetoconductance and conductance fluctuations. We discuss the power spectra of the magnetoconductance and the conductance fluctuations for inhomogeneous magnetic fields and for spin-orbit interaction.

6.1 Introduction and overview

Since its discovery, the Berry phase [78] has been a subject of continued interest. As this geometrical phase emerges from the very basic laws of quantum mechanics, see Sec. 1.6, it has implications for a broad range of physical systems [82]. Even though the Berry phase has been observed in single-particle experiments, its manifestation in condensed matter systems is still under investigation. Some settings were proposed [83, 85, 86, 87, 187], where the Berry phase, resulting from the motion of a spin-carrying particle through an inhomogeneous magnetic field $\mathbf{B}(\mathbf{x})$, can be observed in mesoscopic structures. The expected effects are measurable as persistent currents [83, 86, 188] as well as in the magnetoconductance [85, 87, 189, 190, 191] and the universal conductance fluctuations (UCFs) [85, 87]. The first experiments reporting such effects were realized with semiconductor structures: the conductance was investigated in an InAs sample [79], where the Berry phase can emerge through the Rashba effect [84], in a very similar way as produced by an inhomogeneous field. Magnetoconductance measurements were performed where a ferromagnetic dot, placed slightly above a GaAs sample, produced an inhomogeneous field [192]. Measurements on metallic systems also showed effects, which have been explained in terms of the Berry phase [193, 194, 195]. Further experiments on metallic systems are in progress [196]. An additional scenario was proposed, where domain walls of mesoscopic ferromagnets lead to a Berry phase [187].

During orbital motion in a magnetic field, a spin acquires a Berry phase in a similar way as a charge collects an Aharonov-Bohm phase. Thus, these two phases lead to similar implications for interference phenomena in mesoscopic samples. However, in the first case the phase originates from the change in local field direction, whereas in the second case it results from an enclosed magnetic flux. As these field properties can be varied individually, the interplay of the two phases yields a rich variety of behaviour. These quantum phases are distinguished by another important difference: while Aharonov-Bohm effects appear for arbitrarily small magnitudes B of the magnetic field, Berry phase effects appear to their full extent only in the adiabatic limit, i.e. for large enough fields (specified below). The physical situation required for this limit to be satisfied can be pictured [87, 191] as a spin which must complete many precessions $\omega_B t_o / 2\pi$ around the local magnetic field, while it moves during a time t_o through a region of size ℓ_B over which the direction of the field changes significantly. Here we have introduced the Bohr

frequency $\omega_B = g\mu_B B/2\hbar$, where g is the Landé g -factor and μ_B is the Bohr magneton. For ballistic motion as it occurs in clean semiconductors, one has $v_F t_o \sim \ell_B$ and there is general consensus about the criterion for adiabaticity, i.e. $\omega_B \ell_B/v_F \gg 2\pi$, with v_F being the Fermi velocity. However, for diffusive systems there were recently some discussions [189, 87, 190, 191] whether t_o can be correctly set as the diffusion time $t_d = \ell_B^2/D$ or if one should replace it by the elastic scattering time τ . The first criterion is more optimistic, in the sense that much lower field magnitudes are required to reach adiabaticity, as due to diffusive motion the electrons effectively move more slowly (compared to the ballistic motion) through the changing magnetic field and thus have more time to adjust their spins to the local field orientation. For magnetoconductance quantitative values for the required field magnitudes have been obtained [191]. Solving the special case of a cylindrically symmetrical texture exactly, it was confirmed [191] that the more favorable criterion is indeed sufficient. We remark that, if the ballistic criterion was appropriate for diffusive systems, the large fields required for adiabaticity would imply a strong curvature of the semiclassical trajectories (apart from the case of very large g factors). This curvature in turn is in conflict with the approximation of the orbital motion by its zero-field value and therefore an approach beyond weak localization theory would be required for a self-consistent theory. At this point it should also be noted that Berry phase effects occur even if the adiabatic limit is not fully reached; there is no sharp cutoff where the Berry phase disappears completely. Thus, calculations without assuming adiabaticity are very desirable, as they can be used to study how the Berry phase effects gradually emerge while the magnetic field is increased from low to adiabatic strengths. The adiabatic limit can still be taken at the end of the calculation, so the formal appearance of the Berry phase and the associated dephasing [191] can be identified.

Besides having a spin following the direction of an inhomogeneous external field, there is another scenario which produces a Berry phase: spin-orbit coupling [84]. If an electron moves through an electrical field perpendicular to the ring plane, an effective magnetic field, which is produced in the rest frame of the electron, couples to the electron spin. As this effective field is in radial direction of the ring and perpendicular to the direction of motion, the field rotates while the electron moves around the ring and can therefore produce a Berry phase. By switching on, in addition, an external magnetic field, an arbitrary tilt angle of the total effective field can be realized and so this Berry phase can be tuned. For ballistic motion, the Berry phase manifests

itself in precisely the same way [84] as in the case with an inhomogeneous external magnetic field [83, 85, 86]. However, for diffusive motion the situation becomes more complicated, as the change of the direction of motion of the electron due to a elastic scattering event abruptly changes the effective field direction. Now the picture of a spin, moving adiabatically through a slowly varying field, is no longer valid and needs to be modified. This leads to a new physical situation which has to be considered separately from the situation with inhomogeneous fields.

The outline of this chapter is as follows. In Sec. 6.2 we study the conductance fluctuations $\delta g^{(2)}$ of quasi-1D diffusive rings in inhomogeneous magnetic fields. While $\delta g^{(2)}$ has already been calculated within the adiabatic approximation [87], i.e. for strong magnetic fields, the behavior outside the adiabatic limit and the influence of inhomogeneous fields on dephasing were not discussed so far. We address these issues in this thesis, starting in Sec. 6.2.1 with a calculation of an exact expression for $\delta g^{(2)}$ (i.e. allowing arbitrarily small field magnitudes) for a special texture [see Eq. (6.1)] of the magnetic field. In this process we derive a new form of the diffuson differential equation, which includes inhomogeneous magnetic fields. We evaluate the adiabatic limit of the UCFs, $\delta g_{\text{ad}}^{(2)}$, in Sec. 6.2.2 and compare our results with those derived in previous work [87]. Further, we investigate in Sec. 6.2.3 the finite temperature behavior of the conductance fluctuations. In Sec. 6.3 the effects of the Berry phase on the UCFs and their dependence on magnetic field strengths are discussed in detail. We identify in Sec. 6.3.1 a new effect of the Berry phase by showing that the amplitudes of the $h/2e$ Aharonov-Bohm oscillations depend directly on the value of the Berry phase. In particular, we find some magic tilt angles of the magnetic field, where these Aharonov-Bohm oscillations are completely suppressed. This effect provides a tool for experimental searches of the Berry phase. We use this observation to illustrate the gradually appearing effects of the Berry phase for increasing field strengths and thus give a direct demonstration of the onset of adiabaticity. Then, in Sec. 6.3.2, we give quantitative values of the fields strengths needed for reaching adiabaticity. We show that the criterion for adiabaticity is less stringent for diffusive than for ballistic motion. An exact evaluation of magnetoconductance δg_{SO} and conductance fluctuations $\delta g_{SO}^{(2)}$ in the presence of spin-orbit coupling and homogeneous magnetic fields is given in Sec. 6.4. These results show how the amplitudes of the Aharonov-Bohm oscillations in $\delta g_{SO}^{(2)}$ depend non-monotonously on the direction of an effective field, similarly as it is the case for inhomogeneous magnetic fields. In Sec. 6.5.1 we show how frequency

shift of the Aharonov-Bohm oscillations appear in δg and $\delta g^{(2)}$ caused by the Berry phase. We then point out in Sec. 6.5.2 that the Zeeman term can also produce frequency shifts even in the case of homogeneous fields. In Sec. 6.5.3 we plot and discuss the exact expressions for δg and $\delta g^{(2)}$ for inhomogeneous fields and for spin-orbit coupling as well as the corresponding power spectra. In three appendices we provide details of our calculations.

6.2 Conductance fluctuations

As foundation for further discussions of Berry phase effects and adiabaticity, we will first calculate the conductance fluctuations $\delta g^{(2)}$ in the weak-localization regime. To motivate the analysis of the conductance fluctuations, we would like to emphasize the advantage of studying the UCFs instead of the magnetoconductance. The latter quantity has only contributions from the cooperon, which are suppressed by moderately large magnetic fields penetrating the ring arms [197]. This suppression is in direct competition with the requirement of having large fields to satisfy adiabaticity. In contrast, the conductance fluctuations also have contributions from the diffuson, which is only sensitive to the *difference* of the two magnetic fields, for which the conductance correlator is considered. Therefore, if both fields are taken of similar magnitude, Aharonov-Bohm oscillations and Berry phase effects in the UCFs will still be visible at high magnetic fields where the adiabatic criterion is certainly satisfied.

6.2.1 Exact solution

We shall concentrate on rings with circumference L and study the conductance-conductance correlator $\delta g^{(2)}(\mathbf{B}, \tilde{\mathbf{B}}) = \langle g_{\mathbf{B}} g_{\tilde{\mathbf{B}}} \rangle - \langle g_{\mathbf{B}} \rangle \langle g_{\tilde{\mathbf{B}}} \rangle$, where we have two different magnetic fields \mathbf{B} and $\tilde{\mathbf{B}}$. We consider a special texture [86, 190, 191] for which we obtain exact results (i.e. without making the adiabatic assumption of strong magnetic fields). We assume the magnetic fields to be applied in such a way that they wind f times around the z -axis in one turn around the ring, with tilt angles $\eta, \tilde{\eta}$, see Fig. 6.1. The position along the direction of the ring is described by the coordinate x , varying from 0 to L , so the special texture of the magnetic field is expressed as

$$\mathbf{B} = B \mathbf{n} = B (\sin \eta \cos (\frac{2\pi f x}{L} + \theta), \sin \eta \sin (\frac{2\pi f x}{L} + \theta), \cos \eta), \quad (6.1)$$

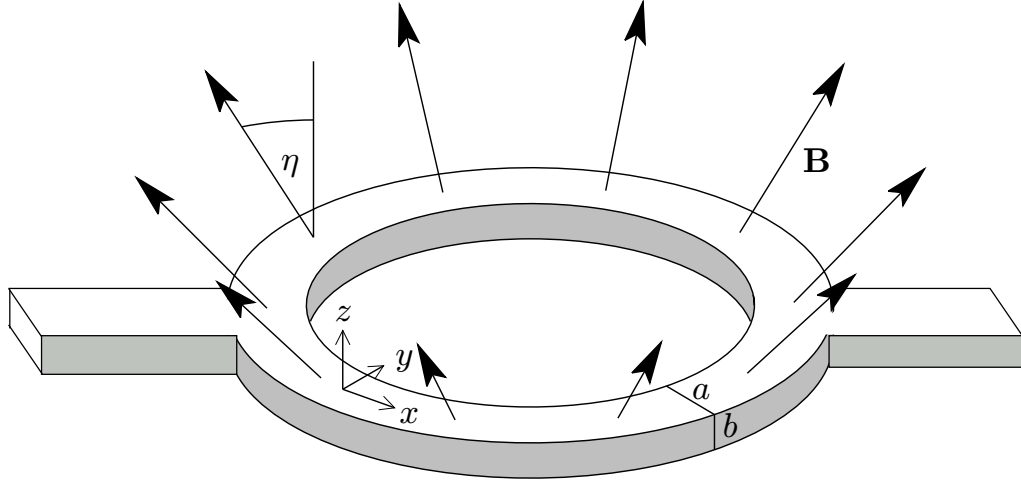


Figure 6.1: A mesoscopic ring of width a and height b in an inhomogeneous magnetic field with tilt angle η , winding once around the z -Axis. The texture of the magnetic field drawn here corresponds to Eq. (6.1) with $f = 1$ and $\theta = 0$.

and similarly for $\tilde{\mathbf{B}}$. We have introduced θ , so we can describe the textures with a field component radial to the ring, i.e. $\theta = 0$, as well as textures with a field component tangential to the ring, i.e. $\theta = \pi/2$.

The starting point of our calculation is the conductance correlator derived in Ref. [87] and given by

$$\delta g^{(2)} = \left(\frac{2e^2 D}{hL^2} \right)^2 \int d\epsilon d\epsilon' n'(\epsilon) n'(\epsilon') \left\{ \frac{1}{d} \text{Tr} \hat{\chi}_\omega^C \hat{\chi}_\omega^{C\dagger} + 2 \text{Re} \text{Tr} \hat{\chi}_\omega^C \hat{\chi}_\omega^C + [\hat{\chi}^C \rightarrow \hat{\chi}^D] \right\}, \quad (6.2)$$

where $n'(\epsilon)$ is the derivative of the Fermi function and $\hbar\omega = \epsilon - \epsilon'$. The dimensionality of the system with respect to the diffusive motion is denoted by d , which describes the relation of the mean free path ℓ to the diffusion coefficient D , i.e. $D = v_F \ell / d$. The propagators $\hat{\chi}^{C/D}$ can be evaluated explicitly by using the operator equation Eq. (G.5):

$$\hat{\chi}^{C/D} = \frac{L^2}{(2\pi)^2 D} \frac{1}{i\omega + \gamma^{C/D} - h^{C/D}}. \quad (6.3)$$

We have defined $w = (L/2\pi L_T)^2 (\epsilon - \epsilon') / kT$, with the thermal diffusion length

$L_T = \sqrt{D\hbar\beta}$. [198] The (non-hermitian) Hamiltonian is given by

$$h^{C/D} = \frac{L^2}{(2\pi)^2} \frac{\partial^2}{\partial x^2} + i\kappa \mathbf{n} \cdot \boldsymbol{\sigma}_1 - i\tilde{\kappa} \tilde{\mathbf{n}} \cdot \boldsymbol{\sigma}_2^{(*)}, \quad (6.4)$$

where the star means complex conjugation in h^D and where we have introduced an adiabaticity parameter [87, 191, 190]

$$\kappa = \frac{\omega_B}{D} \frac{L^2}{(2\pi)^2}, \quad (6.5)$$

and equivalently for $\tilde{\kappa}$ and $\omega_{\tilde{B}}$. We have inserted a phenomenological damping constant $\gamma^{C/D} = (L/2\pi L_{C/D})^2$ expressed in terms of the magnetic dephasing length $L_{C/D}$ [197, 87]:

$$\gamma^{C/D} = \frac{L^2}{(2\pi)^2 L_\varphi^2} + \frac{1}{3(4\pi)^2} \left(\frac{A |B_z \pm \tilde{B}_z|}{2\pi\phi_0} \right)^2. \quad (6.6)$$

The first term of this damping constant incorporates the loss of phase due to inelastic scattering events. The second term takes into account magnetic flux penetration into the arms of the ring with a finite width a and a surface area $A = aL$, while the height b is assumed to be small compared to a . This field penetration leads to averaging over closed paths of different lengths, each of which collects a different Aharonov-Bohm phase, resulting finally in dephasing.

Next we define the basis in which we evaluate the Hamiltonian $h^{C/D}$. As done in Ref. [190] for the cooperon propagator, we now introduce the operators

$$J^{C/D} = \frac{L}{2\pi i} \frac{\partial}{\partial x} + \frac{1}{2} f(\sigma_{1z} \pm \sigma_{2z}), \quad (6.7)$$

which commute with $h^{C/D}$ [199].

We will now go to the basis of eigenvectors $|j, \alpha\beta\rangle_{C/D}$ of $J^{C/D}$. This basis is orthonormal with the following wave functions:

$$\langle x, \alpha'\beta' | j, \alpha\beta \rangle_{C/D} = \frac{\delta_{\alpha'\alpha} \delta_{\beta'\beta}}{\sqrt{L}} \exp \left\{ \frac{2\pi i x}{L} \left(j - \frac{f}{2} \alpha \mp \frac{f}{2} \beta \right) \right\}. \quad (6.8)$$

Because of the periodic boundary conditions in x , the eigenvalues j of $J^{C/D}$ have to be integers. The matrix elements of $h^{C/D}$ in the basis $\{|j, \uparrow\uparrow\rangle_{C/D}, |j, \uparrow\downarrow\rangle_{C/D}, |j, \downarrow\uparrow\rangle_{C/D}, |j, \downarrow\downarrow\rangle_{C/D}\}$ become:

$${}_{C/D} \langle j, \alpha\beta | h^{C/D} | j', \alpha'\beta' \rangle_{C/D} = \delta_{jj'} \left(-h_j^{C/D} + h_\sigma^{C/D} \right), \quad (6.9)$$

where h_j^C and h_j^D are diagonal 4×4 matrices with the entries $\{(j-f)^2, j^2, j^2, (j+f)^2\}$, and $\{j^2, (j-f)^2, (j+f)^2, j^2\}$, *resp.*, and the $\eta, \tilde{\eta}$ dependent matrices are

$$h_\sigma^{C/D} = \begin{pmatrix} i\kappa \cos \eta - i\tilde{\kappa} \cos \tilde{\eta} & -i\tilde{\kappa} e^{\mp i\theta} \sin \tilde{\eta} & i\kappa e^{-i\theta} \sin \eta & 0 \\ -i\tilde{\kappa} e^{\pm i\theta} \sin \tilde{\eta} & i\kappa \cos \eta + i\tilde{\kappa} \cos \tilde{\eta} & 0 & i\kappa e^{-i\theta} \sin \eta \\ i\kappa e^{i\theta} \sin \eta & 0 & -i\kappa \cos \eta - i\tilde{\kappa} \cos \tilde{\eta} & -i\tilde{\kappa} e^{\mp i\theta} \sin \tilde{\eta} \\ 0 & i\kappa e^{i\theta} \sin \eta & -i\tilde{\kappa} e^{\pm i\theta} \sin \tilde{\eta} & -i\kappa \cos \eta + i\tilde{\kappa} \cos \tilde{\eta} \end{pmatrix}. \quad (6.10)$$

To take the Aharonov-Bohm flux into account, we replace $j \rightarrow m = j - (\phi/\phi_0 \pm \tilde{\phi}/\phi_0)$, where $\phi, \tilde{\phi}$ are the fluxes of the fields $\mathbf{B}, \tilde{\mathbf{B}}$ through the ring and $\phi_0 = h/e$ is the magnetic flux quantum [200]. Now it is straightforward to evaluate the exact conductance fluctuations $\delta g^{(2)}$ by calculating the propagators by matrix inversion and inserting the result into Eq. (6.2). This can be done with the help of the computer program Mathematica, which however leads to lengthy expressions which we will not reproduce here. We merely point out that the phase factors in θ cancel each other in $\delta g^{(2)}$ and δg .

6.2.2 Adiabatic approximation

To evaluate the adiabatic limit, we shall consider the regime of large magnetic fields with B and \tilde{B} of similar magnitude. If we define $\Delta\kappa = \tilde{\kappa} - \kappa$, this adiabatic regime is described by

$$\kappa \gg 1 \quad \text{and} \quad \kappa \gg |\Delta\kappa|. \quad (6.11)$$

The exact propagators $\chi^{C/D}$ turn out to be rational functions which are of order two in κ in both numerator and denominator. Now we will keep only the terms of highest order in κ ; terms with large j can be neglected as the sum over j converges rapidly. This leads us to the UCFs in the adiabatic regime:

$$\delta g_{\text{ad}}^{(2)} = \left(\frac{e^2}{h}\right)^2 \frac{1}{4\pi^4} \int d\epsilon d\epsilon' n'(\epsilon) n'(\epsilon') \sum_{j=-\infty}^{\infty} \sum_{\alpha=\pm 1} (G_{\alpha,C}^{\text{ad}} + G_{\alpha,D}^{\text{ad}}) \quad (6.12)$$

$$\begin{aligned} G_{\alpha,C/D}^{\text{ad}} &= \frac{1}{d} \left\{ (w - \alpha\Delta\kappa)^2 + \delta_{-\alpha}^{C/D}(j)^2 + P \right\} \left\{ \left[(w - \alpha\Delta\kappa)^2 + \right. \right. \\ &\quad \left. \left. \delta_{-\alpha}^{C/D}(j)^2 - P \right] \left[(w + \alpha\Delta\kappa)^2 + \delta_{\alpha}^{C/D}(j)^2 - P \right] \right. \\ &\quad \left. + 4P [w^2 + f^2 m^2 (\cos \eta \pm \cos \tilde{\eta})^2] \right\}^{-1} \\ &\quad + 2\text{Re} \left[\left\{ \left[iw - i\alpha\Delta\kappa + \delta_{-\alpha}^{C/D}(j) \right]^2 + P \right\} \left\{ \left[iw - i\alpha\Delta\kappa + \delta_{-\alpha}^{C/D}(j) \right] \right. \right. \\ &\quad \left. \left. \times \left[iw + i\alpha\Delta\kappa + \delta_{\alpha}^{C/D}(j) \right] - P \right\}^{-2} \right], \end{aligned} \quad (6.13)$$

where

$$P = \frac{f^4}{4} \sin^2 \eta \sin^2 \tilde{\eta}, \quad (6.14)$$

$$\delta_{\alpha}^{C/D}(j) = \tilde{\gamma}_{\eta, \tilde{\eta}}^{C/D} + \left(m - \frac{f}{2} \alpha \cos \eta \mp \frac{f}{2} \alpha \cos \tilde{\eta} \right)^2, \quad (6.15)$$

with

$$\tilde{\gamma}_{\eta, \tilde{\eta}}^{C/D} = \gamma^{C/D} + \frac{f^2}{4} \sin^2 \eta + \frac{f^2}{4} \sin^2 \tilde{\eta}. \quad (6.16)$$

The sum over α has been introduced here artificially to facilitate the following interpretation. As it is also seen in Ref. [191] for the case of the magnetoconductance δg , the terms $f^2(\sin^2 \eta + \sin^2 \tilde{\eta})/4$ in Eq. (6.16) act as additional dephasing sources and are here absorbed in the phenomenological dephasing parameter $\tilde{\gamma}_{\eta, \tilde{\eta}}^{C/D}$. However, in Eq. (6.13) there are further $\eta, \tilde{\eta}$ -dependent terms P , which cannot be formally absorbed in $\tilde{\gamma}_{\eta, \tilde{\eta}}^{C/D}$. P reduces the effect of the additional dephasing terms in Eq. (6.16), as we can see by the following numerical evaluation. We consider equal fields $\mathbf{B} = \tilde{\mathbf{B}}$ and low temperatures, thus $\Delta\kappa, \omega = 0$, and assume $\eta, \tilde{\eta}$ to be close to $\pi/2$. Then we estimate the amplitude of the Aharonov-Bohm oscillations by taking the difference between the values of $G_{\alpha,C}^{\text{ad}}$ [Eq. (6.13)] for the two phases $m = 0$

and $m = \pm 1/2$ (i.e. we are considering only the main contributions in the sum over j [Eq. (6.12)]). We then see by numerical evaluation that the oscillations are suppressed if we set $P = 0$ instead of using Eq. (6.14), thus P indeed reduces dephasing.

We can compare now with previous calculations [87] where the UCFs $\delta g_{\text{LSG}}^{(2)}$ have been derived for arbitrary textures and adiabatic evolution of the spin. These results can be recovered from Eq. (6.12) by the replacement $\tilde{\gamma}_{\eta, \tilde{\eta}}^{C/D} \rightarrow \gamma_{\text{LSG}}^{C/D}$ and $P \rightarrow 0$. The dephasing terms due to inhomogeneous fields coupling to the spin [see Eqs. (6.14), (6.16)] were not explicitly given in Ref. [87]; to account for such dephasing these terms must be included in the phenomenological parameter $\gamma_{\text{LSG}}^{C/D}$, and thus $\gamma_{\text{LSG}}^{C/D} \neq \gamma^{C/D}$ and $\gamma_{\text{LSG}}^{C/D} \neq \tilde{\gamma}_{\eta, \tilde{\eta}}^{C/D}$ in general [191].

We also recognize a strong simplification in the special case where one field is homogeneous, $\eta = 0$, i.e., P vanishes. Thus the comparison of $\delta g_{\text{ad}}^{(2)}$ with the solution for arbitrary textures $\delta g_{\text{LSG}}^{(2)}$ yields the simple relation $\gamma_{\text{LSG}}^{C/D} = \tilde{\gamma}_{0, \tilde{\eta}}^{C/D}$. Finally we note that in this case the dephasing due to the orientational inhomogeneity of $\tilde{\mathbf{B}}$ measured by the winding f grows like $f^2 \sin^2 \tilde{\eta}$ [cf. Eq. (6.16)].

6.2.3 Finite temperatures

Now we consider the effects of finite temperatures $T > 0$ on the UCFs $\delta g_{\text{ad}}^{(2)}$ in the adiabatic regime. In the case of $\eta = 0$, i.e. $P = 0$, the factors containing $\delta_{-\alpha}^{C/D}(j)$ in Eq. (6.13) cancel, so we obtain

$$G_{\alpha, C/D}^{\text{ad}} \Big|_{\eta=0} = \frac{1}{d} \left\{ (w + \alpha \Delta \kappa)^2 + \delta_{\alpha}^{C/D}(j)^2 \right\}^{-1} + 2 \text{Re} \left\{ iw + i\alpha \Delta \kappa + \delta_{\alpha}^{C/D}(j) \right\}^{-2}. \quad (6.17)$$

This strong simplification allows us to evaluate the integrals over ϵ and ϵ' in Eq. (6.12) explicitly by using standard Matsubara techniques, as described

in App. H, and we obtain for the UCFs $\delta g_{\text{ad}}^{(2)} = \delta g_{\text{ad},C}^{(2)} + \delta g_{\text{ad},D}^{(2)}$,

$$\begin{aligned} \delta g_{\text{ad},C/D}^{(2)} \Big|_{\eta=0} &= \left(\frac{e^2}{h}\right)^2 \frac{1}{8\pi^6} \left(\frac{L^2}{L_T^2}\right)^2 \\ &\times \text{Re} \sum_{\alpha=\pm 1} \sum'_{j,n,m} \left\{ \frac{1}{d \delta_{\alpha}^{C/D}(j) \cdot \left[\frac{L^2}{4\pi L_T^2}(m+n) + \delta_{\alpha}^{C/D}(j) - i\alpha\Delta\kappa\right]^3} \right. \\ &\quad \left. + \frac{6}{\left[\frac{L^2}{4\pi L_T^2}(m+n) + \delta_{\alpha}^{C/D}(j) - i\alpha\Delta\kappa\right]^4} \right\}. \end{aligned} \quad (6.18)$$

Here n and m are odd, positive integers. For plotting, it is advantageous to calculate the sum in Eq. (6.18) analytically, which gives an expression containing Psi-functions.

We can now obtain a qualitative criterion when the thermal dephasing effects can be ignored. If we ignore thermal effects, i.e. assume low temperatures, we can simplify our calculation leading to Eq. (6.18) by replacing $n'(\epsilon)$ by a delta function $\delta(\epsilon)$ in Eq. (6.12). This yields for $\eta = 0$ the same result as applying Poisson's summation formula to Eq. (6.18) in order to replace the summations over n and m by integrations. We are only allowed to perform this step if the summand varies slowly in n , m , which is the case for $L_T^2 \gg 2\pi L_{C/D}^2$. From a physical point of view, this is an evident requirement: the smearing of the conductance fluctuations due to nonzero temperatures, described by the thermal diffusion length L_T , can only be neglected if the dephasing lengths related to inelastic scattering or penetrating magnetic fields are much shorter than L_T .

In App. I we evaluate the dephasing behavior of the UCFs $\delta g_{\text{hom}}^{(2)}$ for homogeneous fields and finite temperatures. Then we confirm the result of Ref. [87] [Eq. (6.2)] and show that our calculation in the homogeneous limit indeed reproduces known results [198, 201, 202].

6.3 Berry phase and Adiabaticity

6.3.1 Magic Angles—Qualitative criterion for Adiabaticity

We now consider the qualitative effects of the Berry phase on the conductance fluctuations $\delta g^{(2)}$. They emerge from the Berry phase in $\delta_\alpha^{C/D}(j)$ in the adiabatic solution [Eq. (6.12)] and lead to vanishing Aharonov-Bohm oscillations at special “magic” tilt angles of the magnetic fields. This effect has some similarities with the phenomenon of beating, where the superposition of two oscillations with different but fixed frequencies leads to a periodic vanishing of the envelope. However, in our case we have two frequencies which will change when the perpendicular field B_z is increased, since then the Berry phase is altered, too. Thus a suppression of the Aharonov-Bohm oscillations can only be observed at two special tilt angles of the magnetic field, i.e. the Berry phase has a highly non-periodic effect on the envelope of these oscillations as a function of B_z .

From now on we shall only study the experimentally realizable field texture with one winding, $f = 1$. The other configurations with $f > 1$ are solely of academic interest. To illustrate expected experimental results, we will use some material parameters recently determined [203]. The sample Au-1 given in Table I of Ref. [203] has the values $D = 9 \times 10^{-3} \text{ m}^2 \text{ s}^{-1}$ and $L_\varphi = \sqrt{D\tau_\varphi} = 5.54 \text{ } \mu\text{m}$. We assume a ring with diameter of $4 \text{ } \mu\text{m}$, so $L = 12.6 \text{ } \mu\text{m}$, and an arm width $a = 60 \text{ nm}$, which lies well within present-day experimental reach. Finally we assume low temperatures, i.e. $L_T \gg L, L_\varphi$, so we can ignore the dephasing due to thermal fluctuations.

Now we shall consider two equal fields, so no phase terms appear in the diffuson contribution $\delta g_D^{(2)}$. The cooperon contribution $\delta g_C^{(2)}$ is $h/2e$ periodic in the magnetic flux, as a shift of $m = \phi/\phi_0 + \tilde{\phi}/\phi_0 + j = 2\phi/\phi_0 + j$ by 1 is absorbed in the sum over j in Eq. (6.12). For the next argument we take the dephasing due to inhomogeneous fields only phenomenologically into account, i.e. we use the result $\delta g_{\text{LSG}}^{(2)}$ from Ref. [87] or equivalently set $P = 0$ [Eqs. (6.12, 6.17)], so the factors containing $\delta_{-\alpha}^{C/D}(j)$ cancel in Eq. (6.13). If the tilt angle η is such that $\cos \eta = 1/4$, the phase dependent term in $\delta_\alpha^{C/D}(j)$ [Eq. (6.15)] becomes $m - \alpha/4$. One sees that in this special case shifting m by $1/2$ does not affect the value of $\delta g_C^{(2)}$, as it leads solely to an exchange $\alpha \rightarrow -\alpha$. The very same argument applies to $\cos \eta = 3/4$. Thus, for these

magic angles η , where $\cos \eta = 1/4, 3/4$, the UCFs $\delta g^{(2)}$ are $h/4e$ periodic and therefore their *power spectrum shows a vanishing $h/2e$ amplitude*. If we take the exact solution in the adiabatic regime $\delta g_{\text{ad}}^{(2)}$ instead of $\delta g_{\text{LSG}}^{(2)}$, the magic angles are still present, but at shifted values. The angle at $\cos \eta = 3/4$ is nearly unaffected, as $P \approx 0.05$ is very small at this angle. The suppression of the Aharonov-Bohm oscillations is illustrated in Fig. 6.2 (see also Sec. 6.5.3 and Fig. 6.9) by plotting the $h/2e$ amplitude of the exact solution $\delta g^{(2)}$ with varying tilt angle η and for different radial field components. As one can readily see from Fig. 6.2, the effect described here is fully developed for $B \geq 200\text{G}$. For smaller fields, the $h/2e$ amplitude does not completely vanish at the magic angles, as adiabaticity is not yet reached. It should be noted that even if the adiabatic regime is not fully reached, an effect of the Berry phase is still visible as a distinct non-monotonic behavior of the UCFs $\delta g^{(2)}$ as a function of the tilt angle η , unlike the UCFs for a configuration with a homogeneous field texture (also shown in Fig. 6.2).

Another interesting situation arises for $B \neq \tilde{B}$. Now, phase effects from the diffuson contribution to $\delta g^{(2)}$ emerge and remain present even for large fields, since the dephasing due to flux penetrating the arms of the ring depends only on the difference of the fields and not on the sum as for the cooperon contribution, see Eq. (6.6). For illustration, we consider the configuration where \mathbf{B} is homogeneous with $\eta = 0$. The other field $\tilde{\mathbf{B}}$ is assumed to have a radial component so that for a tilt angle $\tilde{\eta} = \pi/3$ the magnitudes of both fields are equal, i.e. $\tilde{B}_{\parallel} = (\sqrt{3}/2)B_z$. In the adiabatic approximation $\delta g_{\text{ad}}^{(2)}$ [Eq. (6.12)] P vanishes, yielding the simple relation Eq. (6.16) between the dephasing due to the inhomogeneous field textures and $\gamma^{C/D}$: the effective dephasing will be increased by $3/16$ at the most interesting angle, $\tilde{\eta} = \pi/3$, in the situation considered here. The contribution of the penetrating fields to $\gamma^{C/D}$ will be three times larger for the cooperon than for the diffuson, as can be seen from Eq. (6.6). Varying \tilde{B}_z changes the Aharonov-Bohm phase $\tilde{\phi}/\phi_0$, while $\phi/\phi_0 = \text{const.}$, leading to h/e oscillations. At $\tilde{B}_z = B_z/2$ two features are worth mentioning. First, the magnitudes of both fields become equal, therefore $\Delta\kappa$ vanishes and so the second part of the criterion in Eq. (6.11) is fulfilled and we can use the adiabatic approximation $\delta g_{\text{ad}}^{(2)}$ [Eq. (6.12)]. Second, we have $\cos \tilde{\eta} = 1/2$, so the phase dependent terms $m \mp \alpha/4$ arise in $\delta_{\alpha}^{C/D}(j)$, as can be seen from Eq. (6.15). With the same argument as above, the UCFs $\delta g^{(2)}$ become $h/2e$ periodic at this magic angle $\pi/3$, so the h/e amplitude vanishes in the power spectrum. We note that, in the adiabatic

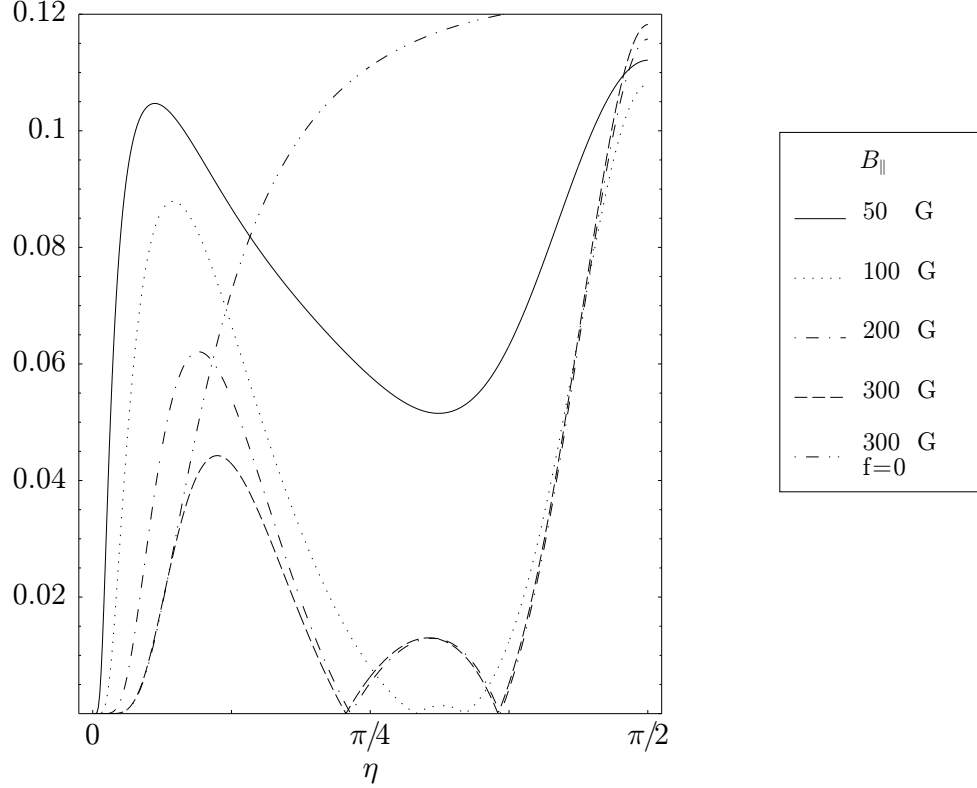


Figure 6.2: The normalized amplitudes of the $h/2e$ oscillations in the UCFs $\delta g^{(2)}$, as a function of the tilt angle η . The magnetic fields are chosen equal, i.e. $\mathbf{B} = \tilde{\mathbf{B}}$, and wind once around the ring (i.e. $f = 1$). The power spectrum of the exact UCFs $\delta g^{(2)}$ has been calculated at every tilt angle η by varying the Aharonov-Bohm flux $0 \leq \phi = \tilde{\phi} \leq 1$. The component of the $h/2e$ oscillation in this spectrum was then normalized by the 0th order Fourier component and is plotted here as a function of η . Four configurations of radial fields $B_{||} = \tilde{B}_{||}$ are shown; the perpendicular field components $B_z = \tilde{B}_z$ are determined by the tilt angles $\eta = \tilde{\eta}$. These field components and so also γ^C , as it depends on the arm-penetrating field, increase for small η . The strong dephasing γ^C at $\eta \approx 0$ can be observed as vanishing oscillations. The most remarkable effects show up for the stronger fields $B_{||} = 200$ G, 300 G at the magic angles $\eta = 0.72, 1.15$. Here the Berry phase eliminates the $h/2e$ oscillations, as it is described in Section 6.3.1. For comparison, we also show the conductance fluctuations for a homogeneous field, i.e. setting $f = 0$. We here set $T = 0$ and used the material parameters $L = 12.6 \mu\text{m}$, $a = 60 \text{ nm}$, $D = 9 \times 10^{-3} \text{ m}^2 \text{ s}^{-1}$, and $L_\varphi = 5.54 \mu\text{m}$.

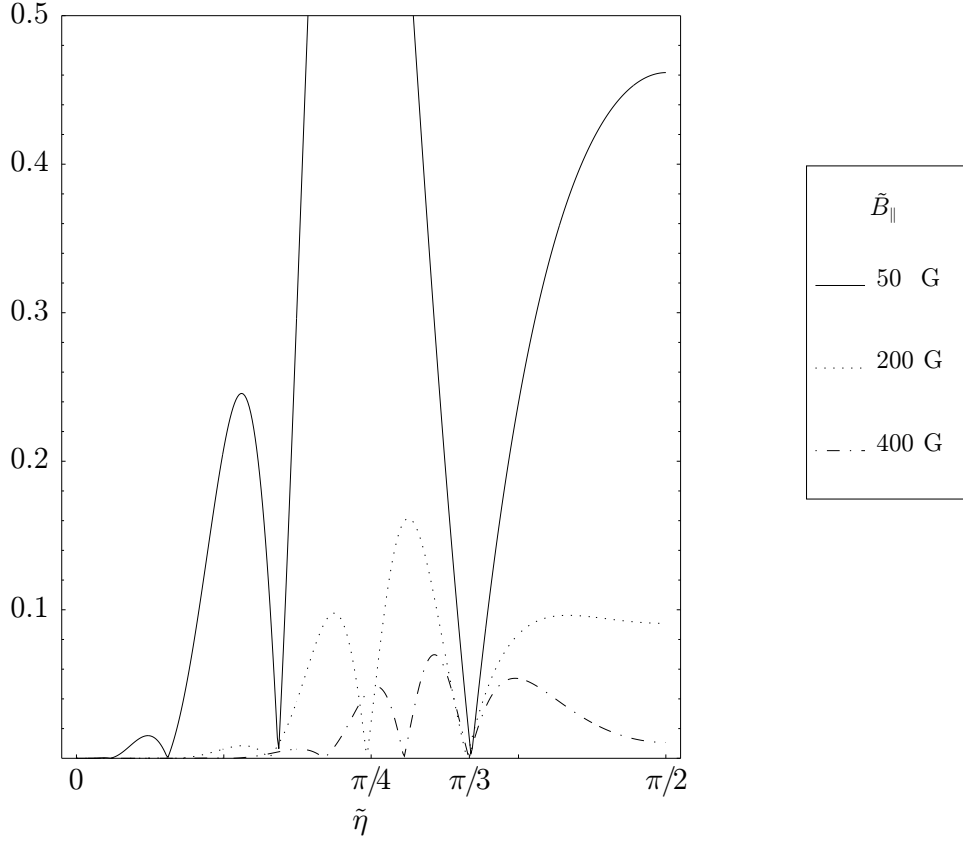


Figure 6.3: The normalized amplitudes of the h/e oscillations in the UCFs $\delta g^{(2)}$, with $\eta = 0$, as a function of the tilt angle $\tilde{\eta}$. The field were taken as $\mathbf{B} = (2/\sqrt{3})\tilde{B}_{\parallel}\mathbf{e}_z$, $\tilde{B}_{\parallel} = \text{const.}$, and \tilde{B}_z was determined through the tilt angle $\tilde{\eta}$. We use the same methods and parameters as described in Fig. 6.2 for $\tilde{B}_{\parallel} = 50$ G, 200 G, and 400 G. We notice that the h/e oscillations become suppressed by the Berry phase at the magic angle $\cos \tilde{\eta} = \pi/3$.

regime, this magic angle is exact, since for the configuration $\eta = 0$ we have $\delta g_{\text{ad}}^{(2)} = \delta g_{\text{LSG}}^{(2)}$. This is shown in Fig. 6.3, again as a function of the tilt angle $\tilde{\eta} = \cot(B_z/B_z)$, see also Sec. 6.5.3 and Fig. 6.10.

6.3.2 Quantitative criterion for Adiabaticity

In order to obtain a quantitative criterion for adiabaticity, we numerically compare the exact solution of the conductance fluctuations $\delta g^{(2)}$ with the adiabatic approximation $\delta g_{\text{ad}}^{(2)}$ [Eq. (6.12)]. We take equal magnitudes for both fields, i.e. $B = \tilde{B}$. We search for a minimal κ_{min} so that the relative difference $|\delta g^{(2)} - \delta g_{\text{ad}}^{(2)}|/\delta g^{(2)}$ is below a certain value. This is done with a bisection algorithm (in κ) and by sampling over the parameter subspace $[0, \pi/2]^2 \times [0, 1]^2 \times [\frac{1}{100}, 10]^2 \subset \{(\eta, \tilde{\eta}, \phi/\phi_0, \tilde{\phi}/\phi_0, \gamma^C, \gamma^D)\}$ with a grid resolution of 10 intersections in the first four dimensions. A finer resolution has been chosen for $\gamma^{C/D}$. As can be seen from Fig. 6.4, for $0.01 \leq \gamma^D \leq 1$, $\gamma^D \leq \gamma^C$ and a field strength such that $\kappa \geq 3$, the numerical values for $\delta g^{(2)}$ and $\delta g_{\text{ad}}^{(2)}$ are already within five percent of each other.

However, as we are interested in the Aharonov-Bohm oscillations rather than in the absolute value of the UCFs $\delta g^{(2)}$, we now use a different method of comparison: We consider the oscillations in the conductance fluctuations resulting from different Aharonov-Bohm fluxes through the ring. As a measure for accuracy we take the relative error of these amplitudes, i.e.

$$\Delta(\kappa, \gamma^C, \gamma^D, \eta, \tilde{\eta}) = \frac{\max_{\phi, \tilde{\phi}} \left| (\delta g^{(2)} - \delta g_{\text{ad}}^{(2)})|_{\phi=\tilde{\phi}=0} - (\delta g_{\text{ad}}^{(2)} - \delta g_{\text{ad}}^{(2)})|_{\phi=\tilde{\phi}=0} \right|}{\max_{\phi, \tilde{\phi}} \left| \delta g^{(2)} - \delta g_{\text{ad}}^{(2)} \right|_{\phi=\tilde{\phi}=0} |_{\eta, \tilde{\eta}=0}}. \quad (6.19)$$

Again we search for a minimal κ_{min} so that Δ is bounded from above by a certain percentage over the whole parameter subspace. We notice from the results shown in Fig. 6.5 that in the regime with only moderate damping $\gamma^C = \gamma^D = 0.1$, adiabaticity is already reached at $\kappa \sim 2$. If we put this in the context of the experimental parameters given in the beginning of Sec. 6.3.1, we expect adiabaticity to be fully reached at magnetic fields of magnitude larger than 500 G. By comparing this value with Fig. 6.2, we note that the qualitative effect of the Berry phase can already be seen for fields which are an order of a magnitude smaller, i.e. for $B, \tilde{B} \gtrsim 50$ G.

We now discuss the effects of different parameters on κ and on the minimal magnetic fields required to reach adiabaticity, thus indicating favorable

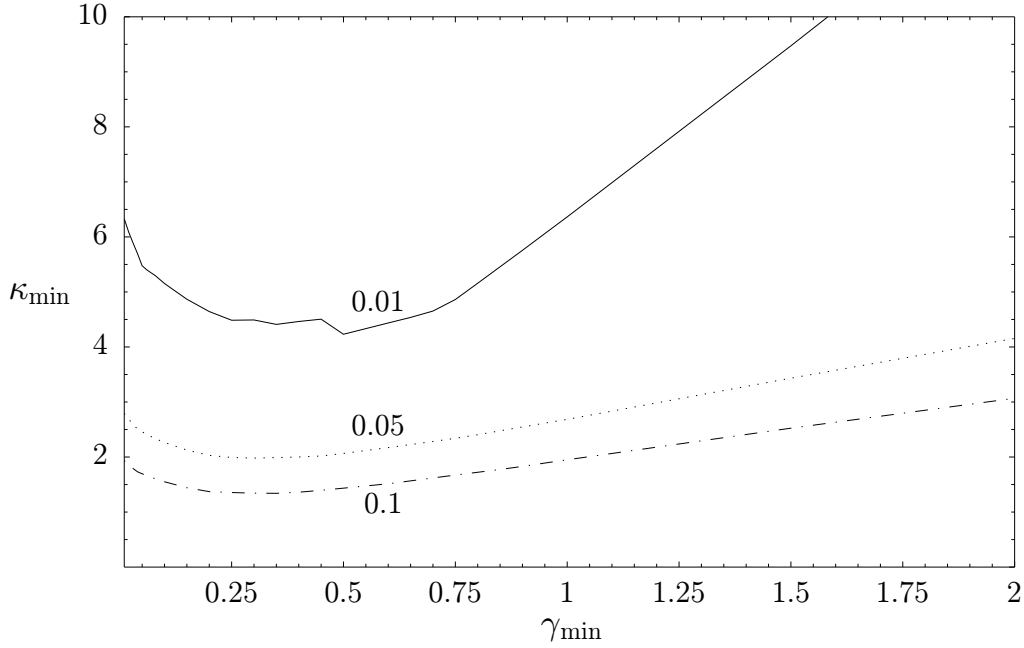


Figure 6.4: This plot shows the minimal κ_{\min} required so that the normalized difference $|\delta g^{(2)} - \delta g_{\text{ad}}^{(2)}|/\delta g^{(2)}$ is smaller than 0.01, 0.05, and 0.1; i.e. the plot shows for which magnitudes of the magnetic field the exact solution of the UCFs $\delta g^{(2)}$ agrees with the adiabatic approximation $\delta g_{\text{ad}}^{(2)}$ [Eq. (6.12)] to a certain accuracy. κ_{\min} is plotted against $\gamma_{\min} = \min\{\gamma^C, \gamma^D\}$; as the two fields \mathbf{B} , $\tilde{\mathbf{B}}$ may have different orientations, γ^D can become larger than γ^C . As $\delta g^{(2)}$ vanishes for large $\gamma^{C/D}$, our normalization is no longer well defined for $\gamma^{C/D} \gtrsim 1$ and the value for κ_{\min} diverges.

experimental setups. If we consider rings of increasing circumference L , we can see from Eq. (6.5) that the minimal magnetic field strength needed decreases as $B_{\text{ad}} \propto L^{-2}$. However, to observe the Berry phase, dephasing must not be too strong, so the condition $L \lesssim 2L_{C/D}$ should still be met. We note that for two equal fields, the first term of $\gamma^C \propto L_C^{-2}$ in Eq. (6.6) depends on L^2 , which restrains us from taking $L > 2L_\varphi$, whereas the second one depends for $B = B_{\text{ad}}$ on L^{-2} . So not only the high magnetic fields needed for adiabaticity, but also the small arm widths a required to minimize strong dephasing due to the penetrating flux, disfavors experimental setups with very small L .

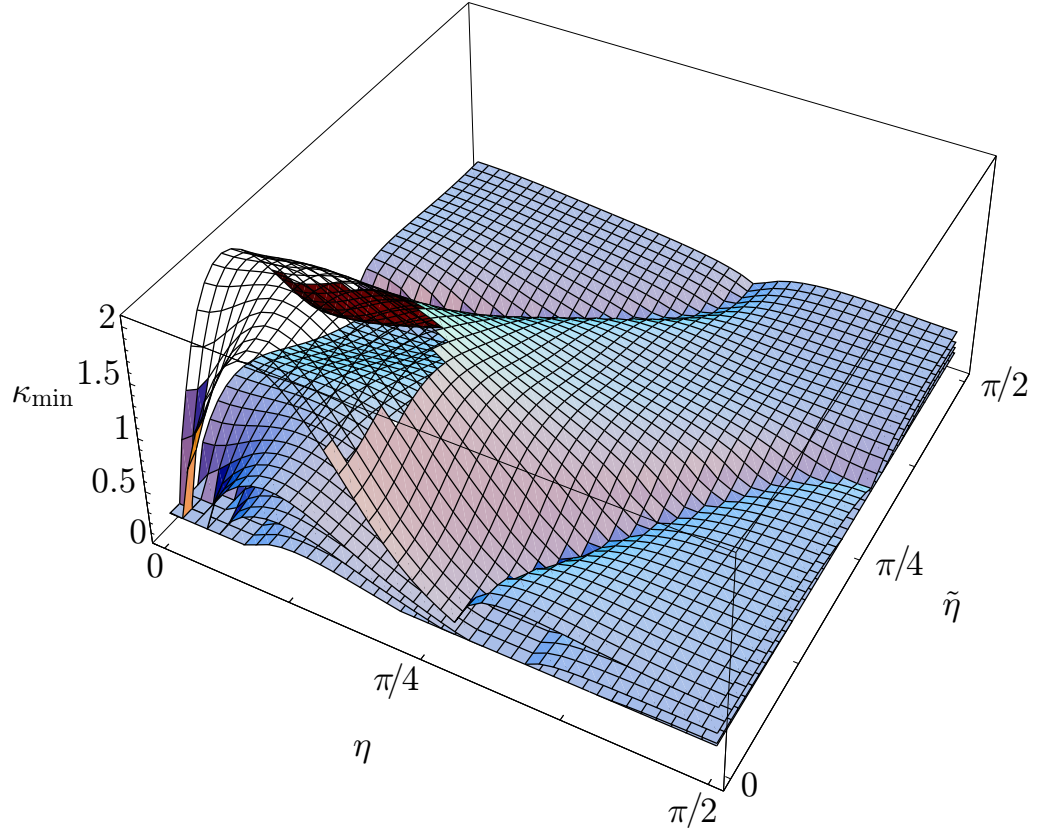


Figure 6.5: Here the quality of the adiabatic approximation $\delta g_{\text{ad}}^{(2)}$ [Eq. (6.12)] in describing the Aharonov-Bohm oscillations is shown. We used Eq. (6.19) and set $\gamma^C = \gamma^D = 0.1$. The surfaces shown are, from top to bottom, the minimal value of κ_{min} required for an agreement $\Delta < 0.01, 0.05, 0.1$, and 0.2 [Eq. (6.19)]. As expected, for $\eta = \tilde{\eta} = 0$ we have $\delta g^{(2)} = \delta g_{\text{ad}}^{(2)}$. For tilt angles $\eta, \tilde{\eta} \approx \pi/2$, the agreement is obtained at low κ_{min} , whereas at $\eta = \tilde{\eta} \approx 0.25$ larger fields are necessary.

Introducing more impurities and thus decreasing the diffusion coefficient D leads to slower motion of the electrons around the ring, giving their spins more time to adjust to the local magnetic texture. Thus, the field strengths required for adiabaticity to occur decrease as $B_{\text{ad}} \propto D$, which can be seen from Eq. (6.5). However, such slow diffusion also leads to shorter dephasing lengths L_T , $L_\varphi \propto D^{1/2}$; assuming that τ_φ remains constant. To avoid such an additional dephasing, i.e. leaving $\gamma^{C/D}$ unaffected, the sample size must also be decreased as $L \propto D^{1/2}$. Thus, because of $\kappa \propto D^{-1}L^2$, no net decrease of the required fields for adiabaticity can be gained by decreasing the diffusion coefficient.

6.4 Exact calculations with spin-orbit interaction in diffusive limit

We turn now to the discussion of Berry phases induced by spin-orbit interaction. Instead of considering an inhomogeneous field, we use here an effective (non-hermitian) Hamiltonian

$$h_{so}^{C/D} = \frac{L}{(2\pi)^2} \frac{\partial^2}{\partial x^2} + i\kappa\sigma_{1z} - i\tilde{\kappa}\sigma_{2z} + i\frac{\alpha}{\hbar^2} \frac{L^2}{D(2\pi)^2} (\mathbf{e}_z \times \boldsymbol{\sigma}^{(*)}) \cdot \mathbf{p}, \quad (6.20)$$

with spin-orbit interaction, using a coupling constant α as defined in Ref. [204], and with a Zeeman term from an external magnetic field, which is perpendicular to the ring plane. One arrives at this Hamiltonian by starting from the Feynman path integral representation of the transition amplitude with spin-orbit coupling, as it is given in Ref. [205]. One can then formally decouple orbital and spin motion, and following the steps given in App. A of Ref. [87], one arrives at the effective Schrödinger equation for the cooperon propagator with the Hamiltonian h_{so}^C . The equation with h_{so}^D for the diffuson, which will be required in Sec. 6.4.2, can be obtained by applying the techniques explained in App. G.

Note that in Eq. (6.20) the momentum operator is still in the Cartesian coordinate system. Now we adopt a polar coordinate system, with $(x', y') = (r \cos \frac{2\pi x}{L}, r \sin \frac{2\pi x}{L})$ and $(\partial_{x'}, \partial_{y'}) = (-\frac{1}{2}\{\sin \frac{2\pi x}{L}, \partial_x\}, \frac{1}{2}\{\cos \frac{2\pi x}{L}, \partial_x\})$, where x denotes the position along the ring and runs from 0 to L . The curly braces denote the anticommutator, which ensures the hermiticity of the momentum

operator. We now have

$$h_{so}^{C/D} = \frac{L^2}{(2\pi)^2} \frac{\partial^2}{\partial x^2} + i\kappa\sigma_{1z} - i\tilde{\kappa}\sigma_{2z} + \frac{\alpha}{\hbar} \frac{L^2}{D(2\pi)^2} \frac{1}{2} \left\{ \sigma_{1x} \cos \frac{2\pi x}{L} + \sigma_{1y} \sin \frac{2\pi x}{L} - \sigma_{2x} \cos \frac{2\pi x}{L} \mp \sigma_{2y} \sin \frac{2\pi x}{L}, \frac{\partial}{\partial x} \right\}. \quad (6.21)$$

To diagonalize the Hamiltonian, we follow the ideas used above and use the operators defined in Eq. (6.7), but now with $f = \tilde{f} = 1$:

$$J^{C/D} := \frac{L}{2\pi i} \frac{\partial}{\partial x} + \frac{1}{2} \sigma_{1z} \pm \frac{1}{2} \sigma_{2z}, \quad (6.22)$$

which commute with the Hamiltonians $h_{so}^{C/D}$, as can be seen using $[\{n(x), \partial_x\}, \partial_x] = -\{n'(x), \partial_x\}$. We can now calculate the matrix elements of $h_{so}^{C/D}$ in the basis defined in Eq. (6.8), with $f = \tilde{f} = 1$, as

$$\begin{aligned} \langle j, \alpha\beta | h_{so}^C | j', \alpha'\beta' \rangle &= \delta_{jj'} \\ \times \begin{pmatrix} -(j-1)^2 + i\kappa - i\tilde{\kappa} & iS(j-\frac{1}{2}) & iS(-j+\frac{1}{2}) & 0 \\ iS(j-\frac{1}{2}) & -j^2 + i\kappa + i\tilde{\kappa} & 0 & iS(-j-\frac{1}{2}) \\ iS(-j+\frac{1}{2}) & 0 & -j^2 - i\kappa - i\tilde{\kappa} & iS(j+\frac{1}{2}) \\ 0 & iS(-j-\frac{1}{2}) & iS(j+\frac{1}{2}) & -(j+1)^2 - i\kappa + i\tilde{\kappa} \end{pmatrix}, \end{aligned} \quad (6.23)$$

and

$$\begin{aligned} \langle j, \alpha\beta | h_{so}^D | j', \alpha'\beta' \rangle &= \delta_{jj'} \\ \times \begin{pmatrix} -j^2 + i\kappa - i\tilde{\kappa} & iS(j-\frac{1}{2}) & iS(-j-\frac{1}{2}) & 0 \\ iS(j-\frac{1}{2}) & -(j-1)^2 + i\kappa + i\tilde{\kappa} & 0 & iS(-j+\frac{1}{2}) \\ iS(-j-\frac{1}{2}) & 0 & -(j+1)^2 - i\kappa - i\tilde{\kappa} & iS(j+\frac{1}{2}) \\ 0 & iS(-j+\frac{1}{2}) & iS(j+\frac{1}{2}) & -j^2 - i\kappa + i\tilde{\kappa} \end{pmatrix}. \end{aligned} \quad (6.24)$$

In Eqs. (6.23) and (6.24), we have introduced a dimensionless spin-orbit coupling parameter

$$S = \frac{\alpha}{\hbar D} \frac{L}{2\pi}. \quad (6.25)$$

By comparing Eqs. (6.5) and (6.25), we note that while κ is quadratic in L , the parameter S is only linearly dependent on L . If we define an effective field angle for diffusive motion with spin-orbit coupling

$$\tan \eta_{SO} = S/\kappa, \quad (6.26)$$

and anticipate the Berry phase to be of the form $\Phi^g = \cos \eta$, we obtain for $S \gg \kappa$ the dependency $\Phi^g \approx \kappa/S \propto L$. Thus the phase can now be enhanced by increasing the size of the ring. However, the phase cannot be increased arbitrarily; for large L , the assumption $S \gg \kappa$ becomes invalid.

6.4.1 Magnetoconductance

We shall now calculate the magnetoconductance with the formula from Ref. [87]

$$\delta g_{SO} = -\frac{e^2}{\pi \hbar} \frac{L}{(2\pi)^2} \sum_{\alpha, \beta = \pm 1} \left\langle x, \alpha, \beta \left| \frac{1}{\gamma - h_{SO}^C} \right| x, \beta, \alpha \right\rangle. \quad (6.27)$$

With Eq. (6.23), we obtain the magnetoconductance

$$\begin{aligned} \delta g_{SO} = & -\frac{e^2}{\pi \hbar} \sum_{j=-\infty}^{\infty} \left\{ 2 \left[4\kappa^2 + (m^2 + \gamma)^2 \right] (m^2 + \gamma + 1) \right. \\ & \left. + S^2 \left[8m^4 + 2m^2 (4\gamma - 1) + 2\gamma + 1 \right] \right\} \times \left\{ \left[4\kappa^2 + (m^2 + \gamma)^2 \right] \right. \\ & \times \left[m^4 + 2m^2 (\gamma - 1) + (\gamma + 1)^2 \right] \\ & \left. + S^2 (m^2 + \gamma) \left[4m^4 + m^2 (4\gamma - 3) + \gamma + 1 \right] \right\}^{-1}, \quad (6.28) \end{aligned}$$

where $m = j - 2\phi/\phi_0$ contains the Aharonov-Bohm flux. In Sec. 6.5 we will see that in the ‘‘adiabatic’’ limit $\kappa, S \gg 1$ the magnetoconductance δg_{SO} will show some similar properties as for inhomogeneous fields, in particular a peak-splitting in the power spectrum, see Fig. 6.11.

6.4.2 Conductance fluctuations

We turn now to a discussion of the recent experiment by Morpurgo et al [79]. by specifying the parameters of the effective Hamiltonian $h_{SO}^{C/D}$, as given in Eqs. (6.20), (6.23), and (6.24). In Ref. [79], conductance measurements were performed on an InAs ring, with nearly ballistic transport. For the

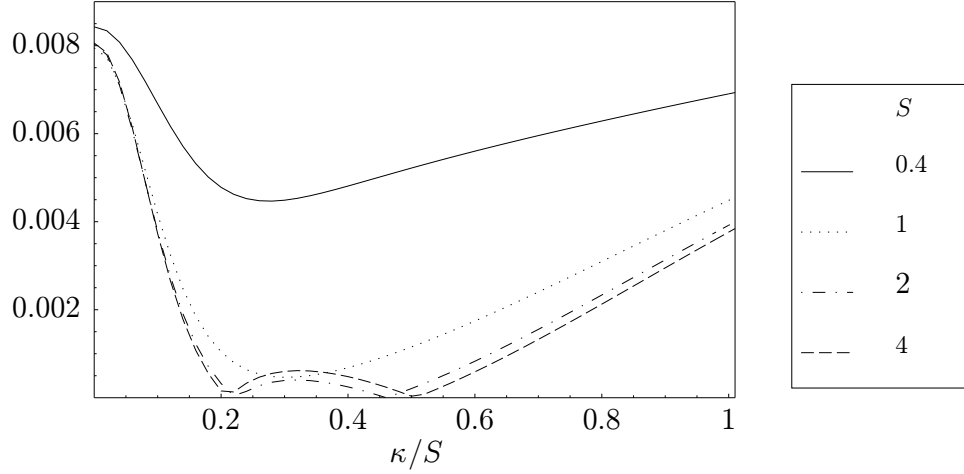


Figure 6.6: The normalized amplitudes of the $h/2e$ oscillations of the UCFs with spin-orbit coupling, $\delta g_{so}^{(2)}$. The power spectrum of the Aharonov-Bohm oscillations was calculated at different values $\kappa = \tilde{\kappa}$ of the perpendicular fields by varying the Aharonov-Bohm flux $0 \leq \phi = \tilde{\phi} \leq 1$. From the power spectrum, the frequency contribution of the $h/2e$ oscillation was normalized by the zero frequency contribution and is shown here as a function of κ/S . We have assumed $T = 0$ and $\gamma^C = \gamma^D = 0.1$.

parameters given [79], $\alpha = 5.5 \times 10^{-10}$ eV cm, $L = 6.6 \mu\text{m}$, $v_F = 9.8 \times 10^7$ cm/s, $\ell = 1.0 \mu\text{m}$, and $D = v_F \ell / 2 = 4.9 \times 10^3$ cm²/s, we calculate with Eq. (6.25) a numerical value of $S \approx 1/50$. Compared to this, the strength of the Zeeman term $\kappa \approx 1/2$ (with $|g| = 15$) is much larger. Within the diffusive approximation, this spin-orbit coupling $S \ll \kappa$ gives only a negligible contribution to the effective Hamiltonian $h^{C/D}$ [Eq. (6.20)] and thus does not produce any Berry phase effects. This very same finding has also been obtained in Ref. [206], based on a slightly different reasoning. Still, we show in Sec. 6.5 that a spin-splitting produced by spin-orbit interaction can be obtained in the “adiabatic regime” $\kappa, S \gg 1$, which, however, is in the opposite limit to the one reported in Ref. [79]. So although we cannot give a quantitative explanation of the experiment [79] here, we can offer a qualitative interpretation, see Fig. 6.13. Further, there is an uncertainty in the spin-orbit coupling parameter α in InAs, as it was recently pointed out [207], and more experiments might be needed to clarify this issue.

To this end we calculate the exact, i.e. without assuming any form of adiabaticity, expression for the conductance fluctuations $\delta g_{sO}^{(2)}$ in the presence of spin-orbit interaction. With the block-diagonalization of the Hamiltonian $h_{sO}^{C/D}$ [Eqs. (6.23), (6.24)] we obtain the propagators required in the formula for the conductance correlator [Eq. (6.2)]. We use Mathematica to obtain an explicit algebraic expression for $\delta g_{sO}^{(2)}$ (which is lengthy and thus not reproduced here) and plot it in Fig. 6.6 (see also Figs. 6.12 and 6.13). From this plot we deduce that in a configuration with spin-orbit coupling, the Aharonov-Bohm oscillations vanish for certain values of S and κ . It is remarkable that this happens, for $S \geq 2$, at the fixed ratios $\kappa/S = 0.2$ and 0.5 , which can be ascribed again to some effective magic angles. Thus we see that Berry phase-like effects occur in $\delta g_{sO}^{(2)}$ as the amplitudes of the Aharonov-Bohm oscillations become dependent on κ/S . This resembles the case for inhomogeneous fields, where the amplitudes of the Aharonov-Bohm oscillations became dependent on the tilt angle η of the magnetic field due to the Berry phase, as it was shown in Sec. 6.3.1.

6.5 Peak splittings in power spectra

6.5.1 Frequency shifts in δg and $\delta g^{(2)}$

We discuss now the emergence of the Berry phase in terms of a splitting of the frequencies of the Aharonov-Bohm oscillations in the magnetoconductance [87, 189] δg and in the UCFs [87] $\delta g^{(2)}$, which can be made visible in the power spectrum [79]. Both quantities depend on the spin-dependent total phase Φ_α , given here for the special case of the texture defined in Eq. (6.1) and for two equal fields $\mathbf{B} = \tilde{\mathbf{B}}$,

$$\begin{aligned} \Phi_{\pm 1} &= 2\phi/\phi_0 \pm \cos \eta = 2\phi/\phi_0 \pm \frac{1}{\sqrt{1 + (B_{\parallel}/B_z)^2}} \\ &\approx 2\phi/\phi_0 \pm B_z/B_{\parallel} = B_z \left(2B_{\phi_0}^{-1} \pm B_{\parallel}^{-1} \right). \end{aligned} \quad (6.29)$$

The approximation used here is valid for small perpendicular fields $B_z \ll B_{\parallel}$. We have introduced $B_{\phi_0} = \phi_0/A$ as the perpendicular field which produces a flux of one flux quantum ϕ_0 through the ring, i.e. the period of an Aharonov-Bohm oscillation in ϕ . The Berry phase is not sensitive to the area enclosed by the ring; thus we prefer here to describe oscillations in B_z rather than in

ϕ . As both δg and $\delta g^{(2)}$ contain periodic terms in Φ_1 and Φ_{-1} , they exhibit oscillations in B_z with the Aharonov-Bohm frequency for homogeneous fields, $2B_{\phi_0}^{-1}$, shifted (at $B_z = 0$) by the frequency

$$\frac{1}{\Delta B_1} = \pm \frac{1}{B_{\parallel}}, \quad (6.30)$$

which results in a peak splitting in the power spectrum.

These splittings are, however, generally on the order of the resolution of the spectrum, which makes it difficult to make them visible. If the perpendicular field is varied from $-B_{\max}$ to B_{\max} , the discrete Fourier transform (DFT) of such an interval has a resolution of $1/2B_{\max}$, i.e. the sampling frequencies are separated by this value. Thus, the peak-splitting term can only be made visible if this resolution is high enough, i.e. $1/2B_{\max} \leq 1/B_{\parallel}$, or

$$B_{\max} \geq \frac{1}{2}B_{\parallel}. \quad (6.31)$$

We note that this restriction is still consistent with the approximation made in Eq. (6.29), since for $B_z = B_{\parallel}/2$ the approximated value of the Berry phase is larger than the exact value by only a factor of $\sqrt{5}/2 \approx 1.1$.

Now we consider the case beyond the above approximation. Here, an estimate for the frequency shifts can be obtained by counting the additional oscillations upon increasing B_z . In this estimation we again neglect the change in frequency of the Aharonov-Bohm oscillations while B_z is increased. However, now we take the mean value of the frequency instead of the frequency at $B_z = 0$ as in Eq. (6.30). Varying B_z from 0 to B_{\max} changes the Berry phase contribution to $\Phi_{\pm 1}$ [Eq. (6.29)] from 0 to $\pm \cos \eta|_{B_z=B_{\max}}$, and so we obtain the mean frequency shift

$$\frac{1}{\Delta B_2} = \pm \frac{1}{\sqrt{B_{\max}^2 + B_{\parallel}^2}} \approx \pm \frac{1}{B_{\parallel}} \left(1 - \frac{B_{\max}^2}{2B_{\parallel}^2} \right). \quad (6.32)$$

When we have calculated the DFT of δg and $\delta g^{(2)}$, we have confirmed the predictions given above, i.e. we do not observe a peak splitting in the $2B_{\phi_0}^{-1}$ frequency for low B_{\max} , due to an insufficient resolution of the DFT. However, we do see a peak splitting in the DFT for higher fields (see Figs. 6.8, 6.9), which vanishes again for $B_{\max} \gg B_{\parallel}$. Since studies of the DFT suffer from

a restricted resolution, it might be more promising to search for the Berry phase via the effects discussed in Sec. 6.3.1.

Finally, we point out that an anisotropic g factor affects the size of the frequency splitting. If the g factor perpendicular to the ring, g_z , is larger than the one in the plane of the ring, g_{\parallel} , the Berry phase dependence on B_z increases while the Aharonov-Bohm phase remains unaffected. As the total phase is $\Phi_{\pm 1} \approx 2\phi/\phi_0 \pm g_z B_z/g_{\parallel} B_{\parallel}$, the frequency splitting is increased by a factor of g_z/g_{\parallel} .

6.5.2 Frequency shifts in $\delta g_{\text{hom}}^{(2)}$ for homogeneous fields

At this point it is important to realize that frequency shifts can also appear in the conductance fluctuations $\delta g^{(2)}$ for homogeneous fields, i.e. even when there is no Berry phase present. For homogeneous fields the evaluation of Eq. (6.2) is straightforward, as $h^{C/D}$ [Eq. (6.10)] becomes diagonal, see also App. I. We evaluate the DOS terms, i.e. the terms containing $\text{Re Tr } \hat{\chi}_{\omega} \hat{\chi}_{\omega}$ in Eq. (6.2), in the low temperature limit for $\eta = \tilde{\eta} = 0$:

$$\begin{aligned} \delta g_{\text{DOS}, C/D}^{(2)} &\propto \text{Re} \sum_{\substack{j \\ \alpha, \tilde{\alpha} = \pm 1}} \frac{1}{[\gamma + (j - \Phi^{C/D})^2 + i(\alpha\kappa + \tilde{\alpha}\tilde{\kappa})]^2} \\ &\approx \frac{2\pi}{\gamma^{3/2}} + \sum_{\alpha, \tilde{\alpha}} \sum_{n=1}^{\infty} \frac{2\pi^2 n}{\gamma} e^{-2\pi n \sqrt{\gamma}} \cos \left[2\pi n \left(\Phi^{C/D} + \frac{\alpha\kappa + \tilde{\alpha}\tilde{\kappa}}{2\sqrt{\gamma}} \right) \right], \end{aligned} \quad (6.33)$$

where we have defined $\Phi^{C/D} = \phi/\phi_0 \pm \tilde{\phi}/\phi_0$. The approximation on the second line of Eq. (6.33) is valid for $\gamma \gg 1/4\pi^2$, $\alpha\kappa + \tilde{\alpha}\tilde{\kappa}$. From Eq. (6.33), we see that the Zeeman term itself already leads to a frequency splitting. So, for instance, if we take the Fourier transform of $\delta g^{(2)}(B_z, -B_z)$ with respect to B_z , we can observe a frequency splitting of the h/e oscillations of the diffuson contribution in the DOS term $\delta g_{\text{DOS}, D}^{(2)}$, given by

$$\frac{1}{\Delta B_{\text{Zeeman}}} = \pm \frac{g\mu_B}{4\hbar D} \frac{L_D L}{2\pi}. \quad (6.34)$$

We checked numerically that the estimated frequency splitting [Eq. (6.34)] is correct within 20 percent even for parameters beyond the assumptions made for the second line of Eq. (6.33). It is important to keep this property of

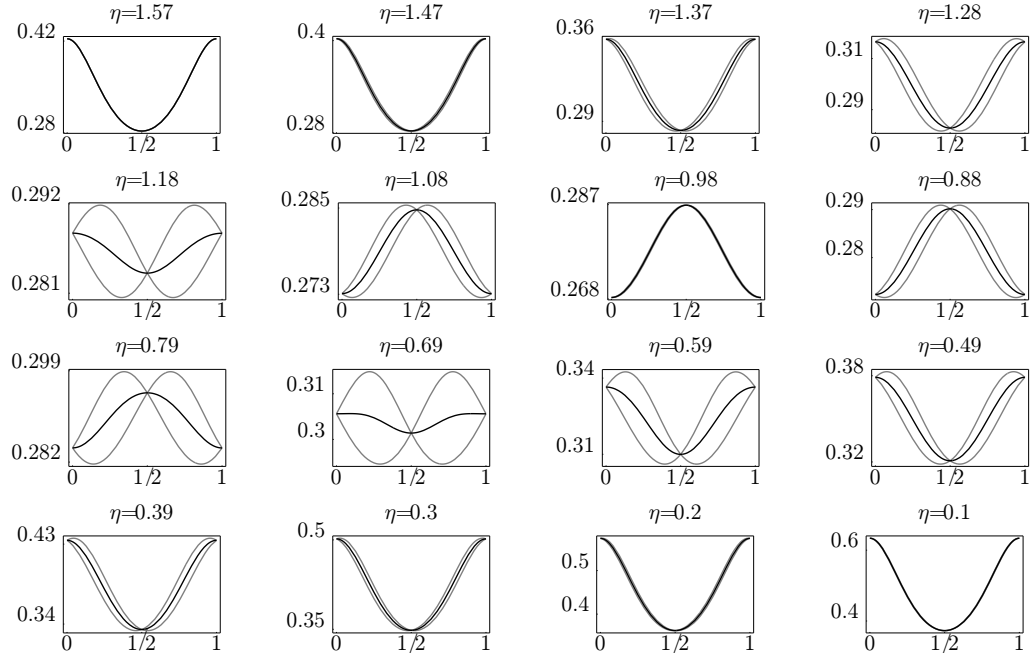


Figure 6.7: The magnetoconductance δg in units of $-2e^2/h$ as a function of the Aharonov-Bohm flux $2\phi/\phi_0$, for different tilt angles η of the external field. We have chosen the dephasing $\gamma = 0.1$ and the field B_{\parallel} parallel to the ring plane to be constant, defined through $B_{\parallel} \propto \kappa_{\parallel} = \kappa \sin \eta = 2.0$. The magnetoconductance is shown in black, while its contribution from the different spins $\alpha = \pm 1$ are scaled by a factor of two and drawn in gray.

the conductance fluctuations $\delta g^{(2)}$ in mind, when searching for Berry phase effects. If vanishing Aharonov-Bohm oscillations or peak splittings in the power spectrum are used to identify the presence of a Berry phase, one has to rule out effects coming from the Zeeman term in the UCFs, e.g. by comparison with the results for homogeneous fields.

6.5.3 Numerical evaluations

We shall now numerically evaluate the magnetoconductance δg for a ring in an inhomogeneous field. We base our analysis on the calculations from Ref. [191]. In Fig. 6.7 we show the Aharonov-Bohm oscillations for different tilt angles η of the external field \mathbf{B} , which is set so strong that we are well within the adiabatic regime. We can readily see that for $\eta \approx \pi/3$ a phase

shift of π occurs, which comes directly from the Berry phase, compared to the oscillations at $\eta = 0$ and $\eta = \pi/2$. For the intermediate tilt angles the effect of the Berry phase is only visible in the amplitude of the Aharonov-Bohm oscillations, as the phase shifts for the two spin directions occur with opposite signs and thus—if both spin directions contribute equally—no phase-shift effect is visible.

As such a phase shift at $\pi/3$ might not be easy to observe, studying signs in the power spectrum provides an interesting alternative [79], even though it requires a sufficiently high resolution, as discussed in Sec. 6.5.1. Indeed, we can observe a peak splitting in the spectrum of the magnetoconductance, as shown in the inset of Fig. 6.8. We notice an even more distinct feature: the Aharonov-Bohm oscillations vanish at two magic tilt angles, $\cos \eta = 0.4, 0.75$, of the field. The mechanism for this effect is exhibited in Fig. 6.7, where it is shown how the two contributions of the different spins suppress the oscillations.

At this point, we would like to stress that the peak splitting depends strongly on the different dephasing terms. In particular, one cannot rely on calculations where the dephasing due to the inhomogeneous fields is not properly taken into account. So if the dephasing γ due to homogeneous effects is very small, e.g. on the order of $1/100$, the amplitude of the oscillations gets reduced drastically as soon as the tilt angle η changes from $\pi/2$ to a smaller, nonzero value, since the field inhomogeneity causes additional dephasing. Thus the Fourier transform of such oscillations has a dominant contribution only from the first few oscillations close to $\pi/2$. This suppression of the remaining oscillations acts as a narrowing of the data window [209] and leads to a widening of the peaks in the power spectrum, masking the peak splitting. The oscillations are further suppressed by the additional dephasing arising from an increasing perpendicular field, which penetrates the ring arms. Of course, it is possible to remove this unwanted over-emphasizing of certain oscillations from experimental data in a post-processing step; using a standard windowing function (we used the Hann window [209] for the inset of Fig. 6.8) for DFTs greatly reduces this problem, in addition to the usual reduction of components leakage of neighboring frequencies in the power spectrum [209].

For the conductance fluctuations $\delta g^{(2)}$, we will further illustrate the effects of the two configurations discussed in Section 6.3.1. In Fig. 6.9 we show the Aharonov-Bohm oscillations occurring in $\delta g^{(2)}$ when the fields are equal, i.e. $\mathbf{B} = \tilde{\mathbf{B}}$. Taking the discrete Fourier transform of $\delta g^{(2)}$ over the range $B_z = 0, \dots, 1$ T, yields a clear peak splitting of the contribution of

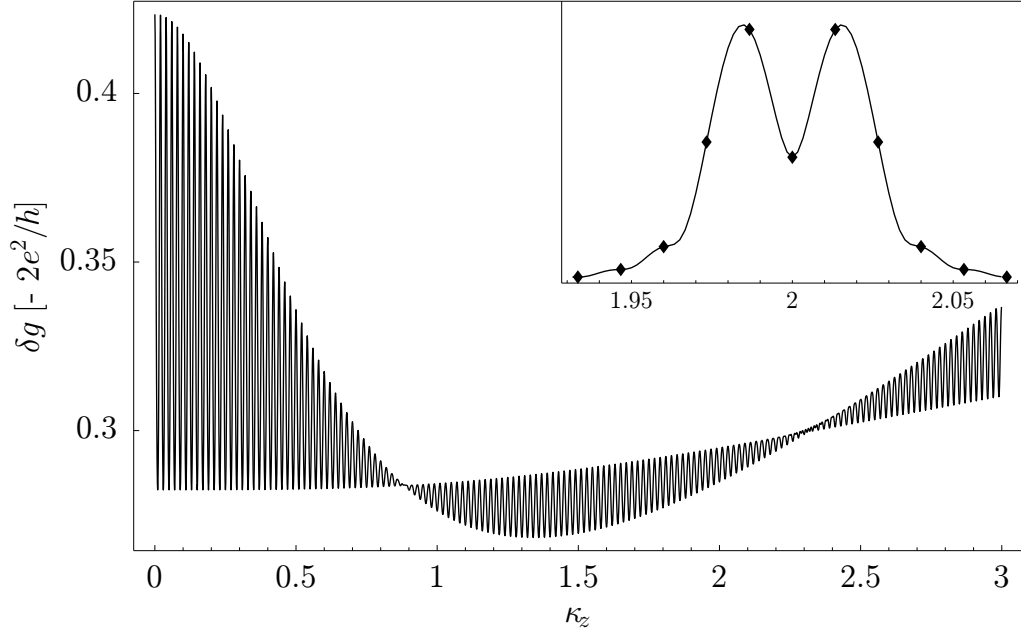


Figure 6.8: The Aharonov-Bohm oscillations in the magnetoconductance δg as a function of the perpendicular field B_z , shown here as $\kappa_z = \kappa \cos \eta$. The radial field component has a magnitude of $B_{\parallel} \propto \kappa_{\parallel} = \kappa \sin \eta = 2.0$ and $\gamma = 0.1$. The vanishing oscillations near $\kappa_z \approx 0.9, 2.3$ (for the magic angle $\cos \eta \approx 0.4, 0.75$) are striking; this a direct consequence of the Berry phase, arising from a canceling of the oscillating contributions of opposite spin directions. The inset shows the power spectrum [208] where a peak splitting is visible.

the $h/2e$ oscillations to the power spectrum, see left inset in Fig. 6.9. We notice a splitting into four peaks of the contribution of the $h/4e$ oscillations (right inset of Fig. 6.9). They only occur in the exact solution $\delta g^{(2)}$, whereas $\delta g_{\text{ad}}^{(2)}$ exhibits only two peaks if we ignore the $\eta, \tilde{\eta}$ -dependent dephasing, i.e. set $\tilde{\gamma}_{\eta, \tilde{\eta}}^{C/D} \rightarrow \gamma^{C/D}$ and $P \rightarrow 0$ in Eq. (6.12). We point out that the frequency shifts for the n th harmonics of the Aharonov-Bohm oscillations increase with n and are thus better resolved in the power spectrum with increasing n .

We plot $\delta g^{(2)}(\tilde{\mathbf{B}})$ in Fig. 6.10 for the special case $\tilde{\mathbf{B}} = (0, 0, \tilde{B}_z)$ homogeneous (see also Sec. 6.3.1).

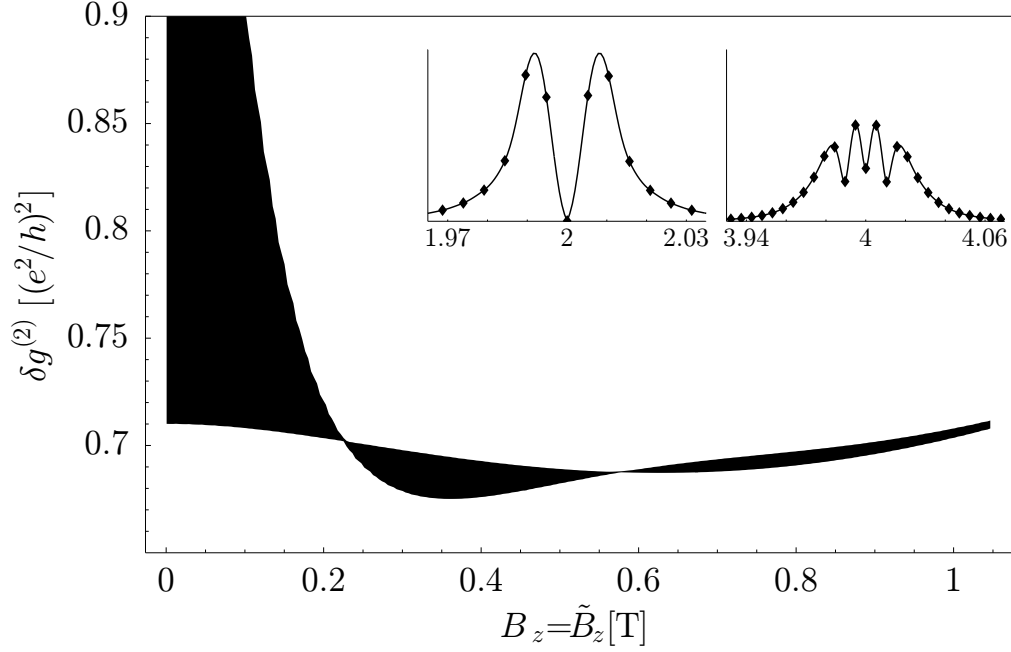


Figure 6.9: The UCFs $\delta g^{(2)}$ for $\mathbf{B} = \tilde{\mathbf{B}}$ plotted as function of B_z (see first part of Sec. 6.3.1). While the printing resolution is not high enough to show the Aharonov-Bohm oscillations, the envelope clearly illustrates the non-monotonic behavior of their amplitudes, which vanish at the magic angles $\eta = 0.72, 1.15$. We have taken a fixed radial component for both fields of $B_{\parallel} = \tilde{B}_{\parallel} = 0.5$ T. We have assumed $L = 3 \mu\text{m}$, $D = 65 \text{ cm}^2/\text{s}$, and $T = 0$. The dephasing was taken into account according to Eq. (6.6), with the parameters $L_{\varphi} = 1.5 \mu\text{m}$, and $a = 60 \text{ nm}$. The two insets show the contributions of the $h/2e$ and $h/4e$ oscillations to the power spectrum [208] in arbitrary units plotted against the frequency in units of ϕ_0^{-1} . The right inset was scaled by a factor of 10. For the particular range of B_z chosen here, there is a peak splitting visible for the $h/2e$ oscillations, while we observe four peaks around the $h/4e$ frequency.

Finally, we consider the power spectrum of the magnetoconductance δg_{so} in the presence of spin-orbit coupling. We use Eq. (6.28) and ignore for simplicity dephasing due to the external magnetic fields penetrating the arms of the ring. Indeed, taking the Fourier transform of the magnetoconductance, a spin splitting can be observed. However, the splitting is not as pronounced as in the case for inhomogeneous fields. Especially important, the splitting is only visible for sufficiently large dephasing parameters γ (produced by inelastic scattering), which can be seen in Fig. 6.11. In contrast to the effects discussed before, using a windowing function was not sufficient to identify a peak splitting for moderately small dephasing parameters $\gamma \lesssim 0.3$. Qualitatively, however, the power spectra of the magnetoconductance for inhomogeneous magnetic fields and for spin-orbit coupling agree, with both showing a peak splitting.

The UCFs with spin-orbit interaction $\delta g_{so}^{(2)}$ are plotted in Fig. 6.12 as a function of the perpendicular fields $B_z = \tilde{B}_z$. We observe a Berry phase-like frequency splitting in the power spectrum. However, as this splitting is rather small, it is only visible in the $h/4e$ oscillations, where the splitting is twice as large as in the $h/2e$ oscillations. Again, the suppression of the Aharonov-Bohm oscillations at $\kappa/S \approx 0.25$ is a distinct feature of a Berry phase-like effect.

A quantity, which was subject of recent studies [79, 206], is the disorder-averaged squared power spectrum of the conductance

$$\langle |g(\nu)|^2 \rangle = |\langle g(\nu) \rangle|^2 + \langle |g(\nu) - \langle g(\nu) \rangle|^2 \rangle. \quad (6.35)$$

On the one hand, we recognize that the first term contains the Fourier transform of the (averaged) magnetoconductance δg , which has frequency contributions from its $h/2e$ oscillations. On the other hand, the second term of Eq. (6.35) is given through the conductance fluctuations $\delta g^{(2)}$ as $\int \int dB_z d\tilde{B}_z \exp\{2\pi i\nu(B_z - \tilde{B}_z)\} \delta g^{(2)}(\mathbf{B}, \tilde{\mathbf{B}})$. This term contributes frequencies corresponding to h/e oscillations, coming from the diffusion term $\delta g_D^{(2)}$ in the conductance fluctuations. Thus, if we now investigate h/e oscillations, we can restrict our studies to the second term of Eq. (6.35). We have evaluated $\langle |g(\nu)|^2 \rangle$ for inhomogeneous fields, with the parameters given in the caption of Fig. 6.9. A splitting of the frequency corresponding to the h/e oscillations was observed and was identified not to result from the Berry phase but from the Zeeman term already present in the case of homogeneous fields [Eq. (6.34)]. Then we examined $\langle |g_{so}(\nu)|^2 \rangle$ with spin-orbit coupling

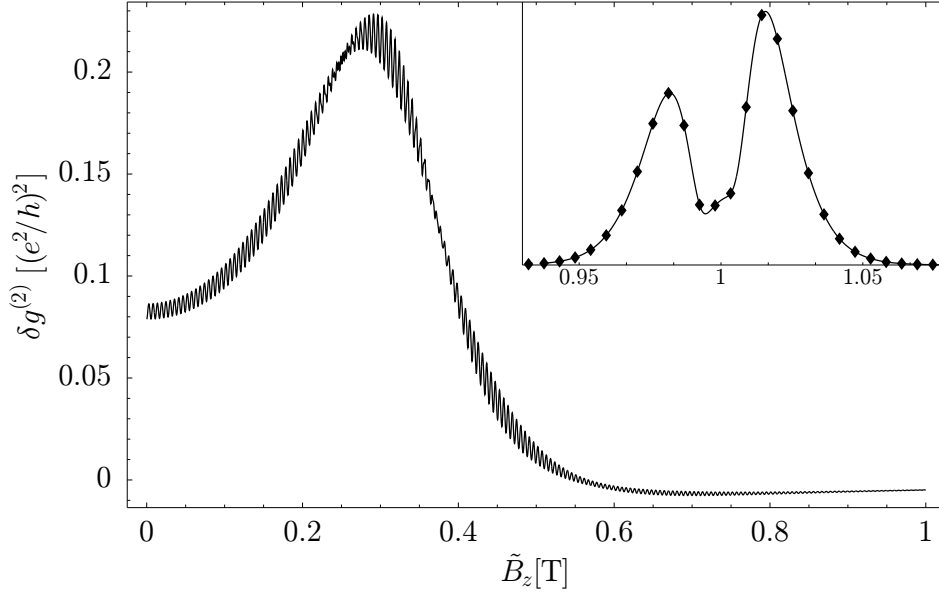


Figure 6.10: The UCFs $\delta g^{(2)}$ for a homogeneous texture of \mathbf{B} plotted as function of \tilde{B}_z (see second part of Sec. 6.3.1). We have taken the homogeneous field as $B_z = 0.5$ T, and $B_{\parallel} = 0$ G and have fixed the radial component for the other field as $\tilde{B}_{\parallel} = 0.43$ T. The remaining parameters are chosen as in Fig. 6.9. The inset shows the power spectrum [208] in arbitrary units plotted against the frequency in units of ϕ_0^{-1} , which exhibits a splitting in the h/e contributions.

for various parameters. An additional peak splitting to the one produced by the Zeeman term [Eq. (6.34)] appears for some specific parameters, i.e. for S large enough to reach “adiabaticity” and for large enough sampling intervals of B_z , \tilde{B}_z to obtain a sufficiently high resolution in the power spectrum. In Fig. 6.13 we see such a splitting of the h/e contribution into four peaks. However, using the parameters given in Ref. [79], we have $S \approx 1/50$ and $\kappa \approx 1/2$ (see Sec. 6.4.2) and in this regime we do not observe any peak splitting, in accordance with Ref. [206].

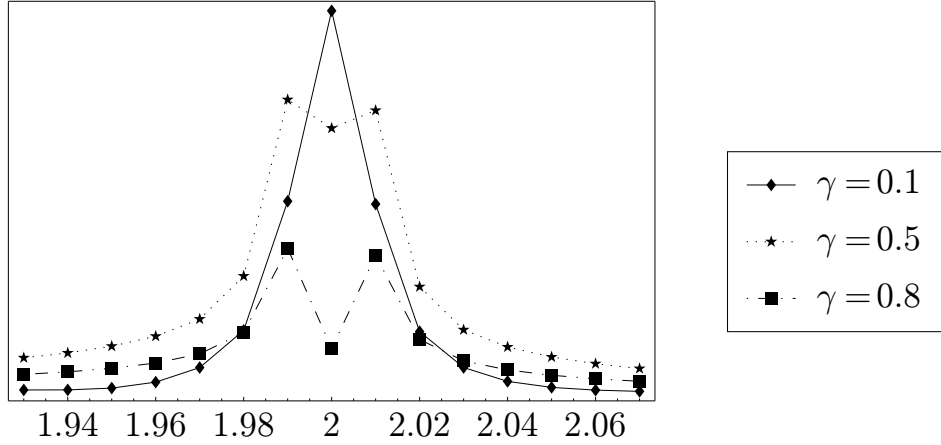


Figure 6.11: The power spectrum of the magnetoconductance $\delta g_{SO}(B)$ with spin-orbit coupling, Eq. (6.28), in arbitrary units plotted against the frequency in units of ϕ_0^{-1} . We have chosen $S = 4$ and taken the Fourier transform of the magnetoconductance for $0 \leq \kappa \leq 4$. We show the power spectrum for three different values of the dephasing parameter γ , where we have down-scaled the values for $\gamma = 0.1$ by a factor of 10. Note that a peak splitting occurs only for the cases with larger dephasing.

6.6 Berry phase controlled Spin Filter

An Aharonov-Bohm ring in an orientationally inhomogeneous magnetic field can be used as a spin filter (cf. Sec. 2.5.1). The idea of this proposal is to use a quantum interference effect, where one component of the spin current is filtered out via destructive interference while the other component remains unaffected. We first consider a ballistic ring in the adiabatic regime where the spin α acquires a Berry phase Φ_α^g when it moves once around the ring. For instance, for the crown-shaped field texture [Eq. (6.1)] with tilt angle η of the magnetic field, the Berry phase is $\Phi_\pm^g = \pm\pi(1 - \cos \eta)$. To obtain a spin filter, η is tuned such that $\cos \eta = \frac{1}{2}$, e.g., by varying in addition a homogeneous external field in z direction. Thus, the Berry phase difference of the two spin components is $\Phi_-^g - \Phi_+^g = \pi$. Further, the Aharonov-Bohm phase $2\pi\phi/\phi_0$ can be tuned independently of η , since generally only a small modulation of the magnetic field in z direction is required to change the flux ϕ through the ring on the order of $\phi_0 = h/e$. The spin filter effect is then obtained, when ϕ

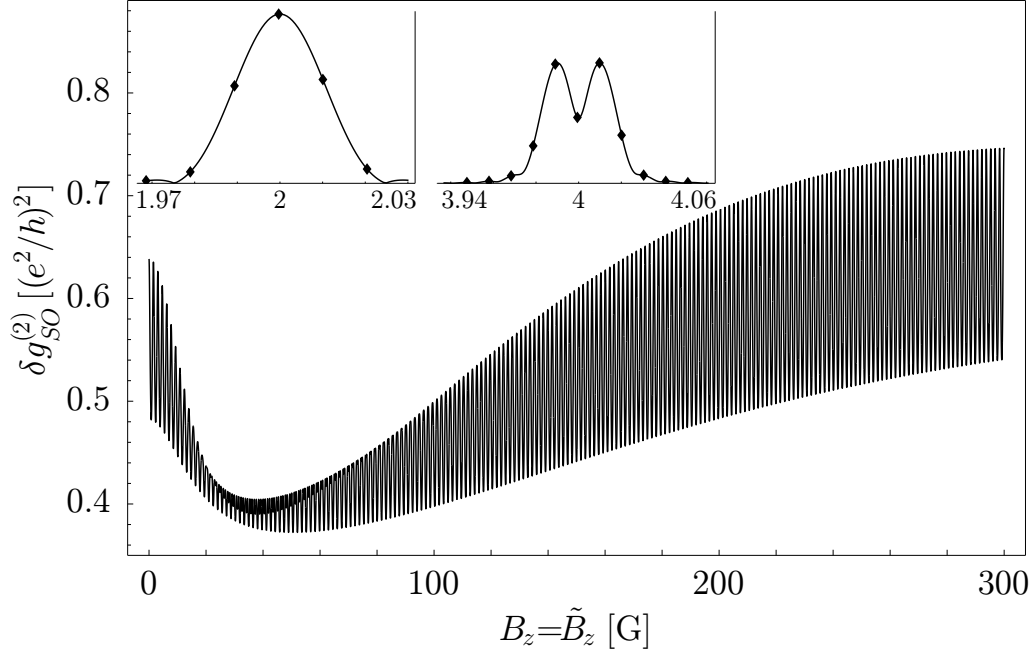


Figure 6.12: The UCFs $\delta g_{SO}^{(2)}$ with spin-orbit interaction for $\mathbf{B} = \tilde{\mathbf{B}}$ plotted as function of B_z . We have taken $\alpha = 1.0 \times 10^{-9}$ eV cm, $L = 12.5 \mu\text{m}$, $D = 2.0 \times 10^{-2}$ m²/s, $g = 15$, and have assumed $T = 0$. This gives us $S = 1.6$ [Eq. (6.25)], and $\kappa(B_z = 300\text{G}) = 4.2$ [Eq. (6.5)]. The dephasing was taken into account according to Eq. (6.6), with the parameters $L_\varphi = 5.0 \mu\text{m}$, and $a = 120$ nm. The envelope of the Aharonov-Bohm oscillations shows a non-monotonic behavior, which also appears in the UCFs for inhomogeneous fields $\delta g^{(2)}$ (see Fig. 6.9). The $h/2e$ oscillations are strongly suppressed at $B_z \approx 30$ G, which corresponds to $\kappa/S \approx 0.25$, as can also be seen from Fig. 6.6. However, this suppression is not very obvious in this figure, since $h/4e$ oscillations are present for $B_z \approx 30$ G. The two insets show the contributions of the $h/2e$ and $h/4e$ oscillations to the power spectrum in arbitrary units [208] plotted against the frequency in units of ϕ_0^{-1} . The right inset was scaled by a factor of 10. For the particular range of B_z chosen here, there is only a single peak visible for the $h/2e$ oscillations, while we observe a small peak splitting around the $h/4e$ frequency.

is tuned such that one spin channel interferes constructively; the other spin channel is offset by a phase π and thus will be suppressed due to destructive interference. A similar effect occurs for diffusive rings in an inhomogeneous magnetic field, the system which we have studied in this chapter. In the impurity-averaged magnetoconductance δg , coherence effects occur with a period $h/2e$ and the Berry phase contribution is $\pm 2\pi(1 - \cos \eta)$. Then, to obtain a phase difference of π for the two spin channels, η must be tuned to a “magic angles”, i.e., $\cos \eta = 1/4, 3/4$. For these angles η , a spin filtering effect is again possible [88]. This becomes apparent in Fig. 6.7, where the two contributions of spin $\alpha = \pm 1$ to the conductance (gray lines) are different for specific values of the Aharonov-Bohm flux.

6.7 Conclusion

We have calculated the exact conductance fluctuations $\delta g^{(2)}$ for a special texture [Eq. (6.1)] and given its adiabatic approximation $\delta g_{\text{ad}}^{(2)}$. In addition to the already known differential equations for the cooperon we have derived the ones for the diffuson in inhomogeneous magnetic fields (App. G). With the result $\delta g_{\text{ad}}^{(2)}$ the dephasing due to inhomogeneous fields became explicit and could be compared with previous calculations [87] where adiabatic eigenstates were used and this dephasing was only implemented with a phenomenological parameter. Then we have described some magic tilt angles of the magnetic field at which the Berry phase suppresses the Aharonov-Bohm oscillations. We have used this effect to illustrate how the adiabatic criterion becomes gradually satisfied. We have calculated numerically the required magnetic field strength for which the adiabatic approximation becomes valid and have shown that the adiabatic criterion is less stringent for diffusive than for ballistic motion, thus confirming previous findings [87, 191].

Furthermore, we have calculated the magnetoconductance and the conductance fluctuations for a diffusive conductor in the presence of spin-orbit coupling. A numerical analysis revealed a non-monotonic behavior of the amplitudes of the Aharonov-Bohm oscillations and peak-splittings in the power spectrum—observations that are similar to the Berry phase effects we have found for inhomogeneous magnetic fields.

Finally, we have described the mechanisms which lead to peak splittings in the power spectrum of magnetoconductance and UCFs and have discussed numerical requirements to make such peaks splittings visible.

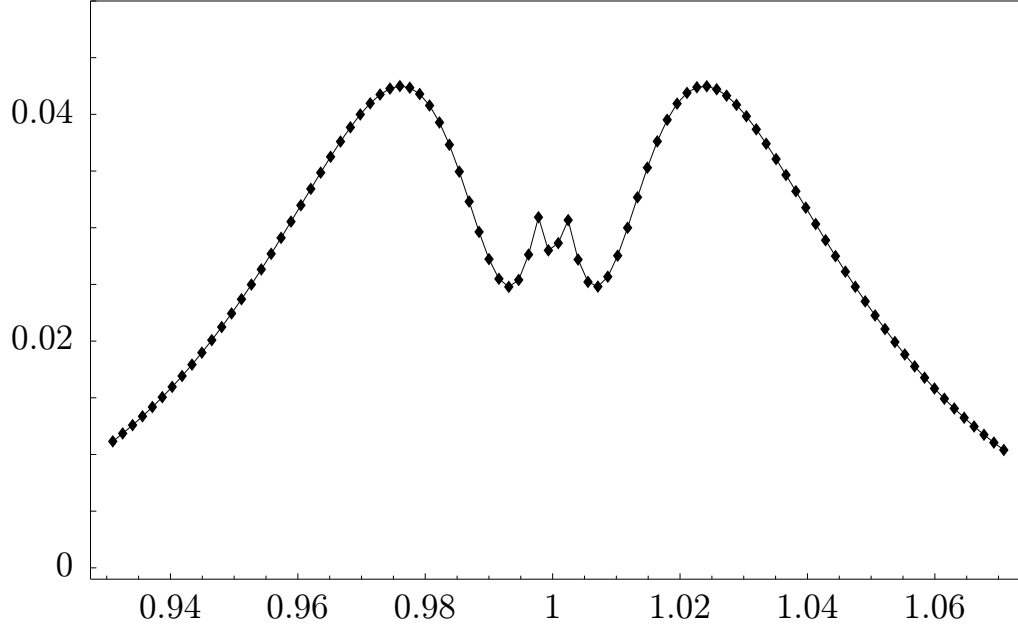


Figure 6.13: The disorder-averaged squared power spectrum of the conductance $\langle |g_{so}(\nu)|^2 \rangle$ [Eq. (6.35)] with spin-orbit interaction plotted as function of ν in units of ϕ_0^{-1} , normalized by the zero frequency contribution. We have taken the same parameters as in Fig. 6.12, but now with $\alpha = 2.0 \times 10^{-9}$ eV cm, and thus $S = 3.2$ [Eq. (6.25)]. We have calculated the second term of Eq. (6.35) explicitly (see text), while taking $B_z, \tilde{B}_z \in [-B_{\max}, B_{\max}]$ with $B_{\max} = 0.1$ T, which gives us a maximal value $\kappa_{\max} = 14$ [Eq. (6.5)]. The peak splitting into the inner two peaks is produced by the spin-orbit interaction, while the larger satellite peaks result from the Zeeman term [Eqs. (6.33) and (6.34)].

Appendix A

Energy Shifts due to Tunneling H_T

In this appendix, we evaluate the integrals over the Fermi function $f(\epsilon) = 1/[1 + e^{(\epsilon-\mu)/kT}]$, which appear in chapter 2 and 4. We calculate

$$\int_0^\infty dt \int_0^\infty d\epsilon f(\epsilon) e^{it(\epsilon-\Delta)} = \pi f(\Delta) + i\mathcal{P} \int_0^\infty d\epsilon \frac{f(\epsilon)}{\epsilon - \Delta} \quad (\text{A.1})$$

for real Δ and where \mathcal{P} denotes the Cauchy principal value. We assume that Δ is near the Fermi energy, thus $\beta\Delta, \beta\mu \gg 1$ with $\beta = 1/kT$. To evaluate the principal value in Eq. (A.1), we now symmetrize the integrand,

$$\begin{aligned} \mathcal{P} \int_0^\infty \frac{f(\epsilon)d\epsilon}{\epsilon - \Delta} &= \log \frac{\mu + \Delta}{\Delta} + \mathcal{P} \int_0^\infty \frac{d\epsilon}{1 + e^{\beta(\epsilon-\mu)}} \left[\frac{1}{\epsilon - \Delta} - \frac{1}{\epsilon + \Delta} \right] \\ &= \log \frac{\mu + \Delta}{\Delta} + \mathcal{P} \int_{-\infty}^\infty \left[\frac{1}{1 + e^{\beta(\epsilon-\mu)}} - \frac{1}{1 + e^{\beta(\epsilon+\mu)}} \right] \frac{\Delta}{\epsilon^2 - \Delta^2} d\epsilon. \end{aligned} \quad (\text{A.2})$$

We can now close the integration contour at $+i\infty$, see App. H for details. We see that that the contribution from the poles at $\epsilon = \pm\Delta$ cancel and the

remaining poles are at $\pi i n/\beta$ for odd n ,

$$\begin{aligned}
\mathcal{P} \int_0^\infty \frac{f(\epsilon) d\epsilon}{\epsilon - \Delta} &= \log \frac{\mu + \Delta}{\Delta} + 2\pi i \sum_{n \text{ odd} > 0} \frac{-1}{\beta} \left[\frac{\Delta}{(\mu + \pi i n/\beta)^2 - \Delta^2} \right. \\
&\quad \left. - \frac{\Delta}{(-\mu + \pi i n/\beta)^2 - \Delta^2} \right] \\
&= \log \frac{\mu + \Delta}{\Delta} + \frac{1}{2} \left[\psi \left(\frac{1}{2} + \frac{i\beta(-\mu + \Delta)}{2\pi} \right) - \psi \left(\frac{1}{2} + \frac{i\beta(-\mu - \Delta)}{2\pi} \right) \right. \\
&\quad \left. - \psi \left(\frac{1}{2} + \frac{i\beta(\mu + \Delta)}{2\pi} \right) + \psi \left(\frac{1}{2} + \frac{i\beta(\mu - \Delta)}{2\pi} \right) \right] \\
&= \log \frac{\mu + \Delta}{\Delta} + \text{Re} \left[\psi \left(\frac{1}{2} + \frac{i\beta|\Delta - \mu|}{2\pi} \right) - \psi \left(\frac{1}{2} + \frac{i\beta(\mu + \Delta)}{2\pi} \right) \right]. \tag{A.3}
\end{aligned}$$

We have introduced the psi (or digamma) function ψ and we have used $\sum_{k=0}^\infty iy/[y^2 + (x + \alpha k)^2] = \{\psi[(x + iy)/\alpha] - \psi[(x - iy)/\alpha]\}/2\alpha$ with $x = \pm\mu + \pi i/\beta$, $y = i\Delta$, $\alpha = 2\pi i/\beta$ and $\psi(z^*) = \psi(z)^*$. For large arguments z , we use $\psi(z) = \log z + O(1/z)$ and we obtain

$$\mathcal{P} \int_0^\infty \frac{f(\epsilon) d\epsilon}{\epsilon - \Delta} = \log \frac{2\pi kT}{\Delta} + \text{Re} \psi \left(\frac{1}{2} + i \frac{\Delta - \mu}{2\pi kT} \right). \tag{A.4}$$

This energy shift [Eq. (A.4)] becomes $\log(kT/\Delta) - \gamma + \log \frac{\pi}{2} \approx \log(kT/\Delta) - 0.1256$, for $|\mu - \Delta| \ll kT$ (“Stark shift”), and $\log(|\mu - \Delta|/\Delta)$ for $|\mu - \Delta| \gg kT$ (“Lamb shift”). Inserting in Eq. (A.1), we arrive at our final result,

$$\int_0^\infty dt \int_0^\infty d\epsilon f(\epsilon) e^{it(\epsilon - \Delta)} = \pi f(\Delta) + i \log \frac{2\pi kT}{\Delta} + i \text{Re} \psi \left(\frac{1}{2} + i \frac{\Delta - \mu}{2\pi kT} \right). \tag{A.5}$$

We also evaluate

$$\begin{aligned}
\int_0^\infty dt \int_0^{\epsilon_c} d\epsilon [1 - f(\epsilon)] e^{i\tau(\epsilon - \Delta)} &= \pi [1 - f(\Delta)] + i \log \frac{\epsilon_c - \Delta}{\Delta} \\
&\quad - i \mathcal{P} \int_0^{\epsilon_c} d\epsilon \frac{f(\epsilon)}{\epsilon - \Delta} \\
&= \pi [1 - f(\Delta)] - i \log \frac{2\pi kT}{\epsilon_c - \Delta} - i \text{Re} \psi \left(\frac{1}{2} + i \frac{\Delta - \mu}{2\pi kT} \right). \tag{A.6}
\end{aligned}$$

Here, we have introduced an upper bandwidth cutoff ϵ_c to ensure convergence of the integral.

Appendix B

Stationary Current for cw ESR

Here, we give the various formulas for the stationary current through the dot in the sequential tunneling regime and in the presence of an ESR field as discussed in chapter 2. We have calculated the current by evaluating the stationary solution of the master equation (Sec. 2.3) and with Eq. (2.22). For odd-to-even sequential tunneling, the spin \uparrow polarized current in lead 2 is

$$\begin{aligned}
 I_2^\uparrow &= e\gamma_2^\uparrow \left(\gamma_1^\uparrow \sum_{l,l'} (-1)^l \gamma_{l'}^\downarrow f_l(\Delta_{S\downarrow}) f_{l'}(\Delta_{S\uparrow}) - \sum_l \frac{W_{\uparrow\downarrow} - W_{\downarrow\uparrow}}{2} \right. \\
 &\quad \times \left\{ (-1)^l \gamma_1^\uparrow f_l(\Delta_{S\downarrow}) + \gamma_l^\downarrow [f_2(\Delta_{S\downarrow}) + f_l(\Delta_{S\uparrow}) - 2f_2(\Delta_{S\downarrow}) f_l(\Delta_{S\uparrow})] \right\} \\
 &\quad + \sum_l \frac{2W_\omega + W_{\uparrow\downarrow} + W_{\downarrow\uparrow}}{2} \left\{ (-1)^l \gamma_1^\uparrow f_l(\Delta_{S\downarrow}) + \gamma_l^\downarrow [f_2(\Delta_{S\downarrow}) - f_l(\Delta_{S\uparrow})] \right\} \Bigg) \\
 &\quad \times \left(\sum_{l,l'} \gamma_l^\uparrow \gamma_{l'}^\downarrow \{1 - [1 - f_l(\Delta_{S\downarrow})][1 - f_{l'}(\Delta_{S\uparrow})]\} + \sum_{l,\sigma \neq \sigma'} (W_\omega + W_{\sigma'\sigma}) \right. \\
 &\quad \left. \times \left\{ \gamma_l^\sigma + \gamma_{l'}^{\sigma'} [1 - f_l(\Delta_{S\sigma})] \right\} \right)^{-1}. \tag{B.1}
 \end{aligned}$$

The spin- \downarrow polarized current I_2^\downarrow is obtained from Eq. (B.1) by exchanging all \uparrow and \downarrow in the numerator (the denominator remains unaffected by such an exchange). The currents in lead 1, $I_1^{\uparrow,\downarrow}$, are obtained from the formulas for $I_2^{\uparrow,\downarrow}$ by exchanging indices 1 and 2 and by a global change of sign. The charge current is $I_l = \sum_\sigma I_l^\sigma$ and is equal in both leads, $I = I_1 = I_2$, due to

charge conservation. For large Zeeman splitting, $\Delta_z > \Delta\mu$, kT , and around the spin satellite peak, $\mu_1 > \Delta_{S\downarrow} > \mu_2$ (see Sec. 2.3.1), we have $f_l(\Delta_{S\uparrow}) = 0$, and the current is

$$\begin{aligned}
I &= e(W_\omega + W_{\downarrow\uparrow}) \left[(\gamma_1^\uparrow \gamma_2^\uparrow + \gamma_1^\uparrow \gamma_2^\downarrow) f_1(\Delta_{S\downarrow}) - (\gamma_1^\downarrow \gamma_2^\uparrow + \gamma_1^\downarrow \gamma_2^\downarrow) f_2(\Delta_{S\downarrow}) \right] \\
&\quad \times \left\{ (2\gamma^\downarrow - W_{\uparrow\downarrow} - W_\omega) \left[\gamma_1^\uparrow f_1(\Delta_{S\downarrow}) + \gamma_2^\uparrow f_2(\Delta_{S\downarrow}) \right] \right. \\
&\quad \left. + 2(W_{\uparrow\downarrow} + W_{\downarrow\uparrow} + 2W_\omega) (\gamma^\downarrow + \gamma^\uparrow) \right\}^{-1}, \tag{B.2}
\end{aligned}$$

for which we have given special cases in Eqs. (2.29), (2.30), (2.31) and (2.44).

For completeness, we also give the results for even-to-odd sequential tunneling, as discussed in Sec. 2.4. By applying the replacements given in Sec. 2.4 to Eq. (B.1), we obtain the spin- \downarrow polarized stationary current in lead 2,

$$\begin{aligned}
I_2^\downarrow &= e\gamma_2^\downarrow \left(\gamma_1^\downarrow \sum_{l,l'} (-1)^l \gamma_{l'}^\uparrow f_l(\Delta_{\downarrow\bar{S}}) [1 - f_{l'}(\Delta_{\uparrow\bar{S}})] - \sum_l \frac{W_{\uparrow\downarrow} - W_{\downarrow\uparrow}}{2} \right. \\
&\quad \times \left\{ (-1)^l \gamma_1^\downarrow f_l(\Delta_{\downarrow\bar{S}}) - \gamma_l^\uparrow [f_2(\Delta_{\downarrow\bar{S}}) + f_l(\Delta_{\uparrow\bar{S}}) - 2f_2(\Delta_{\downarrow\bar{S}}) f_l(\Delta_{\uparrow\bar{S}})] \right\} \\
&\quad \left. + \sum_l \frac{2W_\omega + W_{\uparrow\downarrow} + W_{\downarrow\uparrow}}{2} \left\{ (-1)^l \gamma_1^\downarrow f_l(\Delta_{\downarrow\bar{S}}) + \gamma_l^\uparrow [f_2(\Delta_{\downarrow\bar{S}}) - f_l(\Delta_{\uparrow\bar{S}})] \right\} \right) \\
&\quad \times \left(\sum_{l,l'} \gamma_l^\downarrow \gamma_{l'}^\uparrow \{1 - f_l(\Delta_{\downarrow\bar{S}}) f_{l'}(\Delta_{\uparrow\bar{S}})\} + \sum_{l,\sigma \neq \sigma'} (W_\omega + W_{\sigma'\sigma}) \right. \\
&\quad \left. \times \left\{ \gamma_l^{\sigma'} + \gamma_l^\sigma f_l(\Delta_{\sigma\bar{S}}) \right\} \right)^{-1}. \tag{B.3}
\end{aligned}$$

Appendix C

Exact Current and Noise for a Quantum Dot

We consider a quantum dot which is coupled to Fermi leads and which has only a single level. We model this system with the Hamiltonian

$$H = H_0 + H_T = \varepsilon_d a^\dagger a + \sum_{lk} \epsilon_{lk} c_{lk}^\dagger c_{lk} + \sum_{lk} (t_l c_{lk}^\dagger a + t_l^* c_{lk} a^\dagger), \quad (\text{C.1})$$

where a^\dagger creates an electron on the dot and c_{lk}^\dagger an electron in lead $l = 1, 2, \dots$ with orbital state k . (Since there is only a single level, only one spin direction is involved and we drop the spin index here.) This model can be solved exactly, since the Hamiltonian [Eq. (C.1)] is bilinear. We assume that the interaction H_T is switched on at the time t_0 and that at t_0 the full density matrix is $\rho(t_0) = \rho_D^0 \rho_R^0$, where ρ_R^0 is the density matrix of the leads in thermal equilibrium. Now, we calculate the time evolution of the dot and the lead operators. Using the Heisenberg equation, we find $\dot{c}_{lk}(t) = i[H, c_{lk}(t)] = -i\epsilon_{lk} c_{lk}(t) - it_l a(t)$. We integrate and obtain

$$c_{lk}(t) = e^{-i\epsilon_{lk}(t-t_0)} c_{lk}(t_0) - it_l \int_{t_0}^t d\tau e^{-i\epsilon_{lk}(t-\tau)} a(\tau). \quad (\text{C.2})$$

For these Heisenberg operators at the initial time t_0 , we have $\langle c_{lk}^\dagger(t_0) c_{lk}(t_0) \rangle = \text{Tr} c_{lk}^\dagger c_{lk} \rho(t_0) = \text{Tr} c_{lk}^\dagger c_{lk} \rho_D^0 \rho_R^0 = f_l(\epsilon_{lk})$ with the Fermi function f_l of lead l . This motivates denoting $c_{lk}(t_0) = c_{lk}$ from now on. For the dot annihilation

operator a , we get

$$\dot{a}(t) = -i\varepsilon_d a(t) - i \sum_{lk} t_l^* c_{lk}(t) = (-i\varepsilon_d - \gamma) a(t) - i \sum_{lk} t_l^* e^{-i\varepsilon_{lk}(t-t_0)} c_{lk}. \quad (\text{C.3})$$

Here, we have inserted Eq. (C.2) and assumed a constant density of states ν_l of the leads. We define the width γ of the dot level, $\gamma = \frac{1}{2} \sum_l \gamma_l$, and the tunneling rates $\gamma_l = 2\pi\nu_l |t_l|^2$. We integrate Eq. (C.3) and let $t_0 \rightarrow -\infty$ ¹ to obtain

$$a(t) = \sum_{lk} t_l^* \frac{e^{-i\varepsilon_{lk}(t-t_0)}}{\varepsilon_{lk} - \varepsilon_d + i\gamma} c_{lk}. \quad (\text{C.4})$$

Finally, we insert Eq. (C.4) into (C.2) which yields

$$c_{lk}(t) = e^{-i\varepsilon_{lk}(t-t_0)} c_{lk} - i \int_{t_0}^t d\tau \sum_{l'k'} t_l t_{l'}^* \frac{e^{-i\varepsilon_{lk}(t-\tau)} e^{-i\varepsilon_{l'k'}(\tau-t_0)}}{\varepsilon_{l'k'} - \varepsilon_d + i\gamma} c_{l'k'}. \quad (\text{C.5})$$

C.1 Current

The current operator I_l is defined as the time derivative of the charge of the electrons in the lead l , $e \sum_k c_{lk}^\dagger c_{lk}$, i.e.,

$$I_l(t) = ie \left[H, \sum_k c_{lk}^\dagger(t) c_{lk}(t) \right] = \sum_k ie t_l^* a^\dagger(t) c_{lk}(t) + \text{H.c.} \quad (\text{C.6})$$

To simplify the further evaluation of $I_l(t)$, we define

$$g_{k'}(t) := i t_l^* t_{l'} \frac{e^{i(\varepsilon_{l'k'} - \varepsilon_{lk})(t-t_0)}}{\varepsilon_{l'k'} - \varepsilon_d - i\gamma}, \quad (\text{C.7})$$

$g_{k'} := g_{k'}(0)$, and $\tilde{g}_{k'} := g_{k'}[\varepsilon_{lk} \rightarrow \varepsilon_{l\tilde{k}}]$ which have the properties $g_k(t) = g_k$ and $g_{k'}(t) g_{k'}^*(t) = g_{k'} g_{k'}^*$. We can now evaluate the current [Eq. (C.6)] by inserting $a(t)$ and $c_{lk}(t)$ [Eqs. (C.4) and (C.5)]. We decompose the current, $I_l = I_l^a + I_l^b$, corresponding to the two terms in Eq. (C.5). We find

$$\begin{aligned} I_l^a(t) &= e \sum_{k'l'k'} i t_l^* t_{l'} \frac{e^{i(\varepsilon_{l'k'} - \varepsilon_{lk})(t-t_0)}}{\varepsilon_{l'k'} - \varepsilon_d - i\gamma} c_{l'k'}^\dagger c_{lk} + \text{H.c.} \\ &= e \sum_{k'l'k'} g_{k'}(t) c_{l'k'}^\dagger c_{lk} + g_{k'}^*(t) c_{lk}^\dagger c_{l'k'}, \end{aligned} \quad (\text{C.8})$$

¹An oscillatory factor in t_0 remains in Eqs. (C.4) and (C.5). This factor will be cancelled when we evaluate the averaged current and the noise.

$$\begin{aligned}
I_l^b(t) &= e \frac{\gamma_l}{2} \sum_{\nu'k'\nu''k''} t_{\nu'} t_{\nu''}^* \frac{e^{i\epsilon_{\nu'k'}(t-t_0)}}{\epsilon_{\nu'k'} - \epsilon_d - i\gamma} \frac{e^{-i\epsilon_{\nu''k''}(t-t_0)}}{\epsilon_{\nu''k''} - \epsilon_d + i\gamma} c_{\nu'k'}^\dagger c_{\nu''k''} + \text{H.c.} \\
&= e \frac{\gamma_l}{|t_l|^2} \sum_{\nu'k'\nu''k''} g_{k'}(t) g_{k''}^*(t) c_{\nu'k'}^\dagger c_{\nu''k''}.
\end{aligned} \tag{C.9}$$

We finally get the (exact) current operator

$$I_l(t) = e \sum_{kk'} \left[g_{k'}(t) c_{\nu'k'}^\dagger c_{lk} + g_k^*(t) c_{lk}^\dagger c_{\nu'k'} \right] + e \frac{\gamma_l}{|t_l|^2} \sum_{\nu'k'\nu''k''} g_{k'}(t) g_{k''}^*(t) c_{\nu'k'}^\dagger c_{\nu''k''}. \tag{C.10}$$

Equation (C.10) is a good starting point for evaluating the average current, the noise, and higher order correlations.

C.1.1 Averaged current $\langle I_l \rangle$

Using Eq. (C.10), it is straightforward to find the ensemble averaged current,

$$\langle I_l \rangle = e \sum_k (g_k + g_k^*) f_l(\epsilon_{lk}) + e \frac{\gamma_l}{|t_l|^2} \sum_{\nu'k'} g_{k'} g_{k'}^* f_{\nu'}(\epsilon_{\nu'k'}). \tag{C.11}$$

For two leads, $l = 1, 2$, we find

$$\begin{aligned}
\langle I_1 \rangle &= e \frac{\gamma_1}{2\pi} \int d\epsilon \left[-\frac{\gamma_1 + \gamma_2}{(\epsilon - \epsilon_d)^2 + \gamma^2} f_1(\epsilon) + \sum_{\nu'} \frac{\gamma_{\nu'}}{(\epsilon - \epsilon_d)^2 + \gamma^2} f_{\nu'}(\epsilon) \right] \\
&= -e \frac{\gamma_1 \gamma_2}{2\pi} \int d\epsilon \frac{f_1(\epsilon) - f_2(\epsilon)}{(\epsilon - \epsilon_d)^2 + \gamma^2}.
\end{aligned} \tag{C.12}$$

C.2 Asymmetric shot noise

We consider the asymmetric noise, defined as

$$S_{ll}(\omega) = \int_{-\infty}^{\infty} dt e^{i\omega t} [\langle I_l(t) I_l \rangle - \langle I_l \rangle \langle I_l \rangle]. \tag{C.13}$$

We now calculate the various contributions from I_l^a and I_l^b to $\langle I_l(t) I_l \rangle$. To make our results more compact, we define $f_l = f_l(\epsilon_{lk})$; $f_{\nu'} = f_{\nu'}(\epsilon_{\nu'k'})$; and

$f_{\bar{l}} = f_l(\epsilon_{l\bar{k}})$. Using Wick's theorem, we find

$$\begin{aligned} \langle I_l^a(t) I_l^a(0) \rangle &= \left[e \sum_k (g_k + g_k^*) f_l \right]^2 + e^2 \sum_{k\bar{k}} [\tilde{g}_k(t) g_{\bar{k}} + g_{\bar{k}}^*(t) \tilde{g}_k^*] f_l [1 - f_{\bar{l}}] \\ &+ \sum_{k'l'k'} \{ g_{k'}(t) g_{k'}^* f_{l'} [1 - f_l] + g_{k'}^*(t) g_{k'} f_l [1 - f_{l'}] \}. \end{aligned} \quad (\text{C.14})$$

$$\begin{aligned} \langle I_l^a(t) I_l^b(0) + I_l^b(t) I_l^a(0) \rangle &= \frac{e^2 \gamma_l}{|t_l|^2} \sum_{kl'k'} 2g_{k'} g_{k'}^* (g_k + g_k^*) f_l f_{l'} \\ &+ \frac{e^2 \gamma_l}{|t_l|^2} \sum_{kl'k'} \{ g_{k'}(t) g_{k'}^* f_{l'} [1 - f_l] + g_{k'}^*(t) g_{k'} f_l [1 - f_{l'}] \} (g_k + g_k^*), \end{aligned} \quad (\text{C.15})$$

$$\begin{aligned} \langle I_l^b(t) I_l^b(0) \rangle &= \frac{e^2 \gamma_l^2}{|t_l|^4} \sum_{l'k'l''k''} g_{k'} g_{k'}^* g_{k''} g_{k''}^* f_{l'} f_{l''} \\ &+ \frac{e^2 \gamma_l^2}{|t_l|^4} \sum_{l'k'l''k''} g_{k'}^* g_{k'}(t) g_{k''} g_{k''}^*(t) f_{l'} [1 - f_{l''}]. \end{aligned} \quad (\text{C.16})$$

When we sum the first terms of each of Eqs. (C.14)-(C.16), we obtain $\langle I_l \rangle \langle I_l \rangle$. Thus, these terms are cancelled in Eq. (C.13). We get the correlation function in time space,

$$\begin{aligned} \langle I_l(t) I_l(0) \rangle - \langle I_l \rangle \langle I_l \rangle &= e^2 \sum_{kl'k'} \left\{ g_{k'}(t) g_{k'}^* f_{l'} [1 - f_l] + g_{k'}^*(t) g_{k'} f_l [1 - f_{l'}] \right\} \\ &\times \left[1 + \frac{(g_k + g_k^*) \gamma_l}{|t_l|^2} \right] + e^2 \sum_{k\bar{k}} [\tilde{g}_k(t) g_{\bar{k}} + g_{\bar{k}}^*(t) \tilde{g}_k^*] f_l [1 - f_{\bar{l}}] \\ &+ \frac{e^2 \gamma_l^2}{|t_l|^4} \sum_{l'k'l''k''} g_{k'}(t) g_{k'}^* g_{k''}^*(t) g_{k''} f_{l'} [1 - f_{l''}]. \end{aligned} \quad (\text{C.17})$$

Finally, we resolve the symbols $g_{k'}(t)$ [Eq. (C.7)] and evaluate the Fourier transform of the correlation function. We find the (exact) asymmetric shot

noise,

$$\begin{aligned}
S_{ll}(\omega) = & \frac{e^2}{2\pi} \iint \frac{d\epsilon d\epsilon'}{[(\epsilon - \epsilon_d)^2 + \gamma^2][(\epsilon' - \epsilon_d)^2 + \gamma^2]} \left(\sum_{l'} \gamma_l \gamma_{l'} \left[(\epsilon - \epsilon_d)^2 + \gamma^2 \right. \right. \\
& \left. \left. - 2\gamma_l \gamma_{l'} \right] \left\{ \delta(\epsilon - \epsilon' - \omega) f_{l'}(\epsilon') [1 - f_l(\epsilon)] + \delta(\epsilon - \epsilon' + \omega) f_l(\epsilon) [1 - f_{l'}(\epsilon')] \right\} \right. \\
& + 2\gamma_l^2 \delta(\epsilon - \epsilon' + \omega) [\gamma^2 - (\epsilon - \epsilon_d)(\epsilon' - \epsilon_d)] f_l(\epsilon) [1 - f_l(\epsilon')] \\
& \left. + \gamma_l^2 \delta(\epsilon - \epsilon' + \omega) \sum_{l''} \gamma_{l'} \gamma_{l''} f_{l'}(\epsilon) [1 - f_{l''}(\epsilon')] \right). \tag{C.18}
\end{aligned}$$

C.2.1 Symmetrized noise

For comparison with the literature [149], let us consider the symmetrized noise, $S_{ll}^{\text{sym}}(\omega) = \frac{1}{2} [S_{ll'}(\omega) + S_{l'l}(\omega)]$ and evaluate S_{11}^{sym} in the case of two leads. For this, we use that S_{11}^{sym} is composed of expressions of the form $\sum_{\pm} \iint d\epsilon d\epsilon' (\epsilon - \epsilon' \pm \omega) F(\epsilon) G(\epsilon')$, which are invariant under the replacement $F(\epsilon) G(\epsilon') \rightarrow F(\epsilon') G(\epsilon)$. In the following, we separately discuss the different contributions to S_{11}^{sym} . We first collect the terms containing the factor $f_1(\epsilon) [1 - f_1(\epsilon')]$, i.e., set $l' = l'' = 1$ in Eq. (C.18). We find two contributions, which are proportional to $(\epsilon' - \epsilon_d)^2 + (\epsilon - \epsilon_d)^2 - 2(\epsilon - \epsilon_d)(\epsilon' - \epsilon_d) = (\epsilon - \epsilon')^2 = \omega^2$ and to $2(\gamma^2 - 2\gamma_l \gamma_1 + \gamma^2 + \frac{1}{2}\gamma_1^2) = \gamma_2^2$, resp. Second, we take the term for $l' = l'' = 2$ in last line of Eq. (C.18). Finally, for the term with $l' = 2$ in the first and $l' \neq l''$ in the last line of Eq. (C.18), we use $\gamma_1 \gamma_2 (\gamma^2 - 2\gamma_l \gamma_1 + \gamma_1^2) = \gamma_1 \gamma_2 (\gamma_1 - \gamma_2)^2 / 4$. In total, we obtain

$$\begin{aligned}
S_{ll}^{\text{sym}}(\omega) = & \frac{e^2}{4\pi} \sum_{\pm} \iint \frac{d\epsilon d\epsilon' \delta(\epsilon - \epsilon' \pm \omega)}{[(\epsilon - \epsilon_d)^2 + \gamma^2][(\epsilon' - \epsilon_d)^2 + \gamma^2]} \left(f_1(\epsilon) [1 - f_1(\epsilon')] \right. \\
& \times \gamma_1^2 (\omega^2 + \gamma_2^2) + f_2(\epsilon) [1 - f_2(\epsilon')] \gamma_1^2 \gamma_2^2 + \left\{ f_2(\epsilon') [1 - f_1(\epsilon)] \right. \\
& \left. \left. + f_1(\epsilon) [1 - f_2(\epsilon')] \right\} \gamma_1 \gamma_2 [(\epsilon - \epsilon_d)^2 + (\gamma_1 - \gamma_2)^2 / 4] \right). \tag{C.19}
\end{aligned}$$

This result [Eq. (C.19)] agrees with Eq. (9) of [149], apart that our last term of Eq. (C.19) is larger by factor 4 and has exchanged energies ϵ and ϵ' in $f_2(\epsilon') [1 - f_1(\epsilon)]$, with respect to the result from Ref. [47]. We think that our result is correct since in the regime $|\mu_l - \epsilon_d| > kT > \gamma > \omega$, the noise is given by this term and we obtain the well-known result $S_{11}(0) =$

$e^2\gamma_1\gamma_2(\gamma_1^2 + \gamma_2^2)/(\gamma_1 + \gamma_2)^3$ from Eq. (C.19). Furthermore, note the difference of a global factor 2, since in Ref. [47], the definition $S'_{ll}(\omega) = 2S_{ll}^{\text{sym}}(\omega)$ was used for the noise (see Sec. 1.5).

C.2.2 Quantum noise in sequential tunneling regime

We next consider the sequential tunneling regime, $kT > \gamma$, and evaluate the shot noise in the quantum limit, $\omega > \gamma$. Here, γ is the smaller energy scale and we use $1/(E^2 + \gamma^2) \rightarrow (\pi/\gamma)\delta(E)$. The highest order contribution in ω/γ to the noise is

$$S_{ll}(\omega) = \sum_{\nu'} \frac{\gamma_1\gamma_{\nu'}}{2\pi} \iint \frac{d\epsilon d\epsilon'}{(\epsilon' - \epsilon_d)^2 + \gamma^2} \left\{ \delta(\epsilon - \epsilon' - \omega) f_{\nu'}(\epsilon') [1 - f_1(\epsilon)] \right. \\ \left. + \delta(\epsilon - \epsilon' + \omega) f_1(\epsilon) [1 - f_{\nu'}(\epsilon')] \right\} \quad (\text{C.20})$$

$$= \sum_{\nu'} \frac{\gamma_1\gamma_{\nu'}}{2\gamma} \{ f_{\nu'}(\epsilon_d) [1 - f_1(\epsilon_d + \omega)] + f_1(\epsilon_d - \omega) [1 - f_{\nu'}(\epsilon_d)] \}. \quad (\text{C.21})$$

This result [Eq. (C.21)] is displayed in Eq. (4.13).

C.2.3 Quantum noise in coherent regime

Finally, we analyze the case when tunneling through the dot is coherent, $\gamma > kT$, and again evaluate the shot noise in the quantum limit, $\omega > \gamma$. In this low temperature limit, we can set $f(\epsilon) \rightarrow \theta(\mu - \epsilon)$ and $1 - f(\epsilon) \rightarrow \theta(\epsilon - \mu)$ and we use $\int d\epsilon' / [(\epsilon' - \epsilon_d)^2 + \gamma^2] = h(\epsilon) = \arctan\left(\frac{\epsilon - \epsilon_d}{\gamma}\right) / \gamma$. We can now evaluate the highest order contribution in ω/γ to the noise, Eq. (C.20), and find

$$S_{ll}(\omega) = \sum_{\nu'} \frac{\gamma_1\gamma_{\nu'}}{2\pi} \left[\theta(\omega + \mu_{\nu'} - \mu_1) \int_{\mu_1 - \omega}^{\mu_{\nu'}} \frac{d\epsilon'}{(\epsilon' - \epsilon_d)^2 + \gamma^2} + \theta(\omega + \mu_1 - \mu_{\nu'}) \right. \\ \left. \times \int_{\mu_{\nu'}}^{\mu_1 + \omega} \frac{d\epsilon'}{(\epsilon' - \epsilon_d)^2 + \gamma^2} \right] \\ = \sum_{\nu', \pm} \frac{\pm\gamma_1\gamma_{\nu'}}{2\pi\gamma} \theta(\omega \pm \mu_{\nu'} \mp \mu_1) [h(\mu_{\nu'}) - h(\mu_1 \mp \omega)]. \quad (\text{C.22})$$

We display this result in Eq. (4.12).

Appendix D

Sequential Tunneling Quantum Noise

In this appendix, we give the explicit expression for the quantum shot noise in the sequential tunneling regime. We consider the regime (a) of chapter 4, where the dot has only a single dot level with energy E_\uparrow . To calculate the noise, we use Eqs. (4.4) and (4.6)-(4.11) and obtain

$$\begin{aligned}
 S_{11}^a(\omega) = & \sum_{\nu'} \frac{\gamma_1 \gamma_{\nu'}}{\gamma_1 + \gamma_2} \{f_{\nu'}(E_\uparrow)[1 - f_1(E_\uparrow + \omega)] + f_1(E_\uparrow - \omega)[1 - f_{\nu'}(E_\uparrow)]\} \\
 & - \frac{e^2 \gamma_1^2 (\gamma_1 + \gamma_2) \{f_1(E_\uparrow)[1 - f_1(E_\uparrow + \omega)] + f_1(E_\uparrow - \omega)[1 - f_1(E_\uparrow)]\}}{\omega^2 + (\gamma_1 + \gamma_2)^2} \\
 & - \sum_{\pm} \frac{e^2 \gamma_1^2 \gamma_2^2 [f_1(E_\uparrow) - f_2(E_\uparrow)] [f_1(E_\uparrow \pm \omega) - f_2(E_\uparrow \pm \omega)]}{(\gamma_1 + \gamma_2) [\omega^2 + (\gamma_1 + \gamma_2)^2]} \\
 & + \sum_{\pm} \frac{\pm e^2 \gamma_1^2 \gamma_2^2 [f_1(E_\uparrow) - f_2(E_\uparrow)] [p_1(E_\uparrow \pm \omega) - p_2(E_\uparrow \pm \omega)]}{\pi \omega [\omega^2 + (\gamma_1 + \gamma_2)^2]} \\
 & - \frac{e^2 \omega \gamma_1^2 \{p_1(E_\uparrow) - [1 - f_1(E_\uparrow)]p_1(E_\uparrow - \omega) - f_1(E_\uparrow)p_1(E_\uparrow + \omega)\}}{\pi [\omega^2 + (\gamma_1 + \gamma_2)^2]}, \quad (\text{D.1})
 \end{aligned}$$

where $p_l(\epsilon) = \text{Re} \psi[\frac{1}{2} + i(\epsilon - \mu_l)/2\pi kT]$. In the quantum limit $\omega > \gamma$, only the first term in Eq. (D.1) does not vanish and we recover Eq. (4.13).

Appendix E

Double dot and QPC: Master Equation and Current

We consider a double quantum dot coupled to a QPC, cf. chapter 3. We will now derive the master equation for this system and calculate the QPC current. Using standard superoperators techniques [105, 56, 57], we write $H = H_0 + V$ [Eq. (3.3)] and find the contribution of V in Born-Markov approximation to the r.h.s. of the master equation,

$$- \int_0^\infty d\tau \text{Tr}_Q [V, e^{-iH_0\tau} [V, \rho_Q^0] e^{iH_0\tau}]. \quad (\text{E.1})$$

Here, ρ_Q^0 is the equilibrium density matrix of the leads of the QPC, at chemical potentials $\mu_{\text{in, out}}$ and temperature T , with applied bias $\Delta\mu = \mu_{\text{in}} - \mu_{\text{out}}$. The trace Tr_Q is taken over these leads. We allow for an arbitrary inter-dot tunnel coupling, i.e. we keep V_d exactly. We now evaluate the kernel in the eigenbasis of $H_0 = H_{\text{dot}} + V_d$ which is $|\pm\rangle = \alpha_\pm|L\rangle + \beta_\pm|R\rangle$ with

$$\alpha_\pm/\beta_\pm = \frac{\varepsilon \pm \sqrt{4t_d^2 + \varepsilon^2}}{2t_d} \quad (\text{E.2})$$

and with energies

$$E_\pm = \frac{1}{2}(E_L + E_R) \pm \frac{1}{2}\sqrt{4t_d^2 + \varepsilon^2}.$$

The expectation values, $\text{Tr}_Q \dots \rho_Q^0$, of the QPC contributions to the kernel gives rise to a product of Fermi functions, one for each QPC leads, integrated

over the states in both leads. We evaluate the δ -function (neglecting the principal value contribution) which arises from the time integration in Eq. (E.1) and one integration over the states in the leads remains,

$$F(\Delta) = \int_{-\infty}^{\infty} d\epsilon f(\epsilon) [1 - f(\epsilon + \Delta)] = \int_0^{\infty} \frac{du}{\beta} \frac{1}{1+u} \frac{1}{e^{-\beta\Delta} + u} = \frac{\Delta}{1 - e^{-\beta\Delta}}, \quad (\text{E.3})$$

with $F(\Delta) - F(-\Delta) = \Delta$ and $F(-\Delta) = g(\Delta) \Delta\mu$ in the notation of Ch. 3. We define $s(x) = [F(x + \Delta\mu) + F(x - \Delta\mu)]/\Delta\mu = 1 + x/\Delta\mu + g(\Delta\mu + x) + g(\Delta\mu - x)$. Evaluating all the matrix elements of Eq. (E.1), we find the master equation,

$$\dot{\rho}_- = W_Q [s(E) \rho_+ - s(-E) \rho_-] - s(0) \sqrt{2V_Q W_Q} \text{Re}[\rho_{+-}], \quad (\text{E.4})$$

$$\dot{\rho}_+ = W_Q [s(-E) \rho_- - s(E) \rho_+] + s(0) \sqrt{2V_Q W_Q} \text{Re}[\rho_{+-}], \quad (\text{E.5})$$

$$\begin{aligned} \dot{\rho}_{+-} = & -[s(0)V_Q + iE] \rho_{+-} - i[s(E) + s(-E)] W_Q \text{Im}[\rho_{+-}] \\ & + \sqrt{V_Q W_Q/2} [s(E) \rho_+ - s(-E) \rho_-], \end{aligned} \quad (\text{E.6})$$

where $\rho_{+-} = \langle +|\rho|-\rangle$. We have defined $W_Q = 2\pi\nu^2 \Delta\mu |\langle +|V_{\text{dot}}|-\rangle|^2$ and

$$V_Q = \frac{1}{2e} (\sqrt{\mathcal{I}_+} - \sqrt{\mathcal{I}_-})^2, \quad (\text{E.7})$$

where $\mathcal{I}_{\pm} = 2\pi\nu^2 e \Delta\mu |\langle \pm|V_{\text{dot}}|\pm\rangle|^2$. Rotating to the basis $\{|L\rangle, |R\rangle\}$, we find Eqs. (3.6)-(3.7)

For evaluating the QPC current, we count the number of electrons q which have accumulated since $t = 0$ in the outgoing lead of the QPC. Thus, the time evolution of $\rho(q, t)$ is now depends on q . We find the master equation by observing that the matrix elements of Eq. (E.1) from the contributions $VV\rho_Q^0\rho$ or $\rho_Q^0\rho VV$ do not change q , while those containing $V\rho_Q^0\rho V$ will increase or decrease q by one. Thus, the master equation is of the form $\dot{\rho}(q) = \mathcal{M}_+\rho(q-1) + \mathcal{M}_0\rho(q) + \mathcal{M}_-\rho(q+1)$. Using $\rho = \sum_q \rho(q)$, we can easily go back to the charge-independent master equation, $\dot{\rho} = \sum_q \dot{\rho}(q) = (\mathcal{M}_- + \mathcal{M}_0 + \mathcal{M}_+)\rho =: \mathcal{M}\rho$, i.e., \mathcal{M} is given by Eqs. (3.6)-(3.7). We now give the contribution $\mathcal{M}_+\rho(q-1)$ to the master equation explicitly,

$$\begin{aligned} \dot{\rho}_L(q) &= \frac{I_L}{e} (1 + g_0) \rho_L(q-1) - \frac{t_d^2 \Gamma_I^+ (2g_0 - g_\Sigma)}{2E^2} \rho_L(q-1) \\ &\quad + t_d \Gamma_I^+ \left[\frac{(1 + \lambda)}{4\Delta\mu} + \frac{(2g_0 - g_\Sigma) \varepsilon}{4E^2} \right] \text{Re}[\rho_{RL}(q-1)] + \dots, \quad (\text{E.8}) \end{aligned}$$

$$\begin{aligned} \dot{\rho}_R(q) &= \frac{I_R}{e} (1 + g_0) \rho_R(q-1) + \frac{t_d^2 \Gamma_I^- (2g_0 - g_\Sigma)}{2E^2} \rho_R(q-1) \\ &\quad - t_d \Gamma_I^- \left[\frac{(1 + \lambda)}{4\Delta\mu} - \frac{(2g_0 - g_\Sigma) \varepsilon}{4E^2} \right] \text{Re}[\rho_{RL}(-1 + q)] + \dots, \quad (\text{E.9}) \end{aligned}$$

$$\begin{aligned} \dot{\rho}_{RL}(q) &= t_d \Gamma_I^+ \frac{(2g_0 - g_\Sigma) \varepsilon}{8E^2} [\rho_L(q-1) + \rho_R(q-1)] \\ &\quad - t_d \Gamma_I^+ \frac{(1 + \lambda)}{8\Delta\mu} [\rho_L(q-1) - \rho_R(q-1)] + \left[\frac{(2g_0 - g_\Sigma) t_d^2 \Gamma_Q}{E^2} \right. \\ &\quad \left. - \frac{(1 + g_0) (2e\Gamma_Q - I_L - I_R)}{2e} \right] \rho_{RL}(q-1) + \dots, \quad (\text{E.10}) \end{aligned}$$

with $\Gamma_I^\pm = (I_L - I_R)/e \pm 2\Gamma_Q$. The remaining contributions are $\mathcal{M}_0 = \mathcal{M} - \mathcal{M}_+ - \mathcal{M}_-$ and the matrix elements of \mathcal{M}_- are given by \mathcal{M}_+ with the replacement $\Delta\mu \rightarrow -\Delta\mu$. The current through the QPC is defined as $\langle I \rangle = e \langle \dot{q} \rangle$. We find,

$$\begin{aligned} \langle I \rangle &= e \partial_t \langle q \rangle = e \partial_t \sum_q \text{Tr} q \rho(q) \\ &= e \sum_q \text{Tr} q [\mathcal{M}_+ \rho(q-1) + \mathcal{M}_0 \rho(q) + \mathcal{M}_- \rho(q+1)] \\ &= e \sum_q \text{Tr} (\mathcal{M}_+ - \mathcal{M}_-) \rho(q) = e \text{Tr} (\mathcal{M}_+ - \mathcal{M}_-) \rho, \quad (\text{E.11}) \end{aligned}$$

where we have used $\text{Tr} \mathcal{M} = 0$. Evaluating $\text{Tr} (\mathcal{M}_+ - \mathcal{M}_-)$, we find Eq. (3.11).

Appendix F

Two-level system in an electromagnetic field

We consider the interaction of a two-level system in an electromagnetic field. For example, in the system studied in chapter 5, the two levels are a quantum dot with a single spin, $|\downarrow\rangle$, and the dot after creation of a (charged) exciton, $|X_{\downarrow}^{-}\rangle$. Transitions between these states are then produced by the field of a circularly polarized laser.

F.1 Light-matter interaction with a classical field

In a semi-classical picture, we use a classical (non-quantized) description for the electromagnetic field, while we keep a quantum mechanical description for the other parts of the system. There are two ways to describe coupling between light and matter:

1. We consider coupling of electric or magnetic fields to a (transition) dipole operator, $H_{\text{int}} = -\boldsymbol{\mu}_{\text{el}} \cdot \mathbf{E}$ or $H_{\text{int}} = -\boldsymbol{\mu}_{\text{mag}} \cdot \mathbf{B}$. For example, this description is appropriate for the electron spin, where the coupling to the magnetic field is given by the Zeeman term, Eq. (1.3). Generally, however, it is not obvious how to define the dipole moment. (Below, we see that the dipole approximation corresponds to take $e^{i\mathbf{k}\mathbf{r}} \approx 1$.)

2. We can avoid this dipole picture and use a more microscopical description. We consider a charged particle, e.g., an electron with mass m_0 and

charge e in a electromagnetic field. The corresponding Hamiltonian,

$$H = \frac{1}{2m_0} \left(\mathbf{p} - \frac{e}{c} \mathbf{A}(\mathbf{r}, t) \right)^2 + e\phi(\mathbf{r}, t) + V(\mathbf{r}, t), \quad (\text{F.1})$$

depends on the vector potential $\mathbf{A}(\mathbf{r}, t)$, the electrostatic potential $\phi(\mathbf{r}, t)$, and an external potential $V(\mathbf{r}, t)$ for the electron. We choose the Coulomb (or transverse) gauge, $\text{div} \mathbf{A}(\mathbf{r}, t) = 0$, and obtain

$$H = \frac{\mathbf{p}^2}{2m_0} + V(\mathbf{r}, t) - \frac{e}{mc} \mathbf{A}(\mathbf{r}, t) \cdot \mathbf{p} + \frac{e^2}{2mc^2} \mathbf{A}^2(\mathbf{r}, t) + e\phi(\mathbf{r}, t). \quad (\text{F.2})$$

We consider a cubic volume of length L , with L much bigger than the photon wavelength λ (i.e., in the far-field regime). Then, the vector potential $\mathbf{A}(\mathbf{r}, t)$ can be decomposed in plane waves,

$$\mathbf{A}(\mathbf{r}, t) = \frac{1}{\sqrt{\epsilon_0 \epsilon_r L^3}} \sum_{\mathbf{k}} \mathbf{A}_{\mathbf{k}}(t) e^{i\mathbf{k} \cdot \mathbf{r}}, \quad (\text{F.3})$$

with Fourier coefficients $\mathbf{A}_{\mathbf{k}}(t)$. The components of the vector \mathbf{k} take the values $k_\alpha = 2\pi n_\alpha / L$, where $\alpha = x, y, z$ and $n_\alpha \in \mathbb{Z}$. In the Coulomb gauge, $\mathbf{A}(\mathbf{r}, t)$ satisfies the homogeneous wave equation [210]

$$\nabla^2 \mathbf{A}(\mathbf{r}, t) - \frac{1}{c^2} \frac{\partial}{\partial t^2} \mathbf{A}(\mathbf{r}, t) = 0.$$

This leads to $\mathbf{A}_{\mathbf{k}}(t) = \mathbf{c}_{\mathbf{k}} \exp(-i\omega t) + \mathbf{c}_{-\mathbf{k}}^* \exp(i\omega t)$ with $\omega = ck$. We introduce two orthogonal unit polarization vectors $\boldsymbol{\epsilon}_{\mathbf{k}s}$ ($s = 1, 2$) which satisfy transversally $\mathbf{k} \cdot \boldsymbol{\epsilon}_{\mathbf{k}s} = 0$ ($s = 1, 2$), orthonormality $\boldsymbol{\epsilon}_{\mathbf{k}s}^* \cdot \boldsymbol{\epsilon}_{\mathbf{k}'s'} = \delta_{ss'} \delta^3(\mathbf{k} - \mathbf{k}')$, and right-handedness $\boldsymbol{\epsilon}_{\mathbf{k}1} \times \boldsymbol{\epsilon}_{\mathbf{k}2} = \mathbf{k}/k \equiv \boldsymbol{\kappa}$. Then, we can write $\mathbf{c}_{\mathbf{k}}$ as $\mathbf{c}_{\mathbf{k}} = \sum_{s=1}^2 c_{\mathbf{k}s} \boldsymbol{\epsilon}_{\mathbf{k}s}$ since $\mathbf{A}_{\mathbf{k}} \perp \mathbf{k}$. The basis $\boldsymbol{\epsilon}_{\mathbf{k}s}$ is understood as follows. When both $\boldsymbol{\epsilon}_{\mathbf{k}s}$ are real, this corresponds to two orthogonal linear polarizations (which are by definition parallel to the electric field vector). For a circular polarization, one chooses complex unit polarization vectors $\boldsymbol{\epsilon}_{\mathbf{k}s} = (1, \pm i)/\sqrt{2}$.

We write $\mathbf{A}_{\mathbf{k}}(t)$ in terms of $\boldsymbol{\epsilon}_{\mathbf{k}s}$, define the complex amplitudes $u_{\mathbf{k}s}(t) = c_{\mathbf{k}s} \exp(-i\omega t)$, and obtain

$$\mathbf{A}(\mathbf{r}, t) = \frac{1}{\sqrt{\epsilon_0 \epsilon_r L^3}} \sum_{\mathbf{k}, s} (u_{\mathbf{k}s}(t) \boldsymbol{\epsilon}_{\mathbf{k}s} e^{i\mathbf{k} \cdot \mathbf{r}} + u_{\mathbf{k}s}^*(t) \boldsymbol{\epsilon}_{\mathbf{k}s}^* e^{-i\mathbf{k} \cdot \mathbf{r}}). \quad (\text{F.4})$$

This is an expansion of $\mathbf{A}(\mathbf{r}, t)$ in the *fundamental vector mode functions* $\boldsymbol{\epsilon}_{\mathbf{k}s} \exp(i\mathbf{k} \cdot \mathbf{r})$.

F.2 Canonical quantization of the electromagnetic field

We now quantize the electromagnetic field. For this, we introduce a pair of real canonical variables, $q_{\mathbf{k}s}(t) = u_{\mathbf{k}s}(t) + u_{\mathbf{k}s}^*(t)$ and $p_{\mathbf{k}s}(t) = -i\omega [u_{\mathbf{k}s}(t) - u_{\mathbf{k}s}^*(t)]$. Expressed in these canonical variables, the vector potential reads

$$\mathbf{A}(\mathbf{r}, t) = \frac{1}{\sqrt{\epsilon_0 \epsilon_r L^3}} \sum_{\mathbf{k}, s} \left\{ \left[q_{\mathbf{k}s}(t) + \frac{i}{\omega} p_{\mathbf{k}s}(t) \right] \boldsymbol{\varepsilon}_{\mathbf{k}s} e^{i\mathbf{k} \cdot \mathbf{r}} + c.c. \right\}. \quad (\text{F.5})$$

The Hamiltonian of the electromagnetic field can be expressed in terms of the field energy [210] and becomes, in terms of $q_{\mathbf{k}s}(t)$ and $p_{\mathbf{k}s}(t)$,

$$H_f = \frac{1}{2} \sum_{\mathbf{k}, s} [p_{\mathbf{k}s}^2(t) + \omega^2 q_{\mathbf{k}s}^2(t)], \quad (\text{F.6})$$

which is the energy of a system of uncoupled harmonic oscillators. So every mode \mathbf{k} with polarization s corresponds to one of these independent harmonic oscillators.

We now replace the canonically conjugate variables $q_{\mathbf{k}s}(t)$ and $p_{\mathbf{k}s}(t)$ by operators $\hat{q}_{\mathbf{k}s}(t)$ and $\hat{p}_{\mathbf{k}s}(t)$ which satisfy $[\hat{q}_{\mathbf{k}s}(t), \hat{p}_{\mathbf{k}'s'}(t)] = i\hbar \delta_{ss'} \delta^3(\mathbf{k} - \mathbf{k}')$, and $[\hat{q}_{\mathbf{k}s}(t), \hat{q}_{\mathbf{k}'s'}(t)] = [\hat{p}_{\mathbf{k}s}(t), \hat{p}_{\mathbf{k}'s'}(t)] = 0$ [since according to Eq. (F.6) the classical modes are uncoupled]. We then define the non-Hermitian operators

$$\begin{aligned} \hat{a}_{\mathbf{k}s}(t) &= \frac{1}{\sqrt{2\hbar\omega}} [\omega \hat{q}_{\mathbf{k}s}(t) + i \hat{p}_{\mathbf{k}s}(t)] = \hat{a}_{\mathbf{k}s}(0) e^{-i\omega t}, \\ \hat{a}_{\mathbf{k}s}^\dagger(t) &= \frac{1}{\sqrt{2\hbar\omega}} [\omega \hat{q}_{\mathbf{k}s}(t) - i \hat{p}_{\mathbf{k}s}(t)] = \hat{a}_{\mathbf{k}s}^\dagger(0) e^{-i\omega t}. \end{aligned}$$

These operators $\hat{a}_{\mathbf{k}s}(t)$ and $\hat{a}_{\mathbf{k}s}^\dagger(t)$ satisfy the usual commutation relations of the annihilator and the creation operator of a harmonic oscillator, i.e., $[\hat{a}_{\mathbf{k}s}(t), \hat{a}_{\mathbf{k}'s'}^\dagger(t)] = \delta(\mathbf{k} - \mathbf{k}') \delta_{ss'}$. The Hamiltonian of the quantized electromagnetic field in the Heisenberg picture can finally be written as

$$H_f = \sum_{\mathbf{k}, s} \hbar\omega \left[\hat{a}_{\mathbf{k}s}^\dagger(t) \hat{a}_{\mathbf{k}s}(t) + \frac{1}{2} \right], \quad (\text{F.7})$$

with the usual term proportional to $1/2$ due to the zero-point contribution. The quantized form of the vector potential is

$$\mathbf{A}(\mathbf{r}, t) = \frac{1}{\sqrt{\epsilon_0 \epsilon_r L^3}} \sum_{\mathbf{k}, s} \left[\hat{a}_{\mathbf{k}s}(0) \boldsymbol{\varepsilon}_{\mathbf{k}s} e^{i(\mathbf{k} \cdot \mathbf{r} - \omega t)} + \hat{a}_{\mathbf{k}s}^\dagger(0) \boldsymbol{\varepsilon}_{\mathbf{k}s}^* e^{-i(\mathbf{k} \cdot \mathbf{r} - \omega t)} \right]. \quad (\text{F.8})$$

Note that this is just Eq. (F.6) after replacing $u(t) \rightarrow \hat{a}(t)$, $u^*(t) \rightarrow \hat{a}^\dagger(t)$ and thus $\hat{a}_{\mathbf{k}s}^\dagger$ creates a fundamental vector mode. In the following, we will omit the hat for the operators \hat{a} and \hat{a}^\dagger .

F.3 Interaction of a two-level system with the electromagnetic field

We consider an atom with two electronic levels $|1\rangle$ and $|2\rangle$. In the following, we describe how the coupling to the electromagnetic field leads to transitions between these levels. We describe the system with the Hamiltonian given in Eq. (F.2), but with a quantized vector potential [Eq. (F.8)],

$$H = H_0 + H_f + H_{\text{int}},$$

where,

$$\begin{aligned} H_0 &= \frac{\mathbf{p}^2}{2m_0} + V(\mathbf{r}, t), \\ H_{\text{int}} &= -\frac{e}{mc} \mathbf{A}(\mathbf{r}, t) \cdot \mathbf{p} + \frac{e^2}{2mc^2} \mathbf{A}^2(\mathbf{r}, t), \end{aligned}$$

and we have set the electrostatic potential to zero for simplicity. The field energy H_f is given by Eq. (F.7). We now neglect the term $e^2 \mathbf{A}^2(\mathbf{r}, t)/2mc^2$ in H_{int} , assuming that it is small compared to the one linear in \mathbf{A} . This is a good approximation for most optical experiments. For optical interactions one can usually expand $\exp(\pm i\mathbf{k} \cdot \mathbf{r})$ in the decomposition of \mathbf{A} [Eq. (F.8)] because the wavelength of the radiation field is much larger than the atomic wave function extension. This is the so-called multipole expansion. We now transform to the Schrödinger picture [removing $\exp(\pm i\omega t)$] and apply the electric dipole approximation, $\exp(\pm i\mathbf{k} \cdot \mathbf{r}) \approx 1$. We obtain

$$H_{\text{int}} = -\frac{e}{mc} \sum_{\mathbf{k}, s} A_{\mathbf{k}} \left[a_{\mathbf{k}s} \boldsymbol{\varepsilon}_{\mathbf{k}s} \cdot \mathbf{p} + a_{\mathbf{k}s}^\dagger \boldsymbol{\varepsilon}_{\mathbf{k}s}^* \cdot \mathbf{p} \right], \quad (\text{F.9})$$

where $A_{\mathbf{k}} = \sqrt{\hbar/2\omega\epsilon_0 L^3}$.

We consider H_{int} in the subspace spanned by $|1\rangle$ and $|2\rangle$ and only one mode of the field with a given polarization. We obtain

$$H_{\text{int}} = -\frac{e}{mc} A_{\mathbf{k}} \left[a_{\mathbf{k}s} (|2\rangle\langle 1|\langle 2|\varepsilon_{\mathbf{k}s} \cdot \mathbf{p}|1\rangle + |1\rangle\langle 2|\langle 1|\varepsilon_{\mathbf{k}s} \cdot \mathbf{p}|2\rangle) + a_{\mathbf{k}s}^\dagger (|2\rangle\langle 1|\langle 2|\varepsilon_{\mathbf{k}s}^* \cdot \mathbf{p}|1\rangle + |1\rangle\langle 2|\langle 1|\varepsilon_{\mathbf{k}s}^* \cdot \mathbf{p}|2\rangle) \right].$$

For coupling to a general polarization mode, one usually makes the rotating wave approximation, i.e., only keeping the energy conserving interaction terms. If we restrict ourselves to only one circular polarization mode that couples the transition $|2\rangle \leftrightarrow |1\rangle$ and transitions to other levels (which are possible in real atoms) are excluded, angular momentum conservation removes the energy non-conserving terms. We then obtain the interaction Hamiltonian

$$H_{\text{int}} = -\frac{e}{mc} A_{\mathbf{k}} \left(a_{\mathbf{k}s} |2\rangle\langle 1|\langle 2|\varepsilon_{\mathbf{k}s} \cdot \mathbf{p}|1\rangle + a_{\mathbf{k}s}^\dagger |1\rangle\langle 2|\langle 1|\varepsilon_{\mathbf{k}s}^* \cdot \mathbf{p}|2\rangle \right).$$

Finally, we define the optical Rabi frequency $\hbar\Omega_{\mathbf{k}s} = -eA_{\mathbf{k}}\langle 2|\varepsilon_{\mathbf{k}s} \cdot \mathbf{p}|1\rangle/mc = -e\langle 2|\varepsilon_{\mathbf{k}s} \cdot \mathbf{p}|1\rangle \sqrt{\hbar/2m_0^2 c^2 V \epsilon_0 \omega}$.

Appendix G

Differential equations for Cooperon and Diffuson

In this appendix, we transform the exact conductance correlator for diffusive systems and arbitrary magnetic textures to make a Schrödinger equation approach [86] possible. Further, we will derive the explicit differential equation for the diffuson propagator (the one for the cooperon has been derived previously [87]).

The conductance correlator has been derived in Ref. [87], using diagrammatic techniques, and is given by

$$\begin{aligned} \delta g^{(2)} &= \left(\frac{2e^2 D}{hL^2} \right)^2 \int d\epsilon d\epsilon' n'(\epsilon) n'(\epsilon') \int d\mathbf{x} d\mathbf{x}' \\ &\times \sum_{\alpha_1, \alpha_2, \alpha_3, \alpha_4} \left\{ \frac{1}{d} |\chi_{\alpha_1 \alpha_2, \alpha_3 \alpha_4}^C(\mathbf{x}, \mathbf{x}', \omega)|^2 \right. \\ &+ 2 \operatorname{Re} [\chi_{\alpha_1 \alpha_2, \alpha_3 \alpha_4}^C(\mathbf{x}, \mathbf{x}', \omega) \chi_{\alpha_2 \alpha_1, \alpha_4 \alpha_3}^C(\mathbf{x}', \mathbf{x}, \omega)] \\ &\left. + [\chi^C \rightarrow \chi^D] \right\}, \end{aligned} \quad (\text{G.1})$$

where $n'(\epsilon)$ is the derivative of the Fermi function, $\hbar\omega = \epsilon - \epsilon'$, and d describes the dimension of the system with respect to the mean free path l . The inverse Fourier transform of the cooperon/diffuson propagators $\chi^{C/D}(\mathbf{x}', \mathbf{x}, \omega)$ were

obtained [87, 205] as

$$\begin{aligned}
\chi_{\alpha_1\alpha_2,\alpha_3\alpha_4}^{C/D}(\mathbf{x}', \mathbf{x}; t', t) &= \theta(t' - t) \int_{\mathbf{R}(t)=\mathbf{x}}^{\mathbf{R}(t')=\mathbf{x}'} \mathcal{D}\mathbf{R} \exp \left\{ -\frac{1}{4D} \int_t^{t'} d\tau |\dot{\mathbf{R}}|^2 \right\} \\
&\times \exp \left\{ i \frac{e}{\hbar} \int_t^{t'} d\tau \left[\dot{\mathbf{R}} \cdot \mathbf{A}^{\text{em}}(\mathbf{R}(\tau)) + \dot{\mathbf{R}}^\pm \cdot \tilde{\mathbf{A}}^{\text{em}}(\mathbf{R}^\pm(\tau)) \right] \right\} \\
&\times \left\langle \alpha_4 \alpha_2 \left| \mathcal{T} \exp \left\{ i \frac{g\mu_B}{2\hbar} \int_t^{t'} d\tau \left[\mathbf{B}(\mathbf{R}(\tau)) \cdot \boldsymbol{\sigma}_1 \right. \right. \right. \right. \\
&\quad \left. \left. \left. - \tilde{\mathbf{B}}(\mathbf{R}^\pm(\tau)) \cdot \boldsymbol{\sigma}_2 \right] \right\} \right| \alpha_3 \alpha_1 \right\rangle, \tag{G.2}
\end{aligned}$$

where $\mathbf{R}^-(\tau) = \mathbf{R}(t' + t - \tau)$ is the time-reversed path of $\mathbf{R}^+ \equiv \mathbf{R}$.

For explicit evaluation it is convenient to transform this path-integral representation into a differential equation. In the case of the diffuson we first have to eliminate the time-reversed paths. As a result of reverting the time integration, an additional sign appears in the second term of the electromagnetic vector potential. For the Zeeman interaction we can use the relation

$$\begin{aligned}
&\left\langle \alpha_2 \left| \mathcal{T} \exp \left\{ -i \frac{g\mu_B}{2\hbar} \int_t^{t'} d\tau \tilde{\mathbf{B}}(\mathbf{R}^-(\tau)) \boldsymbol{\sigma} \right\} \right| \alpha_1 \right\rangle \\
&= \left\langle \alpha_1 \left| \mathcal{T} \exp \left\{ i \frac{g\mu_B}{2\hbar} \int_t^{t'} d\tau \tilde{\mathbf{B}}(\mathbf{R}(\tau)) \boldsymbol{\sigma} \right\} \right| \alpha_2 \right\rangle^* \\
&= \left\langle \alpha_1 \left| \mathcal{T} \exp \left\{ -i \frac{g\mu_B}{2\hbar} \int_t^{t'} d\tau \tilde{\mathbf{B}}(\mathbf{R}(\tau)) \boldsymbol{\sigma}^* \right\} \right| \alpha_2 \right\rangle. \tag{G.3}
\end{aligned}$$

The latter equation can be proven by writing the time-ordered product as a Dyson series and by inserting a resolution of unity in spin space between all products $(\mathbf{B}(x_j)\boldsymbol{\sigma})(\mathbf{B}(x_{j+1})\boldsymbol{\sigma})$, thereby arriving at an expression with terms of the form $\langle \alpha | B_i(x_j)\sigma_i | \beta \rangle^*$. Such terms are the complex conjugate of Pauli matrix elements multiplied by the real number $B_i(x_j)$. So we can rewrite them as $\langle \alpha | B_i(x_j)\sigma_i^* | \beta \rangle$, remove the previously inserted unities, and go back to the time-ordered product.

Now we can give the differential equations for the propagators

$$\begin{aligned} & \left(\frac{\partial}{\partial t'} + D \left[-i \frac{\partial}{\partial \mathbf{x}'} - \frac{e}{\hbar} \left[\mathbf{A}^{\text{em}}(\mathbf{x}') \pm \tilde{\mathbf{A}}^{\text{em}}(\mathbf{x}') \right] \right] \right)^2 \\ & \quad - i \frac{g\mu_{\text{B}}}{2\hbar} \left[\mathbf{B}(\mathbf{x}') \cdot \boldsymbol{\sigma}_1 - \tilde{\mathbf{B}}(\mathbf{x}') \cdot \boldsymbol{\sigma}_2^{(*)} \right] \hat{\chi}^{C/D}(\mathbf{x}', \mathbf{x}; t', t) \\ & = \delta(\mathbf{x}' - \mathbf{x}) \delta(t' - t) \hat{\mathbb{1}}, \end{aligned} \quad (\text{G.4})$$

where $\hat{\chi}^{C/D}(\mathbf{x}', \mathbf{x}; t', t)$ is a matrix in four-dimensional spin space. The upper sign is for the cooperon [87], the lower sign and the complex conjugate of $\boldsymbol{\sigma}_2$ for the diffuson. Passing to Fourier space and operator notation, the above equation becomes

$$\left(i\omega - D \frac{(2\pi)^2}{L^2} h^{C/D} \right) \hat{\chi}_\omega^{C/D} = \hat{\mathbb{1}}, \quad (\text{G.5})$$

where the effective Hamiltonian $h^{C/D}$ is defined in Eq. (6.4).

Finally we express the conductance correlation in terms of the operators $\chi_\omega^{C/D}$. We note that with $\chi_{\alpha_1\alpha_2, \alpha_3\alpha_4}^C(\mathbf{x}, \mathbf{x}', \omega)^* = \langle \mathbf{x}', \alpha_4\alpha_2 | \hat{\chi}_\omega^C | \mathbf{x}, \alpha_3\alpha_1 \rangle^* = \langle \mathbf{x}, \alpha_3\alpha_1 | \hat{\chi}_\omega^{C\dagger} | \mathbf{x}', \alpha_4\alpha_2 \rangle$, and $\chi_{\alpha_1\alpha_2, \alpha_3\alpha_4}^D(\mathbf{x}, \mathbf{x}', \omega)^* = \langle \mathbf{x}', \alpha_4\alpha_1 | \hat{\chi}_\omega^D | \mathbf{x}, \alpha_3\alpha_2 \rangle^* = \langle \mathbf{x}, \alpha_3\alpha_2 | \hat{\chi}_\omega^{D\dagger} | \mathbf{x}', \alpha_4\alpha_1 \rangle$ we can simplify the terms in Eq. (G.1):

$$\int d\mathbf{x} d\mathbf{x}' \sum_{\alpha_1, \dots, \alpha_4} |\chi_{\alpha_1\alpha_2, \alpha_3\alpha_4}^{C/D}(\mathbf{x}, \mathbf{x}', \omega)|^2 = \text{Tr} \hat{\chi}_\omega^{C/D} \hat{\chi}_\omega^{C/D\dagger}, \quad (\text{G.6})$$

and

$$\int d\mathbf{x} d\mathbf{x}' \sum_{\alpha_1, \dots, \alpha_4} \chi_{\alpha_1\alpha_2, \alpha_3\alpha_4}^{C/D}(\mathbf{x}, \mathbf{x}', \omega) \chi_{\alpha_2\alpha_1, \alpha_4\alpha_3}^{C/D}(\mathbf{x}', \mathbf{x}, \omega) = \text{Tr} \hat{\chi}_\omega^{C/D} \hat{\chi}_\omega^{C/D}. \quad (\text{G.7})$$

Appendix H

Finite Temperature Integrals for UCFs

We shall explain here the integrals used in Sec. 6.2.3 to obtain Eq. (6.18). We are interested in

$$I = \int d\epsilon' n'(\epsilon') J = \int d\epsilon' n'(\epsilon') \int d\epsilon n'(\epsilon) \left(\frac{1}{d} \frac{1}{(\epsilon - \epsilon' + a)^2 + c^2} + 2\text{Re} \frac{1}{(i\epsilon - i\epsilon' + ia - c)^2} \right) \quad (\text{H.1})$$

with a, c real and $c > 0$. We consider a rectangular integration contour Γ with one side lying on the real axis, extending $M = 2\pi l/\beta$ towards the positive imaginary axis and the same amount on each side of the real axis. For any positive integer l , the absolute value of the Fermi function is bounded above on such a contour: $|n(z)| \Big|_{\Gamma} < 2$. The integrands considered further below are a product of the Fermi function and a rational function decaying with at least $|z|^{-2}$. The integral of these products over the section of Γ in the upper half plane, will thus vanish for $M \rightarrow \infty$, as we have $|z| \geq M$ on this contour. We further note, that the complex expansion of the Fermi function $n(z)$ has its poles at $z = i\omega_n$, where $\omega_n = \pi n/\beta$ are the Matsubara frequencies and n is an odd integer.

We expand the first rational function in Eq. (H.1) into partial fractions

and then integrate J by parts:

$$\begin{aligned}
 J &= \int d\epsilon n(\epsilon) \left\{ \frac{1}{d} \frac{1}{2ic} \left(\frac{1}{(\epsilon - \epsilon' + a - ic)^2} - \frac{1}{(\epsilon - \epsilon' + a + ic)^2} \right) \right. \\
 &\quad \left. + 2\text{Re} \frac{-2}{(\epsilon - \epsilon' + a + ic)^3} \right\} \\
 &= \text{Re} \int d\epsilon n(\epsilon) \left\{ \frac{1}{d} \frac{i}{c(\epsilon - \epsilon' + a + ic)^2} - \frac{4}{(\epsilon - \epsilon' + a + ic)^3} \right\}. \quad (\text{H.2})
 \end{aligned}$$

We now evaluate the integral along the contour described above. As the poles of the rational functions in Eq. (H.2) are in the lower half plane at $\epsilon' - a - ic$, they are not within the integration contour. Applying Cauchy's residue theorem and accounting for the residues of the Fermi function $\text{res } n(z)|_{z=i\omega_n} = (-1/\beta)$ yields

$$J = \frac{2\pi}{\beta} \text{Re} \sum_{n \text{ odd} > 0} \left\{ \frac{1}{d} \frac{1}{c(i\omega_n - \epsilon' + a + ic)^2} + \frac{4i}{(i\omega_n - \epsilon' + a + ic)^3} \right\}. \quad (\text{H.3})$$

For the second integration in Eq. (H.1), we replace the expression in braces in the above equation by its complex conjugate. As before, we first integrate by parts over ϵ' and apply the residue theorem afterwards. This results in

$$\begin{aligned}
 I &= \frac{4\pi}{\beta} \text{Re} \sum_{n \text{ odd} > 0} \int d\epsilon' n(\epsilon') \left\{ \frac{1}{d} \frac{1}{c(i\omega_n + \epsilon' - a + ic)^3} + \frac{6i}{(i\omega_n + \epsilon' - a + ic)^4} \right\} \\
 &= \frac{8\pi^2}{\beta^2} \text{Re} \sum_{n, m \text{ odd} > 0} \left\{ \frac{1}{d} \frac{1}{c(\omega_n + \omega_m + ia + c)^3} + \frac{6}{(\omega_n + \omega_m + ia + c)^4} \right\}. \quad (\text{H.4})
 \end{aligned}$$

Appendix I

UCFs $\delta g_{\text{hom}}^{(2)}$ for Homogeneous Fields

We evaluate the UCFs for homogeneous fields to compare the results which we have used in chapter 6 from Ref. [87] [used in Eq. (6.2)] with earlier calculations [198, 201, 202]. For homogeneous fields we have $\eta = \tilde{\eta} = 0$ and $f = 0$, thus the Hamiltonians $h^{C/D}$ [Eq. (6.9)] become diagonal with the matrix elements $j^2 + i\alpha\kappa - i\tilde{\alpha}\tilde{\kappa}$. Now we evaluate the propagators $\hat{\chi}^{C/D}$ [Eq. (6.3)] and by evaluating the integrals over the Fermi functions in Eq. (6.2) explicitly by using standard Matsubara techniques, as explained in App. H. We obtain $\delta g_{\text{hom}}^{(2)} = \delta g_{\text{hom},C}^{(2)} + \delta g_{\text{hom},D}^{(2)}$, where

$$\begin{aligned} \delta g_{\text{hom},C/D}^{(2)} &= \left(\frac{e^2}{h}\right)^2 \frac{1}{8\pi^6} \left(\frac{L^2}{L_T^2}\right)^2 \text{Re} \sum_{\alpha, \tilde{\alpha}=\pm 1} \sum_{j=-\infty}^{\infty} \sum'_{n,m} \\ &\left\{ \frac{1}{-d} (\gamma^{C/D} + j^2) [b_{nm} + \gamma^{C/D} + j^2 + i(\alpha\kappa - \tilde{\alpha}\tilde{\kappa})]^3 \right. \\ &\left. + \frac{6}{[b_{nm} + \gamma^{C/D} + j^2 + i(\alpha\kappa - \tilde{\alpha}\tilde{\kappa})]^4} \right\}, \end{aligned} \quad (\text{I.1})$$

and we have introduced $b_{nm} = (n+m)(L/L_T)^2/4\pi$. Here n and m are positive, odd integers. The Aharonov-Bohm flux is implemented by replacing $j \rightarrow j - (\phi/\phi_0 \pm \tilde{\phi}/\phi_0)$. For further evaluation we now set $\kappa = \tilde{\kappa}$. We describe the summation of cooperon and diffuson terms with a prefactor β , which is 1 if both terms contribute and 2 if time-reversal symmetry is broken, so the cooperon contribution vanishes. Thus we have $\delta g_{\text{hom}}^{(2)} \approx (2/\beta)\delta g_{\text{hom},D}^{(2)}$

and from now on we only consider the dephasing parameter $\gamma = \gamma^D = L^2/(2\pi L_\varphi)^2$, according to Eq. (6.6).

If the spin-channel mixing is suppressed (i.e. $\kappa \gg \gamma$) in Eq. (I.1), we can replace the sum over the spins $\sum_{\alpha\bar{\alpha}}$ by the number of spin states g_s . For weaker magnetic fields ($\kappa \ll \gamma$) we have full spin degeneracy and obtain the factor g_s^2 . Accounting for valley degeneracy yields a factor g_v^2 .

Since we will check our results against the ones given in Ref. [202], where one-dimensional systems were considered, we take $d = 1$. Since we will evaluate some limiting cases below, where $L \gg 2\pi L_\varphi$, we have $\gamma \gg 1$ and can therefore replace the j -sum in Eq. (I.1) by an integral. The Aharonov-Bohm phase can then be removed by shifting the integration variable j and we finally obtain

$$\delta g_{\text{hom}}^{(2)} = \left(\frac{e^2}{h}\right)^2 \frac{1}{8\pi^6} \frac{2g_s^2 g_v^2}{\beta} \left(\frac{L^2}{L_T^2}\right)^2 \times \sum'_{n,m} \int_{-\infty}^{\infty} dj \left\{ \frac{1}{d(\gamma + j^2) [b_{nm} + \gamma + j^2]^3} + \frac{6}{[b_{nm} + \gamma + j^2]^4} \right\}. \quad (\text{I.2})$$

In the limit $(2\pi)^2 L_\varphi^2 \ll L^2, 2\pi L_T^2$, we have

$$\frac{2\pi L_T^2}{L^2} (\gamma + j^2) \geq \frac{L_T^2}{2\pi L_\varphi^2} \gg 1. \quad (\text{I.3})$$

Thus, we can use Poisson's summation formula to replace the summation over n and m in Eq. (I.2) by integration to arrive at

$$\delta g_{\text{hom}}^{(2)} = \frac{3}{4\pi^4} \frac{g_s^2 g_v^2}{\beta} \left(\frac{e^2}{h}\right)^2 \int_{-\infty}^{\infty} \frac{dj}{(\gamma + j^2)^2} = 3 \frac{g_s^2 g_v^2}{\beta} \left(\frac{e^2}{h}\right)^2 \left(\frac{L_\varphi}{L}\right)^3. \quad (\text{I.4})$$

We now consider another limit, $2\pi L_T^2 \ll L^2, (2\pi)^2 L_\varphi^2$. Again, we start from Eq. (I.2), but now we first calculate the integral over j , which has the dominant contribution $\pi\gamma^{-1/2}b^{-3}$ since $1 \ll \gamma \ll b_{nm}$. Thus we obtain

$$\begin{aligned} \delta g_{\text{hom}}^{(2)} &= \frac{4}{\pi} \frac{g_s^2 g_v^2}{\beta} \left(\frac{e^2}{h}\right)^2 \frac{L_T^2 L_\varphi}{L^2 L} \sum'_{n,m} \frac{1}{[\frac{1}{2}(n+m)]^3} \\ &= \frac{2\pi}{3} \frac{g_s^2 g_v^2}{\beta} \left(\frac{e^2}{h}\right)^2 \frac{L_T^2 L_\varphi}{L^2 L}. \end{aligned} \quad (\text{I.5})$$

Indeed, our results $\delta g_{\text{hom}}^{(2)}$ given in Eqs. (I.4) and (I.5) agrees with these of Ref. [202]. Thus, on the one hand, we have confirmed that the result from Ref. [87] [used in Eq. (6.2)] is consistent with earlier calculations [198, 201, 202]. On the other hand, in Eq. (I.1) we have given an explicit formula (not known before as far as we are aware of) describing how the spin-channel mixing becomes suppressed for increasing magnetic fields, such that $\delta g_{\text{hom}}^{(2)}$ contains a prefactor g_s^2 for low and g_s for high magnetic fields.

Appendix J

Energy Scales

For an electron spin in a magnetic field of a few Tesla, one typically needs to know the Zeeman splitting in meV or the Larmor frequency in s^{-1} . For estimating these and similar numerical values, Table J.1 is useful. We obtain it by equating the energies $g|\mu_{\text{B}}|B$, kT , $\hbar\omega$, $h\nu$, and E pairwise and using $g = 2$, $|\mu_{\text{B}}| = 9.27 \times 10^{-24} \text{ J/T}$, $k = 1.38 \times 10^{-23} \text{ J/K}$, and $\hbar = 1.05 \times 10^{-34} \text{ Js}$. For the rows, we set $B = 1 \text{ T}$ (Tesla), $T = 1 \text{ K}$ (Kelvin), $\omega = 1 \text{ rad s}^{-1}$, $\nu = 1 \text{ Hz}$, and $E = 1 \text{ meV} = 1.60 \times 10^{-19} \text{ mJ}$, resp., and fill the obtained values of the parameters B , T , ω , ν , and E into the corresponding columns.

-	Tesla	Kelvin	rad s^{-1}	GHz	meV
Tesla		1.3	1.8×10^{11}	28	0.12
Kelvin	0.74		1.3×10^{11}	21	0.086
rad s^{-1}	5.7×10^{-12}	7.6×10^{-12}		1.6×10^{-10}	6.6×10^{-13}
GHz	0.036	0.048	6.3×10^9		0.0041
meV	8.6	12	1.5×10^{12}	242	

Table J.1: Comparing parameters. For example, the Zeeman splitting in a magnetic field $B = 1 \text{ T}$ corresponds to the thermal energy at $T = 1.3 \text{ K}$.

References

- [1] G. Prinz, Phys. Today **45**(4), 58 (1995); G. A. Prinz, Science **282**, 1660 (1998).
- [2] M.A. Nielsen, I.L. Chuang, *Quantum Computation and Quantum Information* (Cambridge U. Press, New York, 2000).
- [3] D. Loss and D.P. DiVincenzo, Phys. Rev. A **57**, 120 (1998).
- [4] J.M. Kikkawa and D.D. Awschalom, Phys. Rev. Lett. **80**, 4313 (1998).
- [5] R. Fiederling, M. Keim, G. Reuscher, W. Ossau, G. Schmidt, A. Waag, and L.W. Molenkamp, Nature (London) **402**, 787 (1999); Y. Ohno, D.K. Young, B. Beschoten, F. Matsukura, H. Ohno, and D.D. Awschalom, *ibid.* **402**, 790 (1999).
- [6] Y. Ohno, D. K. Young, B. Beschoten, F. Matsukura, H. Ohno, and D.D. Awschalom, Nature **402**, 790 (1999).
- [7] F.G. Monzon and M.L. Roukes, J. Magn. Magn. Mater. **198**, 632 (1999).
- [8] S. Lüscher, T. Heinzel, K. Ensslin, W. Wegscheider, and M. Bichler, Phys. Rev. Lett. **86**, 2118 (2001).
- [9] D.P. DiVincenzo and D. Loss, J. Magn. Magn. Mater. **200**, 202 (1999).
- [10] P. Recher, E.V. Sukhorukov, and D. Loss, Phys. Rev. B **63**, 165314 (2001).
- [11] P. Recher and D. Loss, Phys. Rev. Lett. **91**, 267003 (2003).
- [12] G. Burkard, D. Loss, E.V. Sukhorukov, Phys. Rev. B **61**, R16303 (2000).

- [13] C.H. Bennett and D.P. DiVincenzo, *Nature* **404**, 247 (2000).
- [14] N. Gisin, G. Ribordy, W. Tittel, and H. Zbinden, *Rev. Mod. Phys.* **74**, 145 (2002).
- [15] F. Bloch, *Phys. Rev.* **70**, 460 (1946).
- [16] A. Abragam and B. Bleaney, *Electron Paramagnetic Resonance of Transition Ions* (Clarendon Press, Oxford, 1970).
- [17] R. Shankar, *Principles of Quantum Mechanics* (Plenum Press, NY/London, 1994).
- [18] L.P. Kouwenhoven, G. Schön, and L.L. Sohn, in *Mesoscopic Electron Transport*, Vol. 345 of *NATO Advanced Study Institute, Series E*, edited by L.L. Sohn, L.P. Kouwenhoven, and G. Schön (Kluwer Academic Publishers, Dordrecht, 1997).
- [19] S. Tarucha, D.G. Austing, T. Honda, R.J. van der Hage, and L.P. Kouwenhoven, *Phys. Rev. Lett.* **77**, 3613 (1996).
- [20] J. M. Elzerman, R. Hanson, J.S. Greidanus, L.H. Willems van Beveren, S.De Franceschi, L.M.K. Vandersypen, S. Tarucha, L.P. Kouwenhoven, *Phys. Rev. B* **67**, 161308 (2003).
- [21] F.R. Waugh, M.J. Berry, D.J. Mar, R.M. Westervelt, K. L. Campman and A. C. Gossard, *Phys. Rev. Lett.* **75**, 705 (1995); C. Livermore, C.H. Crouch, R.M. Westervelt, K.L. Campman, and A.C. Gossard, *Science* **274**, 1332 (1996).
- [22] T.H. Oosterkamp, S.F. Godijn, M.J. Uilenreef, Y.V. Nazarov, N.C. van der Vaart, and L.P. Kouwenhoven, *Phys. Rev. Lett.* **80**, 4951 (1998).
- [23] R.H. Blick, D. Pfannkuche, R.J. Haug, K. v. Klitzing, and K. Eberl, *Phys. Rev. Lett.* **80**, 4032 (1998); R.H. Blick, D.W. van der Weide, R.J. Haug, and K. Eberl, *Phys. Rev. Lett.* **81**, 689 (1998); T.H. Oosterkamp, T. Fujisawa, W.G. van der Wiel, K. Ishibashi, R.V. Hijman, S. Tarucha, L.P. Kouwenhoven, *Nature* **395**, 873 (1998); I.J. Maasilta and V.J. Goldman, *Phys. Rev. Lett.* **84**, 1776 (2000).
- [24] T. Hayashi, T. Fujisawa, H.-D. Cheong, Y.-H. Jeong, and Y. Hirayama, *Phys. Rev. Lett.* **91**, 226804 (2003).

- [25] P. Recher, E.V. Sukhorukov, D. Loss, Phys. Rev. Lett. **85**, 1962 (2000).
- [26] A.V. Khaetskii and Y.V. Nazarov, Phys. Rev. B **64**, 125316 (2001).
- [27] S.I. Erlingsson and Y.V. Nazarov, Phys. Rev. B **66**, 155327 (2002).
- [28] L.S. Levitov and E.I. Rashba, Phys. Rev. B **67**, 115324 (2003).
- [29] V. Golovach, A. Khaetskii, and D. Loss, cond-mat/0310655.
- [30] G. Burkard, D. Loss, and D.P. DiVincenzo, Phys. Rev. B **59**, 2070 (1999).
- [31] A.Khaetskii, D. Loss, and L. Glazman, Phys. Rev. Lett. **88**, 186802 (2002).
- [32] A.Khaetskii, D. Loss, and L. Glazman, Phys. Rev. B **67**, 195329 (2003).
- [33] J.A. Gupta, D.D. Awschalom, X. Peng, and A.P. Alivisatos, Phys. Rev. B **59**, R10 421 (1999).
- [34] T. Fujisawa, Y. Tokura, and Y. Hirayama, Phys. Rev. B **63** R081304 (2001).
- [35] R. Hanson, B. Witkamp, L.M.K. Vandersypen, L.H. Willems van Beveren, J.M. Elzerman, and L.P. Kouwenhoven, Phys. Rev. Lett. **91**, 196802 (2003).
- [36] L.K. Grover, Phys. Rev. Lett. **79**, 325 (1997).
- [37] P.W. Shor, in *Proc. 35th Symposium on the Foundations of Computer Science*, (IEEE Computer Society Press), 124 (1994).
- [38] B. Schneier, *Applied Cryptography* (John Wiley & Sons, NY, 1995).
- [39] F. Weissbaum, *Introduction to Cryptology*, 2001 (unpublished).
- [40] L.M.K. Vandersypen, M. Steffen, G. Breyta, C.S. Yannoni, M.H. Sherwood, I.L. Chuang, Nature **414**, 883 (2002).
- [41] J.I. Cirac and P. Zoller, Phys. Rev. Lett. **74**, 4091 (1995); C. Monroe, D.M. Meekhof, B.E. King, W.M. Itano, and D.J. Wineland, *ibid.* **75**, 4714 (1995).

- [42] Q.A. Turchette, C.J. Hood, W. Lange, H. Mabuchi, and H.J. Kimble, Phys. Rev. Lett. **75**, 4710 (1995).
- [43] D. Cory, A. Fahmy, and T. Havel, Proc. Nat. Acad. Sci. U.S.A. **94**, 1634 (1997); N.A. Gershenfeld and I. L. Chuang, Science **275**, 350 (1997).
- [44] V. Privman, I. D. Vagner, and G. Kventsel, Phys. Lett. A **239**, 141 (1998).
- [45] B.E. Kane, Nature (London) **393**, 133 (1998).
- [46] A. Shnirman, G. Schön, and Z. Hermon, Phys. Rev. Lett. **79**, 2371 (1997).
- [47] D.V. Averin, Solid State Commun. **105**, 659 (1998).
- [48] L.B. Ioffe, V.B. Geshkenbein, M.V. Feigel'man, A.L. Fauchère, and G. Blatter, Nature **398**, 679 (1999).
- [49] T.P. Orlando, J.E. Mooij, L. Tian, C.H. van der Wal, L.S. Levitov, S. Lloyd, and J.J. Mazo, Phys. Rev. B **60**, 15398 (1999); C.H. van der Wal, A.C.J. ter Haar, F.K. Wilhelm, R.N. Schouten, C.J.P.M. Harmans, T.P. Orlando, S. Lloyd, and J.E. Mooij, Science **290**, 773 (2000).
- [50] D. P. DiVincenzo, cond-mat/9612126; in *Mesoscopic Electron Transport, Vol. 345 of NATO Advanced Study Institute, Series E: Applied Sciences*, edited by L. Sohn, L. Kouwenhoven, and G. Schön (Kluwer, Dordrecht, 1997).
- [51] D.P. DiVincenzo, Fortschr. Phys. **48**, 771 (2000).
- [52] G. Burkard, H.-A. Engel, and D. Loss, Fortschr. Phys. **48**, 965 (2000).
- [53] G. Salis, Y. Kato, K. Ensslin, D.C. Driscoll, A.C. Gossard, and D.D. Awschalom, Physica E **16**, 99 (2003).
- [54] Y. Kato, R.C. Myers, D.C. Driscoll, A.C. Gossard, J. Levy, and D.D. Awschalom, Science **299**, 1201 (2003).
- [55] G. Burkard, G. Seelig, and D. Loss, Phys. Rev. B **62**, 2581 (2000).
- [56] H.-A. Engel and D. Loss, Phys. Rev. Lett. **86**, 4648 (2001).

- [57] H.-A. Engel and D. Loss, Phys. Rev. B **65**, 195321 (2002).
- [58] H.-A. Engel, V. Golovach, D. Loss, L.M.K. Vandersypen, J.M. Elzerman, R. Hanson, and L.P. Kouwenhoven, cond-mat/0309023.
- [59] L.D. Landau and E.M. Lifshitz, *Statistical Physics*, Course in Theoretical Physics Vol. 5, §118 (Pergamon, London/Paris, 1958).
- [60] M.B. Johnson, Phys. Rev. **29**, 367 (1927); H. Nyquist, Phys. Rev. **32**, 110 (1928).
- [61] W. Schottky, Ann. Phys. (Leipzig) **57**, 541 (1918).
- [62] D. Rogovin, D.J. Scalapino, Ann. Phys. (NY) **86**, 1 (1974).
- [63] E.V. Sukhorukov, G. Burkard, and D. Loss, Phys. Rev. B **63**, 125315 (2001).
- [64] G.B. Lesovik, R. Loosen, JETP Lett. **65** (3), 295 (1997).
- [65] Ya.M. Blanter and M. Büttiker, Phys. Rep. **336**, 1 (2000).
- [66] C. Beenakker and C. Schönberger, Phys. Today (5), 37 (2003).
- [67] C.W.J. Beenakker and M. Büttiker, Phys. Rev. B **46**, 1889 (1992); K.E. Nagaev, Phys. Lett. A **169**, 103 (1992).
- [68] B.R. Bulka, J. Martinek, G. Michalek, and J. Barnas, Phys. Rev. **60**, 12246 (1999).
- [69] A. Cottet, W. Belzig, and C. Bruder, cond-mat/0308564.
- [70] L.S. Levitov and G.B. Lesovik, JETP Lett. **58**, 230 (1993).
- [71] L.S. Levitov, H.-W. Lee, and G.B. Lesovik, J. Math. Phys. **37**, 4845 (1996).
- [72] M.J.M. de Jong, Phys. Rev. B **54**, 8144 (1996).
- [73] Yu.V. Nazarov, Ann. Phys. (Leipzig) **8**, special Issue, SI-193 (1999).
- [74] W. Belzig and Yu.V. Nazarov, **87**, 197006 (2001).
- [75] L.S. Levitov and M. Reznikov, cond-mat/0111057.

- [76] B. Reulet, J. Senzier, and D. E. Prober, *Phys. Rev. Lett.* **91**, 196601 (2003).
- [77] C. W. J. Beenakker, M. Kindermann, and Yu. V. Nazarov, *Phys. Rev. Lett.* **90**, 176802 (2003).
- [78] M.V. Berry, *Proc. R. Soc. London, Ser. A*: **392**, 45 (1984).
- [79] A. F. Morpurgo, J. P. Heida, T. M. Klapwijk, B. J. van Wees, and G. Borghs, *Phys. Rev. Lett.* **80**, 1050 (1998).
- [80] J.-B. Yau, E.P. De Poortere, and M. Shayegan, *Phys. Rev. Lett.* **88**, 146801 (2002).
- [81] M.J. Yang, C.H. Yang, K.A. Cheng, Y.B. Lyanda-Geller, *cond-mat/0208260*.
- [82] For a collection of relevant reprinted articles and commentary, see A. Shapere and F. Wilczek, *Geometric Phases in Physics* (World Scientific, Singapore, 1989).
- [83] D. Loss, P.M. Goldbart and A.V. Balatsky, *Phys. Rev. Lett.* **65**, 1655 (1990).
- [84] A.G. Aronov and Y.B. Lyanda-Geller, *Phys. Rev. Lett.* **70**, 343 (1993).
- [85] D. Loss, P.M. Goldbart and A.V. Balatsky, 1990, in *Granular Nanoelectronics*, D.K. Ferry, J.R. Barker and C. Jacoboni (eds.), *NATO ASI Series B: Physics* 251 (Plenum, New York, 1991).
- [86] D. Loss and P.M. Goldbart, *Phys. Rev. B* **45**, 13544 (1992).
- [87] D. Loss, H. Schoeller, and P.M. Goldbart, *Phys. Rev. B* **48**, 15218 (1993).
- [88] H.-A. Engel and D. Loss, *Phys. Rev. B* **62**, 10238 (2000).
- [89] M. Paillard, X. Marie, P. Renucci, T. Amand, A. Jbeli, and J. M. Gérard, *Phys. Rev. Lett.* **86**, 1634 (2001).
- [90] J.A. Gupta, R. Knobel, N. Samarth, and D.D. Awschalom, *Science* **292**, 2458 (2001).

- [91] A. Imamoglu, D.D. Awschalom, G. Burkard, D.P. DiVincenzo, D. Loss, M. Sherwin, and A. Small, Phys. Rev. Lett. **83**, 4204 (1999).
- [92] C.H.W. Barnes, J.M. Shilton, and A.M. Robinson, Phys. Rev. B **62**, 8410 (2000).
- [93] R. Vrijen, E. Yablonovitch, K. Wang, H.W. Jiang, A. Balandin, V. Roychowdhury, T. Mor, and D. DiVincenzo, Phys. Rev. A **62**, 012306 (2000).
- [94] J. Levy, Phys. Rev. A **64**, 052306 (2001).
- [95] X. Hu, R. de Sousa, and S. Das Sarma, Phys. Rev. Lett. **86**, 918 (2001).
- [96] J.P. Gordon and K.D. Bowers, Phys. Rev. Lett. **1** 368 (1958).
- [97] P.C. Hammel, Z. Zhang, G.J. Moore, and M.L. Roukes, J. Low Temp. Phys. **101**, 59 (1995); J.A. Sidles, J.L. Garbini, K.J. Bruland, D. Rugar, O. Züger, S. Hoen, and C.S. Yannoni, Rev. Mod. Phys. **67**, 249 (1995).
- [98] V.N. Golovach and D. Loss, Europhys. Lett. **62**, 83 (2003).
- [99] T. Brandes, F. Renzoni, and R.H. Blick, Phys. Rev. B **64**, 035319 (2001).
- [100] C.J.P.M. Harmans (private communication).
- [101] R.H. Blick, V. Gudmundsson, R.J. Haug, K. von Klitzing, and Karl Eberl, Phys. Rev. B **57**, R12 685 (1998).
- [102] M. Dobers, K. von Klitzing, J. Schneider, G. Weimann, and K. Ploog, Phys. Rev. Lett. **61**, 1650 (1988).
- [103] S. Tarucha, D.G. Austing, T. Honda, R.J. van der Hage, and L.P. Kouwenhoven, Phys. Rev. Lett. **77**, 3613 (1996).
- [104] One distinguishes between μ_{dot} , which is the energy required for an electron of the lead to tunnel onto the dot, and the addition energy $E_{\text{add}} = \mu_{\text{dot}}(N+1) - \mu_{\text{dot}}(N) = e^2/C + \varepsilon_{N+1}^\sigma - \varepsilon_N^\sigma$. When lead l provides enough energy such that an electron can tunnel onto the dot [$\mu_l > \mu_{\text{dot}}(N)$], the addition energy is the extra energy the lead must provide such that an *additional* electron can tunnel onto the dot as well, $\mu'_l = \mu_l + E_{\text{add}} > \mu_{\text{dot}}(N+1)$. The current as function of the gate voltage shows sequential tunneling peaks at $\mu_{\text{dot}}(N)$. Thus, E_{add} is proportional to the distance of two subsequent peaks.

- [105] E. Fick and G. Sauermaun, *The Quantum Statistics of Dynamic Processes*, Springer Series in Solid State Sciences Vol. 86 (Springer, Berlin, 1990).
- [106] At this point, one usually makes a secular approximation (Ref. [107]) by neglecting terms in M^I [Eq. (2.8)] that rapidly oscillate with the energy difference of different states on the dot. However, it is noteworthy that for the system considered here, no such terms appear and thus no such secular approximation is required.
- [107] K. Blum, *Density Matrix Theory and Applications* (Plenum Press, New York, 1996), Chap. 8.
- [108] B. Thimmel, P. Nalbach, and O. Terzidis, *Eur. Phys. J. B* **9**, 207 (1999); F. Bloch and A. Siegert, *Phys. Rev.* **57**, 522 (1940).
- [109] PAT effects are due to the electric rf field component (see Sec. 2.2.1) and thus are less sensitive to changes in B_z , compared to the magnetic ESR effects described here.
- [110] It has been suggested to test the functionality of spin filtering by an electron interference experiment with an Aharonov-Bohm (AB) ring, with one dot in each arm of the ring (Ref. [211]). On the one hand, if both dots allow the same spin to pass, the flux enclosed by the electron moving through the upper as well as through the lower arm will lead to interference and the resulting AB oscillations are observable in the current. On the other hand, if the dots filter out different electron spins—say, all spin- \uparrow electrons go through the upper arm while all spin- \downarrow electrons go through the lower arm of the ring—no magnetic flux is enclosed by either spin current and thus no interference occurs. However, there is still a leakage (cotunneling) current of the opposite spin through the spin filters (Ref. [25]); thus there is still a small current contribution showing AB oscillations.
- [111] E. Merzbacher, *Quantum Mechanics*, 3rd ed. (Wiley, New York, 1998), Chap. 20.
- [112] For nonmagnetic photon-assisted pumps see, e.g., Ref. [18] and B.L. Hazelzet, M.R. Wegewijs, T.H. Stoof, and Yu.V. Nazarov, *Phys. Rev. B* **63**, 165313 (2001).

- [113] Generically this is satisfied. However, if there is no complete basis of eigenvectors of \mathcal{M} , there is power law admixture. For instance, for $\Delta_{\perp} = \Sigma_W - V_{\uparrow}$, the last two eigenvalues, λ_{\pm} , in Eq. (2.48) are degenerate. Then, the time evolution of ρ can contain terms proportional to $t e^{\lambda_{\pm} t}$.
- [114] D.V. Averin and Yu.V. Nazarov, in *Single Charge Tunneling*, Vol. 294 of *NATO Advanced Study Institute, Series B*, edited by H. Grabert and M.H. Devoret, (Plenum Press, New York, 1992).
- [115] H. Schoeller and G. Schön, *Phys. Rev. B* **50**, 18 436 (1994); J. König, H. Schoeller, and G. Schön, *ibid.* **58**, 7882 (1998).
- [116] D. Loss and E.V. Sukhorukov, *Phys. Rev. Lett.* **84**, 1035 (2000).
- [117] M. Ciorga, A.S. Sachrajda, P.Hawrylak, C. Gould, P. Zawadzki, S. Jullian, Y. Feng, and Z. Wasilewski, *Phys. Rev. B* **61**, R16 315 (2000).
- [118] M.H. Devoret and R.J. Schoelkopf, *Nature* **406**, 1039 (2000).
- [119] For the measurement process in Josephson qubits, see Y. Makhlin, G. Schön, and A. Shnirman, *Phys. Rev. Lett.* **85**, 4578 (2000).
- [120] Note that by using transport involving many states of the dot, the read-out current could be increased and thus the read-out time further decreased. Further, if instead resonant tunneling is considered, e.g., into an SET device, faster read out could be achieved.
- [121] Note that in general $I_1(t) \neq I_2(t)$, since charge can accumulate on the dot for some typical time, which is limited from above by the inverse tunneling rates. Here, charge accumulation occurs with the period of the Rabi oscillations Δ_x^{-1} .
- [122] An alternative application of pulsed ESR for measuring T_2 is spin echo, where a well-defined sequence of pulses is applied to cancel the effect of dephasing (Refs. [212],[96] and [16]). At the end of the sequence, the dot spin (in the σ_z basis) can be measured by one of the techniques discussed in Secs. 2.9, 2.10.1, and 2.11. Here, spin echo compensates for dephasing of an array of quantum dots in an inhomogeneous magnetic field B_z or in time series measurements (on a single dot), where the magnetic field B_z fluctuates in time. More care must be taken for inhomogeneities in the g factor (Rabi frequency Δ_x), since then a pulse does not rotate the spin

by an equal angle for every dot. To compensate this, one could, e.g., use Carr-Purcell-Meiboom-Gill pulse sequences (Ref. [212]).

- [123] A. Peres, *Quantum Theory* (Kluwer Academic, Amsterdam, 1993).
- [124] We note that similar concepts have been used in recent experiments (Ref. [213]), however with a separation of time scales, $T_\Omega, t_p \ll \gamma^{-1}$. We show here that such concepts can be applied more generally for regimes where $T_\Omega, t_p \lesssim \gamma^{-1}$.
- [125] C. Schöenberger, H. van Houten, and H.C. Donkersloot, *Europhys. Lett.* **20**, 249 (1992).
- [126] D. Porath and O. Millo, *J. Appl. Phys.* **81**, 2241 (1996).
- [127] C.J. Chen, *Introduction to Scanning Tunneling Microscopy* (Oxford University Press, New York, 1993).
- [128] L.M.K. Vandersypen, R. Hanson, L.H. Willems van Beveren, J.M. Elzerman, J.S. Greidanus, S. De Franceschi, L.P. Kouwenhoven in *Quantum Computing and Quantum Bits in Mesoscopic Systems*, eds. A.J. Leggett, B. Ruggiero, and P. Silvestrini (Kluwer, NY, 2003), quant-ph/0207059.
- [129] In other words, we assume a sufficient signal-to-noise ratio of the apparatus to distinguish the measurement outcome A_0 from A_1 .
- [130] For a qubit in an arbitrary superposition $\alpha|0\rangle + \beta|1\rangle$, the expectation value of the measurement is $\langle \hat{A} \rangle = |\alpha|^2 \langle \hat{A} \rangle_0 + |\beta|^2 \langle \hat{A} \rangle_1$, which allows to determine $|\alpha|^2$ and $|\beta|^2 = 1 - |\alpha|^2$. (To measure the phase $\arg \alpha/\beta$, first some single qubit rotations need to be performed.) In order to differentiate a given $|\alpha|^2$ from a value $|\alpha'|^2$, a sufficient n is given by Eqs. (3.1) and (3.2) after replacing $p_0 \rightarrow |\alpha|^2 p_0 + (1 - |\alpha|^2)(1 - p_1)$ and $p_1 \rightarrow 1 - |\alpha'|^2 p_0 - (1 - |\alpha'|^2)(1 - p_1)$.
- [131] K. Bosch, *Grosses Lehrbuch der Statistik* (R. Oldenbourg, Munich, 1996), pp. 379.
- [132] If n is small, one can use Clopper-Pearson confidence intervals. However, if read out of one state is perfect, say $p_0 = 1$, we can no longer approximate with a normal distribution, even for large n . In that case, finding A_0 as outcome n times in a row, even if the qubit is $|1\rangle$, i.e., read

out fails, occurs with probability $(1 - p_1)^n$. Thus, $n \geq \log(\alpha)/\log(1 - e)$ is sufficient for read out.

- [133] T. Fujisawa, D.G. Austing, Y. Tokura, Y. Hirayama, S. Tarucha, *Nature* **419**, 278 (2002).
- [134] B.E. Kane, N.S. McAlpine, A.S. Dzurak, R.G. Clark, G.J. Milburn, H.B. Sun, and H. Wiseman, *Phys. Rev. B* **61**, 2961 (2000).
- [135] Instead of a reference dot, the qubit dot can be coupled to a lead. To ensure that only electrons with, say, spin \downarrow can tunnel, one can use spin-polarized leads or a Zeeman splitting on the dot and properly tuned energy levels [56, 57].
- [136] M. Field, C. G. Smith, M. Pepper, D. A. Ritchie, J. E. F. Frost, G. A. C. Jones, and D. G. Hasko, *Phys. Rev. Lett.* **70**, 1311 (1993).
- [137] W. Lu, Z.Q. Ji, L. Pfeiffer, K.W. West, and A.J. Rimberg, *Nature* **423** (6938), 422 (2003).
- [138] This can be generated with (i) locally different magnetic fields. Or, with an inhomogeneous g factor as follows. (ii) Spatial variation of dot location in a heterostructure, i.e., moving electrons up/down by gates etc. (iii) Similarly, produce a spatial variation with different orbital states by filling each dot with a different number of electrons. (iv) Different hyperfine interaction in each dot, say, by inducing a nuclear polarization in one dot by the QPC current. (v) Different Rashba interaction, (vi) optical Stark effect [C. Cohen-Tannoudji, J. Dupont-Roc, *Phys. Rev. A* **5**, 968 (1972); [90]], or (vii) differently distributed magnetic impurities in each dot.
- [139] K. Ono, D.G. Austing, Y. Tokura, S. Tarucha, *Science* **297**, 1313 (2002).
- [140] S.A. Gurvitz, *Phys. Rev. B* **56**, 15215 (1997).
- [141] A.N. Korotkov, *Phys. Rev. B* **63**, 115403 (2001).
- [142] H.-S. Goan, G.J. Milburn, H.M. Wiseman, H.B. Sun, *Phys. Rev. B* **63**, 125326 (2001).

- [143] We map the two-level system $\{|L\rangle, |R\rangle\}$ onto a pseudo spin $\frac{1}{2}$ with Hamiltonian $H(t) = \frac{1}{2}\varepsilon\sigma_z + t_d\sigma_x + X(t)\sigma_z + \frac{1}{2}(t_L^Q + t_R^Q)V_{\text{QPC}}(t)$. The fluctuations due to the QPC are $X(t) = \frac{1}{2}(t_L^Q - t_R^Q)V_{\text{QPC}}(t)$ with $V_{\text{QPC}}(t) = e^{iH_{\text{QPC}}t}V_{\text{QPC}}e^{-iH_{\text{QPC}}t}$.
- [144] We define $\mathbf{P} = \frac{1}{2}\text{Tr} \rho \boldsymbol{\sigma}$ and write the master equation in the standard Bloch notation, $\dot{\mathbf{P}} = \boldsymbol{\omega} \times \mathbf{P} + \Gamma(\mathbf{P} - \mathbf{P}_0)$, with $\boldsymbol{\omega} = (2t_d, -t_d\Gamma_Q/\Delta\mu - t_d\Gamma_Q(g_\Sigma - 2g_0)\varepsilon/E^2, \varepsilon + t_d\Gamma_Q/\Delta\mu)$, and where Γ is symmetric with elements $\Gamma_{xy} = \Gamma_{yx} = -t_d\Gamma_Q/\Delta\mu$; $\Gamma_{xz} = \Gamma_{zx} = \Gamma_{xy} - t_d\Gamma_Q(g_\Sigma - 2g_0)\varepsilon/E^2$; $\Gamma_{yy} = -\Gamma_Q(1 + g_\Sigma) + \Gamma_Q(g_\Sigma - 2g_0)\varepsilon^2/E^2$; $\Gamma_{xx} = 2\Gamma_{xy} + \Gamma_{yy}$; $\Gamma_{yz} = \Gamma_{zy} = \Gamma_{zz} = 0$. Finally, $P_{0x} = P_{0y} = 0$ and $P_{0z} = [t_d\Gamma_Q(2t_d + \varepsilon)/(1 + g_\Sigma)\Delta\mu^2 - \Gamma_{xy}]/\Gamma_{xz}$.
- [145] R. Aguado and L.P. Kouwenhoven, Phys. Rev. Lett. **84**, 1986 (2000).
- [146] U. Gavish, Y. Levinson, and Y. Imry, Phys. Rev. B **62**, 10637 (2000).
- [147] Using the antisymmetric noise contribution to isolate quantum effects can be compared with conductance measurements in Aharonov-Bohm (AB) rings, where the contribution showing AB oscillations can easily be separated and is purely due to quantum mechanical phase coherence.
- [148] H. Birk, M.J.M. de Jong, and C. Schönenberger, Phys. Rev. Lett. **75**, 1610 (1995).
- [149] D.V. Averin, J. Appl. Phys. **73**, 2593 (1993).
- [150] A.N. Korotkov, Phys. Rev. B **49**, 10381 (1994).
- [151] S. Hershfield, J.H. Davies, P. Hyldgaard, C.J. Stanton, and J.W. Wilkins, Phys. Rev. B **47**, 1967 (1993).
- [152] The formal solution of Eq. (4.2) corresponds to resumming an infinite number of terms. Since we evaluate the self-energy \mathcal{M} in leading order, we only resum a certain subset of the higher order terms in $\rho^c(\omega)$.
- [153] Evaluating $\hat{M}(\tau)$ explicitly, we find that it decays on a time scale $\tau_c \sim 1/kT$, i.e., the correlations induced in the leads decay within τ_c . Thus, the Markov approximation is justified for $\omega\tau_c, \gamma\tau_c \ll 1$.

- [154] This is apparent from Eq. (4.5). More general, it is straightforward to prove that in Born-Markov approximation, the autocorrelation function is always symmetric in ω for operators \dot{X} with $[X, H_0] = [X, \rho_Q^0] = 0$.
- [155] This linear map $G \mapsto g$ is the identity on operators, however, here G is a superoperator. With this notation, Eq. (4.6) is reminiscent of the Lindblad form, $\sum_i [A_i \rho A_i^\dagger - A_i^\dagger A_i \rho] + \text{h.c.}$
- [156] A.N. Korotkov, *Europhys. Lett.* **43**, 343 (1998).
- [157] This system is equivalent to the one with an additional electron on the dot and where the ground state with two electrons is a singlet $|S\rangle$ [56, 57].
- [158] The steps coming from the θ -function are suppressed by the last factor of Eq. (4.12).
- [159] R. Deblock, E. Onac, L. Gurevich, and L.P. Kouwenhoven, *Science* **301**, 203 (2003).
- [160] *Semiconductor Spintronics and Quantum Computation*, eds. D.D. Awschalom, D. Loss, and N. Samarth. Series on Nanoscience and Technology, Springer (2002).
- [161] N.H. Bonadeo, J. Erland, D. Gammon, D. Park, D.S. Katzer and D.G. Steel, *Science* **282**, 1473 (1998).
- [162] J.A. Gupta, D.D. Awschalom, X. Peng, and A.P. Alivisatos, *Phys. Rev. B* **59**, R10421 (1999).
- [163] B. Ohnesorge, M. Albrecht, J. Oshinowo, A. Forchel, and Y. Arakawa, *Phys. Rev. B* **54**, 11532 (1996).
- [164] S. Raymond, S. Fafard, P. J. Poole, A. Wojs, P. Hawrylak, S. Charbonneau, D. Leonard, R. Leon, P. M. Petroff, and J. L. Merz, *Phys. Rev. B* **54**, 11548 (1996).
- [165] R.J. Epstein, D.T. Fuchs, W.V. Schoenfeld, P.M. Petroff, and D.D. Awschalom, *Appl. Phys. Lett.* **78**, 733 (2001).
- [166] A. Gruber, A. Dräbenstedt, C. Tietz, L. Fleury, J. Wrachtrup, and C. von Borczyskowski, *Science* **276**, 2012 (1997).

- [167] E. Lifshitz, I. Dag, I.D. Litvitn, and G. Hodes, *J. Phys. Chem. B* **102** (46), 9245 (1998).
- [168] N. Zurauskiene, G. Janssen, E. Goovaerts, A. Bouwen, D. Shoemaker, P.M. Koenraad, and J.H. Wolter, *phys. stat. sol. (b)* **224**, 551 (2001).
- [169] For a recent discussion, see, e.g., T. Calarco , A. Datta, P. Fedichev, E. Pazy, and P. Zoller, *Phys. Rev. A* **68**, 012310 (2003).
- [170] S. Cortez, O. Krebs, S. Laurent, M. Senes, X. Marie, P. Voisin, R. Ferreira, G. Bastard, J.M. Gérard, and T. Amand, *Phys. Rev. Lett.* **89**, 207401 (2002).
- [171] M. Baier, F. Findeis, A. Zrenner, M. Bichler, and G. Abstreiter, *Phys. Rev. B* **64**, 195326 (2001).
- [172] M. Bayer, G. Ortner, O. Stern, A. Kuther, A.A. Gorbunov, A. Forchel, P. Hawrylak, S. Fafard, K. Hinzer, T.L. Reinecke, S.N. Walck, J.P. Reithmaier, F. Klopff, and F. Schäfer, *Phys. Rev. B* **65**, 195315 (2002).
- [173] J.J. Finley, D.J. Mowbray, M.S. Skolnick, A.D. Ashmore, C. Baker, A.F.G. Monte, and M. Hopkinson, *Phys. Rev. B* **66**, 153316 (2002).
- [174] J.G. Tischler, A.S. Bracker, D. Gammon, and D. Park, *Phys. Rev. B* **66**, 081310 (2002).
- [175] M. Fricke, A. Lorke, J.P. Kotthaus, G. Medeiros-Ribeiro, and P.M. Petroff, *Europhys. Lett.* **36**, 197 (1996).
- [176] K.H. Schmidt, G. Medeiros-Ribeiro, M. Oestreich, P.M. Petroff, and G.H. Döhler, *Phys. Rev. B* **54**, 11346 (1996).
- [177] For dot shapes of lower than circular symmetry, mixing of different band states can become significant. See, e.g., L.-W. Wang , J. Kim, and A. Zunger, *Phys. Rev. B* **59**, 5678 (1999).
- [178] Al.L. Efros, *Phys. Rev. B* **46**, 7448 (1992).
- [179] Al.L. Efros and A.V. Rodina, *Phys. Rev. B* **47**, 10005 (1993).
- [180] In B_z , we have absorbed the Overhauser field which could possibly arise from dynamically polarized nuclear spins.

- [181] A linearly oscillating magnetic field, $\mathbf{B}_x(t) = B_x^0 \cos(\omega_{\text{ESR}}t)\hat{\mathbf{x}}$, can also be applied, cf. J.J. Sakurai, *Modern Quantum Mechanics, Revised Edition*, Addison-Wesley (1995). This leads, in the rotating wave approximation (RWA), to the same result as the rotating field for $B_{\perp} \rightarrow B_x^0/2$.
- [182] We use the standard description $H_{\text{d-L}} = -e\mathbf{A} \cdot \mathbf{p}/m_0c$, with vector potential \mathbf{A} and charge e , bare mass m_0 , and momentum \mathbf{p} of the electron. Since excitonic electric fields are present, we neglect the typically smaller electric fields of the laser that are contained in second order in the term $\propto \mathbf{A}^2$. We apply the electric dipole approximation and assume a coherent photon state for the laser. Then, $\Omega_L = \alpha e \langle X_{\downarrow}^- | \mathbf{e}_L \cdot \mathbf{p} | \downarrow \rangle \sqrt{2\hbar/m_0^2 c^2 V \epsilon_0 \epsilon_r \omega_L}$, with volume V , unit polarization vector \mathbf{e}_L , and mean photon number $|\alpha|^2$ of the laser mode. The relative permittivity of the semiconductor is ϵ_r , and ϵ_0 is the dielectric constant. See also Appendix F and Ref. [210].
- [183] Excitation of a charged exciton state containing an electron triplet would require an additional energy of ~ 40 meV [170] and can be excluded by the low laser bandwidth.
- [184] The single-spin relaxation time T_1 can be measured via a similar double resonance scheme as discussed in this work. For this, we assume that the laser polarization is σ^+ and the temperature is sufficiently low that $|X_{\downarrow}^- \rangle$ is decoupled from the three-level system $|\uparrow \rangle$, $|\downarrow \rangle$, and $|X_{\uparrow}^- \rangle$, cf. Figs. 5.1,5.2. In the regime $\Omega_L, W_{\text{em}} \gg \Omega_{\text{ESR}}, W_{\uparrow\downarrow}$, the mean time of fluorescence interruptions due to ESR excitation provides T_1 , similarly as for a single atom [H.J. Kimble, R.J. Cook, and A.L. Wells, Phys. Rev. A **34**, 3190 (1986)].
- [185] T. Flissikowski, I.A. Akimov, A. Hundt, and F. Henneberger, Phys. Rev. B **68**, R161309 (2003).
- [186] J.A. Gupta, R. Knobel, N. Samarth, and D.D. Awschalom, Science **292**, 2458 (2001); C.E. Pryor and M.E. Flatté, quant-ph/0211160.
- [187] Y. Lyanda-Geller, I.L. Aleiner, and P.M. Goldbart Phys. Rev. Lett. **81**, 3215 (1998).
- [188] D. Loss and P.M. Goldbart, Phys. Lett. A **215**, 197 (1996).
- [189] A. Stern, Phys. Rev. Lett. **68**, 1022 (1992)

- [190] S.A. van Langen, H.P.A. Knops, J.C.J. Paasschens, and C.W.J. Beenakker, Phys. Rev. B **59**, 2102 (1999).
- [191] D. Loss, H. Schoeller, and P.M. Goldbart, Phys. Rev. B **59**, 13328 (1999).
- [192] P.D. Ye, S. Tarucha and D. Weiss, Proceeding of ICPS 24, Israel (1998).
- [193] T.M. Jacobs and N. Giordano, Superlattices and Microstructures **23**, 635 (1998).
- [194] P. Mohanty and R.A. Webb, Phys. Rev. Lett. **84**, 4481 (2000).
- [195] R. Häussler, PhD thesis, Universität Karlsruhe, 1999.
- [196] G. Nunes, APS Centennial Meeting (1999) QC21,6.
- [197] A.G. Aronov and Yu.V. Sharvin, Rev. Mod. Phys. **59**, 755 (1987).
- [198] P.A. Lee, A.D. Stone and H. Fukuyama, Phys. Rev. B **35**, 1039 (1987).
- [199] Implementing magnetic textures with different winding numbers f and \tilde{f} can be easily done by replacing the coefficient of σ_{2z} in Eq. (6.7) with $\pm\tilde{f}/2$. This will result in different diagonal elements in the matrices given below. As we have verified, within this approach the only further generalization of the magnetic texture is an arbitrary rotation axis of the field [214]. Otherwise it is not possible to find a linear combination of ∂_x and Pauli matrices which commutes with $h^{C/D}$.
- [200] As every quantity $\sum_{j=-\infty}^{\infty} f(j + \Phi)$ is periodic in Φ with period one, we see that $\delta g^{(2)}$ has a periodic dependence on the Aharonov-Bohm fluxes $\phi, \tilde{\phi}$.
- [201] B.L. Al'tshuler and D.E. Khmel'nitskii, Pis'ma Zh. Eksp. Teor. Fiz. **42**, 291 (1985) [JETP Lett. **42**, 359 (1985)].
- [202] C.W.J. Beenakker and H. van Houten, Phys. Rev. B **37**, 6544 (1988).
- [203] P. Mohanty, E.M.Q. Jariwala, and R.A. Webb, Phys. Rev. Lett. **78**, 3366 (1997).
- [204] Yu. A. Bychkov, V.I. Mel'nikov and E.I. Rashba, Sov. Phys. JETP **71**, 401 (1990) [Zh. Eksp. Teor. Fiz. **98**, 717 (1990)].

- [205] S. Chakravarty and A. Schmid, Phys. Rep. **140**, 193 (1986).
- [206] A.G. Mal'shukov, V.V. Shlyapin and K.A. Chao, Phys. Rev. B **60**, 2161 (1999).
- [207] S. Brosig, K. Ensslin, R.J. Warburton, C. Nguyen, B. Brar, M. Thomas, and H. Kroemer, Phys. Rev. B **60**, 13989 (1999).
- [208] The full line in the power spectrum is provided as a guide to the eye. It was obtained by zero-padding the data before calculating the DFT [209].
- [209] W.H. Press, S.A. Teukolsky, W.T. Vetterling, and B.P. Flannery, *Numerical Recipes in C* (Cambridge University Press, England, 1993), Chap. 12.
- [210] L. Mandel and E. Wolf, *Optical Coherence and Quantum Optics*, Cambridge University Press (1995).
- [211] J.A. Folk, R.M. Potok, A.C. Johnson, S.M. Cronenwett, C.M. Marcus, W.G. van der Wiel, and L.P. Kouwenhoven, APS March Meeting (2001) C25.4.
- [212] C.P. Slichter, *Principles of Magnetic Resonance* (Springer, Berlin, 1990).
- [213] Y. Nakamura, Yu.A. Pashkin, and J.S. Tsai, Nature (London) **398**, 786 (1999).
- [214] H.-A. Engel, Diploma thesis, Universität Basel, 1999.

Curriculum Vitae

Hans-Andreas Engel

Born: (see printed version)

Nationality: Swiss

Education

- | | |
|---------------|---|
| 1982-1987 | Primarschule, Rünenberg and Marly, Switzerland |
| 1987-1991 | Progymnasium, Binningen, Switzerland |
| 1991-1993 | Matura (Typus C) <ul style="list-style-type: none">• Gymnasium Oberwil, Switzerland; skipped first year |
| 1994-1999 | Study of physics, University of Basel, Switzerland <ul style="list-style-type: none">• minor subjects: mathematics and biology |
| October 1999 | Diploma in Condensed Matter Theory <ul style="list-style-type: none">• <i>Berry phase in diffusive rings</i>• supervisor: Prof. D. Loss |
| 2000-2003 | PhD student <ul style="list-style-type: none">• University of Basel, Switzerland• Teaching assistant |
| December 2003 | Submission of PhD thesis in Theoretical Physics <ul style="list-style-type: none">• <i>Electron Spins in Dots and Rings: Coherence, Read Out, and Transport</i>• supervisor: Prof. D. Loss• co-referees: Prof. C. Bruder and Prof. L.S. Levitov• summa cum laude |

During my studies at the University of Basel I attended lectures of the following professors:

N. A'Campo, G. Bauer, T. Bickle, C. Bruder, R. Capitelli, F.-J. Elmer, D. Graudenz, H.-J. Güntherodt, H.P. Hauri, E.W. Heri, A. Khaetskii, D. Kotschick, H. Kraft, D. Loss, D. Masser, E. Meyer, H. Mühry, G.-R. Plattner, H. Rudin, B. Scarpellini, C. Schönenberger, G. Schatz, J. Seelig, I. Sick, P. Talkner, L. Tauscher, F.-K. Thielemann, D. Trautmann, and C. Ullrich.

Publications

1. Hans-Andreas Engel and Daniel Loss,
Asymmetric Quantum Shot Noise in Quantum Dots,
cond-mat/0312107.
2. Hans-Andreas Engel, Vitaly Golovach, Daniel Loss, L.M.K. Vandersypen,
J.M. Elzerman, R. Hanson, and L.P. Kouwenhoven,
Measurement efficiency and n-shot read out of spin qubits,
cond-mat/0309023.
3. Oliver Gywat, Hans-Andreas Engel, Daniel Loss, Ryan Epstein, Yuichiro
Kato, and David D. Awschalom,
Optical Detection of Single-Electron Spin Decoherence in a Quantum Dot,
cond-mat/0307669, accepted for Phys. Rev. B.
4. Hans-Andreas Engel and Christoph Leuenberger,
Benford's law for exponential random variables,
Statistics & Probability Letters **63** (4), 361 (2003).
5. Hans-Andreas Engel and Daniel Loss
*Single Spin Dynamics and Decoherence in a Quantum Dot via Charge Trans-
port*,
Phys. Rev. B **65**, 195321 (2002).
6. Hans-Andreas Engel und Daniel Loss,
Berry-Phase gemessen,
Physik Journal **1** (6), 19 (2002).
7. Simon Scheuring, Daniel J. Müller, Henning Stahlberg, Hans-Andreas Engel,
and Andreas Engel,
*Sampling the conformational space of membrane protein surfaces with the
AFM*,
Eur Biophys J. **31** 172 (2002).
8. Hans-Andreas Engel and Daniel Loss,
*Detection of Single Spin Decoherence in a Quantum Dot via Charge Cur-
rents*,
Phys. Rev. Lett. **86**, 4648 (2001).

9. Hans-Andreas Engel, Patrik Recher, and Daniel Loss,
Electron spins in quantum dots for spintronics and quantum computation,
Solid State Commun. **119**, 229-236 (2001).
10. Daniel Loss, Patrik Recher, and Hans-Andreas Engel,
*Electron spins for spintronics and quantum communication in quantum dots
and wires*,
XXXVI Rencontres de Moriond, Electronic Correlations: From meso- to
nano-physics, 525 (2001).
11. Hans-Andreas Engel and Daniel Loss,
*Conductance fluctuations in diffusive rings: Berry phase effects and criteria
for adiabaticity*,
Phys. Rev. B **62**, 10238 (2000).
12. Guido Burkard, Hans-Andreas Engel, and Daniel Loss,
*Spintronics and Quantum Dots for Quantum Computing and Quantum Com-
munication*,
Fortschritte der Physik **48**, 965 (2000) (special issue on Experimental Pro-
posals for Quantum Computation), eds. H.-K. Lo and S. Braunstein.